QUANTUM MECHANICAL STUDY OF SEMICONDUCTING CLUSTERS

THESIS SUBMITTED FOR THE AWARD OF THE DEGREE OF

Doctor of Philosophy

In

Applied Physics

By

Deep Kumar

Enrollment No.: 434/10

Under the Supervision of

Dr. Devesh Kumar

DEPARTMENT OF APPLIED PHYSICS
SCHOOL FOR PHYSICAL SCIENCES
BABASAHEB BHIMRAO AMBEDKAR UNIVERSITY,
LUCKNOW – 226025 (U. P.), INDIA
2018

DEDICATED

TO

MY FAMILY

DECLARATION

I declare that the thesis entitled **"Quantum Mechanical Study of Semiconducting Clusters"** has been prepared by me under the supervision of **Prof. Devesh Kumar**, Department of Applied Physics, School for Physical Sciences, Babasaheb Bhimrao Ambedkar University, Lucknow. No part of this thesis has formed the basis for the award of any degree, diploma or fellowship previously. Further, I declare that the material embodied in the present work is based on original research work and the indebtedness to others has been duly acknowledged at relevant places. This is also declared that the thesis is essentially free from all kinds of plagiarism.

Deep Kumar

Deep Kumar

Department of Applied Physics
School for Physical Sciences
Babasaheb Bhimrao Ambedkar University
Vidya Vihar, Rae Bareilly Road
Lucknow, (U.P.), India-226025

Date: 25-09-2018
Place: Lucknow

CERTIFICATE

This is to certify that the thesis titled **"Quantum Mechanical Study of Semiconducting Clusters "** submitted by **Mr. Deep Kumar** is an original research work and has not been previously submitted in part or full for the award of any other degree or diploma to this or any other university or institutions.

The thesis submitted to the Babasaheb Bhimrao Ambedkar University, Lucknow. satisfies all the requirements as stipulated in the *Doctor of Philosophy (Ph.D.) regulations -1999 as amended in 2010* and it is fit for submission and evaluation for the award of Doctor of Philosophy of the University.

Date : 25-9-2018

D kumar 25/9/18
(Supervisor)

D kumar 25/9/18
(Head of the Department)

ACKNOWLEDGEMENT

Foremost, I am highly grateful to God for His blessings that continue to flow into my life, and because of You, I made this through against all odds.

I am very much indebted to my supervisor **Prof. Devesh Kumar** for his generous support, encouragement, guidance and providing me inspiring research atmosphere during the period of my research work. I am thankful to him for introducing the subject to me as well as keeping me on the right track throughout my research activities. I would like to extend my thanks for his patience with which he dealt me, his critical remarks, valuable suggestions and his attachment on personal level have proven guiding lamp on the road to success.

I would like to give my sincere thanks to Prof. Devesh Kumar, Head of Department, for providing me all the necessary facilities available in the Department during my research work.

am also grateful to my teachers Prof. B.C. Yadav, Dr. Ramesh Chandra, Dr. Anil Kumar Yadav and Dr. Devendra Singh and Dr. K. B. Thapa for their blessings. I deeply acknowledge the help of office staff of the department who was always ready to support me at every stage of my research work.

Further, I would like to thank the facilities of Central Library and the Computer Center of Babasaheb Bhimrao Ambedkar University, Lucknow which were useful at every stage of the research work.

I am also thankful to my colleagues Mr. Jitendra, Mr. Pranav, Asheesh, Mr. Suresh, Mr. Dharmveer, Mr. Narinder, Ms. Ruchi, Ms. Rolly, Ms. Nidhi, Ms. Anamika and Ms. Shivani of my group for being with me as well as for helping and supporting me in every manner.

I gratefully acknowledge the financial support from the University Grant Commission (UGC), Government of India, New Delhi.

Finally, I have no words to express my feelings of gratitude towards my family. My parents have been constant torch bearers for me constantly encouraging and providing all necessary guidance, supports and inspiration towards acquiring new skills. My wife supports need no mention, without her it would have not been such a smooth task. I am highly indebted to all my family members, they helped me glide smoothly during times of despairs.

Last but not least, I would like to thank one and all, who directly or indirectly helped me during my studies leading to this thesis.

Deep Kumar

(Deep Kumar)

ABSTRACT

Materials possessing an electrical resistivity between that of conductor and insulator are called semiconductors. All the devices based on semiconductos materials, such as transistors, solar cells, light-emitting diodes, digital integrated circuits, solar photovoltaics, and much more, are the base of modern electronics. Silicon is used in most of the semiconductor devices while other materials such as germanium, gallium arsenide, and Gallium nitride are used for specialized applications. The continuing development of material science and clusters technologies make evident the need for detailed theoretical understanding of these systems. Many theoretical approximations have been developed to study their basic properties. Most of these methods provide excellent information on the ground state, although the ab initio methods demand demands in general a substantial computational effort.

PREFACE

The thesis entitled **"Quantum Mechanical Study of Semiconducting Clusters"** encapsulates the results of theoretical investigations carried out in the Department of Applied Physics, Babasaheb Bhimrao Ambedkar University during 2013 under the supervision of Dr. Devesh Kumar, Professor of this department.

Semiconductors are used in the production of transistors and diodes, as the basic components of modern electronic devices. This technology has completely changed the world we live in, semiconductors have been widely used in electronics, integrated circuits and computer industry because it can produce better, faster, cheaper electronic devices. Man has known industrial applications of these semiconductor clusters but their mechanism was unknown until chemistry developed, both experimental as well as theoretically. The lack of technology may impair characterization of given substrate but theoreticians emerged with promising tools that blossomed fruitful results and gave deep insights into stability of these clusters and had a great impact on the semiconductor industry.

Nowadays computational techniques have matured to a level, which is widely tested, and benchmarked and different sets of processes have been developed that generate reliable results capable of predicting experimental data for last few decades. There are many instances when experimentalists have reproduced and validated the already predicted theoretical results.

The thesis is divided in seven chapters. **Chapter 1** reviews the theoretical work done on semiconductor cluster and also discusses the suitability of various computational quantum mechanical methods available in terms of accuracy etc.

In **Chapter 2**, development and mathematical details of quantum mechanical methods has been discussed.

Chapter 3 deals with the results obtained from the calculation for Ga_xAs_x fullerene like clusters. An attempt was also made to correlate the calculated results with experimental data.

Chapter 4 is focused on the results obtained from Structural Stability and Electronic Properties of $(Ga_nN_n)_m$ clusters. A comparison of cluster stability based on quantum mechanically obtained eneregetic profile was also made in this chapter.

Chapter 5 presents chapter study of Stability of $Cd_xS_{x\pm4}$ fullerene like clusters.

Chapter 6 is focused on the results obtained from the Quantum chemical studies of Phosphorus doped ZnO cluster stability and electronic properties. The general conclusions drawn from the present thesis are summarized in the **Chapter 7**.

Hopefully, a better understanding of these important semiconducting clusters will enable more efficient and effective work of computational chemistry to be performed, well into the future.

LIST OF ABBREVIATION

1.	BS	Basis Set
2.	BLYP	Becke Lee Yang Parr
3.	CdS	Cadmium Sulfide
4.	CT	Charge-Transfer
5.	CI	Configuration-Interaction
6.	DZ	Double Zeta
7.	DFT	Density Functional Theory
8.	EA	Electron Affinity
9.	EE	Electrostatic Embedding
10.	ECP	Effective Core Potential
11.	EPR	Electron Paramagnetic Resonance
12.	FT-ICR	Fourier Transform-Ion Cyclotron Resonance
13.	GaAs	Gallium Arsenide
14.	GaN	Gallium Nitride
15.	GTO	Gaussian type orbital
16.	Ge	Germanium
17.	HAT	Hydrogen Atom Abstraction
18.	HF	Hartree-Fock
19.	HOMO	Highest Occupied Molecular Orbital
20.	IE	Ionization Energy
21.	IR	Infra Red
22.	LCAO	Linear Combination of Atomic Orbital
23.	LUMO	Lowest Unoccupied Molecular Orbital
24.	Mgn	Magnetic
25.	MM	Molecular Mechanics
26.	MD	Molecular Dynamics
27.	MS	Mass Spectrometry
28.	PES	Potential Energy Surface

29.	QM	Quantum Mechanics
30.	RHF	Restricted Hartree-Fock
31.	SCF	Self Consistent Field
32.	STO	Slater Type Orbital
33.	TM	transition metal
34.	UHF	Unrestricted Hartree-Fock
35.	ZPE	Zero Point Energy
36.	ZnO	Zinc Oxide

LIST OF TABLES

LIST OF FIGURES

TABLES OF CONTENTS

CHAPTER 1

INTRODUCTION

The beginning of the 20^{th} century saw the treatment of matter through its constituent elements viz. atoms and molecules. The material was then seen to be comprising of a large number of atoms or molecules whose properties can be well explained by assuming the substance as periodic arrangement of atoms. However little information existed regarding the manner in which atoms or molecules aggregated to form a bulk. It was proposed that a few to a few hundreds of atoms aggregated in a peculiar manner. This subunit may be called as cluster if its properties differ drastically from its bulk analog. The study of clusters has gained significance because they explain transition of properties from atomic to bulk regime.

Cluster science grew up exponentially since the late 1970's because of two main reasons:

(a) The first reason was the desire to comprehend as to how the reduced dimensions lead to a significant change from fundamental physics point of view.

(b) The second reason was the motivation to manipulate and interplay with properties of matter to obtain materials for specific applications in modern and future technologies.

The clusters are composed of atoms and molecules intermediated in size between the individual atoms to the bulk matter.

The cluster can be categorized depending upon the number of atoms that constitute them: small, medium and large. The cluster whose "properties" change drastically as

we change their size and shape are categorised under small clusters. When clusters are made up of same atoms then such cluster are said to be homogeneous but when clusters are comprised of a kind of atoms or molecules then they are said to be heterogeneous cluster. As far as the properties of these cluster are concerned from individual atoms or molecules to bulk, the properties change drastically.[1, 2] While comparing the cluster with bulk materials, it can be easily observed that the cluster exhibits a very large surface to bulk volume ratio i.e. on the surface, a large fraction of the constituents particle can be identified. Due to this the chemistry of the surface now plays an extremely important role in determining the important properties. The molecules can be classified by their different composition and structure while the clusters differ in both. The clusters may be comprised of any number of atoms or molecules. The clusters that can be said to obtain the most stable structure depend upon the number of particles associated with it. In a particular size and composition, there may be a number of isomers, and among these isomers, one would get the most stable configuration which is known as ground state isomer. With the increase in the number of atoms constituting the clusters, the number of possible isomers increases rapidly. Thus important parameters like binding energy, relative stability, energy level spacing, magnetism and bonding change sharply with the different structures as the number of atoms that make up the clusters are changed.

1.1. Clusters Science

Cluster science from the view point of potential technological applications as well as from the scientific view point is very important. It has been the most evolving fields of research in both chemistry and physics. As discussed before, these systems (cluster) help to establish the connection between the atomic and molecular physics

on one side and condensed matter physics on the other. Since the properties of the clusters are dominated by their large surface to volume ratio giving an opportunity to study the interplay between surface and volume effects. The clusters owing a finite size exhibit discrete spectroscopic features.

Nanoclusters are comprised of a few to a few hundred of atoms that have drawn much attention due to their relevance in the nanoscience and nanotechnology. The properties of the nanoclusters are extremely sensitive to the size and composition. Therefore it can be said that these nanoclusters help to bridge gap between the bulk material and atomic or molecular structure. At nanoscale level, the size dependent properties are often observed. Hence by varying the number of atoms, in the clusters, its size and structure changes that help to tune the electronic properties.

Computational modelling of these clusters provides a platform to better understand the science behind their electronic structure properties. The physical and chemical properties of these clusters are quite different from that of the bulk material due to the quantum confinement. The structure of these clusters obtained by the ab-initio quantum mechanical calculations obtained theoretically provides a protocol for the experimentalists to produce nanostructures. During the last several years, many clusters like metals and semiconductor binary nanoclusters were studied that contain small atomic clusters as the building block for the relatively bigger and well controlled nanostructures.[3-10] In order to minimise the size of devices used in the present area, silicon and germanium clusters have been studied extensively both theoretically and experimentally.[6-9] Sometimes while predicting the structure of the stable cluster it is found that a particular composition, resembles the chemical properties of atoms or group of elements in the periodic table. The prediction of such a major findings is termed as superatom concept and this came to light while studying

the aluminium clusters where notable size dependent reactivity can be observed. [10-11] For the hydrogen storage, metal clusters can be used that can also resolve the issues concerned with renewable energy field. Thus theoretical predictions play a significant role to design and model different materials as per requirements which are not always feasible via the experimental techniques as there is a high probability of reaction affinity of small size clusters. Hence one can surely say that theoretical prediction of these clusters and their characterizations is a very hot topic of research in the present scenario.

Hence in the field of cluster science, both experimental and theoretical research are quite important for the further development of this field.

1.2. Importance of Cluster Science

For the last few decades, cluster science has been such a field that is growing and studied at a good pace with time with the involvement of advanced computational and experimental techniques. Hence research on this field has increased exponentially. There are various factors for this: firstly the clusters help to connect the science of isolated atoms, molecules and bulk matter. Hence it is quite interesting to study how these properties vary with the size for a particular composition. This knowledge helps to provide a novel viewpoint that in turns helps to improve our understanding of these clusters. This driving force to reveal the properties of the cluster is the main influential force. The present thesis will touch upon various aspects of the size and different combinations of clusters. The second motivation of the cluster science was to explore the reasons that help to form thermodynamically and chemically stable structure via nucleation at atomic level.

The nanoclusters are the mesoscopic particles ranging from few to hundred of atoms. In contrast to the free molecules in gases, the condensed phases of matter are called as liquid, crystalline, solid and gases depending on their properties in the constant proximity of all their constituent atoms. Clusters are composed of atoms, molecules or ions that under the influence of different forces bind to form the clusters.

While dealing with small sized clusters and nanoclusters, the structural periodicity is found to be absent that is very much required in the case of crystal lattice i.e. in bulk. Some of the common geometries in clusters are hexagonal prism structures, icosahedrons, incomplete icosahedrons or any other polyhedral structure. These clusters cannot grow in the form of periodic lattice but by using computational modelling, one can make clusters in the form of 1-D nanotube or 2-D planer structure. Quantum confinement effect can thus easily be observed by some properties of these clusters that are very rarely found in the bulk.

The present thesis deals with the computational studies of the different clusters like Gallium Nitride (GaN), Cadmium sulphide (CdS), Gallium Arsenide (GaAs) and Zinc Oxide (ZnO) and various important parameters like stability, binding energies, Homo Lumo gap, electron affinity, ionization potential, density of states etc. that were calculated by using the density functional theory (DFT).

1.3. Type of clusters

1.3.1. Zinc Oxide (ZnO) clusters

During the past few decades, notable advancement in the development of wide band gap semiconductor can be observed ranging from blue lasers to solar cells. ZnO is a wide band gap semiconductor which has drawn attention of the scientific and research

community due to its application in different fields.[12] Due to the wide band gap of approximate 3.4 eV at room temperature, ZnO has become an important material for spintronics applications due to the high electron mobility.[13] The ZnO clusters find potential application in the field of spintronics, transparent electronics and optoelectronics.[14-16] Some other important application of ZnO clusters are non-volatile memory systems and ferromagnetism that is required to store data for extended time period.[17]

Semiconductor like ZnO provide the possibility to the devices which combine magnetic and optical effect, such as spin light-emitting diodes (LEDs) [18], spin polarised solar cell,[19] and magneto-optical switches.[20] Zno is an attractive field of research due to the following reasons:

(1) There is a lack of systematic experimental study of the size and dopant concentration which depends upon the optical properties of nanoclusters.

(2) There is a conflict between the magnetic and optical properties of transition metal (TM) doped ZnO nanoclusters.

B. Wang *et al.* proposed perfect cage structure in $(ZnO)_n$, $(ZnO)_{15}$, $(ZnO)_{16}$, and (ZnO) that have relatively higher binding energy (B.E) and wider HOMO-LUMO gaps. Such magic number clusters resemble to (BN)n clusters with similar size.[21] The HOMO-LUMO gap for $(ZnO)_n$ for n=1 and 2 are quite smaller than other clusters that is contrary to the general behaviour of the semiconductor.

In the B-doped ZnO clusters, intrinsic room temperature ferromagnetism has been observed.[22] In the high temperature annealed N-doped ZnO, the green band emission can be easily observed [23] with Co-doped ZnO clusters, few studies have

been reported. C and N co-doped clusters are fabricated using metal-organic chemical vapour deposition.[24] However very few theoretical studies on Co-doped ZnO cluster are reported.

1.3.2. Cadmium Sulfide (CdS) Clusters

Since the past two decades, nanoparticles and semiconductor clusters were the most extensively studied fields by the theoreticians as well as by the experimentalists. By varying the size of the clusters, the electronic and optical properties can be tuned therefore this field drew much attention of the scientific world. This feature is termed as quantum confinement effect or quantum size effect QES.[25-29] This can be mesmerized by the condition of a particle in the box. This problem prevails for example, when an electron is trapped in a confined dimension. This confinment can be observed in one, two or all 3- dimensions. From experimental point of view these confinements can be observed like quantum wells, quantum dots, quantum wire, respectively. For a confined systems i.e. a cluster or nanoparticles, HOMO-LUMO gap i.e. the gap between the single energy levels is inversely proportional to the size of the system. However as the size of the systems is increased, the spacing between energy levels are reduced but as the number of particle increases, the number of energy levels also increases. As a result the system acquires the property of a bulk (eg. the discrete energy levels begin to form bonds). Experimentally it is found that the HOMO-LUMO gap of bulk material is lower than that of nanoparticles. As the particle size is increased, value of energy band gap resemble with that of the bulk materials. II-VI semiconductors like telluride Selenide, Cadmium Sulfide are extremely important from the viewpoint that these have various possible crystal structures like wurtzite and zinc blende.

For some compounds, the rock salt crystal structure obtained at high pressure also exists.[30-31] Zinc blende and wurtzite crystal structure are found to be energetically almost degenerate for the bulk, among these two structure, wurtzite structure is more stable structure.[32-34]

In order to calculate the lowest optical transitions of CdS, Se, or Te clusters, some of the studies used the approach of effective mass method.[35-38] Thereby the underlying structure of cluster becomes of only secondary importance. Another approach, the tight-binding was applied to these systems,[40-53] and it was presumed that the structure of the cluster is of a finite part of an infinite crystal system. The structural relaxation is not taken into consideration in most of the studies done so far except by whaley co-workers.[53] They used $sp3s^*$ tight binding model, and also considered the density functional work carried out by Ahlrichs *et al.*[54-55] Chelikowsky *et al.* [56] used TDLDA calculations of small Cd_nSe_n clusters. These structures were taken from the simulated annealing strategy.[57] The size of cluster was quite small. Currently the cadmium sulfide clusters find potential application in the field of material science.[58] since the electronic properties can be easily tuned. Since there are various applications of the CdS clusters like tuning electrical /optical properties,[59-60] solar cells [61] and DNA analysis [62] so CdS clusters are widely studied clusters by many research groups.[63-65]

The applications of CdS clusters in the nonlinear susceptibility measurement,[66] thin films of CdS nanocrystals [67] and nanoparticles [68-70] are worth noticing. However very few theoretical work is carried out on $(CdS)_n$ so this provides an opportunity to work in this field at large. The study of hyper polarizability of monomers was studied by Rapitis *et al.*[71] The $(CdS)_n$ structure was investigated by Joswing *et al.*[72] based on the approach of local density approximation study on the polarizability of

the CdS clusters.[73] Troparevsky and chelikowsky outlined the mean dipole polarizability per atom of (CdS)n which decreses rapidly with cluster size thereby tending to the bulk limit of 23.7 eEh-1 from the tetramer onward.

1.3.3. Gallium Arsenide (GaAs) clusters

GaAs is one of the most important group III-V semiconductor that is suitable for the use in high-efficiency solar cell with a band gap of approx.(1.43eV) for single juction solar cell.[74] It also exhibits high optical absorption which means solar cells made of GaAs needs to be of a few microns thick to absorb sunlight. GaAs also find its application in space industry due to its insensitivity to heat and its high resistance to radiation damage. By various techniques, nanoparticles of the GaAs were prepared that find application in radiofrequency (rf) sputtering, laser ablation, molecular beam epitaxy, and chemical method.[75-79] The application of an external electric field in order to tune the energy gap of a semiconductor nanocrystal can be an important step in the development of electronic and optoelectronic devices. Over the last few years, the effects of the electric fields on the optical and electronic properties of semiconductor nanostructure have been studied widely.[79-83]

The bulk GaAs has a number of applications so its clusters are very crucial from technological point of view.[84] One important application is that of the spin based electronics [85] because with the doping of Mn atoms into GaAs, a diluted magnetic semiconductor clusters in produced.[86] In the field of optoelectronic sensing,[87] these GaAs particles are a promising candidate. They are also used in medical diagnostics,[88] quantum computing [89] as a component of fuel cells.[90] Earlier the studies were confined to the small size of the clusters but with the advancement of theoretical and experimental approaches. The studies on the bigger clusters also

started with the pace of time. The work carried out for GaAs clusters studied theoretically.[91] is noticeable. A review on the theoretical efforts for smaller GaAs clusters provided significant light on the theoretical approaches. Structural data were obtained for the GaAs monomer [92] using resonant two-photon ionization spectroscopy and for Ga_nAs_m clusters [93] with $n+m \leq 5$ using the laser photo detachment spectra of the corresponding anions. Therefore, theoretical studies would provide a useful guide for future experimental studies. On the other hand, one needs to know the structure of large GaAs clusters in order to model metal doped clusters important for fabricating micro devices for spintronic applications.[94] Considerable attention has been directed toward the preparation of the GaAs nanostructures.[95-102]

1.3.4. Carbon Nanoclusters

The C_{60} was discovered in 1985.[103] After studying different carbon clusters it can be concluded that it has rich variety of physical and chemical properties. The synthesis of fullerene clusters has been accomplished in macroscopic quantities, under some specific conditions and they are very helpful for developing some new materials which may be useful in many fields of science. The atomic and electronic structures of fullerene based materials have high degrees of freedom in various dimensions. Some examples are single molecule quantum dots, linear chain in nanotubes, planar nano and crystalline solids.[104] The tuning of electronic and magnetic properties of pure fullerene is realized by the functionalizing or chemical modification of the fullerene.[105] Endohedral doping also represents an interesting possibility of functionalizing the fullerene clusters, instead of exohedral and substitutional doping of the fullerene. The research of endo fullerene has progressed over the last few years and characterization of endohedro TM was reported.[106]

Since many years, theoreticians have occupied the research of carbon based ferromagnetism, and for the dislocations, vacancies and impurity of the atoms, the origin of ferromagnetism has been proposed.[107] Till now, theoreticians have focused to understand the magnetic properties of metellofullerenes. The magnetic properties of C_{60} [108-110] are crucial due to their high stability and large volume available for encapsulation. Lopez *et al.*,[105] have studied the magnetic properties of the carbon clusters, which are present in fullerenes and graphite nanoribbons. After the study, it is observed that, small metallohedral fullerenes remain unchanged and instead of the successful production of many small fullerenes, their magnetic properties have been investigated.[111-114] The smaller fullerene does not follow the isolated pentagon rule and disagree with the pentagon structure. Stability and electronic properties of fullerene are strongly affected by this class. The recent work on the synthesis of endohedral fullerene has got some special significance. By using laser vaporization of mixture of UO_2/graphite, U@C_{28} films were produced successfully.[115] Instead of U@C_{28}, the signals of U@C_{46}, U@C44, and U@C58 were also observed in mass spectrum, with lower intensities. Hence the fullerene cage stabilized by the internal uranium atom and the end point of laser is shrunk by the U@C_{28}. The mass spectrum obtained by laser vaporization of graphite/metal-oxide composites, have been confirmed by the presence of Zr, Hf, Ti, Sc inside C_{28} cage. Many theoretical groups have followed these experiments and performed a systematic series of M@C_{28} (M = Mg, Al, Ca, Sc, Ti, Ge, Zr and Sn),[116] and found that only Sr@C_{28} and Zn@C_{28} are thermodynamically stable due to their large binding energies. Sun *et al.* [117] studied the encapsulation of thirteen atoms from group IA to group VA (i.e. H, Li, Na, K, Be, Mg, Ca, B, N, P) and nine cations from group IA to group IIIA (i.e. Li^+, Na^+, K^+, Be^{2+}, Mg^{2+}, Ca^{2+}, Bi^{2+}, Al^{3+}) inside C_{32}

cage. Chen *et al.* investigated the stabilities and molecular structures of noble gas atoms (i.e. He, Ne, Ar and Kr) inside the C_{32} cage.[118] Kang gave a detailed calculation of possible encapsulation of alkali metals (i.e. Li, Na, K) inside C_{36}.[119] However, the trapping of TM inside the smaller fullerene cage has not been investigated experimentally and theoretically.

1.3.5. Germanium (Ge) Clusters

On Ge clusters, very few theoretical contributions have been made however some groups studied the endohedral doping of (transition metal)TM. Elements in pure as well as hydrogenated germanium cages [120,121] prevails which shows different properties. By the theoretical studies on TM doped caged Ge_nTM (n = 11-16) clusters,[120] the behaviour of growth of these clusters are found to be different from metals which are encapsulated silicon clusters, with the magic number for the cations at =4, 6, 10.[122,123]

Shvartsburg *et al.* on the basis of the binding and the fragmentation energy reported that Ge is relatively more stable than Ge_n clusters having medium sized, are stacks of tri-capped trigonal prism subunits. But the structure of Ge_n and Si_n for n =13, n=15-, 16.[124] HOMO-LOMO for these clusters is much higher as compared to their Si counterpart. The ferromagnetism have been reported in semiconductor of group IV, Mn_xGe_{1-x},[125] Cr_xGe_{1-x} [126] and Cr doped Ge single bulk crystal which show ferromagnetic ordering at 126 K,[127,128] while using molecular beam epitaxy (MBE) method, Cr doped Ge film, has shown weak paramagnetic behaviour between 1.8 K – 300 K.[127] Recent work on germanium crystal has shown Ge clusters doping with halogens.[129-132] Zn,[133] Cu,[134] Fe,[135,136] W,[137] Mn,[138] and Co small Ge_nCr clusters shows high magnetic moment for n = 1.5.[139] In spite of many

theoretical calculations, the origin of magnetism in TM doped, Ge clusters is still an area that needs to be investigated.

1.3.6. Gallium Nitride (GaN) Clusters

Gallium Nitride is the most important semiconductor after Si that is studied widely due to its brilliant light emiting, hardness, high thermal conductivity and electron transport properties.[140] Blue, green and violet light emiting diodes (LEDs) are used in the coloured display.[141,142] Also GaN at high temperatures can be useful materials for transistors, power switching and millimetre-wave applications and microelectronic devices.[143,141] With pure GaN crystals, the electronic industry is revolutionized, helping to laser yields, allowing more controllable wavelength and improving upon the opto-electronic devices. It also noticeable that LEDs could perform better, replacing the century-old incandescent bulb, and be used also for efficient power-handling circuitry in hybrid electric vehicles.[144] Materials and devices made from or containing GaN have been extensively studied since the early 90s experimentally,[142] and theoretically (using ab initio electronic structure methods) for GaN clusters.[141,145-151]

Group III nitrides have bandgaps ranging from red to UV frequencies, with robust thermal and mechanical properties and together with their alloys have acceptable electron transport properties for the applications in optoelectronics high speed devices and high temperature and high power electronic devices.[152,153] In past decade, these materials have remarkable success in electronic devices operating at terahertz frequencies.[143]

1.4. Literature survey

The important role of cluster science is to explore a wide range of nanostructure materials and understand their properties. Metal clusters have been studied both at theoretical and experimental levels. They have drawn attention in various fields due to their attractive physical and chemical properties.[154-157] The recent finding of Os cluster can be utilized as catalysts for methane hydrogenation and dissociation that provides a scope for further experimental and theoretical studies.[158] Chen *et al.* identified and studied the low lying structures of small iridium clusters and performed a systematic study.[159] Zhang *et al.* explored the magnetic and geometrical properties of Tb_n cluster and reported that the local spin magnetic moment shows a weak dependence on the cluster size.[160] In cluster science, the research on mixed metal clusters has become an advanced topic in the present scenario.[161] The structural, electronic and magnetic properties of golden cage clusters can be tuned by the doping with Sc, Ti in Au clusters and these find potential application in the field of electronic devices for tuning.[162] Dong *et al.* found that the doping of Au cluster with the Cr exhibits a magnetic moment which can be used in the field of magnetic storage devices.[163] Sahoo *et al.* studied the small sized Pt capped Fe, Co and Ni clusters that can be utilized by the experimentalists to design the novel materials.[164] Current findings of uranium encapsulated Au14 cage clusters provided a theoretical protocol for the future synthesis for the further study of the mixed clusters that might

facilitate in the application of radio-labeling which is another biomedical application.[165] Among the heterogeneous clusters, the study of the pure and hybrid semiconductor nanoclusters have attracted a lot of attention of the theoreticians and experimentalists as it finds potential applications in the field of electronic industries.[166-169] Due to the presence of the dangling bonds on the clusters surface, the pure semiconductors are chemically reactive. There are two ways to saturate the dangling bonds on the Si and Ge clusters, first by the encapsulation of transition metal (TM) in the cage,[170] and second by adding the hydrogen atoms exohedrally.[171] By considering these two ways it may be concluded that the encapsulation of transition metal in semiconductor cage cluster plays a key role in effectively saturating the dangling bonds of Si and Ge cage clusters.[172] The first bench mark experimental contribution in this field was made by Beck who explored that the transition metals (TM) such as Cr, Mo, W etc in silicon cluster augments the stability of the doped cluster.[173] Recent reports on metal encapsulated caged cluster of germanium [174,175] and silicon [176,177] provided new avenues to develop different nanostructures that may find applications in the field of electronics and luminescence. The role of the transition metal doping has proven to be significant to tune the stability, magnetic and optoelectronic properties.[178] Ma *et al.* reported how the structural, optical, and magnetic properties that changes with the doping of Cu, Ag and Au in the silicon clusters.[179] They also reported their applications in the field

of magneto-optics and photovoltaic cells. Recent study confirms that the physical and chemical properties of silicon cluster can be tuned by the variation of the size and shape of the clusters.[180,181] Li *et al.* found a significant role of the *d*-shell and the atomic radii of the dopant atoms in the cage formation of the transition metal doped Si cluster.[182] The metal encapsulated germanium cage clusters was an interesting topic for scientific community and provided an opportunity to work in this field of research. The theoretical studies on Cr doped germanium cluster explained the origin of magnetic moment in the clusters which is mainly localized at the Cr atom.[183] Kapil *et al.* executed a systematic study on Ni doped germanium clusters in a linear combination of atomic orbital brought to light on the design of Ge based superatom.[184] Manish *et al.* performed a theoretical study and explained the relative stability, chemical, and vibrational properties of cluster on transition metal (TM = Ti, Zr and Hf) doped cluster that are doped with metals.[185] Jorg *et al.* performed a combined theoretical and experimental study on lithium doped germanium clusters and compared the chemical properties in detail using molecular orbitals and density of states.[186] Xiaojun *et al.* studied the bimetallic Au-Ge nanoclusters and studied the effect of size selectivity.[187] They also reported the effect of the size selectivity on the geometry and its electronic properties. Deng *et al.* have studied the structural, electronic and magnetic properties of VGe_n (n = 3-12) cluster using anion photoelectron spectroscopy in combination with DFT and gave a

detailed description on charge transfer mechanism and the minimization of the clusters.[188] They have also investigated the structural and magnetic properties of Co doped germanium anion clusters using photoelectron spectroscopy.[189] Ravi *et al.*, using the density functional theory, studied Mo doped Ge_n cluster and reported important parameters like the stability, electronic and magnetic properties.[190]

These studies performed on the transition metals encapsulated clusters of Ge showed in general that the growth behavior, electronic and magnetic properties are extremely sensitive to the transition metal doping and also they depend upon the size of the clusters.

Torres *et al.* studied the structural and electronic properties of MSi_{16} (M= Sc, Ti, V+) superatom that can help to grow low dimensional system.[191] Vikas *et al.* explored the shell magnetism behaviour in transition metal doped calcium superatom.[192] They reported a stable magnetic $FeCa_8$ cluster with 24 valance electrons distributed in a closed shell sequence.

A recent theoretical study has been carried out that reports of the doping of Zn_{17} nanoparticle with transition metal impurity (TM = Sc, Ti, V, Cr, Mn, Fe, Co, Ni and Cu).[193] It has been investigated extensively that the Zn atomic environment is found to be spin polarized that modulated the total spin moment of these molecular magnets depending on the induced moments and magnetic coupling. Khanna *et al.* found the existence of designer magnetic superatom VNa_8 and reported that VNa_8 is a

magnetic superatom with a filled d-subshell with magnetic moment of 5μB.[194] This study showed a pathway to investigate the spin dependent electronics of the new magnetic motifs. Its low electron affinity is consistent with filled subshell and enhanced stability. Recent studies performed on the $Al_{12}Cu$ superatom by Reveles *et al.* can be used as stable building blocks of ionic salt.[195] Zhang *et al.* performed investigation using the first principle investigation for magnetic superatom in vanadium doped lithium clusters.[196] Acevedo *et al.* studied the gold, aluminum, and gallium superatom complexes and brought to light the superatom analogy in the class of ligand metal clusters.[197] The superatom can be used to create molecular electronic devices for the next generation of faster computers with large memory storage. With the help of magnetic superatom, denser integrated devices, volatile data storage, and higher data processing can be developed. The transition metal doped magnesium cluster can be used for the hydrogen storage and this has become an active area of research since the last two decades. The hydrogen adsorption on Mg doped Aluminium cluster was investigated by Varano and Henery.[198] They investigated the hydrogen adsorption on magnesium doped aluminium clusters using DFT method. Recent studies performed on small metal clusters show that they can be used as a process of hydrogen dissociation.[199,200] These theoretical studies show that how the number of atoms, shape, and the particular electronic spin state in small clusters can drastically change the ability to dissociate hydrogen molecule from the

clusters surface. Giri *et al.* utilized the DFT approach and showed some metal clusters that can be used as hydrogen storage materials.[201]

Jin *et al.* performed theoretical investigation to study the dissociation and adsorption of H2 on $(ZrO_2)_n$ (n=1-6) clusters.[202] They found that the absorption favors the sites with low coordinate number and increasing H-H bond length which helps to dissociate hydrogen molecule on the surface. Srinivasu *et al.* using ab initio quantum mechanical calculation performed a systematic study to confirm the molecular hydrogen adsorption in binary metal system.[203] Chen *et al.* studied the stability of transition metal on Mg surface and focused on the effect on hydrogen adsorption.[204] They showed that (transition metals) TMs doping with second layer on Mg surface is generally more stable than that on clean Mg but weaker than TMs in the first layer. This favors the peripheral positions of TMs atom. Fanjie and Yanfei reported the electronic, structural and magnetic properties of Mg_nX cluster (X= Fe, Co, Ni) and they have found that TMs atom is endohedrally localized in Mg_nX clusters.[205] Guo investigated the possible dissociation mechanism and dissociation pathway of H_2 on Al_nCr (n = 1-13) clusters, and characterized the hydrogen dissociation behavior using the activation number and reaction energy.[206] This study provides a theoretical approach of transition metal doped clusters as highly efficient and cost effective catalysts for hydrogen dissociation. Mananghaya reported the effectiveness and implementation of the ability of nitrogen doped carbon nanotube

(4ND-CNxNT) decorated with Sc for hydrogen storage under the spin-unrestricted density functional theory.[207]

References

1. W. A. de Heer, *Rev. Mod. Phys*., **65**, 611 (1993).
2. M. Brack, *Rev. Mod. Phys*., **65**, 677 (1993).
3. S. A. Shevlin, Z. X. Guo, *Chem. Soc. Rev*., **38**, 211 (2009).
4. A. Zuttel, *Mater Today*, **6**, 24 (2003).
5. R. Coontz, R. Hanson, *Science*, **305**, 957 (2004).
6. C. Milanese, A. Girella, G. Bruni, V. Berbenni, P. Cofrancesco, A. Marini *J. Alloys Comp*., **465**, 396 (2008).
7. A. Zaluska, L. Zaluski, J. O. Strob-Olsen, *Appl. Phys. A Mater Sci. Process*, **72,** 157 (2001).
8. M. Tsuda, W. A. Dino, H. Nakanishi, H. Kasai, *J. Phys. Soc.*, **73**, 2628 (2004).
9. R. A. Varin, T. Czujko, Z. S. Wronski, *Int. J. Hydrogen Energy*, **34**, 8603 (2009).
10. M. Tsuda, W. A. Dino, H. Kasai, H. Nakanishi, H. Aikawa, *Thin Solid Films*, **509**, 157 (2006).
11. L. Zaluski, A. Zaluska, J.O. Stron Olsen, R. Schulz, *J. Alloy Comp*., **288**, 217 (1999).
12. S. J. Pearton, D. P. Norton, K. Ip., Y. W. Heo, T. Steiner, *J. Vac. Set.Technol. B*, **22**, 932 (2004).
13. Y. Chen, D. M. Bagnall, H-J. Koh, K. T. Park, K. Hiraga, Z. Q. Zlm, T. Yao, *J. Appl. Phys.*, **84**, 3912 (1998).
14. G. A. Prinz, *Science*, **282**, 1660 (1998).
15. T. Dietl, H. Olmo, *MRS Bull*., **28**, 714 (2003).
16. S. K. Kamilla, S. Basil, *Bull. Mater. Sci.*, **25**, 54 (2002).
17. S. Parkin, X. Jiang, C. Kaiser, A. Panchula, K. Roche, M. Sainant, *Proe. IEEE*, **91**, 661 (2003).
18. J. M. Kikkawa, D. D. Awschalom, *Nature*, **397**, 139 (1999).
19. I. Zutic, J. Fabian, S. Das Sarnia, *Phys. Rev. B*, **64**, 121201 (2001).
20. Y. S. Didosyan, H. Hauser, G. A. Reider, W. Toriser, *J. Appl. Phys*., **95**, 7339 (2004).
21. B. Wang, S. Nagase, J. Zhao, G. Wang, *J. Phys. Cheni. C*, **111**, 4956 (2007).
22. X. G. Xu, H. L. Yang, Y. Wu, D. L. Zhang, S. Z. Wu, J. Miao, Y. Jiang, X. B.Qin, X. Z. Gao, B. Y. Wang, *Appl. Phys. Lett*, **97**, 232502 (2010).

23. Hui. Chen, X, Zhang, Q. Zhang, X. Hou, Q. Zhou, J. Yan, W. Tan, *J. Luminescence*, **131**,947 (2011).
24. K. Tang, S. Gu, S. Zhu, W. Liu, J. Ye, J. Zhu, R. Zhang, Y. Zheng, X. Sun, *Appl. Phys. Lett.*, **93**, 132107 (2008).
25. A. Henglein, In Topics in Current Chemistry; Steckhan, *E., Ed.; Springer-Verlag: Berlin,* **143**, 113 (1988).
26. A. D. Yoffe, *Adv. Phys.,* **42**, 173 (1993).
27. M. Nirmal, D. J. Norris, M. Kuno, M. G. Bawendi, A. L. Efros, M. Rosen, *Phys. Rev. Lett.*, **75**, 3728 (1995).
28. A. P. Alivisatos, *J. Phys. Chem*., **100**, 13226 (1996).
29. S. Gorer, G. Hodes, In Semiconductor Nanoclusters; Kamat, P.V., Meisel, *D., Eds.; Elsevier Science, B. V. Amsterdam,* (1996).
30. S. Desgreniers, *Phys. Rev. B,* **58**, 14102 (1998).
31. J. M. Recio, M. A. Blanco, V. Luana, R. Pandey, L. Gerward, Staun Olsen, *J. Phys. Rev. B,* **58**, 8949 (1998).
32. C. Y. Yeh, Z. W. Lu, S. Froyen, A. Zunger, *Phys. Rev. B*, **45**, 12130 (1992).
33. V. A. Federov, V. A. Ganshin, Y. N. Korkishko, *Mater. Res. Bull*., **28**, 59 (1993).
34. J. O. Joswig, M. Springborg, G. Seifert, *J. Phys. Chem. B*, **104**, 2617 (2000).
35. L.E. Brus, *J. Chem. Phys.*, **79**, 5566 (1983).
36. L. E. Brus, *J. Chem. Phys*., **80**, 4403 (1984).
37. H. M. Schmidt, H. Weller, *Chem. Phys. Lett.*, **129**, 615 (1986).
38. A.I. Ekimov, A. L. Efros, M.G. Ivanov, A. A. Onushchenko, S. K. Shumilov, *Solid State Commun*., **69**, 565 (1989).
39. G. T. Einevoll, *Phys. Rev. B***, 45**, 3410 (1992).
40. P. E. Lippens, M. Lannoo, *Phys. Rev. B*, **39**, 10935 (1989).
41. M. V. Rama Krishna, R. A. Friesner, *J. Chem. Phys*., **95**, 8309 (1991).
42. N. A. Hill, K. B. Whaley, *J. Chem. Phys*., **100**, 2831 (1994).
43. A. Tomasulo, M.V. Ramakrishna, *J. Chem. Phys*., **105**, 3612 (1996).
44. L.W. Wang, A. Zunger, *Phys. Rev. B*, **53**, 9579 (1996).
45. A. Mizel, M. L. Cohen, *Phys. Rev. B*, **56**, 6737 (1997).
46. S.Y. Ren, S.F. Ren, *J. Phys. Chem. Solids*, **59**. 1327 (1998).
47. L. W. Wang, A. Zunger, J. *Phys. Chem. B*, **102**, 6449 (1998).
48. K. Leung, S. Pokrant, K. B. Whaley, *Phys. Rev. B*, **57**, 12291 (1998).

49. E. Rabani, B. Hetenyi, B. J. Berne, L. E .Brus, *J. Chem. Phys.*, **110**, 5355 (1999).
50. J. Perez-Conde, A. K. Bhattacharjee, *Solid State Commun*., **110**, 259 (1999).
51. A. Franceschetti, H. Fu, L. W. Wang, A. Zunger, *Phys. Rev. B*, **60**, 1819 (1999).
52. S. Pokrant, K.B. Whaley, *Eur. Phys. J. D*, **6**, 255 (1999).
53. K. Leung, K. B. Whaley, *J. Chem. Phys.*, **110**, 11012 (1999).
54. K. Eichkorn, R. Ahlrichs, *Chem. Phys. Lett.*, **288**, 235 (1998).
55. P. Deglmann, R. Ahlrichs, K. Tsereteli, *J. Chem. Phys.*, **116**,1585 (2002).
56. M.C. Troparevsky, J. R. Chelikowsky, *J. Chem. Phys.*, **114**, 943 (2001).
57. M. C. Troparevsky, L. Kronik, J.R. Chelikowsky, *Phys. Rev. B*, **65**, 033311 (2001).
58. A. P. Alivisatos, *Science*, **271**, 933 (1996).
59. T. Vossmeyer, L. Katsikas, M. Giersig, I. G. Popovic, K. Diesner, A. Chemseddine, A. Eychmuller, H. Weller, *J. Phys. Chem.*, **98**, 7665 (1994).
60. S. H. Tolbert, P. A. Alivisatos, Annu. *Rev. Phys. Chem*., **46**, 595 (1995).
61. A. Hanafusa, T. Aramoto, M. Tsuji, T. Yamamoto, T. Nishio, P. Veluchamy, H. Higuchi, S. Kumazawa, S. Shibutani, J. Nakajima, T. Arita, H. Ohyama, T. Hibino, K. Omura, Solar Energy Mater. *Solar Cells*, **67**, 21 (2001).
62. J. R. Lakowicz, I. Gryczynski, Z. Gryczynski, K. Nowaczyk, C. Murphy, *J. Anal. Biochem.*, **280**, 128 (2000).
63. L. Manna, E. C. Scher, L.S. Li, P. A. Alivisatos, *J. Am. Chem. Soc.*, **14**, 7136 (2002).
64. Y. T. Chen, J.B. Ding, Y. Guo, L. B. Kong, H. L. Li, *Mater. Chem. Phys*., **77**, 734 (2002).
65. T. Ni, D. K. Nagesha, J. Robles, N. F. Materer, S. Mussig, N. A. Kotov, *J. Am. Chem. Soc.*, **124**, 3980 (2002).
66. N. Sugimoto, A. Koiwai, S. Hyodo, T. Hioki, S. Noda, *Appl. Phys. Lett*., **66**, 923 (1995).
67. Y. P. Rakovich, M. V. Artemyev, A. G. Rolo, M. I. Vasilevsky, M. J. M. Gomes, *Phys. Stat. Solidi. B*, **224**, 319 (2001).
68. D. G. Fu, M. Li, X. Wang, J. Q. Cheng, Y. Zhang, Z. H. Lu, J. Z. Liu, J. Z. *Supramolecular Science*, **5**, 495(1998).
69. D. G. Fu, Y. Zhang, J. Z. Liu, Z. H. Lu, *Mater. Lett*., **51**, 183 (2001).

70. D.G. Fu, Y. Zhang, J. Z. Liu, Z. Lu, *Mater. Chem. Phys.*, **77**, 285 (2002).
71. S. G. Raptis, M. G. Papadopoulos, A. J Sadlej, *J. Chem. Phys.*, **111**, 7904 (1999).
72. J. O. Joswig, M. Springborg, G. Seiffert, *J. Phys. Chem. B*, **104**, 2617 (2000).
73. M. C Troparevsky, J. R. Chelikowsky, *J. Chem. Phys.*, **114**, 943 (2001).
74. B. G. Streetman, B. Sanjay, Solid state electronic devices, 5thedn. Prentice Hall, *Upper Saddle River*, (2000).
75. Y. Fu, M. Willander, E. L. Sivchenko, *Superlatt Microstruct*, **27**, 255 (2000).
76. M. Hirasawa, N. Ichikawa, Y. Egashira, I. Honma, H. Komiyama, *Appl. Phys. Lett.*, **67**, 3483 (1995).
77. M. A. Malik, P.O. Brien, S. Norager, J. Smith, *J. Mater Chem*.,**13**, 2591 (2003).
78. R. A. Ganeev, A. I. Ryasnyanskiy, T. Usmanov, *Opt Commun*., **272**, 242 (2007).
79. M. Tews, D. Pfannkuche, *Phys. Rev. B*, **65**, 073307 (2000).
80. W. Sheng, J. P. Leburton, *Phys. Rev. Lett.*, **88**, 167401 (2002).
81. W. Sheng, J. P. Leburton, *Phys. Rev. B*, **64**, 153302 (2001).
82. P. Zhang, X. G. Zhao, J Phys. *Condens Matt.*, **13,** 8389 (2001).
83. K. Chang, J. B. Xia, *J. Appl. Phys*., **84**, 1454 (1998).
84. D. D. Nolte, *J. Appl. Phys*., **95**, 6259 (1999).
85. S. A. Wolf, D. D. Awschalom, R. A. Buhrman, J. M. Daughton, S. von Molnár, M. L. Roukes, A. Y. Chtchelkanova, D. M. Treger, *Science*, **294**, 1488 (2001).
86. H. Ohno, A. Shen, F. Matsukura, A. Oiwa, A. Endo, S. Katsumoto, Y. Iye, *Appl. Phys. Lett.*, **69**, 363 (1996).
87. W. Chen, J. Z. Zhang, A. G. Joly, *J. Nanosci. Nanotechnol*., **4**, 919 (2004).
88. X. Michalet, F. F. Pinaud, L. A. Bentolila, J. M. Tsay, S. Doose, J. J. Li, G. Sundaresan, A. M. Wu, S. S. Gambhir, and S. Weiss, *Science*, **2007**, 538 (2005).
89. T. Calarco, A. Datta, P. Fedichev, E. Pazy, and P. Zoller, *Phys. Rev. B*, **68**, 012310 (2003).
90. R. D. Schaller, V. I. Klimov, *Phys. Rev. Lett.*, **96**, 097402 (2006).
91. G. L. Gutsev, R. H. O. Neal, B. C. Saha, M. D. Mochena, E. Johnson, C. W. Bauschlicher, *J. Phys. Chem. A*, **112**, 10728 (2008).
92. G. W. Lemire, G. A. Bishea, S. A. Heidecke, M. D. Morse, *J. Chem. Phys*., **92**, 121 (1990).
93. T. R. Taylor, H. Gómez, K. R. Asmis, D. M. Neumark, *J. Chem. Phys*., **115**, 4620 (2001).

94. J. Wang, L. Ma, J. Zhao, G. Wang, X. Chen, and R. B. King, *J. Chem. Phys*., **129**, 044908 (2008).
95. Y. Masumoto, M. Matsuura, S. Tarucha, H. Okamoto, *Phys. Rev. B*, **32**, 4275 (1985).
96. M. A. Olshavsky, A. N. Goldstein, A. P. Alivisatos, *J. Am. Chem. Soc.*, **112**, 9438 (1990).
97. L. Butler, G. Redmond, D. Fitzmaurice, *J. Phys. Chem.*, **97**, 10750 (1993).
98. Y. Sun, J. A. Rogers, *Nano Lett.*, **4**, 1953 (2004).
99. A. D. Berry, R. J. Tonucci, M. Fatemi, *Appl. Phys. Lett*., **69**, 2846 (1996).
100. X. Duan , J. L.Wang, C. M. Lieber, *Appl. Phys. Lett.*, **76**, 1116 (2000).
101. X. Duan, C. M. Lieber, *Adv. Mater*, **12**, 298 (2000).
102. W. Shi, Y. Zheng, N. Wang, C. S.Lee, S. T. Lee, *Adv. Mater*, **13**, 591 (2001).
103. H. W. Kioto, J. R. Heath, S. C. O. Brien, R. F. Curl, R. E. Smalley, *Nature*, **318**, 162 (1985).
104. H. I. Li, *et al. Phys. Rev. Lett.*, **103**, 056101 (2009).
105. F. Lopez-Urias, *et al., J. Mater. Chern.*, **18**, 1535 (2008).
106. B. Elliot, K. Yang, A. M. Rao, H. P. Annan, *Chern. Comm.*, **20**, 2083 (2007).
107. D. S. Bethune, R. D. Johnson, J. R. Salem, M. S. de Vries, C. S. Yannoni, *Nature*, **366**, 123 (1993).
108. R. Valencia, A. Rodriguez-Fortea, J. M. Poblet, *Chern. Cornrnun*, 4161 (2007).
109. J. Lu, R. Sabirianov, W. N. Mei, Yi Gao, C-G. Duan, X. Zeng, *J. Phys. Chern. B*, **110**, 23637 (2006).
110. H. Shinohara, *Rep. Prog. Phys*., **63**, 843 (2000).
111. H. W. Kioto, *Nature*, **329**, 529 (1987).
112. G. Von Helden, N. G. Gotts, M. T. Bowers, *Nature*, **363**, 6025 (1993).
113. C. Piskoti, J. Yatger, A. Zettl, *Nature*, **393**, 771 (1998).
114. H. Prinzbach, A. Weller, P. Landenberger, F. Wahl, J. Worth, L. T. Scott, M. Golmont, D. Olevano, B.V. Issendorff, *Nature*, **407**, 60 (2000).
115. T. Gau, M. D. Diener, Yan Char, M. J. Alford, R. E. Haulier, S. M. McClure, T. Olmo, J. H. Weaver, G. E. Scuseria and R. E. Smalley, *Science*, **257**, 1661 (1992).
116. T. Gau, R. E. Smalley, G. E. Scuseria, *J. hein. Phys*., **99 (1),** 352 (1993).
117. L. Sun, Y. Chang, B. Hong, R. Yang, *Int. J. Quant. Chem.*, **107**, 1241 (2007).

118. Y. M. Chen, J. Shi, L. Rui, Q. X. Guo, *J. Mol. Struct.: Theoeheni*, **907**, 104 (2009).
119. H. S. Kang, *J. Phys. Cheni. A*, **110,** 4780 (2006).
120. R. Robles, S. N. Klianna, A. W. Castleman, *J. Phys. Rev. B*, **77,** 235441 (2008).
121. C. Xiao, F. Hagelberg, *J. Mol. Struct: THEOCHEM*, **529**, 241 (2000).
122. T. P. Martin, H. Scliaber, *J. Chern. Phys.*, **83**, 855 (1985).
123. W. Schulze, B. Winter, I. Goldenfeld, *J. Chern. Phys.*, **87**, 2402 (1987).
124. A. A. Shvartsburg, B. Liu, Z.Y. Lu, C.Z Wang, M. F. Jarrold, K. M. Ho, *Phy. Rev.Lett.*, **83**, 2167 (1999).
125. F. C. Chuang, Y. Y. Hsieli, C. Hsu and M. A. Albao, *J. Chern. Phys.*, **127**, 144313 (2007).
126. S. Choi, S. C. Hong., S. Cho., *Appl. Phys. Lett.*, **81**, 3606 (2002).
127. Li Ma, J. Zhao, J. Wang, B. Wang, Q. Lu, G. *Wang, Phys. Rev. B*, **73**,125439 (2006).
128. S. Itaya, Y. Yamamoto, H. Hori, *J. Superconductivity: Incorporating Novel Magnetism*, **18**, 83 (2005).
129. K. Kaya, H. Kawamata , Y. Negishi, T. Hayase, R. Kislii, A. Nakajima, *J. Phys. D*, **40**, 5 (1997).
130. J. L. Wang, G. H. Wang, J. J. Zhao, *Phys. Rev. B*, **64,** 205411 (2001).
131. J. G. Han, Z. Y. Ren, Y. W. Zhang, *Chern. Phys*., **305**, 253 (2004).
132. B. X. Li, R L. Cao, *Phys. Rev. B*, **62**, 15788 (2000).
133. J. Wang, J. G. Han, *Chern. Phys*., **342**, 253 (2007).
134. J. Wang, J. G. Han, *J. Chern. Phys*., **123**, 244303 (2005).
135. W.J. Zhao, Z. Yang, Y. L. Yan. X. L. Lei. G. X. Go, Q. L. Wang and Y. Luo, *Acta Phys. Sin.*, **56**, 2596 (2007).
136. W. J. Zhao, Y. X. Yang, *Chern. Phys*., **352**, 291 (2008).
137. J. Wang, J. G. Han, *J. Phys. Chern*., **4110**, 12670 (2006).
138. W. J. Zhao, X. Y. Wang, *J. Mol. Struct., Theochem*, **901**, 18 (2009).
139. X. L. Hou, G. Gopakumar, P. Lievens, M. T. Nguyen, *J. Phys. Chern. A*, **111**, 13544 (2007).
140. J. Goldberger, R. He, Y. Zhang, S. Lee, H. Yan, H. J. Choi, P. Yang, *Nature*, **422**, 599 (2003).
141. S. M. Lee, Y. H. Lee, Y. G. Hwang, C. J. Lee, *J. Korean Phys. Soc*., **34**, S253

(1999).

142. S. Nakamura, M. Senoh, N. Iwasa, S. Nagahama, *Appl. Phys. Lett.*, **67**, 1868 (1995).
143. G. Simin, M. S. Shur, R. Gaska, *Int. J. High Speed Electron. Syst.*, **19**, 7 (2009).
144. R. Stevenson, The World's Best Gallium Nitride. IEEE Spectrum, 40 (2010).
145. J. Nord, K. Albe, P. Erhart, K. Nordlund, *J. Phys. Condens. Matter*, **15**, 5649 (2003).
146. J. Fritsch, O. F. Sankey, K. E. Schmidt, J. B. Page, *Phys. Rev. B*, **57**, 15360 (1998).
147. K. Karch, J. M. Wagner, F. Bechstedt, *Phys. Rev. B*, **57**, 7043 (1998).
148. A. Costales, R. Pandey, *J. Phys. Chem. A,* **107**, 191 (2003).
149. B. Song, C. H. Yao, P. Cao, *Phys. Rev. B*, **74**, 035306 (2006).
150. B. Song, P. L.Cao, *Phys. Lett. A*, **328**, 364 (2004).
151. J. Zhao, B. Wang, X. Zhou, X. Chen, W. Lu, *Chem. Phys. Lett.*, **422**, 170 (2006).
152. J. H. Edgar, Properties of Group III Nitrides; INSPEC, The Institution of Electrical Engineers: London, (1994).
153. C. Bungaro, K. Rapcewicz, J. Bernholc, *Phys. Rev. B*, **61**, 6720 (2000).
154. W. M. Sun, Y. Li, D. Wu, Z. R. Li , Phys. Chem. Phys. Chem., 14, 16467 (2012).
155. C. N. Van Dijk, T. Rasing, A. Kirilyuk, J. Bowlan, A. Liang, W. A. Heer, *J. App. Phys.*, **107**, 09B526 (2010).
156. Bhattacharya, T. T. Nguyen, J. D. Haeck , K. Hansen , P. Lievens, E. Janssens, *Phys. Rev. B*, **87**, 054103 (2013).
157. B. X. Zheng, D. Dong, L. Wang, J. X.Yang, *J. Phys. Chem.*, **118**, 4005 (2014).
158. K. Takahashi, S. Isobe, S. Ohnuki, *Chem. Phys. Lett.*, **555**, 26 (2013).
159. M. Chen, D. A. Dixon, *J. Phys. Chem. A*, **117**, 3676 (2013).
160. G. L. Zhang, H. K.Yuan , H. Chen, A. L. Kunag, C. L. Tian , J. Z. Wang, *J. Phy. Chem. A,* **118**, 1936 (2014).
161. V. E. Kaydashev, E. Janssens, P. Lievens, *J. Chem. Phys.*, **142**, 034310 (2015).
162. H. F. Li, H. Q. Wang, *Phys. Chem. Chem. Phys.*, **16,** 244 (2014).
163. D. Die, X. Y. Kuang, J. J. Guo, B. X. Zheng, *Physica A*, **389**, 5216 (2010).
164. S. Sahoo, A. Hucht, M. E. Gruner, G. Rollmann , P. Entel, *Phys Rev B*, **82**, 054418 (2010).
165. Y. Gao, X. Dai, S. Kang, C. A. J. Cruz, M. Xin, Y. Meng, J. Han, Z. Wang, R.

Zhou, *Scinetific Report*, **4**, 5862 (2014).

166. Y. Negishi, H. Kawamata, F. Hayakawa, A. Nakajima, Kaya, *Chem. Phys. Lett*., **294**, 370 (1998).
167. J. Atobe, K. Koyasu, S. Furusea, A. Nakajima, *Phys. Chem. Chem. Phys*., **14**, 9403 (2012).
168. V. T. Ngan, P. Gruene, P. Claes, E. Janssens, A. Fielicke, M. T. Nguyen, P. Lievens *J. Am. Chem. Soc*., **132**, 15589 (2010).
169. P. Claes, E. Janssens, V. T. Ngan, P. Gruene, J. T. Lyon , D. J. Harding, A. Fielicke, M. T. Nguyen , P. Lievens , *Phys. Rev. Lett.*, **107**, 173401 (2011).
170. D. Bandopadhyay, P. Sen, *J. Phys. Chem. A*, **114**, 1835 (2010).
171. M. Kumar, B. J. Singh, S. Kajjam , D. Bandopadhyay, *J. Comp. Theo. Nanoscience*, **7**, 296 (2010).
172. D. Bandopadhyay, *J. Mol. Model.*, **18**, 3887 (2012).
173. S. M. Beck, J. Chem. Phys., 87, 4233 (1987).
174. J. Atobe, K. Koyasu, S. Furuseand, A. Nakajima, *Phys. Chem. Chem. Phys.*, **14**, 9403 (2012).
175. K. Mondal, T. K. Ghanty, A. Banerjee, A. Chakarabarti, C. Kamal, *Mol. Phys.*, **111**, 725 (2013).
176. J. Wang, Y. Liu, Y. C. Li, *Phys. Lett. A*, **374**, 2736 (2010).
177. Y. Cao, V. D. Linde, R. F. Hockendrof, M. K. Beyer, *J. Chem. Phys*., **132**, 224307 (2010).
178. K. Dhaka, D. Bandopadhyay, *RSC Adv.*, **20**, 83004 (2015).
179. W. Ma, F. Chen, *J. Mol. Model*., **19**, 4555 (2013).
180. C. S. Lin, W. D. Cheng, J. Y.Wang, R. Q. Zhang , *Chem. Phys. Lett*., **509**, 124 (2011).
181. R. N. Zhao, J. G. Han, J. T. Bai, F. Y. Liu, L. S. Sheng, *Chem. Phys*., **372**, 89 (2010).
182. Y. Li, J. T. Lyon, A. P. Woodham, P. Lievens, A. Fielicke, E. Janssens, *J. Phys. Chem. C*, **119**, 10896 (2014).
183. N. Kapila, I.Garg, V. Jinal, H. Sharma, *J. Magne Mag. Materials*, **324**, 2885 (2012).
184. K. Dhaka, R. Trivedi, D. Bandyopadhyay, *J. Mol. Model*., **19**, 1473 (2012).
185. M. Kumar, N. Bhattacharya, D. Bandyopadhyay, *J. Mol. Model.*, **18**, 405 (2012).

186. J. D. Haeck , T. B.Tai , S. Bhattacharya , H. T. Le, E. Janssens, M. T.Nguyen, P. Lievens, *Phys. Chem. Chem. Phys.*, **15,** 5151 (2013).
187. X. Li, K. Su, X. Yang, L. Song, L.Yang, *Computaional and theoretical Chemistrt.*, **1010**, 32 (2013).
188. X. J. Deng, X. Y. Kong, H. G. Xu, X. L. Xu , G. Feng, W. J. Zheng, *J. Phys. Chem. C*, **119,** 11048 (2015).
189. X. J. Deng, X. Y. Kong , H. G. Xu , X. L. Xu, G. Feng, W. J. Zheng, *Phys. Chem. Chem. Phys.*, **15**, 3987 (2014).
190. R. Trivedi, K. Dhaka, D. Bandopadhyay, *RSC Adv*, **4**, 64825 (2014).
191. M. B. Torres, E. M. Fernandez, L. C. Balbas, **111**, 444 (2011).
192. V. Chouhan, V. M. Medel, J. U. Reveles, S. N. Khanna, *Chem. Phys. Lett.*, **528**, 39 (2012).
193. A. Lebon, A. Aguado, A. Vega, *J. Phys. Chem. C*, **119**, 27838 (2015).
194. X. Zhang, Y. Wang, H. Wang, A. Lim, G. Gantefoer, K. H. Bowen, J. U. Reveles, S. N. Khanna , *J. Amer. Chem. Soc*., **135**, 4856 (2013).
195. J. U. Reveles, T. Baruah, R. R. Zope, *J. Phys. Chem*., **119**, 5129 (2015).
196. M. Zhang, J. Zhang, X. Feng, H. Zhang, L. Zhao, X. Luo, W. Cao, *J. Phys. Chem. A*, **117**, 13025 (2013).
197. O. L. Acevedo, P. A. Clayborne, H. Hakkinen, *Phys. Rev. B*, **84**, 035434 (2011).
198. A. Varano, D. J. Henry, *J. Phys. Chem. A*, **114**, 3602 (2010).
199. I. Pino, G. J. Kroes, M. C. Hemert, *J. Chem. Phys*., **133**, 184304 (2010).
200. X. J. Kuang, X.Q. Wang, G. B. Liu, *J. Chem. Sci*., **123,** 743 (2011).
201. S. Giri, A. Charaborty, P. K. Chattaraj, *J. Mol. Model*. **17**, 777 (2011).
202. R. Jin, S. Zhang, Y. Zhang, S. Huang, P. Wang, H. Tian, *Int. J. Hydrogen Energy*, **36**, 9069 (2011).
203. K. Srinivasu, S. K. Ghosh , R. Das, S. Giri, P. K. Chattaraj, *RSC Adv*., **2**, 2914 (2012).
204. M. Chen, X. B. Yang, J. Cui, J. J. Tang, L. Y. Gan, M. Zhu, Y.J. Zhao, *Int. J. Hydrogen Energy*, **37**, 309 (2012).
205. K. Fanjie, H. Yanfei, *J. Mol. Model*., **20**, 2087 (2012).
206. J. Guo, *J. Phys. Chem*., **117**, 3458 (2013).
207. M. Mananghaya, *Int. J. Hydrogen Energy*, **40**, 9352 (2015).

CHAPTER 2

METHODOLOGY

2.1. Quantum mechanical calculations of atomics orbitals

The science has been put to discover new characteristics in a known material or to explore a novel matter exhibiting unique characteristics that may be dedicated to the service of the living world. A material consists of molecules; latter comprises of atoms; atoms are constituted from electrons, protons and neutrons; latest concepts have evolved from fathoms of quark theory, field theory etc. Although the energy of the system depends on configuration of its constituents broadly, specific properties may largely be attributed to electronic structure. Trajectory of atoms and its constituents can be practically calculated using classical mechanics; atomic systems are best explained by quantum mechanics. Though former aims at deducing trajectory of a particle under study, latter does so by searching not a proper motion but probabilistic distribution function. Although earlier works of Born, Hartee, Pauli, Dirac etc. assisted in earliest development of the subject, the contribution of Schrodinger laid the foundation of the mechanics of atomic world which essentially evolved into current state of science.[1] Modern day science is obliged to Schrodinger because of his marked contribution of wave equation:[2]

$$H\psi = E\psi \qquad (2.1)$$

here, H is Hamiltonian operator of the system-consisting of kinetic energy and potential energy term, E is eigen value representing energy and ψ denotes eigen function. ψ is well behaved mathematical function such that $\psi^*\psi$ represents probability density.[3] This equation is easily solved for atoms like hydrogen,

depending on the property of interest, with little or no approximation. Although this equation is quite simple and is able to fully describe most complex systems correctly, the actual problem lies in solving it for a given system. In fact, it is the beauty of this equation that almost any molecular system can be fully explained by solving it and yet, the basic problem lies in choosing appropriate method of solving it. The eigen values give energy of the system while eigen function leads to probability distribution of constituents viz electron, nucleus etc. The wave function may further be split into electron and nuclear wave function. The Hamiltonian can be written as:

$$H = -\sum_i \frac{\hbar^2}{2m_e}\nabla^2 - \sum_A \frac{\hbar^2}{2m_A}\nabla^2 - \sum_i \sum_A \frac{Z_A e^2}{r_{iA}} + \sum_{i<j} \frac{e^2}{r_{ij}} + \sum_{A<B} \frac{Z_A Z_B e^2}{r_{AB}} \qquad (2.2)$$

where *i*, *j* show summation over electron while *A*, *B* represent nucleus. First and second terms stand for kinetic energy of electrons and nuclei, third term stands for electron-nucleus potential energy, while fourth and fifth terms represent inter electron and inter-nucleon interaction energy. Born-Oppenheimer understood that electrons make instantaneous changes with any change in nucleus; subsequent to this, Schrödinger's equation was solved by variable separable method, to get a resolved form of differential equations solvable for electronic wave function only for a given arrangement of nucleus.[4-6]

To achieve the total energy of a new configuration subject to given atomic conditions, it is necessary to add the nuclear potential energy term to electronic energy. In case of atoms, any variation in nuclear position is easy to deal with. However, same calculations are quite complicated even for simplest molecules. Evidently, Hamiltonian includes (a) kinetic energy, and (b) potential energy term which is, sub divided into (i) nucleus-nucleus interaction (ignored due to Born-Oppenheimer approximation), (ii) electron-nucleus potential energy and (iii) inter-electron

interaction energy. It is this last term that creates complexity. Hamiltonian due to electrons only may be expanded as:

$$H_e = -\sum_i \frac{1}{2}\nabla_i^2 - \sum_A \sum_i \frac{Z_A}{r_{iA}} + \sum_{i<j} \frac{1}{r_{ij}} \tag{2.3}$$

here, first term represents the kinetic energy, second term is nucleus-electron potential energy and last term means electron -electron interaction energy. With this H_e at hand, one gets E_e and ψ_e as:[7]

$$H_e(1,2,...,n)\psi_e(1,2,...,n) = E_e\psi_e(1,2,...,n) \tag{2.4}$$

It is obvious that this provides merely electronic part but not the nuclear part. The result obtained by this electronic equation is used to find total energy and total wave functions of given system. Nuclear interaction is not supposed to play any valuable role in atomic wave function but produces valuable information in molecular wave functions (commonly called as molecular orbitals).

Multi-electron systems can be solved with methods of approximation only and many workers have proposed several ways to solve it. D. R. Hartree assumed the total wave function in 1928 as the product of the electrons' wave function (assuming Z. electron molecule).[8]

$$\psi_e(r_1,\theta_1,\phi_1;r_2,\theta_2,\phi_2;...;r_z,\theta_z,\phi_z) = \psi_1(r_1,\theta_1,\phi_1)\psi_2(r_2,\theta_2,\phi_2)...\psi_z(r_z,\theta_z,\phi_z) \tag{2.5}$$

As Schrödinger's equation includes potential energy operator which if known will provide wave functions and eigen values. But the potential energy for such a system is not fully known. Apart from this, wave function should take coordinates of all Z-electrons. Variable separable method would guarantee Z-independent linear differential equations from a single Schrodinger's equation for Z-electron atom (ignoring electron-electron potential term), which may be resolved into Z-independent

single electron equation. Starting with approximation trial solutions and solving for field iteratively, one gets self-consistent field (SCF) solutions. These equations are solved numerically. Alternatively, variational principle may be used to get desired solutions. However application of such trial wave functions was soon neglected because such total wave function was not anti-symmetric- a condition imposed by Pauli's exclusion principle. After Fermi-Dirac statistics,[9] electrons are supposed to be defined by spatial as well spin functions:

$$\Psi_{tot} = \psi(\vec{r}) \times \xi(\vec{s}) \tag{2.6}$$

here $\psi(\vec{r})$ is spatial wave function while $\xi(\vec{s})$ is spin wave function (commonly represented by α or β).[10] Slater proposed a method for obtaining such total electron wave functions (anti-symmetric) [11] from spatial and spin coordinates with the help of so-called Slater determinant:[12]

$$\psi = \frac{1}{\sqrt{N!}} \begin{vmatrix} \phi_1(r_1)\alpha(s_1) & \phi_2(r_1)\beta(s_1) & \dots & \dots & \dots & \phi_n(r_1)\beta(s_1) \\ \phi_1(r_2)\alpha(s_2) & \phi_2(r_2)\beta(s_2) & \dots & \dots & \dots & \phi_n(r_2)\beta(s_2) \\ \dots & \dots & \dots & & & \dots \\ \dots & \dots & & \dots & & \dots \\ \dots & \dots & & & \dots & \dots \\ \phi_1(r_n)\alpha(s_n) & \phi_2(r_n)\beta(s_n) & & & & \phi_n(r_n)\beta(s_n) \end{vmatrix} \tag{2.7}$$

Alternatively,

$$\psi = \frac{1}{\sqrt{N!}} \begin{vmatrix} \chi_1(1) & \chi_2(1) & \dots & \dots & \dots & \chi_N(1) \\ \chi_1(2) & \chi_2(2) & \dots & \dots & \dots & \chi_N(2) \\ \dots & \dots & \dots & & & \dots \\ \dots & \dots & & \dots & & \dots \\ \dots & \dots & & & \dots & \dots \\ \chi_1(N) & \chi_2(N) & & & & \chi_N(N) \end{vmatrix} \tag{2.8}$$

Using Slater's method, Hartree and Fock improvised the method of SCF theory, Here, each electron is assumed as moving in a fixed field arising due to nucleus and

remaining electrons. This method proved to be a great success as the electron-electron interaction term posed a severe hindrance in variable separable method. The energy of the atom or molecule is provided as:

$$E = \frac{\int \psi^* H \psi d\tau}{\int \psi^* \psi d\tau} \tag{2.9}$$

or, in Dirac Notation,[13-15]

$$E = \frac{\langle \psi \mid H \mid \psi \rangle}{\langle \psi \mid \psi \rangle} \tag{2.10}$$

Besides being anti-symmetric, the wave functions are supposed to be ortho-normal:

$$\int \psi_m^* \psi_n d\tau = \delta_{mn} \qquad \text{OR} \qquad \langle \psi_m \mid \psi_n \rangle = \delta_{mn} \tag{2.11}$$

2.2. Hartree Self-consistent field method

The electrons are lighter than the nuclei, so contribution of latter does not play an important role in atoms. However in the molecules, the structure of the atomic nucleus contributes the nuclear potential. Although Born-Oppenheimer helped solve this kind of problem, this field (being constant value for a given geometry) should be appropriately connected to obtain the total energy of the molecule and the total wave function.[16-17]

Hamiltonian can be rewritten for the N-electron system:

$$H_e = \sum_i h_i + \sum_i \sum_{j>i} g_{ij} + V_{nn} \tag{2.12}$$

where

$$h_i = -\frac{1}{2}\nabla^2 - \sum_A \frac{Z_A}{|R_A - r_i|} \tag{2.13}$$

and

$$g_{ij} = \frac{1}{|r_i - r_j|} \tag{2.14}$$

Note that one electron operator h_i describes the motion of the i[th] electron in the field of all nuclei of given molecule and must be the only operator in absence of any inter electronic or inter nuclear interaction, g_{ij} is two electron operator giving mutual repulsion between two electrons while V_{nn} is nuclear-nuclear interaction energy. From Dirac's notation for energy,

$$E = \sum_i \langle \chi_i \mid h_i \mid \chi_i \rangle + \frac{1}{2} \sum_{i,j} \left(\langle \chi_i \chi_i \mid g_{ij} \mid \chi_j \chi_j \rangle - \langle \chi_i \chi_j \mid g_{ij} \mid \chi_i \chi_j \rangle \right) + V_{nn} \tag{2.15}$$

Alternatively, it may be written as

$$E = \sum_i \langle \chi_i \mid h_i \mid \chi_i \rangle + \sum_{i<j} \left(J_{ij} - K_{ij} \right) + V_{nn} \tag{2.16}$$

here, first term shows energy due to core Hamiltonian operator in absence of any interaction, J_{ij} shows Coulomb operator (classically it is repulsion between two charge distributions), K_{ij} shows exchange operator (for which there is no classical analogue and is a result of Pauli's exclusion principle).[18]Thus, it is essentially a many body problem (unlike hydrogen atom, which is the problem of two bodies) there exists no exact solution to multi body system. Hence, one solution can only be better than another, variational principle is used to find the molecular orbital (MO) having minimum energy (stable configuration).Better wave function will give less energy than lesser corrected functions. Such type of optimization is gained subject to constraint that MOs should remains orthogonal and normalized. For this, the method

of undefined multipliers can be used.[16,19] Thus the problem is minimization of energy subject to orthonormality constraint:

$$S_{ij} = \int \chi_i \chi_j d\tau = \langle \chi_i \mid \chi_j \rangle = \delta_{ij} \tag{2.17}$$

The Lagrange function will now be stationary with respect to variations in orbitals:

$$L = E - \sum_{i,j} \lambda_{ij} \left(\langle \chi_i \mid \chi_j \rangle - \delta_{ij} \right) \tag{2.18}$$

For extremum of Lagrange function:

$$\delta L = \delta E - \delta \sum_{i,j} \lambda_{ij} \left(\langle \chi_i \mid \chi_j \rangle - \delta_{ij} \right) = 0 \tag{2.19}$$

here λ_{ij} is often identified as energy and related to molecular orbital energies. Under such formulation, one is now forced to find solution which takes into consideration motion of all electrons simultaneously, which in turn are so interconnected that change in one's coordinates (spatial or spin) is bound to affected others as well. To avoid such difficulty, one may consider motion of one electron under the influence of field of nuclei and other electrons in their fixed orbitals χ_j. The resulting equation may then be tidied up as follows:[16,20]

$$F_i \chi_i = \sum_j \varepsilon_{ij} \chi_j \tag{2.20}$$

where F_i is called Fock operator:

$$F_i(1) = h_i(1) + \sum_j \left(J_j(1) - K_j(1) \right) \tag{2.21}$$

Here 1 in parentheses denotes operator for one particular electron, J is Coulomb operator (electron repulsion term) and K is exchange operator (spin correlation

term). If Lagrangian multipliers are chosen zero unless indices i and j are same, one gets standard eigen value problem:

$$F_i \chi_i = \varepsilon_i \chi_i \tag{2.22}$$

It should be noted that solutions of above equations are not unique as determinant is unaffected by row/column transformations. Also, Fock operator is evaluable only if orbitals of remaining electrons are known. To counteract this vicious cycle, iterative method is employed which assumes trial solutions to get Fock operator (via Coulomb and Exchange operators) till solutions are 'self-consistent'. The Hartree Fock method is also known as mean field approximation method in which average electron-electron repulsion is taken into account.[21]

2.3. Roothaan Hall equation

Hartree's SCF procedure was improvised by Fock. Slater's determinantal wave functions were introduced (obeying Pauli's exclusion principle).The direct method of solution of Hartee Fock equation was not applied. HF equation was investigated by Roothaan and Hall separately in new form of matrix in line with expansion of MOs in terms of basis functions termed as atomic orbitals. Being advantageous, this method also helps in computability as well as in interpretability of result, which can be traced back to those of comprising atoms. In this scheme, the basis functions are expressed by spatial wave functions:

$$\phi_i = \sum c_{\mu i} \theta_\mu \tag{2.23}$$

In evaluation of coefficients $c_{\mu i}$ energy minimization techniques help fully well. Thus, we can get a set of shell consistent LCAO molecule orbital ϕ_i like that orbital will be

best for any particular set of basis functions. Roothaan Hall equation is obtained after variational technique:[22]

$$\sum_{\nu}\left(F_{\nu\mu}-\varepsilon_i S_{\nu\mu}\right)C_{\nu i}=0 \tag{2.24}$$

where $F_{\nu\mu}$ is the Fock operator and $S_{\nu\mu}$ is the overlap integral:

$$F_{\nu\mu}=\left\langle\theta_\nu\,|\,h\,|\,\theta_\mu\right\rangle+\sum_{\gamma}^{AO}\sum_{\delta}^{AO}D_{\gamma\delta}\left(\left\langle\theta_\nu\theta_\gamma\,|\,g\,|\,\theta_\mu\theta_\delta\right\rangle-\left\langle\theta_\nu\theta_\gamma\,|\,g\,|\,\theta_\delta\theta_\mu\right\rangle\right) \tag{2.25}$$

$$S_{\nu\mu}=\left\langle\theta_\nu\,|\,\theta_\mu\right\rangle \tag{2.26}$$

The density matrix is defined as:

$$D_{\gamma\delta}=\sum_{j}^{occ.MO}C_{\gamma j}C_{\delta j} \tag{2.27}$$

These equations were basically developed by Roothaan [22] and Hall [23] independently. Equations as mentioned above are a set of algebraic equations conveniently written in matrix equations:

$$FC=SCE \tag{2.28}$$

The Fock matrix and C matrix are square matrices, E is a diagonal matrix whose elements are the orbital energies. Here Fock matrix is dependent on orbital coefficients that are seen to be on both side of matrix equations and iterative procedure is adopted.[16]

Roothaan Hall equations may be generalised to solve by standard method:

$$F'C'=C'E \tag{2.29}$$

$$\text{where } F'=S^{-1/2}FS^{-1/2} \text{ and } C'=S^{1/2}C \tag{2.30}$$

Solution exists only if determinant $|F'-EI|$ is zero. For larger matrixes, the diagnalization of matrix F' is chosen. The eigen vectors of F' is given by matrix of coefficients C'.

2.4. Computational method for Roothaan Hall equation

Hartree Fock method is applied in solving Schodinger equation by setting up equation to solve all individual one electron wave functions:

$$F_i(1)\phi_i(1) = \varepsilon_i\phi_i(1) \tag{2.31}$$

where 1 within parenthesis represents one electron equation. With certain basis set at hand, overlap matrix S_{ij} and Fock matrix F_{ij} are evaluated by proper choice of trial functions. For calculating energy ε_i, coefficient $c_{\nu i}$, iteration is applied subject to expected convergence limits. The motion of electron is not assumed to be correlated in HF equations. The electron correlation is included through configuration interaction [25, 26] and Moller-Plesset [27] perturbation theory.

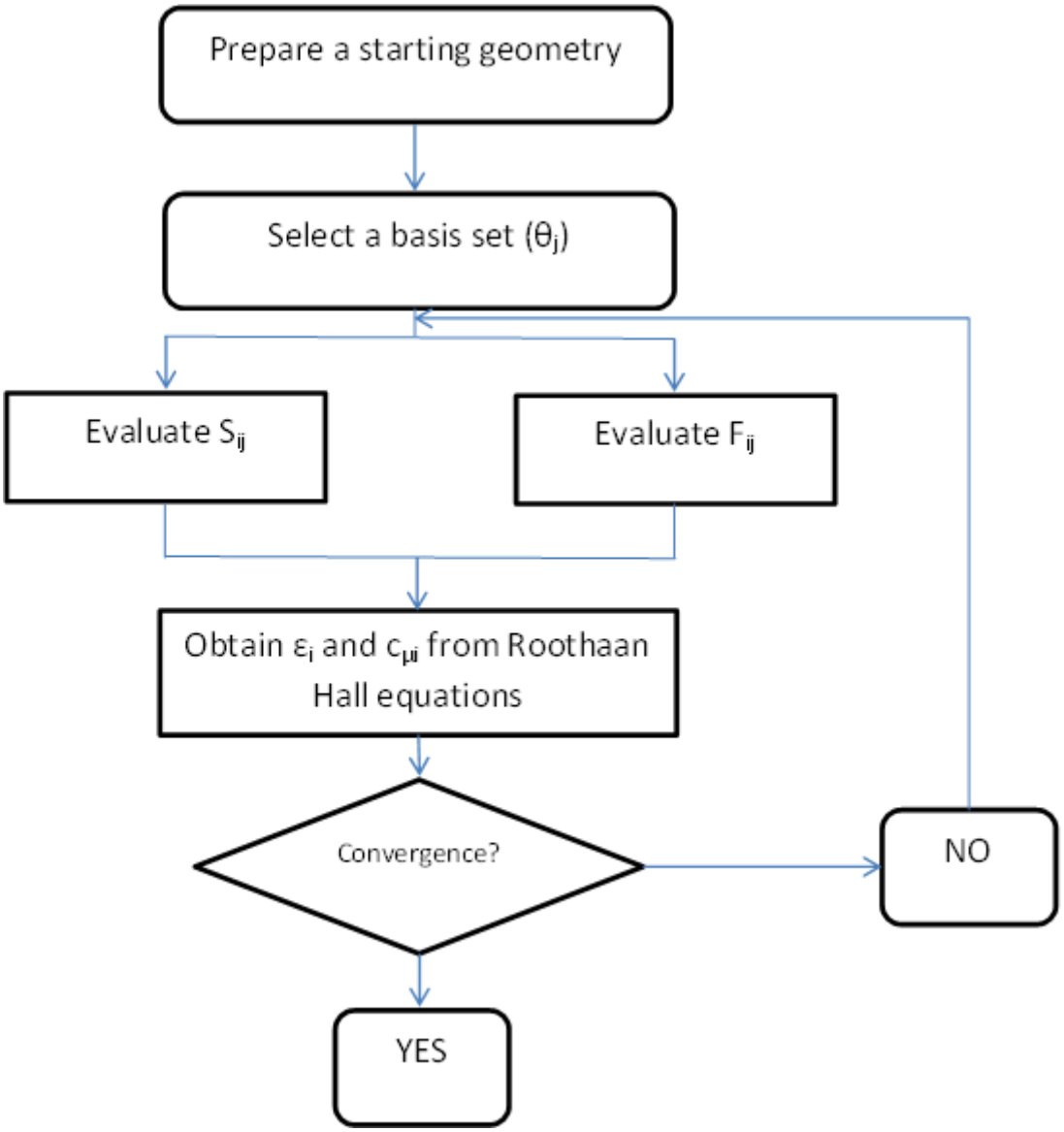

Figure 2.1: Algorithm for solving Roothaan Hall equation

2.5. Basis sets

Basis sets are used to describe the shape of orbitals in atoms or molecules. Ideally, a complete set must represent orbitals completely. Generally infinite number of basis functions is required for getting Hartree Fock energy close to that obtained by variational principle. As this is not feasible from computational viewpoint, the truncation error creeps in and is of unavoidable nature. Therefore it is considered to be necessary to choose a set of lesser number of basis functions(to reduce

computational costs) and to choose them cleverly (to minimize computational effort by getting simpler integrals) and giving least possible error simultaneously. Atomic functions are considered to be obvious choice for basis for functions. For diatomic molecules, atomic orbitals are chosen as basis functions centred on both atoms. Using theory of linear combination of atomic orbitals (LCAO),[28] each atomic orbital can be represented as a linear combination of one or more Slater type Orbitals (STOs).[29, 30] A set of virtual atomic orbitals may also be chosen besides all the occupied orbitals:

$$\phi_i = \sum_r c_{ri} \chi_r \tag{2.32}$$

The quality of molecular orbitals (MO) obtained is decided by number of active and virtual orbitals considered. This choice plays significant role in getting calculated energy converged to within the basis set limit. STOs are a general class of chosen basis set. The STO for s-type atomic orbitals has form:

$$S(r) = N_s e^{-\zeta r} \tag{2.33}$$

where r is radial distance from the nucleus, N_s is called normalization constant and constant ζ represents the orbital exponent governing the size of atomic orbital. Gaussian-type Orbital (GTO) is another popular choice of basis set which has following form for s-type atomic orbital:[16, 31]

$$g(r) = N_g e^{-\zeta r^2} \tag{2.34}$$

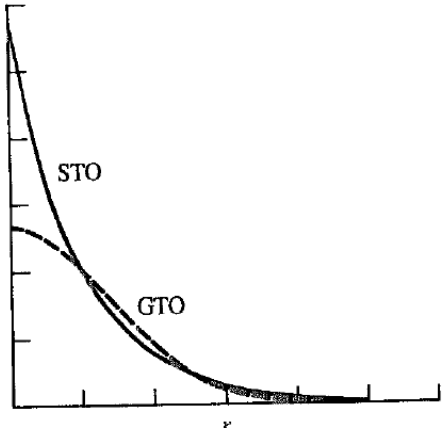

Figure 2.2:1s STO and best Gaussian equivalent.

For getting higher orbitals basis functions, STO or GTO is multiplied by appropriate exponents of coordinate to get p-type d-type or higher functions. In Cartesian coordinate system, general GTO possesses following form:

$$g(r) = N_g x^a y^b z^c e^{-\zeta r^2} \tag{2.35}$$

where, values of a, b and c are chosen suitably for expected orbital type. In the SCF calculation of molecule, atomic orbitals mix to form MOs.

A direct physical interpretation is obtained through STO basis set and hence it is considered to be good basis set for MOs. However, being computationally expensive, STOs are used in MO calculations. The corresponding integrals are simpler and tidy in GTO basis set, even though they are not accurate near and far from nucleus. The linear combination of Gaussian function is however sought to resolve this problem well. It is observed that Gaussian expansions contain two parameters: contraction coefficients and exponents. If both parameters vary, it is known to be uncontracted or primitive Gaussian. If these parameters are predetermined and remain constant and if number of terms in expansion are contracted, they are called contracted Gaussian functions.

For accommodating all filled orbitals in the shell, if the minimum number of the functions are employed such functions constitute a minimal basis set.[32] One basis function for every type of occupied orbital is used. It is observed that at least three Gaussian functions are capable of representing STO closely (Figure 2.3).So, STO-3G is the most popular basis set. The notation indicates that shape of STO is predicted by single contraction of 3 GTOs and gives absolute minima in MO calculations. Usually STO-nG (n=2-6) basis set uses n-Gaussian functions to represent each orbital. However, such minimal basis set is inadequate for systems containing atoms at the end of a period. Non-spherical electronic distribution can also not be described properly. This problem is resolved by using more than one function for each orbital. Increased number of basis functions also helps in getting closer to exact energy value, however computation cost rises.

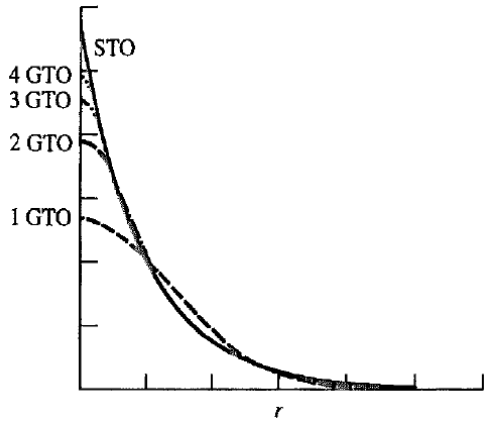

Figure 2.3: Comparison of 1s STO and Gaussian expansions with upto four terms

For more accurate results, number of basis functions employed for calculations exceeds the number of basis functions in minimal basis set. The Double Zeta (DZ)is a basis set that employs two basis functions of each type of minimal basis functions for the separated atoms, varying in their orbital exponents ζ. This type of basis set is capable of geometry optimization in DFT calculations.[33] The results of calculations

in double-ζ quality basis set were compared against experimental data and a benchmark established using hybrid DFT methods. In another approach, double number of functions are utilized to describe valence electrons but single function is used for inner shell and is commonly called slit valence double-ζ basis set. It is suitable for calculations in non isotropic charge distribution. For example, in 3-21G, three Gaussian functions describe the core orbitals while valence electrons are represented by three Gaussians: the contracted part is given by two Gaussians while the diffuse part is represented by one Gaussian. There are numerous other methods, e.g., triple-ζ, quadrupole-ζ etc. which are more complex in nature but may not necessarily ensure improvement in calculations.

In an isolated atom, charge is usually unperturbed than similar atoms in molecules. This distortion occurs due to mixing of different types of occupied or unoccupied orbitals. The polarization functions help in tackling such problem. They usually consist of higher angular momentum orbital. They are represented by '*' and provided flexibility to change in orbital shape. Highly diffuse functions are added into basis set for molecular systems that have electron density significantly far away from molecules. They have small exponents and are represented by '+'. They are called as augumented basis sets, presence of smaller exponents help deal with large spread of Gaussian functions. In DFT calculation, their inclusion changes the relative energies of various geometries.[34, 35]

The Pople basis set is popular for calculations involving organic molecules. It is denoted by 6-31G.[34, 36] The notation implies that six GTO primitives are contracted singly for core orbital and two contractions describe valence shells: one with three primitives, other with one primitive. Sometimes, it is also written as 6-31G* or 6-31G**. A single asterisk (*) indicates addition of d-primitives to atoms

other than hydrogen while two asterisks mean that a set of p-primitives has been added to hydrogen as well. One or two plus signs may be added (6-31+G* or 6-31++G*) which implies addition of diffuse functions in atomic orbitals. A single plus (+) sign indicates addition of diffuse functions to atoms other than hydrogen while two plus signs indicate diffuse function for all atoms.

Transition metals contain large number of electrons. Special basis sets have been developed for then. They include an effective core potential (ECP) for accounting all electrons.[37] Generally core electrons do not participate in bond formation, in a molecular system. Due to this an electric potential in Hamiltonian replaces such orbitals in the ECP treatment. Relativistic corrections help in improving energies. For iron, typical ECP containing basis sets are from Los Alamos type, viz. LACVP or LANL2DZ.[38]

In our work, basis set (B3LYP) has also been used that employs diffuse and polarization functions on cluster. Geometry optimization has been performed without any constraints. Optimized geometries were verified using frequency calculations. Kumar *et al.* have used two different basis sets, namely 6-31G on the cluster in a test calculation on total energy.[39] This resulted in very little changes in optimized geometries. Subsequently, electrical, optical and structural stability was investigated.

2.6. Density functional theory

Schrodinger equation provides a framework for study of systems at microscopic level. While pioneering works of Hartree (self-consistent field method),[40] Fock (electron as fermion),[41] Slater (determinant method for anti-symmetric electron wave function),[42] Dirac (local exchange),[43] Roothaan-Haall (basis functions for molecular orbitals) [22,23] and others have developed a well-tested mechanism for

evaluation of eigen functions which in turn culminate into near accurate physical properties (configuration energies, optical properties, spectral intensities etc.), these methods are limited by their expensive nature (computationally) and time consuming character. The earlier works of Thomas [44] and Fermi [45] (during early 1930s) revolved around explanation of given system by aid of charge densities. Their methods depended on electron number density to represent Coulomb functional energy and served as alternative to wavefunction method. However, it was Hohenberg, Kohn and Sham who provided this methodology a firm foundation. With Hohenberg-Kohn (HK) theorems [46] and Kohn-Sham (KS) formulation [47] for construction of exchange correlation potentials, the Density Functional Theory (DFT) grew enormously. Accurate density functionals were developed and they were easy to implement. This made the DFT approach to many body problems popular amongst researchers in the area of physics, chemistry and material sciences as any ground state observable could be expressed as density functional. A functional enables a function to be mapped to number:

$$Q[f(r)] = \int f(r)dr \tag{2.36}$$

HK theorems ensured one-to-one correspondence between exchange correlation functions and electron density. This helped study electronic structure of atoms, molecules and solids. Initially it was developed to study ground state properties and various physical or chemical processes. However, various researchers are enthusiastically developing theory for excited states as well, viz. Theophilou,[48] Gross, Oliveira, Kohn,[49] Gorling,[50,51] Kryachko, Ludena,[52] Levy, Nagy,[53] Sahni [54] etc.

In Thomas Fermi model, electron density is the prime variable unlike wave function in Schrodinger's approach. The total energy of a system influenced by external potential may be expressed in terms of a functional of electron density:

$$E_{TF}[\rho(r)] = \frac{3}{10}\left(3\pi^2\right)^{2/3}\int \rho(r)^{5/3}\,dr + \int \rho(r)V_{ext}(r)dr + \frac{1}{2}\iint \frac{\rho(r)\rho(r')}{|r-r'|}drdr' \qquad (2.37)$$

where, first term represents kinetic energy of non-interacting electrons in a homogeneous electron gas (HEG), second term indicates classical electrostatic energy of nucleus-electron Coulomb interaction while last term is the classical electrostatic Hartree energy as approximated by classical Coulomb repulsion between electrons. The exchange and correlation amongst electrons were ignored. Dirac introduced local exchange term $-\frac{3}{4}\left(3/\pi\right)^{1/3}\int \rho(r)^{4/3}\,dr$. The ground state energy could be minimized by Lagrange's undetermined multiplier method subject to constraint that number of electrons is conserved. However the approximations in this theory were so crude that bonds between atoms or molecules could not be explained properly which led to its failure in explanations for electrons in solid matter,[55] yet it clearly acted as predecessor to DFT methods.

Hohenberg and Kohn gave an exact theory of many-body systems in 1964 which was capable of explaining not only condensed-matter systems of electrons with fixed nuclei but also applicable to any other system of interacting particles under influence of external potentials. It was based on two basic theorems proposed by them (HK theorems). An additional $E_{XC}(\rho(r))$ was incorporated subject to slowly varying electron density with position in HEG system (local density approximations, LDA). These propositions were later put into practical use by Kohn-Sham (KS) formulations that enabled calculations to be implemented on a personal computer and earned them Nobel prize in 1998.[47]

The exchange correlational functional is not known *apriori*, which necessitates the usage of approximate equations. Vosko, Wilk and Nusair contributed immensely by adding spin densities terms.[56] Later, better exchange and correlational functionals were developed by Lee, Yang Parr (LYP),[57] Perdew, Wang (PW9) [58] and Becke (B96).[59] Next, Becke developed procedures for hybrid density functional procedures to eliminate demerits of existing methods.[60,61] In this method, exchange and correlational functionals were approximated using a three fit parameters (A, B and C) which were optimized against experimental data:

$$E_{XC}^{B3LYP} = AE_X^{Slater} + (1-A)E_X^{HF} + B\Delta E_X^{Becke} + E_C^{VWN} + C\Delta E_C^{LYP} \quad (2.38)$$

Although it is not a truly ab initio method, it provides extremely accurate and low-cost computational method that has been benchmarked extensively against test results. Besides B3LYP, M06 is another class of functional which relies on spin densities, spin density gradients, spin kinetic energy densities and nonlocal hybrid functionals.

References

1. L. I. Shiff, *Quantum Mechanics*, 3rd Edition, McGraw- Hill, NewYork (1968).
2. E. Schroedinger, *Ann. Physik*, **79**, 361 (1926).
3. L. Pauling, E. B. Wilson, *Introduction to Quantum Mechanics*, McGraw-Hill, New York (1935).
4. M. Born, J. R. Oppenheimer, *Ann. Physik*, **84**, 457 (1927).
5. W. Kolos, L.Wolniewicz, *J. Chem. Phys.*, **41**, 3663 (1964).
6. B. T. Sutsliffe, *Adv. Quantum. Chem.*, **28**, 65 (1997).
7. J. A. Pople , D. L. Beveridge, *Approximate Molecular Orbital Theory*, McGraw-Hill Book Co., New York (1970).
8. D. R. Hartree, *Proc. Cambridge Phil. Soc.*, **24,** 89, 111, 426 (1928).
9. G. Uhlenbeck, S. Goudsmit, *Nature wissenschaften*, **13**, 953 (1925).
10. J. A. Pople, D. L. Beveridge, P. A. Dobosh, *J. Chem. Phys.*, **47**, 2026 (1967).
11. W. Pauli, *Z. Physik.*, **31**, 765 (1925).
12. J. C. Slater, *Phys. Rev*., **35**, 509 (1930) and **34**, 1239 (1959).
13. P. A. M. Dirac, *The Principle of Quantum Mechanics*, Oxford University Press, London (1958).
14. J. K. L. McDonald, *Phys. Rev*., **43**, 830 (1933).
15. R. H. Young, *Int. J. Quant. Chem*., **6**, 596 (1972).
16. F. Jenson, *Introduction to Computational Chemistry*, 2nd Edition, John Wiley & Sons Ltd., Chichester (2007).
17. I. N. Levine, *Quantum Chemistry*; Chapter-11, *"The Hartree Fock Self-Consistent Method"*, 5th Edition, Pearson, (2000).
18. I. N. Levine, *Quantum Chemistry.*, Chapter-8, "Perturbation Theory", Pearson, 5th Edition (2000).
19. J. A. Pople, D. L Beveridge, *Z. Physik.*, **61**, 126 (1930).
20. J. E. Lennard-Jones, *Proc. Roy. Soc. (London)*, **A198,** 14 (1949).
21. C. Edimiston, K. Ruedenberg, *Rev. Mol. Phys.*, **34**, 457 (1963); J. *Chem. Phys.*, **43**, 597 (1965).
22. C. C. Roothaan, *J. Rev. Mod. Phys.*, **23**, 69 (1951).
23. G. G. Hall, *Proc. Roy. Soc., (London),* **A205**, 541 (1951).
24. W. J. Hehre, L. Radom, J. A. Pople, P.v.R. Schleyer, *Ab Initio Molecular*

Orbital Theory, Wiley (1986).

25. B. O. Roos, (Ed.) *Lecture Notes in Quantum Chemistry,* Springer-Verleg (1992).
26. J. Olsen, O. Christiansen, H. Koch, P. Jorgensen, *J. Chem. Phys. Lett.*, **261**, 369 (1996).
27. C. Moller, M. S. Plesset, *Phys. Rev.*, **46**, 618 (1934).
28. E. Hückel, *Z. Physik.*, **70**, 204 (1931).
29. D. Feller, E. R. Davidson, *Rev. Comp. Chem.*, **1** (1990).
30. T. Helgaker, P. R. Taylor, "*Modern Electronic Structure Theory*", Part II, D. Yarkony (Ed.), World Scientific, pp. 727 (1995).
31. S. F. Boys, *Proc. Roy. Soc.*, (London), **A 200**, 542 (1950).
32. T. H. Dunning Jr. and P. J. Hay, *Modern Theoretical Chemistry*, H. F. Schaefer III (Ed.), Vol. 3, pp. 1, Plenum, New York (1977).
33. J. S. Binkley, J. A. Pople, *J. Am. Chem. Soc*., **102**, 939 (1980).
34. W. J. Hehre, R. Ditchfield, J. A. Pople, *J. Chem. Phys.*, **56**, 2257 (1972).
35. M. J. Frisch, J. A. Pople, Binkley, *J. Chem. Phys.*, **80**, 3265 (1984).
36. H. Hellmann, *J. Chem. Phys.*, **3**, 61 (1935).
37. P. J. Hay and W. R. Wadt, *J. Chem. Phys.*, **82**, 270 (1985).
38. D. Kumar, B. Karamzadeh, G. N. Sastry and S. P. de Visser, *J. Am. Chem. Soc.*, **132**, 7656 (2010).
39. T. H. Dunning Jr. and P. J. Hay, *Modern Theoretical Chemistry*, H. F. Schaefer III (Ed.), Vol. 3, pp. 1, Plenum, New York (1977).
40. D. R. Hartree, Proc.CambridgePhil.Soc., **24,** 89 (1928).
41. V. Fock, Z. Phys., **61**, 126 (1930).
42. J. C. Slater , Phys. Rev. **81**, 385 (1951); J.C. Slater, Phys. Rev. **82**, 538 (1951); J.C. Slater, Phys. Rev. **91**, 52 (1953).
43. P. A. M. Dirac, Proc. Cambridge Phil. Roy. Soc. **26** 376 (1930).
44. L. H. Thomas *Proc.CambridgePhil.Soc.***23** 542(1926).
45. E. Fermi, *Z.Phys.***48** 73(1928).
46. P. Hohenberg and W. Kohn, Phys.Rev. **136**, B864 (1964).
47. W. Kohn and L. J. Sham, Phys. Rev. **140**: A1133 (1965).
48. A. K. Theophilou *J. Phys. C***12** 5419 (1979).
49. E.K.U. Gross, L.N. Oliveira, and W. Kohn, Phys. Rev. A **37**, 2809 (1988).

50. A. Gorling Phys. Rev. A **54**, 3912 (1996).
51. A. Gorling Phys. Rev. A**59**, 3359 (1999).
52. T. Koga *J. Chem. Phys.***95**, 4306 (1991).
53. M. Levy A .Nagy *Phys. Rev. Lett.***83** 4361 (1999).
54. V. Sahni, Quantal Density Functional Theory, Springer Verlag (2004).
55. E. Teller, Rev. Mod. Phys. **34**, 627 (1962).
56. S. H. Vosko, L. Wolk, M. Nusair, Can. J. Phys., **58**, 1200 (1980).
57. C. Lee, W. Yang, R. G. Parr, *Phys. Rev*., **B37**, 785 (1988).
58. J. P. Perdew, Y. Wang, *Phys. Rev*., **B45**, 13244 (1992).
59. A. D. Becke, *J. Chem. Phys*., **104**, 1040 (1996).
60. A. D. Becke, *J. Chem. Phys*., **98**, 5648 (1993).
61. R. G. Parr, W. Yang, *Density Functional Theory*, Oxford University Press (1989).

CHAPTER 3

Quantum mechanical study of Ga_xAs_x fullerene type micro-clusters for x=10, 13, 15, 18, 20, 25 and 30 atoms

3.1. Introduction

Low-dimensional semi-conducting material is of great interest to researchers in nano science.[1-4] Micro-clusters present a new phase of a solid with novel properties and are formed by aggregation of atoms or molecules, and also exhibit properties significantly different from that of the bulk. The dependence of electronic structure of the micro-cluster on its physical size give rise to new physical, optical [5] electronic [6] chemical as well as magnetic properties.[7] Since the properties of a micro-cluster depend on its composition so it enables to fine tune different properties of micro-clusters, particularly in case of semiconductor clusters, resulting in novel optical and electronic capabilities. Investigation of clusters also enables to study the emergence of bulk crystalline properties from atomic or molecular scale. In order to obtain some desired property from a cluster, a detailed study about the properties of the cluster and its flexibility to control its size is required. The present day computational resources and techniques have enabled to model and investigate these clusters with ease and accuracy.

Fullerenes have a special structure which consists only of pentagonal and hexagonal rings with hollow cage like structure and belongs to the class of micro-clusters. With all possible arrangement of atoms between these pentagon and hexagon many isomers can be constructed by varying the number of atoms.[7] After the discovery of fullerene the interest has now shifted towards the search of new fullerene like structures formed by other elements or combination of different elements because

fullerene type structure offers several unique properties that can be used in different applications like synthesis of nano-structured semiconducting magnets.[6] With the rapid increase in the density of the electrons with the reduced size of components they are used in the electronic devices such as quantum dots and quantum clusters. Currently available technology has already made it possible to fabricate semiconductor clusters by using laser vaporization technique and mass spectroscopy. A great interest in the field of clusters has arisen because of the advancement in computational and theoretical techniques along with development of advanced spectroscopic techniques.

III–V group semiconductor materials have been the focus of numerous experimentalists.[8-9] Due to high electron mobility of III – V compounds such as GaAs these have the capability of replacing Si in the electronics industry. GaAs is a direct band gap semiconductor with band gap energy of ~ 1.43 eV. In the recent years several experimental and theoretical investigations of GaAs clusters have been done. These studies have enabled us to know more about the structural stability, reactivity and nature of bonding in these clusters. It is expected that Gallium Arsenide cluster may exhibit different bonding characteristics than their bulk because of their strong anion-anion bonds.[10] Investigations based on density functional theory (DFT) have proved to be very useful for studying these type of micro-clusters. The DFT scheme is accurate enough to explain the physical properties of the cluster which depend on several parameters like the size, charge or the stoichiometric composition of the cluster.[11-13]

The present work is focused on the structures, as well as electronic properties of fullerene type Ga_xAs_x micro-clusters for x=10, 13, 15, 18, 20, 25 and 30 atoms.

3.2. Computational Method

The fullerene like Ga_xAs_x structures were generated using Gauss View 5.0. The optimization and study of the structures and characteristics of these clusters have been carried out by using the DFT with unrestricted B3LYP exchange-correlation potential as implemented in Guassion 09 program.[14-15] For describing the good geometrical and bonding feature for heavy atom, the basis set with effective core potential, LanL2DZ [16] is used for Gallium (Ga) and Arsenic (As) atoms. The basis set LanL2DZ describes the outermost electrons of $3s^2\ 3p^6\ 4s^2\ 3d^{10}\ 4p^1$for Ga and As atoms. The interaction between core and valence electron was handled by Torullier-Martins norm conserving pseudo potential in their fully separable form and the pseudo potential also includes d orbitals in the valence configuration.[17,18]

Optimized geometries were obtained without any symmetry constraints and continued until the force components on each atom are less than 0.01 eV/Å using a conjugated gradient algorithm. These optimized geometries were subsequently verified by frequency calculations. The presence of real frequency confirms the stability of structure. The gap between energy of the highest occupied molecular orbital and lowest unoccupied molecular orbital levels and the binding energy is also used to determine the stability of the micro-clusters. The method and the basis set used are well established to the similar type study of metal clusters.[19]

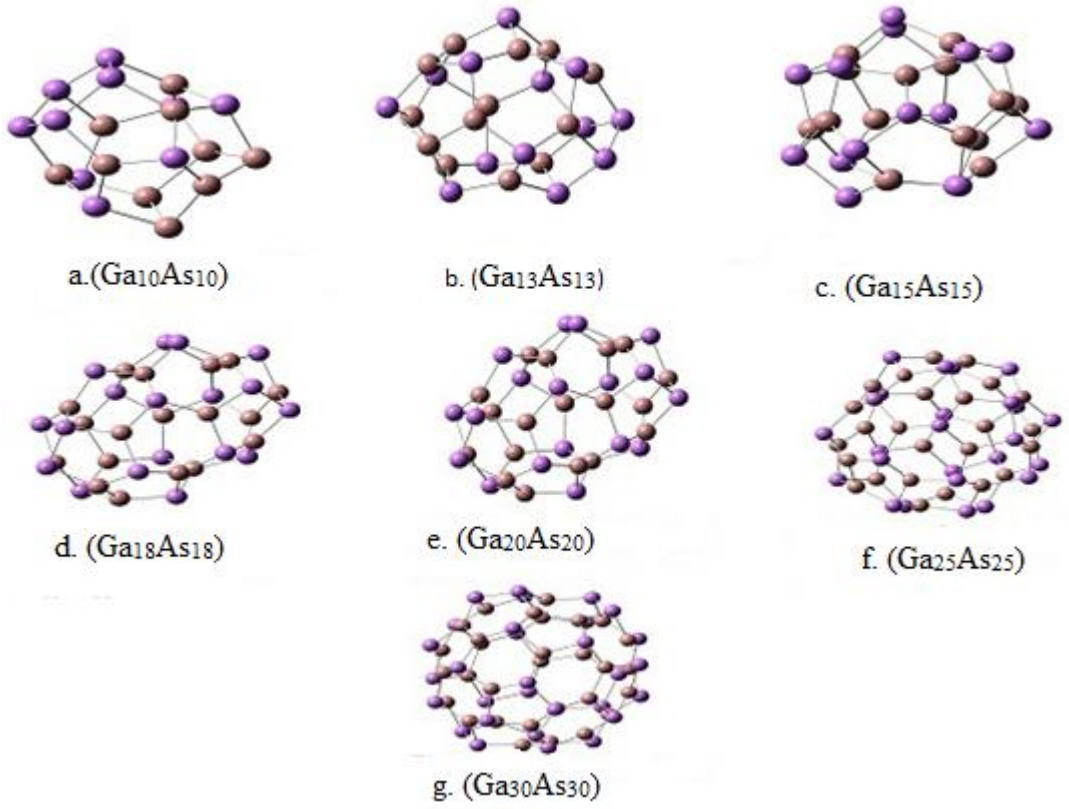

Figure 3.1: The optimized structures of Ga_xAs_x micro-clusters for x= 10, 13, 15, 18, 20, 25 and 30.

3.3.1. Results and Discussion

The optimized structures for gallium arsenide fullerenes (Ga_xAs_x) are presented in Figure 3.1 for x= 10, 13, 15, 18, 20, 25 and 30, the dark red colours represent the Ga atom and violet colours represent the As atoms. Each structure has 12 pentagons and six edges are shared by adjacent pentagons. Common edges of pentagons consist of Ga-Ga and As-As homo nuclear bonds. The Ga-Ga bond length lies in range of 2.50-2.69 A^0, the As-As bond length lies in range 2.58-2.62 A^0 and Ga-As bonds length is in range 2.46-2.52 A^0. The variation of bond lengths for Ga-Ga, As-As and Ga-As is shown in Figure 3.2. The Figure 3.2 clearly indicates the dependency of bond lengths in clusters are significant in cluster size. The homo-nuclear Ga-Ga and As-As bonds are almost constant, except for Ga-Ga bond in case of $Ga_{10}As_{10}$, which confirms their

bonding. The Ga-As-Ga bond angle is 100^0-109^0 but the As-Ga-As bond angles tends to have larger values 113^0-130^0. The As-Ga-Ga bond angle at the shared pentagon edge is $\approx 111^0$ and Ga-As-As bond angles at shared pentagon edge is$\approx 98^0$ but lies between the above bond angle ranges.

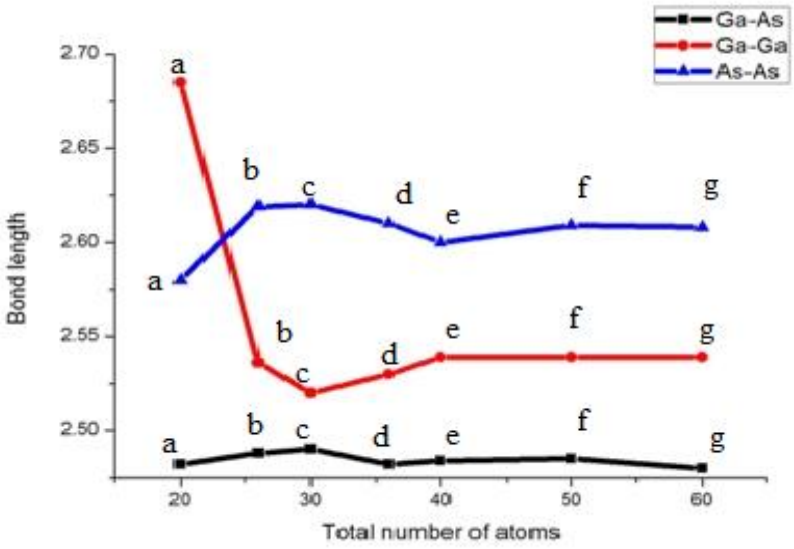

Figure 3.2: Variation of bond lengths in Å the Ga_xAs_x clusters for x = 10, 13, 15, 18, 20, 25 and 30.

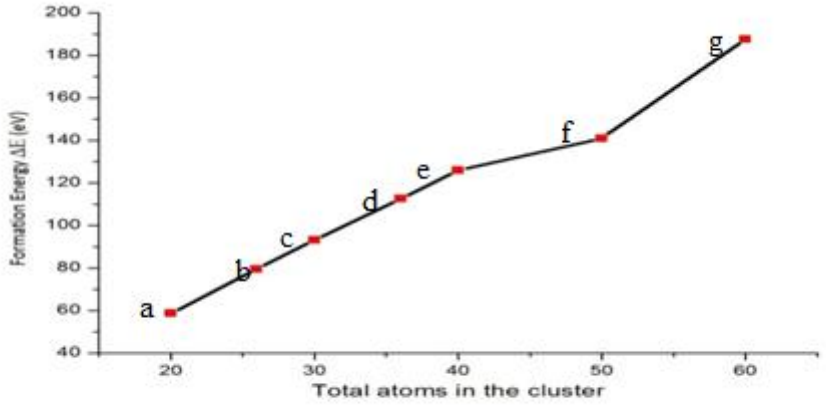

Figure 3.3: Variation of formation energy in eV for Ga_xAs_x clusters for x = 10, 13, 15, 18, 20, 25 and 30.

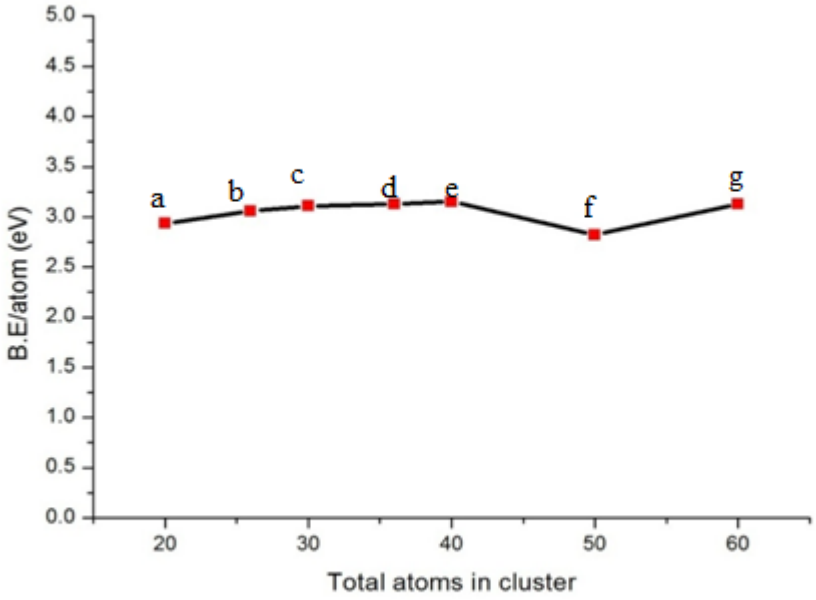

Figure 3.4: The Variation of binding energy in eV for Ga_xAs_x clusters for x = 10, 13, 15, 18, 20, 25 and 30.

The variation of formation energy in eV for Ga_xAs_x clusters for x= 10, 13, 15, 18, 20, 25 and 30 is shown in Figure 3.3. The formation energy of the clusters lies between

0.1078-0.114976 eV. The binding energy in eV for Ga_xAs_x clusters for x= 10, 13, 15, 18, 20, 25 and 30 is shown in Figure 3.4. The binding energy increases monotonically with increase in cluster size.

The energetic of possible reaction from reactants Ga and As to the products i.e. cluster depending on the stoichiometric of the clusters is obtained by the reaction

$$x(GaAs) \rightarrow Ga_xAs_x$$

The binding energy change ΔE shown in Figure 3.4 is a function of total number of atoms x+x in Ga_xAs_x. It is obvious from Figure 3.4 that the binding energy increases as the cluster size increases.

3.3.2. Electronic structure of the gallium arsenide fullerenes

The energy gap E_g is the difference of the highest occupied molecular orbital (HOMO) and energy of lowest unoccupied orbital (LUMO), this also represents the chemical stability of clusters. The E_g of Ga_xAs_x clusters are lie between 2.20-2.50 eV. The variation of E_g of Ga_xAs_x cluster for x = 10, 13, 15, 18, 20, 25 and 30 is shown in Figure 3.5.

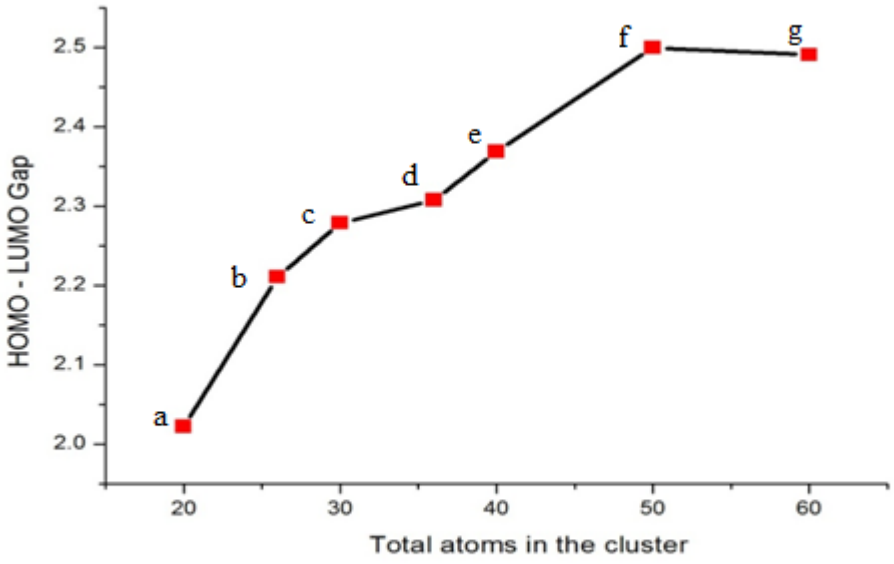

Figure 3.5: The variation of Homo-Lumo gap (E_g) in eV for Ga_xAs_x clusters for x = 10, 13, 15, 18, 20, 25 and 30.

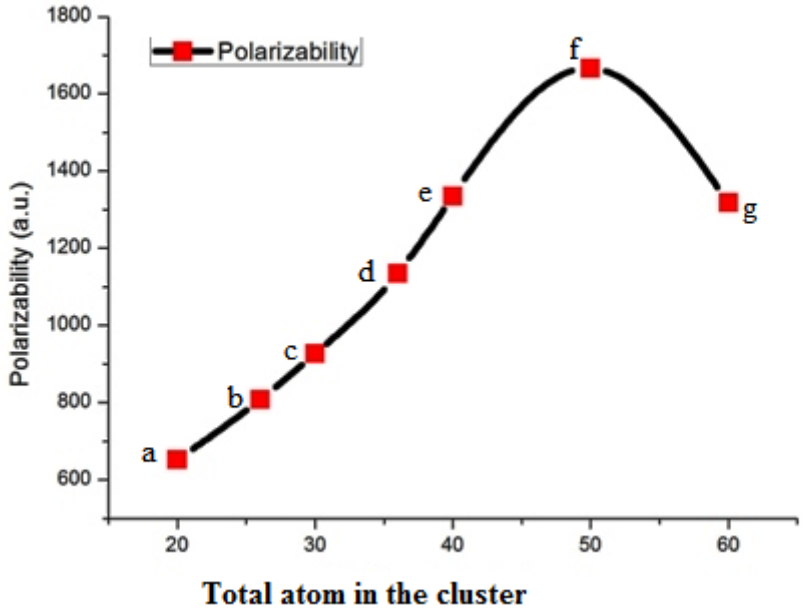

Figure 3.6: The variation of polarizability in atomic unit for Ga_xAs_x clusters for x= 10, 13, 15, 18, 20, 25 and 30.

The optical activity of a cluster is related to its corresponding polarizabillity. The variation of polarizability in au for Ga_xAs_x clusters for x= 10, 13, 15, 18, 20, 25 and 30 is presented in Figure 3.6. The polarizabilty increase gradually till x=25 in Ga_xAs_x cluster and it falls for $Ga_{30}As_{30}$. From Figure 3.6 is clear that $Ga_{25}As_{25}$ is higher than other studied clusters.

3.4. Conclusion

The electronic structure and optical properties of the Ga_xAs_x clusters for x= 10, 13, 15, 18, 20, 25 and 30 were studied using DFT method. The binding energy and HOMO-LUMO gap (E_g) confirms the stability of the clusters. The variation of polarizability, the optical activity with increase in cluster size in the presented study suggests that $Ga_{25}As_{25}$ cluster has more optical activity in comparison with other studied clusters.

References

1. W. Dobwolski, J. Kossut, T. Story Hand *b. Magn. Mater*, **15**, 289 (2003).
2. P. V. Kamat, fullerenes chemistry, physics and technology, Chem. *Rev.*, **93**, 267 (1993).
3. Y. Wang, N. J. Herron, Inclusion phenomena and molecular recognition, *Phys. Chem.*, **92**, 4988, (1988).
4. S. D. Cox, T E Gier, G. D. Stucky, J. Birlein, J. *Am. Chem. Soc*., **110**, 2986, (1988).
5. M. BeziJavan, *J. Mol. Model*, **19**, 2273, (2013).
6. Liu Li-R En, Zhu Hehg-Jiang, Liu Zhi-Feng, Wu Peng, *Chin. Phy. B*, **21**, 123601, (2012).
7. M. Galica, R. Buczko, Physica status solidi B-basic solid state physics, 739 (2013).
8. P. W. Fower, D. E. Manolopoulos, An atlas of fullerenes, *oxford: Clarendon Press* (1995).
9. S. C. O. Brien, Y. Liu, Q. Zhang, J. R. Heath, *J. Chem. Phys.***, 84**, 4074, (1986).
10. R. Schafer, J. A. Becker, *Phys. Rev. B*, **54** , 10296, (2004).
11. L. Wang, L. P. F. Chibante, F. K. Tittel, R.F. R. E. Smalley Curel, *Chem. Phy. Lett*., **172**, 335, (1990).
12. P. Sarkar, M. Springborg, *Phys. Rev. B*, 68, 235409, (2003).
13. C. Ghosh, S. Pal, B. Goswami, P. Sarkar, *Chem. Phys. Lett*., **407**, 498, (2005).
14. B. Brena, L. Ojamae, *J. Phys .Chem. C*, **112**, 13516, (2008).
15. A. D. Becke, *Phys. Rev. A*, **38** ,3098, (1988).
16. C. Lee, W. Yang, R. G. Parr, *Phys. Rev. B***, 37**,785,(1988).
17. R.W. Wadt, J. P. Hay, *J. Chem. Phys*., **82**, 284, (1985).
18. P. W. Fowler, K. M. Rogers, G. Seifert, M. Terrones, H. Terrones, *Chem. Phys. lett*., **299**, 359, (1999).
19. S. P. de Visser, D. Kumar, M. Danovich, N. Nevo, D. Danovich, P. K. Sharma, W. Wu, S. Shaik, *J. Phys. Chem. A***, 110**, 8510 (2006).

CHAPTER 4

Structural Stability and Electronic Properties of $(Ga_nN_n)_m$ Micro Cluster by Using ab-inito and Tight-Binding Study

4.1. Introduction

Carbon nanotubes (CNT), the one dimensional system is gaining momentum with the invention of carbon. The potential application of CNT is due to their high mechanical strength, ballistic transport and other novel properties.[1] The nanotubes and nanowires from Mo-S compound have been extensively studied due to different applications. CNTs have replaced other alternatives.[2,3] Synthesis with unique structural and electronic properties and the ability to advance tune their properties by adding dopants are studied in detail.[4] The 1-D systems of CdS compounds have drawn much attention, leading to the synthesis of their nanowires [5,6] nanotubes,[7] and nanorods[8-10] with controlled dimensions.

Recently it has been proved that the low dimensional semiconductor material have become of great interest to researchers in the field of nanoscience.[11-13] Among these materials of III-V group semiconductor compound due to their paramount technological potential have applications such as photo electronic devices, photonic integrations, ultrahigh frequency microwave and photovoltaic solar cells.

Gallium nitride (GaN) is an important semiconducting material, which has a broad range of potential applications for optoelectronics and high power electronic devices. Light emitting diode has made a boom in the market with its appearance in the recent past year.[14] Its high thermal conductivity also opened new routes in high-temperature and high-power electronic devices[15,16] such as Metal Semiconductor Field Effect Transistor (MESFETs), High Electron Mobility Transistors (HEMTs) and

heterojunction bipolar transistor (HBTs).[17,18] Furthermore high Curie temperature and room temperature ferromagnetic nature has been predicted in GaN-doped with transition metal (MT).[19-20] Recently, there have been an increasing interest in GaN nanostructures likes nanotubes, nanowires and microclusters. Single-crystal GaN nanotubes with inner diameters of 30-200nm and wall thickness of 5-50 nm were synthesized experimentally. There have been several theoretical studies on Ga_nN_n clusters up to n=4-6 by Bel Bruno [21], Kandallam et al. [22-25], and Song et al. [26-27]. To study the lowest–energy of $(Ga_nN_n)_x$ clusters, a number of possible isomers were generated.[28-29] These structures were adopted from those previously proposed for the III-V semiconductor compound cluster such as BN [30-31], AlN [32, 33].

Table 4.1 (a): Illustrates the Binding energy, band gap and bond distance of $(Ga_2N_2)_m$ Clusters.

Cluster	Binding energy/atom (eV)	Band gap (eV)	Bond distance (Å)
$(Ga_2N_2)_1$	10.34	1.49	1.92
$(Ga_2N_2)_2$	10.81	0.84	1.91
$(Ga_2N_2)_3$	11.29	1.30	1.93
$(Ga_2N_2)_4$	11.48	1.33	1.92
$(Ga_2N_2)_5$	11.60	1.54	1.90
$(Ga_2N_2)_6$	11.61	2.43	1.91

Table 4.1(b): Shows the binding energy, band gap and bond distance of $(Ga_3N_3)_m$ Clusters.

Cluster	Binding energy/atom (eV)	Band gap (eV)	Bond distance (Å)
$(Ga_3N_3)_1$	10.92	2.11	1.87
$(Ga_3N_3)_2$	11.54	1.60	1.90
$(Ga_3N_3)_3$	11.83	2.12	1.92
$(Ga_3N_3)_4$	11.96	2.32	1.93
$(Ga_3N_3)_5$	12.05	2.39	1.92
$(Ga_3N_3)_6$	12.10	2.49	1.92

Table 4.1(c): Depicts the binding energy, band gap and bond distance of $(Ga_4N_4)_m$ Clusters.

Clusters	Binding energy/atom (eV)	Band gap (eV)	Bond distance (Å)
$(Ga_4N_4)_1$	11.15	2.65	1.77
$(Ga_4N_4)_2$	11.61	2.35	1.83
$(Ga_4N_4)_3$	11.83	2.52	1.91
$(Ga_4N_4)_4$	11.88	2.43	1.89
$(Ga_4N_4)_5$	12.00	2.69	1.89
$(Ga_4N_4)_6$	11.99	2.42	1.90

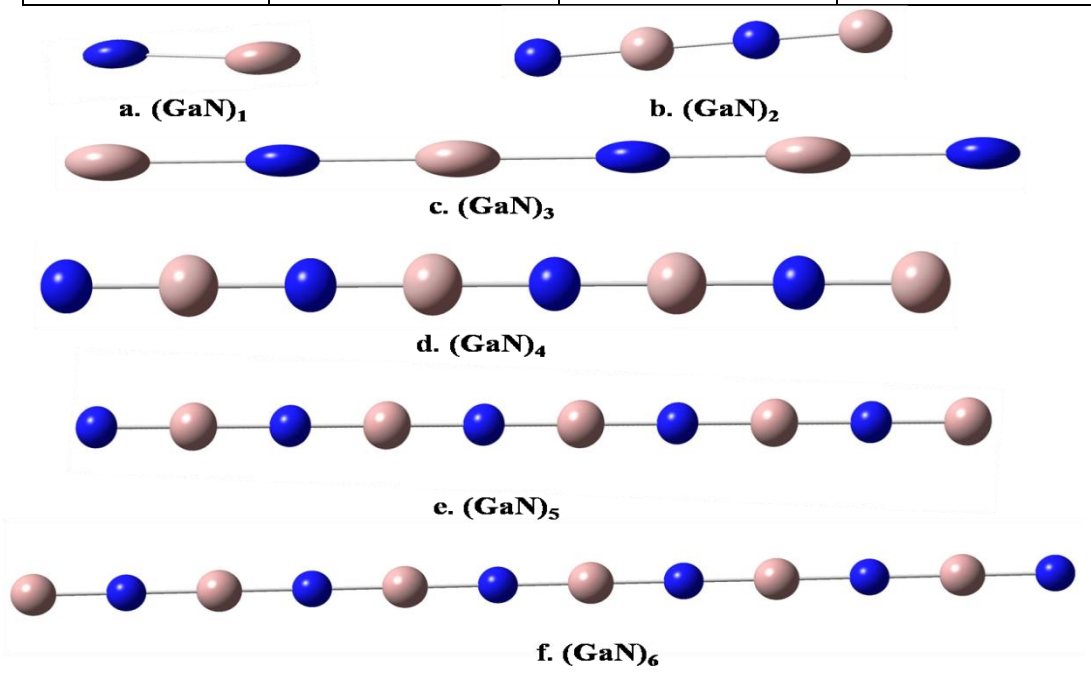

Figure 4.1.a: Illustrates the optimized structures of $(GaN)_m$ micro cluster.

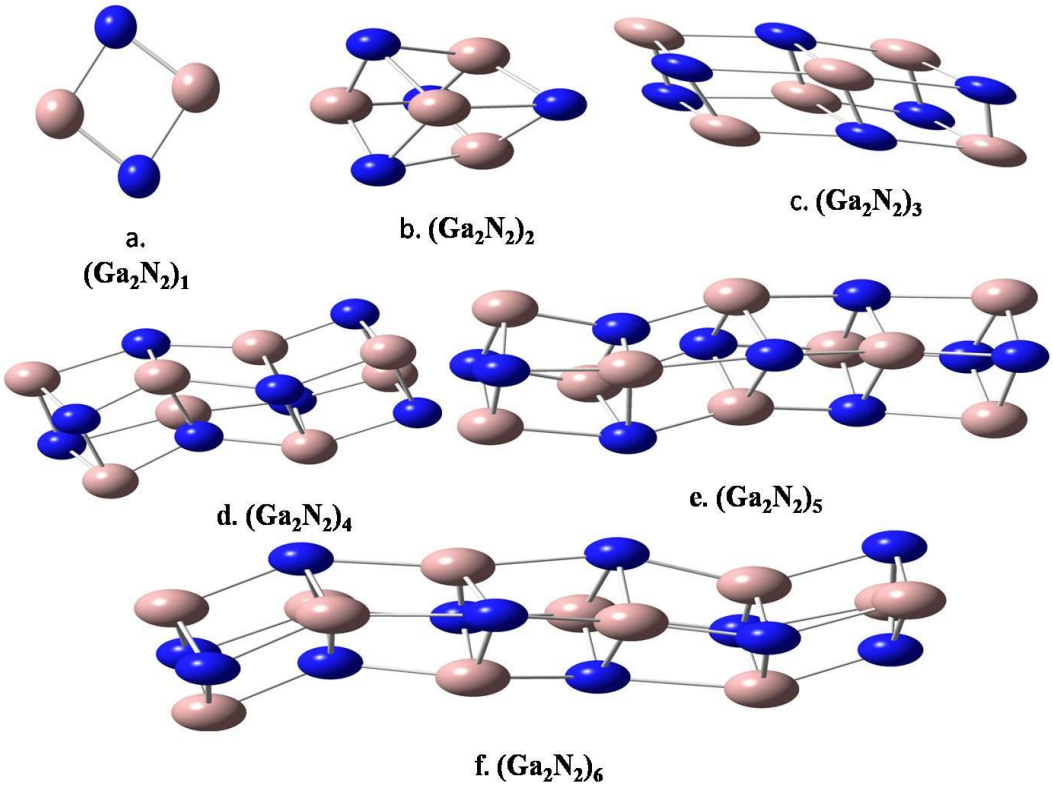

Figure 4.1.b: Illustrates the optimized structures of $(Ga_2N_2)_m$ cluster.

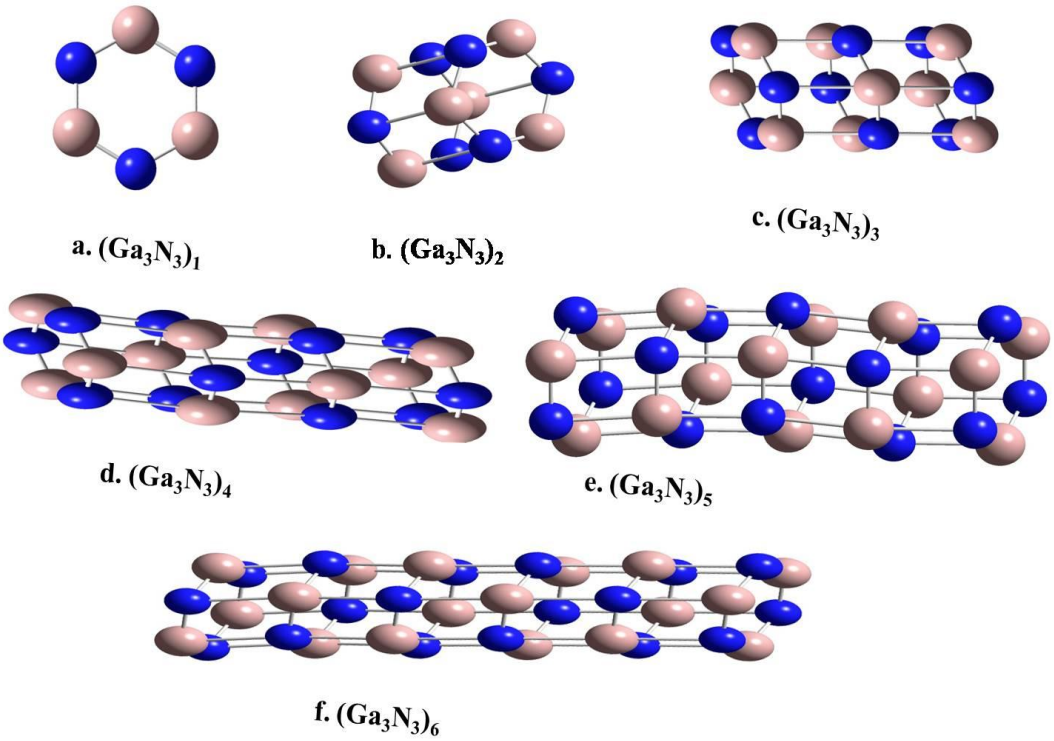

Figure 4.1.c: Illustrates the optimized structures of $(Ga_3N_3)_m$ cluster.

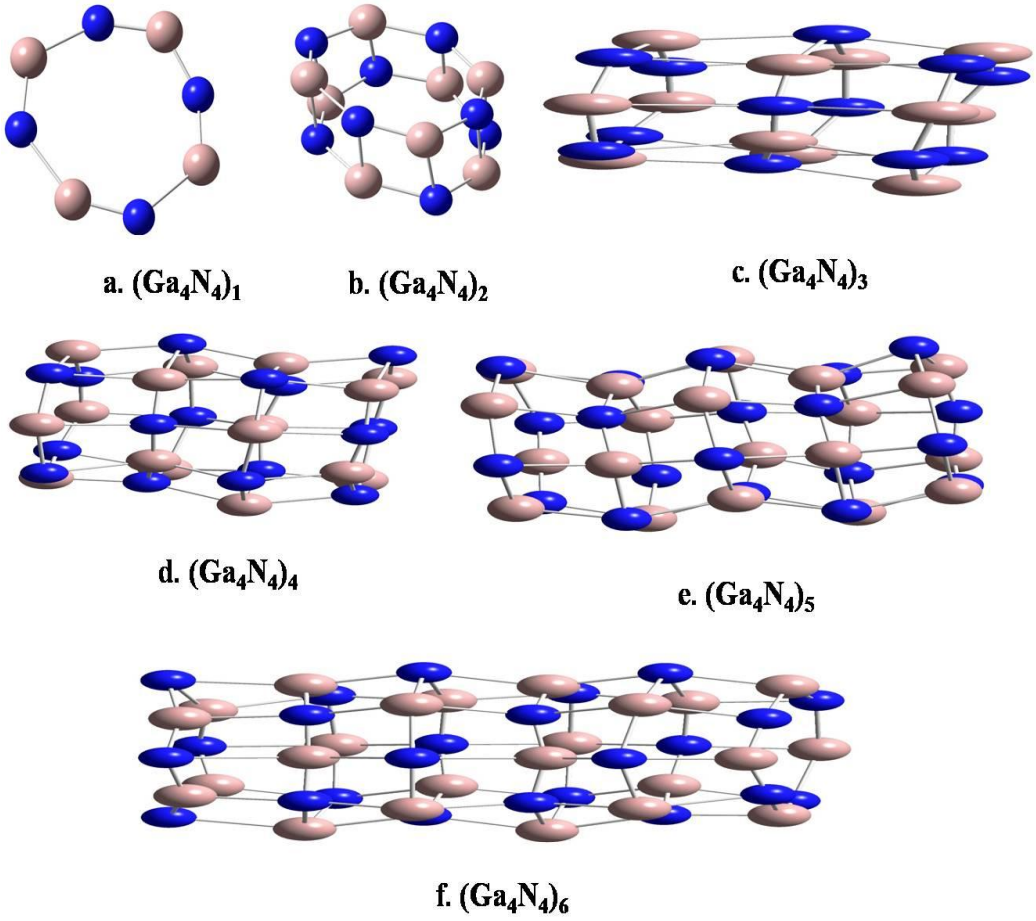

Figure 4.1.d: Illustrates the optimized structures of $(Ga_4N_4)_m$ cluster.

4.2. Computational Method

For the optimization of GaN condensed nanocluster and to calculate their ground and excited state properties, density functional theory has been used. Structural optimizations (i.e. the geometrical parameters) have been performed with no constraints imposed on the nanocluster structures during the optimization. We have constructed various possible structures for each GaN cluster. These structures were drawn using Gauss View 0.5. For geometry optimization, B3LYP level of DFT method, Beck's three parameters with correlation function (Lee-Yang-Parr), and relativistic effective core potential with double zeta basis set, LANL2DZ as implemented in Gaussian 09 program suite were used. DFT is one of the promising

and efficient methods to investigate electronic, optical and structural stability of micro clusters. Also, Gauss Sum 3.0 has been used for the evaluation of density of states (DOS) spectrum.

The binding energy per atom (BE) of a cluster is calculated using the formula:

$$\mathbf{BE} = \frac{\mathbf{nE(Ga)+nE(N)-E(GanNn)}}{\boldsymbol{2n}}$$

Where E (Ga), E (N), and E (Ga_nN_n) are total energy of a single Ga atom, a single N atom, and Ga_nN_n clusters, respectively and n is the number of Ga or N atoms. Similar calculations were extended to cluster to comprehend the first principle calculations on optimized Ga_nN_n nanowires with n=1-4.

4.3. Results and Discussion

4.3.1. Atomic structure of Ga_nN_n cluster

First principle calculations on the various Ga_nN_n (n=1-4) clusters, were performed to obtain the stable isomers in each size range, which acts as a fundamental building block of condensed cluster or nano assemblies. Optimized structures are shown in Figure-4.1(a), 4.1(b), 4.1(c) and 4.1(d), the BE, HOMO-LUMO gap and Ga-N bond distance of stable isomers are reported in Table -4.1(a, b & c). The stable isomers of Ga_nN_n clusters from n=4 to 12 possess ring and cage (37) geometries respectively, which are quite comparable to earlier reports.

4.3.2. Condensed Clusters

With an understanding of stable isomers of Ga_nN_n with different geometries, condensed cluster of $(Ga_nN_n)_m$ are achieved by linear stacking of m up to 7 units of stable Ga_nN_n isomers (n=1-4). We also endeavor the condensation of the stable

isomers of Ga_5N_5, but the important structural distortion was observed due to large aperture in the center of the rings. Hence we did not proceed in this direction.

The optimized structures of condensed clusters are shown in Figure 4.1, the $(Ga_nN_n)_2$ cluster is obtained by condensing one planar Ga_3N_3 isomer at the top while another isomer at the bottom, thus increasing the number of Ga-N bonds in the cluster. Similarly, $(Ga_3N_3)_4$ and other condensed clusters, $(Ga_nN_n)_m$ were obtained ,and optimized structure are shown in Figure 4.1(a) - 4.1(d) further , other–sized $(Ga_nN_n)_2$ cluster are stacked from their basic unit of Ga_nN_n.

The binding energy and HOMO- LUMO gap of all the condensed (Ga_nN_n) clusters and the results are shown in Figure 4.2 along with the cohesive energy per atom and band gap of infinite Ga_nN_n nanowires. As expected, the BE of condensed cluster increases linearly with m and slowly achieves the cohesive energy per atom and band gap of infinite nano wires, as shown in Figure 4.2(a). In the inset, the BEs, of $(Ga_nN_n)_m$ condensed cluster with respect to the diameter (in terms of n) are shown. Even though the diameter of the $(Ga_3N_3)_m$ condensed clusters is smaller than that of the $(Ga_4N_4)_m$ cluster, beyond m= 3. The BE of the cluster is almost equal to that of the latter. The BEs of $(Ga_3N_3)_5$ and $(Ga_4N_4)_5$ are 12.05 and 12.00 eV/atom, respectively. Hence it can be concluded that $(Ga_4N_4)_m$ condensed cluster are more stable as compared to other -sized condensed cluster and preferably this cluster could extend to nanorod and nanowires. Even our calculation on infinite nanowires supports this conclusion as the cohesive energies of $(Ga_3N_3)_3$ and $(Ga_4N_4)_3$ infinite nanowires are almost same (11.83eV/atom).

Figure 4.2(b) depicts the variation of the HOMO- LUMO gap of the cluster. For n= 2,3 the HOMO-LUMO gap increases as the m values increases, and for n= 4 it lies between 2.35 to 2.69 eV. The HOMO-LUMO gap for $(Ga_4N_4)_m$ condensed cluster is

significantly higher than that of other condensed cluster. This supports our previous statement that $(Ga_4N_4)_m$ condensed clusters are more stable among all the clusters. Further, we also noted in Figure 4.2 that beyond m=2, the HOMO-LUMO gap of $(Ga_1N_1)_m$ atomic wire is less than that of other condensed cluster. It is a consequence of the increase in the number of non bonding states with the increase in the length of the atomic wire [34]. Overall, the HOMO-LUMO gap of all $(Ga_nN_n)_m$ clusters is less than the band gap of the bulk GaN compound.

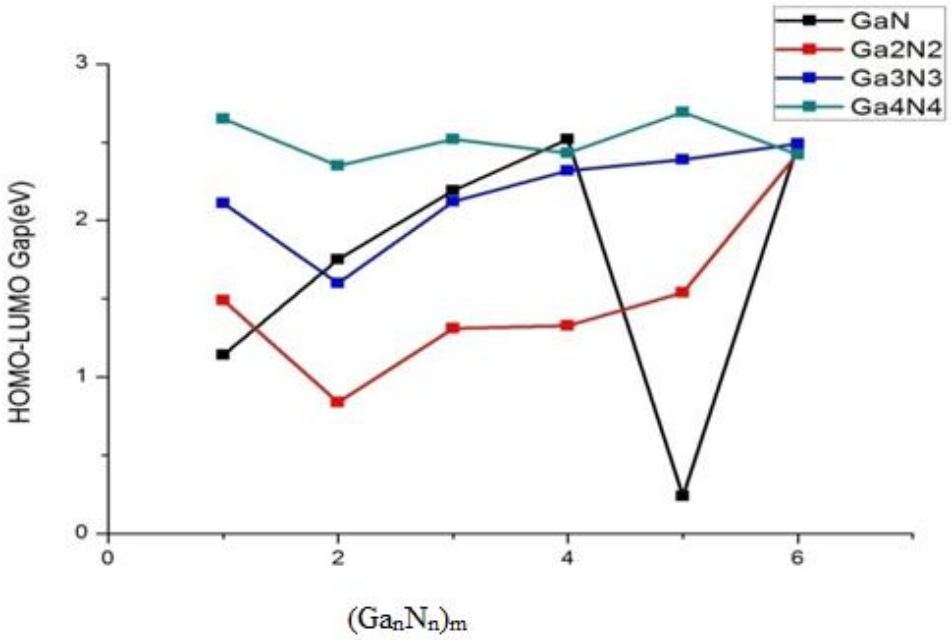

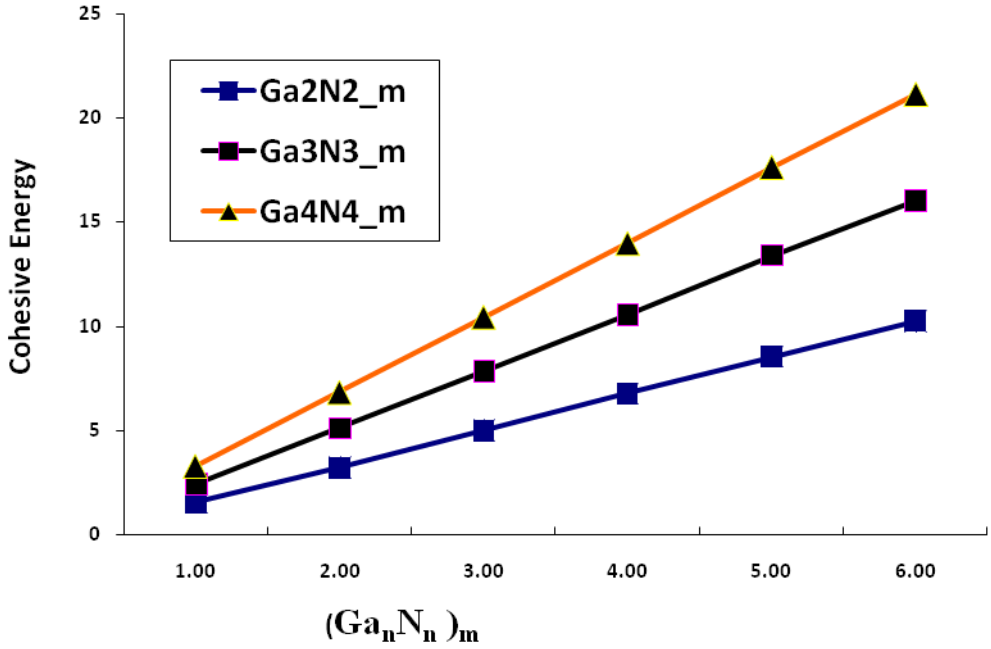

Figure 4.2: (a) Cohesive energy and (b) HOMO – LUMO Gap of $(Ga_nN_n)_m$ are shown. In the inset, BEs of $(Ga_nN_n)_m$ are shown for various n. The band gap shown in figure is less than the bad gap of bulk GaN, which is obtained from the calculation**.**

4.3.3. Electronic Structure

To study the structural stability of $(Ga_3N_3)_m$ cluster the total and partial density of states (DOS) of the cluster with m=2,3 and 4 are studied and it is shown in Figure 4.3. The DOS states are located in the energy range from -13.0 to -0.0 eV, while Ga (S P) states are distributed in the unoccupied region. These clusters can be understood on the structural stability of the molecular orbital theory.

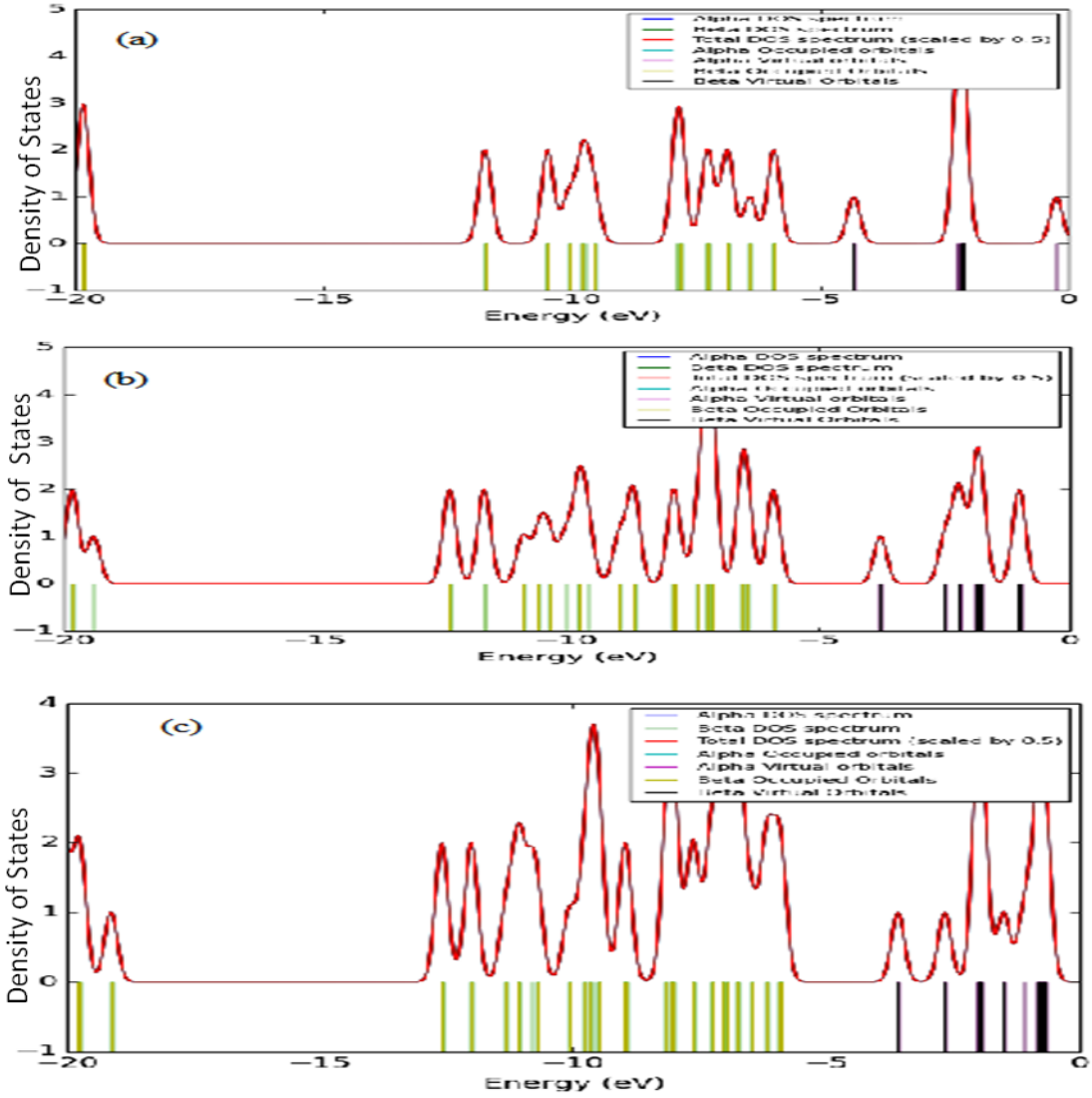

Figure 4.3: Total and partial DOS of $(Ga_3N_3)_m$ cluster with m=2(a), m=3(b), and m=4(c).

4.3.4. Fragmentation of condensed cluster

The fragmentation energy per atom (FE) is calculated by using the formula:

$$FE = \frac{\mathrm{E[(Ga3N3)n] + E[(Ga3N3)m - n] - E[(Ga3N3)m]}}{6m}$$

The $(Ga_3N_3)_m$ may be divided into the following two pieces of a possible cluster: (1,m -1), (2,m-2), (3-m-3), (4, m-4). FE are calculated and shown in Figure 4.4

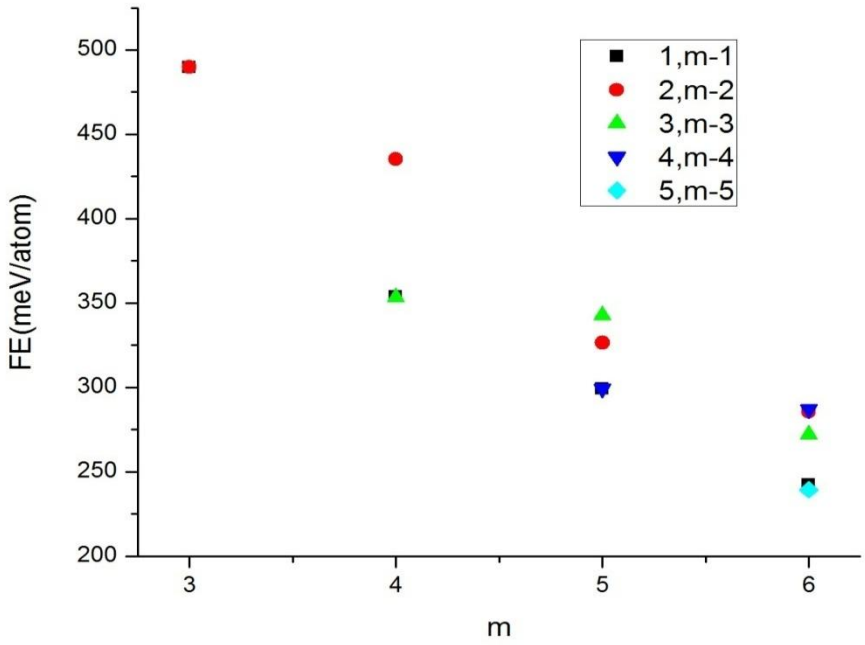

Figure 4.4 show that when a cluster FE decreases, m values increases. This infers that the condensed clusters under the influence of temperature breaks into smaller units on the order of 450K.

We condensed the second derivative of the total energy (Δ^2E) of the cluster and the cluster reveals about the structural stability and it is reported in Figure 4.5. Our calculations shows that the Δ^2E of $(Ga_3N_3)_3$ cluster shows the maximum value, and high structural stability of this cluster.

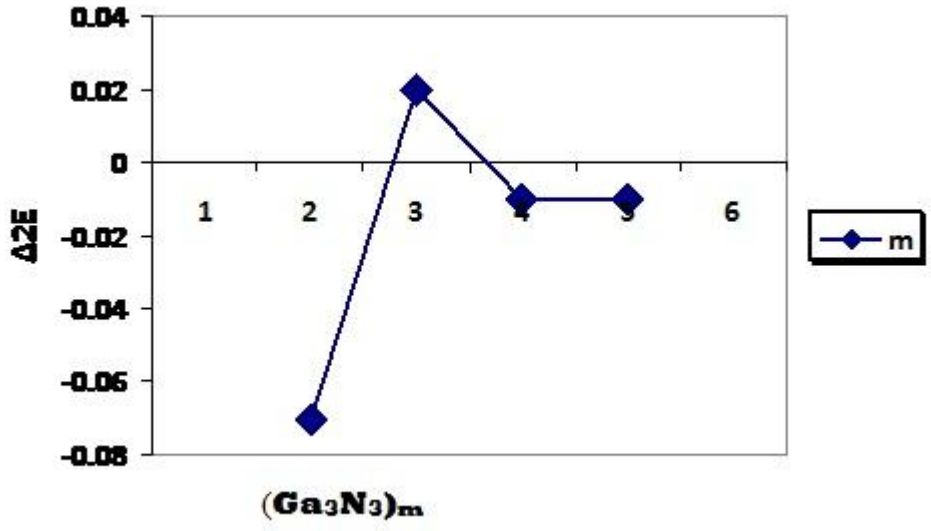

Figure 4.5: Shows the variation of second derivative of energy of $(Ga_3N_3)_m$ cluster with respect to m. The calculated value by using the formula Δ^2E= E (m+1) +E (m-1) - 2E (m).

4.4. Conclusion

The study of the structural stability and electronic properties of $(Ga_nN_n)_m$ (n = 1-4, m = 1-6) cluster by implementing first principle calculations is studied in detail. This structural stability of cluster is explained by the DOS. It is estimated that it creates stability due to sp- hybridization, along with the different-sized condensed clusters, $(Ga_3N_3)_m$ that is found to be more stable. Further, the electronic properties of cluster are shown to have lower energy gap as compared to the bulk GaN system. It could be used as interesting photo-catalytic applications. Our calculations also revealed that more concentrated cluster of structural stability 1- D nanorod is obtained.

References

1. G. Dresselhaus, M. S. Dresselhaus, P. Eklund, *Science of Fullerenes and Carbon Nanotubes*; Academic Press: San Diego, CA, 1995.
2. Y. Feldman, E. Wasserman, D. J. Srolovitz, R. Tenne, *R. Science,* **267**, 222 (1995).
3. **V. Nicolosi, P. D Nellist, S. Sanvito, E. C. Cosgriff, S. Krishnamurthy, W. J. Blau, M. L. H. Green, D. Vengust, D. Dvorsek, D. Mihailovic, G. Compagnini, J. Sloan, V. Stolojan, J. D Carey, S. J Pennycook And J. N. Coleman,** *In* ***Advanced Materials*****, 19, 543 (2007).**
4. I. Laraib, J. Karthikeyan, P. Murugan, *Phys. Chem. Chem. Phys.,* **18**, 5471 (2016).
5. J. H. Zhan, X. G. Yang, W. X. Zhang, D. W. Wang, Y Xie, Y. T. Qian, *J. Mater. Rese.,* **03**, 629(2015).
6. J. Xu, X. Zhuang, P. Guo, Q. Zhang, W. Huang, Q. Wan, W. Hu, X. Wang, X. Zhu, C. Fan, Z. Yang, L.Tong, X. Duan, A. Pan, *Nanowires Nano Lett.,* **12**, 5003 (2015).
7. H. Zhang, D.Yang, Yujie Ji, X. Ma, J. Xu, D. Que, *ACS Nano,* **4**, 91 (2010).
8. H. Zhang, X.Y. Ma, J. Xu, D. R. Yang, *J. Cryst. Growth*, **263**, 372 (2004).
9. A. E Saunders, A. Ghezelbash, P. Sood, B. Korgel, *langmure,* **24**, 9043 (2008).
10. A. S. Barnard, H. Xu, *J. Phys. Chem. C,* **111**, 18112 (2007).
11. S. Nakamura, G. Fasol, The blue laser diode (Springer, Berlin, 1997).
12. S. Nakamura, M. Senoh, N. Iwasa, S. Nagahama, *Appl. Phys. Lett.,* **67,** 1868 (1995).
13. H. Bar-Ilan, S. Zamir, O. Katz, B. Meyler, J. Salzman, *Materials Science and Engineering A,* **302,** 14 (2001).
14. R. J. Trew, M. W. Shin, V. Gatto, *Solid-State Electronics,* **41,** 1561 (1997).
15. S. J. Pearton, F. Ren, A. P. Zhang, K. P. Lee, *Materials Science and Engineering: R. Reports*, **3**, 55 (2000).
16. R. de Paiva, J. L. A. Alves, R. A. Nogueira, J. R. Leite, L. M. R. Scolfaro, *Journal of Physics,* **34**, 647
17. T. Dietl, H. Ohno, F. Matsukura, J. Cibert and D. Ferrand, *Science,* **287,**

1019 (2000).

18. T. Jungwirth, J. Sinova, J. Masek, J. Kucera, A.H. MacDonald, *Rev. Mod. Phys.* **78,** 809 (2006).
19. J. Goldberger, R. He, Y. Zhang, S. Lee, H. Yan, H.J. Choi, P. Yang, *Nature.*, **422,** 599 (2003).
20. S. M. Lee, Y. H. Lee, Y. G. Hwang, J. Elsner, D. Porezag, T. Frauenheim, Phys. Rev. B, **60**, 7788 (1999).
21. J. J. Bel Bruno, *Heteroatom Chem.*, **11**, 281 (2000).
22. A. K. Kandalam, R. Pandy, M.A. Blanco, A. Costales, J. M. Recio, J. M. Newsam, *J. Phys. Chem. B,* **104,** 4361 (2000).
23. A. K. Kandalam, M. A. Blanco, R. Pandy, *J. Phys. Chem. B,* **105,** 6080 (2001).
24. A. K. Kandalam, M. A. Blanco, R. Pandy, *J. Phys., Chem. B,* **106**, 1945 (2002).
25. A. K. Kandalam, M. A. Blanco, R. Pandy, *J. Phys. Chem. B,* **107**, 4508 (2003).
26. B. Song, P. L. Cao, *Phys. Lett. A,* **300,** 485 (2002).
27. B. Song, P. L. Cao, B. X. Li, *Phys. Lett. A,* **315**, 308 (2003).
28. Ch. Chang, A. B .C. Patzer, E. Sedlmayr, T. Steinke, D. Sulzle, *Chem. Phys. Lett,*. **350,** 399 (2001).
29. Jijun Zhao, Baolin Wang Xiaolan, Zhou Xiaoshuang Chen, Wei Lu, *Chem. Phys Lett.*, **422,** 170 (2006).
30. D. L. Strout, *J. Phys. Chem. A*, **104**, 3364 (2000).
31. D. L. Strout, *J. Phys. Chem. A*, **105,** 261 (2001).
32. J. M. Matxain, J. M. Ugalde, M. D. Towler, R. J. Needs, *J. Phys. Chem. A*, **107,** 10004 (2003).
33. H. S. Wu, F. Q. Zhang, X. H. Xu, C. J. Zhang, H. J. Jiao, *J. Phys.Chem. A,* **107,** 204 (2003).
34. R. Hoffmann, solid and surface: A Chemiet's View on Bonding in Extended Structures. *VHC publisher New York,* 1988.

CHAPTER 5

Stability of CdxSx±4 fullerene like micro clusters predicted from ab initio DFT calculations

5.1. Introduction

One-dimensional (1D) nano clusters such as nanowires [1-2] and nanotubes [3] has lead to a growing interest due to their importance in scientific research and their potential technical applications.[4-9] It is recognized that 1D nano clusters are ideal systems for searching a large number of novel devices at the nanoscale with the size dependent functional properties. The approaches of classical mechanics are inadequate and incompetent to study the micro-clusters because of their atomic scale dimensions. So the involvement of quantum mechanics to map theoretical with experimental results plays an important role. Availability of present day state of the art computational resources and techniques have enabled us to model and investigate these clusters easily & accurately.

This 1D structure is interconnected and expected to play a very important role as a key in nanoscale electronics, optoelectronics [10-11], electrical units and electrical equipments.[12-13] A series of 1-D assemblies of various sizes were tetrahedral CdS groups which were synthesized [14] using the bi-functional covalent legend groups. In this context, basic tetrahedral units were obtained by fragmenting the bulk phase of quartzite or zinc blends. In fact, clusters are almost degenerate [15], both bulk phases and their stability increases after adsorption of organic legends.[16-17] CdS II-VI semiconductor, an important discovery was the first semi conductor that found immediate application in light emitting. Perhaps application in nonlinear optical devices, flat panel display, photo catalysts, solar cells, electro chromic windows,

photo detectors and organic applications, electronic and optoelectronic materials as one of the most important diode laser, logic gates etc. are studied.[18-19] It also has a wide range of applications in telecommunication, optical wavelength, lasing material, data storage and near field optical lithography.[20-22]

Fullerenes have a special hollow cage like structure that resembles these clusters. Only Pentagonal and hexagonal rings form the fullerene structure. By using the different permutations of N atoms in the fullerene structure comprising of pentagon and hexagon, several isomers are possible with different arrangements for the collection of the atom with 12 pentagons and (N-2)/10 hexagonal that can be constructed.[23] After the carbon fullerenes, the interest has now inclined towards the research of new fullerene like structures formed by other elements or combination of different elements because fullerene structure offers several unique properties that can be utilised in different nano-technology applications like synthesis of nano-structured semiconducting magnets, optoelectronic devices etc.[24]

Mass spectroscopy and laser vaporization technology are being used for the manufacture of semiconductor clusters. A great interest in the field of clusters has evolved because of the advancement in computational and theoretical techniques along with the development of advanced spectroscopic techniques.

Several experiments have been performed from II-VI group in search of different semiconductor materials.[25-26] II-VI group compounds have high electron mobility such as CdS, therefore the electronics industry may be inclined to replace Si. CdS is a direct band gap semiconductor with band gap energy of ~ 2.42 eV. In the recent years, several experimental and theoretical investigations of CdS clusters have been performed. These studies have enabled us to know more about the structural stability, reactivity and nature of bonding in these clusters. Thus the Cadmium Sulfide cluster

may exhibit different bonding characteristics than their bulk counterpart which have the same bonding because of strong anion-anion interaction.[27] The investigation of such clusters based on first principles methods has proven to be very useful for study. The first principle technique is used to explain the physical properties of the cluster via computational scheme that requires very precise size, charge or cluster variables such as the stoichiometric composition which depends on these variable parameters.

The present work is based on the study of the structures, stabilities and electronic properties of $Cd_{x\pm4}S_{x\pm4}$ clusters possessing fullerene like hollow cage structures. Various possible structures of CdS fullerene depend upon the different composition of Cd and S which are governed by the formula $Cd_{x\pm4}S_{x\pm4}$, where x is the number of single type of atom present in the cluster. The value of x is varied and corresponding clusters so formed were studied.

5.2. Computational Method

The geometries of fullerene like $Cd_{x\pm4}S_{x\pm4}$ structures were made using Gauss View 5.0. Thereafter the geometries were optimized using Gaussian 09 program suite. The method incorporated to optimize and study the structures and characteristics of these clusters is DFT with the unrestricted B3LYP exchange-correlation functions.[31-32] To describe the geometrical and bonding characteristics for heavy atoms, the basis set with effective core potential, LanL2DZ [33] is used to study the fullerenes formed by Cadmium (Cd) and Sulfide (S) atoms. In this basis set, the electronic configuration for Cd is $4s^2\ 3d^{10}\ 4p^6 5s^2 4d^{10}$ and for S is $2s^2\ 2p^6\ 3s^2\ 3p^4$. The interaction between core and valence electron was handled by Torullier-Martins norm conserving pseudo potential [34] in their fully separable form.[35] In Cd pseudo potential, d orbitals are also included in the valence configuration.

All the geometries of fullerenes considered for the study were subjected to full geometry optimizations without any restrictions. The force component in each atom is less than 0.01 eV/Å which is calculated using a conjugate gradient algorithm. The energy gap i.e the highest occupied molecular orbital and lowest unoccupied molecular orbital levels and the binding energy were used to determine the stability of the system.

5.3. Results and Discussion

To determine the stability of Cadmium Sulfide fullerenes, cohesive energy, energy change in a model reaction, energy gap in electronic structure were considered. The structures with lower energies are energetically more favourable and stable than the systems with higher values. The Gaussian works in gaseous medium. So the lower energy of the cluster is utilised to decide which systems are chemically more stable. Smaller energy gap values are used for lower reactivity and thus contribute in the enhanced chemical stability.

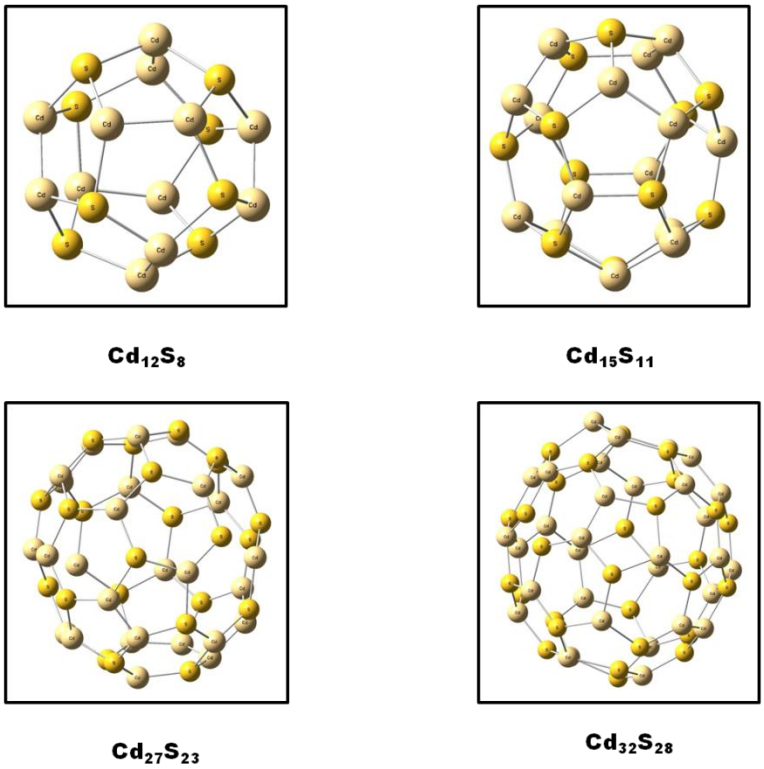

Figure 5.1: The Cd-rich Cd_xS_{x-4} non-IPR fullerenes. The shared edges of the pentagon's are occupied by Cd atoms.

The optimized atomic structure of Cd-rich Cadmium Sulfide fullerenes with the formula of $Cd_{x+4}S_x$ are shown in Figure.5.1 for $8 \leq x \leq 28$ where the light (creamish white) color represents the Cd atoms and yellow color represent the S atom. In each structure there are 12 pentagons and six edges are shared by adjacent pentagons. The Figure 5.1 shows the isomers where Cd and S atoms could be placed to give the minimum number of homo-nuclear bonds. The common edges of adjacent pentagons consist of Cd-Cd bonds. However there are no homo-nuclear bonds. In Cd-rich Cadmium Sulfide fullerenes, Cd-Cd bond length remains 2.81-2.93 Å, Cd-S bond length are in the range of 2.4-2.53 Å. The bond length decides the size of the cluster. Bond angles of Cd-S-Cd are in the range 95^0- 107^0, while the S-Cd-S bond angle tends to have higher values of 114^o-143^o. The S-Cd-Cd bond angle at the shared pentagon edge is $\approx 111^0$. The S-rich cadmium sulfide fullerenes are shown in

Figure.5.2. In S rich fullerenes, the shared edges of adjacent pentagons consists of S-S bonds. In both Cd-rich and S-rich fullerenes, sulfur atoms tend to protrude out of the cluster. The Cd-S-Cd bond angle values are between 105^0- 122^0 and for the S-Cd-S bond angle values are in the range of 118^0-130^0. The S-S bond length varies in the small range of 2.20-3.38 Å in S-rich fullerenes and the Cd-S bond length are in the range of 2.56-2.71 A^o. The Cd-S-S bond angle at the shared edges of pentagons is $\approx 109^o$, which is smaller than the bond angles for the shared edge in Cd-rich fullerenes. All the structures shown in Figure 5.1 and 5.2 are relaxed up to much minimised residual force values, the Cadmium Sulfide fullerenes correspond to local minima in the energy landscape. This information alone is not sufficient to suggest better stoichiometry for the stability. So we compare total energy of fullerenes in sequence to calculate the relative energetic stabilities of various compositions.

The binding energy per atom for cadmium sulfide fullerenes with general formula of Cd_xS_y is shown in Figure.5.3a, where x+y, gives the total number of atoms in a fullerene. The binding energy of Cd-rich fullerene decreases or increases with the increasing size of cluster monoatomotically. On the basis of binding energy, the S-rich fullerenes are more stable than the Cd-rich fullerenes. This was opposite to our naive expectation depending upon the atomic structure, Cd- rich fullerenes acquire the shape of a sphere, and these are expected to be more favourable than the S-rich fullerenes. However, even for CdS surface, S atoms with ground state structure is raised above the surface. A similar criterion remains for our cadmium sulfide fullerenes. Although the cluster is produced from the bulk geometry, it may be optimized to get better cohesive energy results. So, the Cd_xS_y fullerenes are energetically as stable as their counterparts.

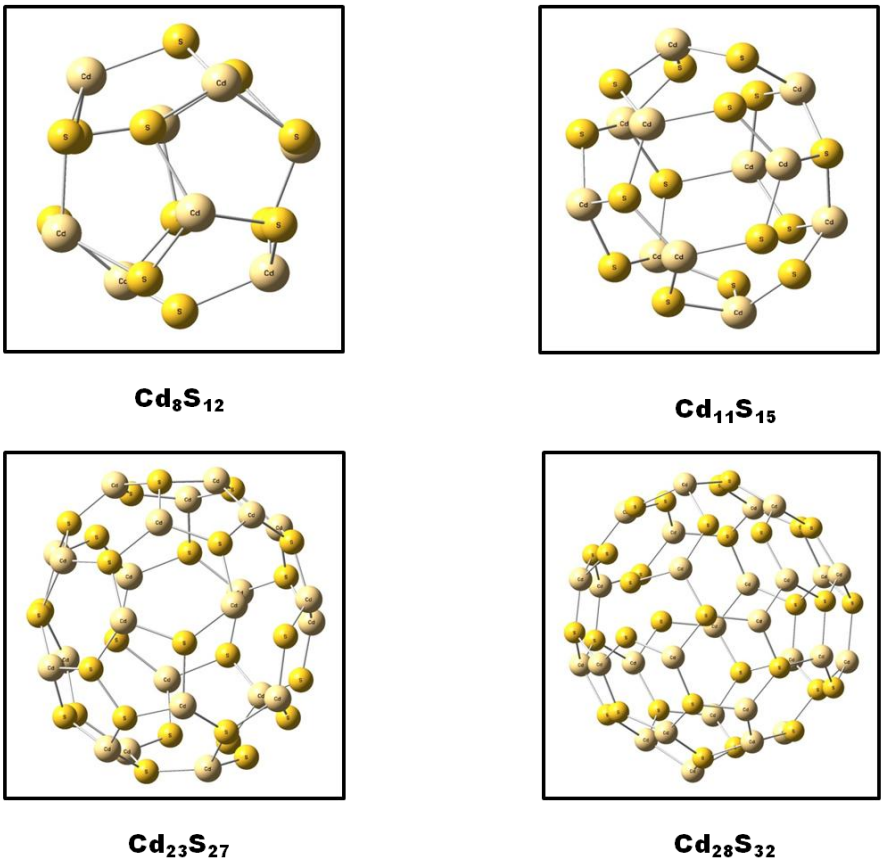

Figure 5.2: The S-rich Cd_xS_{x+4} non-IPR fullerenes. The shared edges of the pentagons are occupied by S atoms.

(a)

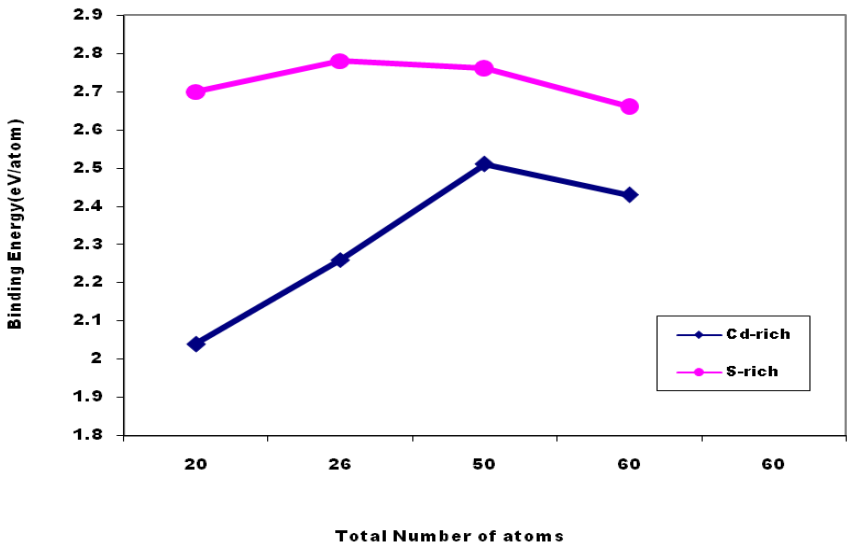

(b)

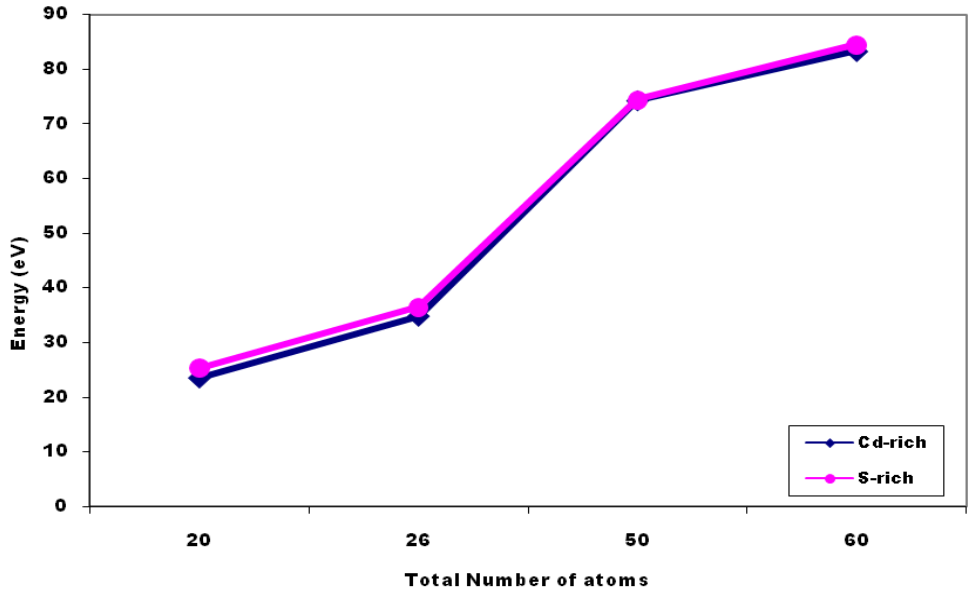

(c)

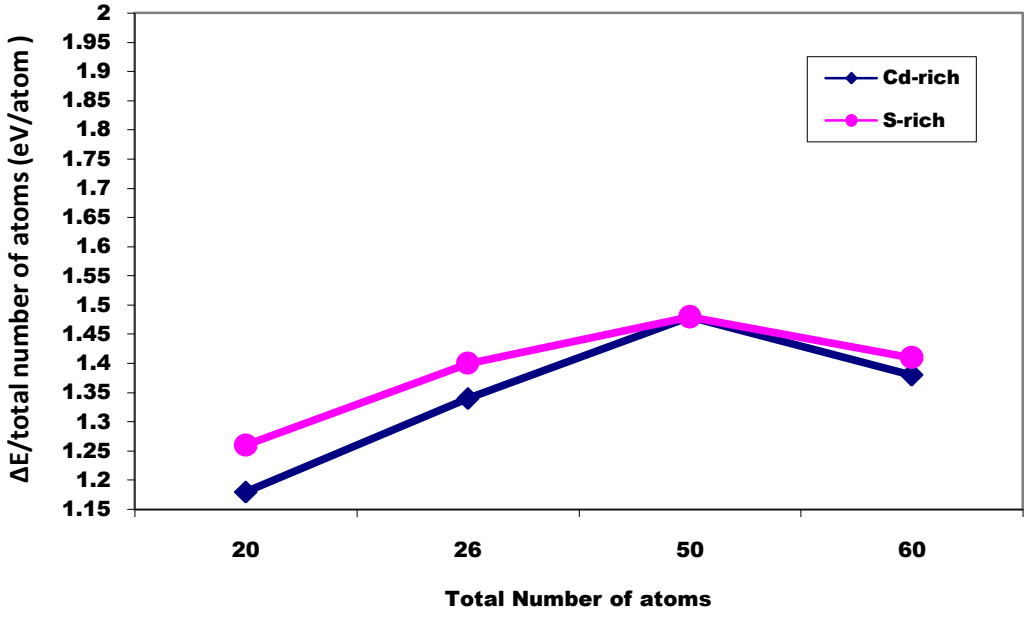

Figure 5.3: The energetics of Cd_xS_y non-IPR fullerenes in Cd-rich fullerenes (x=y+4) and in S-rich fullerenes (y= x+4) are shown. (a) Binding energy of the bulk Cd_xS_y fullerenes as a function of the total number of atom. (b) The reaction energy during a synthesis of the fullerenes starting from bulk CdS and S_2 gas .the reaction energy per atom is shown in(c).

In order to comprehend the energetic, let us consider the energies of possible reaction utilising bulk CdS and S_2 gas as reactants or products, depending on the stoichiometric were considered. The Cd –rich fullerenes are supposed to be processed by the model reaction (n+4) CdS $\rightarrow$ $Cd_n+4S_n+2S_2$ and S-rich fullerenes production is supposed to be processed by conserving S_2 gas in $n+4CdS+2S_2$ Cd_nS_{n+4} reaction. The rate of this reaction may be regulated by altering concentration of S_2 above the CdS bulk sample. The total energy change ΔE or the difference between the total energy of product and reactant is always positive. In another way, the above reaction is endothermic. Total-energy change ΔE is shown in Figure 5.3b as a function of total number of atoms (x+y) in CdxSy fullerenes. The energy for Cd-rich Cadmium Sulfide fullerenes is higher than the S-rich fullerenes. It has been examined that there is a difference between the reaction energies for Cd-rich and S-rich fullerenes. The energy change per atom ΔE/(x+y) is shown in Figure 5.3c. On the basis of calculated reaction energy values, the formation energy per atom for Cd-rich fullerenes lies between 1.18eV to 1.48 eV and an S-rich fullerene is between 1.26 eV to 1.48 eV.

5.3.1: Electronic structure of the Cadmium Sulfide fullerenes

The energy gap E_g, which is the difference between lowest–unoccupied energy level and highest-occupied energy level as a marker for chemical stabilities of the fullerenes is taken into consideration. The Figure 5.4 clearly shows the variation of energy gap on increasing the number of atoms. The Cd-rich fullerenes have Eg of 1.34-2.05 eV, while the Eg of S-rich fullerenes are comparatively lower in the range 1.82-2.03eV.

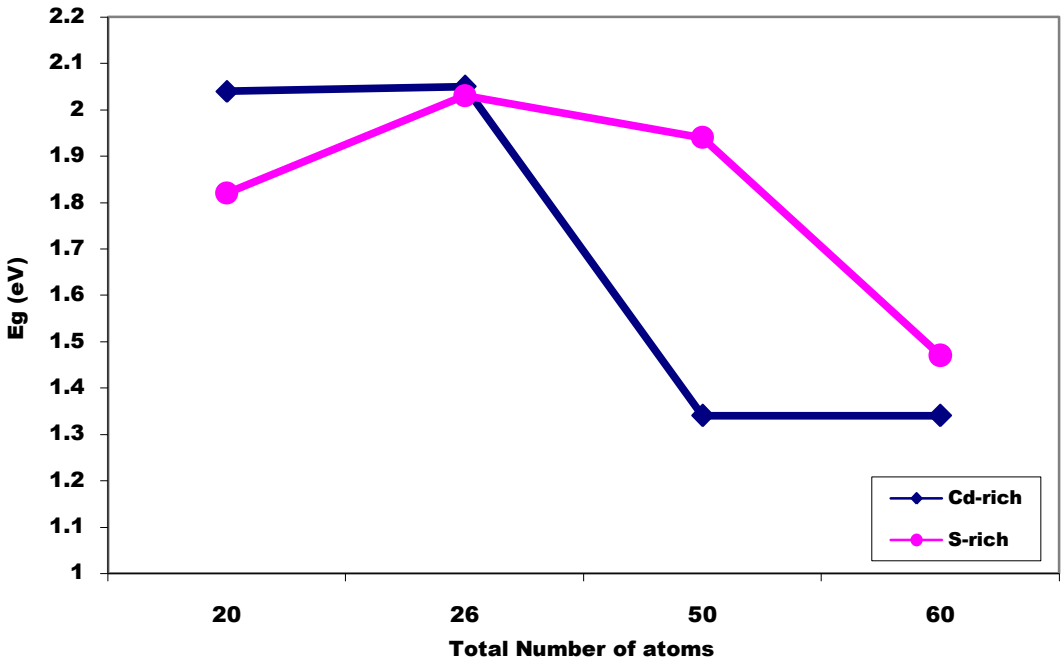

Figure 5.4: The energy gap in the electronic structure of Cd_xS_y non-IPR fullerenes.

5.4. Conclusions

The atomic structure and stability of cadmium Sulfide fullerenes ($Cd_xS_{x\pm4}$) is studied by using DFT method. It has been found that the hollow Cadmium Sulfide fullerenes are stable when the pentagon edges are shared which reduces the number of homo-nuclear bonds. The energetics and the energy gap in electronic structure as indicators, for the stability of Cadmium Sulfide fullerenes are also investigated. The study predicts that these clusters are stable. The stability of the cluster increases when the number of homo-nuclear bonds in the cluster is less.

It is found that the binding energy of S-rich fullerene gets saturated when the size of the cluster is beyond 40 atoms. Therefore, the shared edges of adjacent pentagons, S atoms, bond angle are satisfied by only a small strain energy input. The bond lengths are not adequate to differentiate between the Cd-rich and S-rich fullerenes so this might be the possible reason for the lower total energy in S-rich fullerenes and that S-S bond are energetically more favorable than Cd-Cd bonds. This conclusion is in

agreement with the findings that S atom clusters in small cadmium sulfide fullerenes clusters (S- containing clusers) are more stable.

References

1. D. Kumar, A. Trivedi, D. Kumar, *Advanced Materials Science*, **1**, 1 (2017).
2. F. X. Gu, Z.Y. Yang, H. K. Yu, J. Y. Xu, P. Wang, L. M. Tong, A.L. Pan, *J. Am. Chem. Soc.*, **133**, 2037 (2011).
3. H .Zhang, X.Y. Ma, J. Xu, D.R. Yang, *J. Cryst. Growth*, **263**, 372 (2004).
4. C. M. Lieber, Z. L. Wang, *M. R. S. Bull.*, **32**, 99 (2007).
5. X. S. Fang, Y. Bando, U.K. Gautam, T.Y. Zhai, H. B. Zeng, X. J. Xu, M. Y. Liao, D. Golberg, *Crit. Rev. Solid State Mat. Sci.*, **34**, 190 (2009).
6. D. Golberg, Y. Bando, C. C. Tang, C. Y. Zhi, *Adv. Mater.*, **19**, 2413 **(**2007).
7. Z. J. Gu, Y. Ma, T.Y. Zhai, B. F. Gao, W. S. Yang, J. N. Yao, *Chem. Eur. J.*, **12**, 7717 (2006).
8. M. Law, J. Goldberger, P. D. Yang, *Rev. Mater. Res.*, **34**, 83 (2004).
9. C. N. R. Rao, R. Voggu, A .Govindaraj, *Nanoscale,* **1**, 96 (2009).
10. C. J. Barrelet, A. B. Greytak, C. M. Lieber, *Nano Lett.*, **4**, 1981 (2004).
11. J. L. Zhao, J. A. Bardecker, A. M. Munro, M. S. Liu, Y. H. Niu, I. K. Ding, J. D. Luo, B. Q. Chen, A. K. Y. Jen, D. S. Ginger, *Nano Lett.*, **6**, 463 (2006).
12. Y. N. Xia, P. D. Yang, Sun, Y. G. Wu, B. Mayers, B. Gates, Y. D. Yin, F. Kim, H. Q. Yan, *Adv. Mater.*, **15**, 353 (2003).
13. T. Y. Zhai , X. S. Fang , Y. Bando , Q. Liao , X. J. Xu , H. B. Zeng , Y. Ma , J. N. Yao , D. Golberg , *ACS Nano*, **3**, 949 (2009) .
14. N. F. Zheng, X. H. Bu, H.W. Lu, L. Chen, P. Y. Feng, *J. Am. Chem. Soc.*, **127**, 14990 (2005).
15. J. O. Joswig, M. Springborg, G. Seifert, *J. Phys. Chem. B,* **104**, 2617 (2000).
16. N.V. Soloviev, A. Eichhofer, D. Fenske, U. Banin, *J. Am. Chem. Soc.*, **123**, 2354 (2001).
17. N. F. Zheng, X. H. Bu, H.W. Lu, L. Chen, P. Y. Feng, *J. Am. Chem. Soc.*, **127**, 14990 (2005).
18. T. Y. Zhai, X. S. Fang, Y. Bando, B. Dierre, B. D. Liu, H. B. Zeng, X. J. Xu, Y. Huang, X. L. Yuan, T. Sekiguchi, D. Golberg, *Adv. Funct. Mater.*, **19**, 2423 (2009).
19. M. Zhang,, T. Y. Zhai, X. Wang, Q. Liao, Y. Ma, J. N. Yao, *J. Solid State Chem.*, **182**, 3188 (2009).
20. T. Y. Zhai, X. S. Fang, Y. Bando, Q. Liao, X. J. Xu, H. B. Zeng, Y. Ma, J. N. Yao,

D. Golberg, *A.C.S. Nano*, **3**, 949 **(**2009**)**.

21. X. F. Duan, Y. Huang, R. Agarwal, C. M. Lieber, *Nature*, **421**, 241 (2003).
22. N. V. Hullavarad, S. S. Hullavarad, P. C. Karulkar, *J. Nanosci. Nanotec.*, **8**, 3272 (2008).
23. M. Galica, R. Buczko, *Phys. Status Solidi RRL.*, **7**, 739 (2013).
24. L. R. Liu, H. J. Zhu, Z. F. Liu, P. Wu, *Chin. Phys. B*, **21**, 123601 (2012).
25. M. Galica, R. Buczko, *Phys. Status Solidi RRL.*, **7**, 739 (2013).
26. P.W. Fowerand, D. E. Manolopoulos, An atlas of fullerenes, *Oxford:Clarendon Press*, (1995).
27. R. Schafer, J. A. Becker, *Phys. Rev. B.*, **54**, 10296 (2004).
28. L. Wang, L. P. F. Chibante, F. K. Tittel, R. F. Curel, R. E. Smalley, *Chem. Phys. Lett.*, **172**, 335 (1990).
29. P. Sarkar, M. Springborg, *Phys. Rev. B.*, **68**, 235409 (2003).
30. C. Ghosh, S. Pal, B. Goswami, P. Sarkar, *Chem. Phys. Lett.*, **407**, 498 (2005).
31. B. Brena, L. Ojamae, *J. Phys. Chem. C*, **112,** 13516 **(**2008).
32. A. D. Becke, *Phys. Rev. A*, **38**, 3098 (1988).
33. W. Lee, R. G. P. Yang, *Phys. Rev. B*, **37**, 785 (1988).
34. R. W. Wadt, J. P. Hay, J. *Chem. Phys.*, **82**, 284 (1985).
35. P.W. Fowler, K. M. Rogers, G. Seifert, M. Terrones, H. Terrones, *Chem. Phys. Lett.*, **299**, 359 (1999).

CHAPTER 6

Quantum chemical studies of Phosphorus doped ZnO cluster stability and electronic properties by using ab-inito method

6.1. Introduction

The clusters are finite aggregates of atoms or molecules containing few to a hundred of atoms. They may consist of identical molecules or atoms, or two or more different types of atoms. They may be synthesised by several experimental methods such as molecular beam, vapour phase as in colloidal suspension.[1] Zinc oxide (ZnO) materials are n-type semiconductor have wide band gap 3.37 eV, which exhibits the Wurtzite structure. ZnO in its wurtzite lattice belongs to space group P63mc characterized by two subunits interconnected by Zn^{2+} and O^{2-} ions where zinc is surrounded by tetrahedral oxygen ions and vice versa. Today, there is a great deal of interest in research toward making p-type ZnO that has potential applications in laser diodes emitting ultraviolet light.[2] The ZnO cluster due to its low ionization energy, ionic radius, easy availability, low toxicity and easy handling is widely used in optoelectronic devices such as photo detectors, gas sensors, light emitting diodes, varistors, piezoelectric devices, batteries, fuel cells, photocells as a catalyst.[3-9] ZnO is a very good functional material with different nanostructures existing in various forms, such as nanotubes [10], nanowires [11], nanoribbons [12], nanorods [13], nanorings [14], nano helix [15] and nano boxes [16] that have been extensively investigated. The bandgap of this material is comparable with wide bandgap materials. Many theoretical studies have been reported on ZnO nanoclusters.[17-19] ZnO are composed of stable nanosized crystals Wurtzite. Bahnemann et al.[20] reported that no clear transition is found between the cluster and the size of the quantum dot ZnO. Accurate structural determination of small particles with sizes

below 10 nm, remains a problem in the standard techniques likes X-ray diffraction that could not be satisfactorily resolved. By applying the new techniques of refinement [20-23] ZnO becomes an important material for solar energy applications with improved optical properties. It is a promising multifunctional material with a wide range of technological applications including electrical and light emitting devices.[24-25] The ZnO cluster has a potential application in solar energy conversion . [26] ZnO has been recognized as a valuable optical material in the blue-UV region [27] and has a large exciton binding energy. Very few works are reported based on the density functional theory (DFT) on ZnO clusters. DFT is preferable for application in materials science because it can handle bulk and structural calculations.[28] One of the main advantages of DFT is to tailor the properties of materials without the feeding of the experimental data with a low computational cost relative to other method.[29] To understand extremely efficient optoelectronic devices, it is mandatory to have high-quality single –crystalline p-type ZnO. Recently, enormous effort has been devoted in fabricating p-type ZnO via thin films using I and group V element as p-type dopants.[30] There is a good scope to work on p-type ZnO nanowires (substituting of P and N) as very few works are reported in this field.[31] To study the structural stability of ZnO micro clusters, Phosphorus is added as an impurity. Novel features of the present work are due to enhancement of the p-type character of ZnO micro cluster by substituting P atom in cluster, $Zn_xO_{x-1}P$ micro cluster has been simulated with x=2-5 for different structures (linear 3D, and rings). Their structural stability, dipole moment, binding energy, HOMO-LUMO energy gap, Ionization potential (IP) and Electron affinity are studied in detail.

6. 2 Computational Detail

All Phosphorus doped Zinc Oxide ($Zn_xO_{x-1}P$) clusters for x=2-5 reported in this work are optimized by the B3LYP method as implemented in Gaussian 09 package.[32] Various possible structures for each $Zn_xO_{x-1}P$ clusters are modelled and the stable structure is identified from the energetic. The energy minimization and dipole moment have been calculated by the simulation with Beckes three-parameter hybrid functional combined with Lee-Yang-Parr correlation functional (B3LYP) method with 6-31G basis set [33-35]. Gauss Sum3.0 is used to plot the density of states (DOS) spectrum.

6.3 Results and Discussion

6.3.1 Structure of $Zn_xO_{x-1}P$ micro cluster.

The relevant parameters like energy, dipole moment values and point group of $Zn_xO_{x-1}P$ cluster for (x=2-5) are reported in Table 6.1.

Table 6.1 Illustrate the various models of different cluster size.

Model	Cluster Size	Energy (Hartrees)	Dipole moment (Debye)	Point group
Linear	2	-3974.727373	2.01	Cs
	3	-5829.099738	2.03	Cs
	4	-7683.472522	2.15	C1
	5	-9537.843967	2.14	Cs
Ring	2	-3974.724212	0.28	Cs
	3	-5829.141279	0.29	Cs
	4	7683.537652	0.29	Cs
	5	-9537.922905	0.34	Cs
3D	3	-5829.141279	0.30	C1
	4	-7683.478453	1.05	C1
	5	-9537.903002	1.90	C1

The above tabulated values are as per the structure. The energy decreases when cluster size increases. Also when the number of atoms in the cluster is increased, the stability increases. From energy values, it can be said that all the structures of Zn_5O_4P have less energy and are most stable. The possible structural diagram of $Zn_xO_{x-1}P$ clusters for (x=2-5) are shown in Figure 6.1(a) - 6.4(c). The Zn_2O_1P cluster has two isomers as shown in Figure 6.1 (a) & Figure 6.1(b): linear and ringed structures. In these isomers, the ring structure has lower energy and shows square planar geometry. The bond length between Zn and P atom in linear structure is about 2.32 Å whereas in the ring structure it is 2.43 Å.

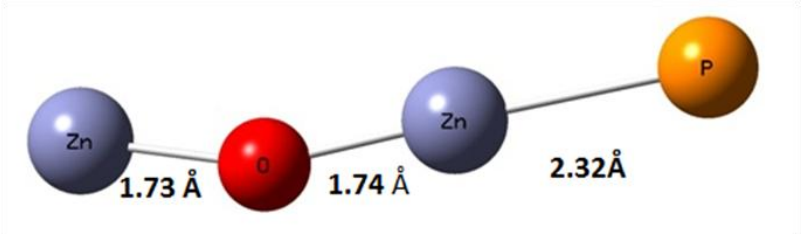

Figure 6.1 (a): B3LYP/6-31G optimized geometrical structure of Zn_2O_1P linear clusters.

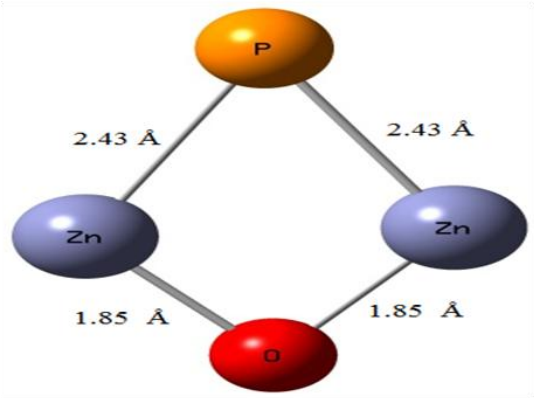

Figure 6.1(b): B3LYP/6-31G optimized geometrical structure of Zn_2O_1P Ring clusters.

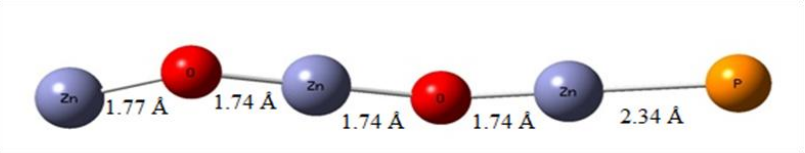

Figure 6.2(a): B3LYP/6-31G optimized geometrical structure of Zn_3O_2P linear clusters.

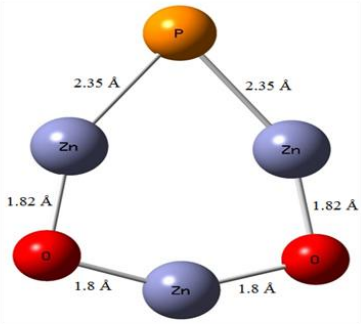

Fig. 6.2(b): B3LYP/6-31G optimized geometrical structure of Zn_3O_2P Ring clusters.

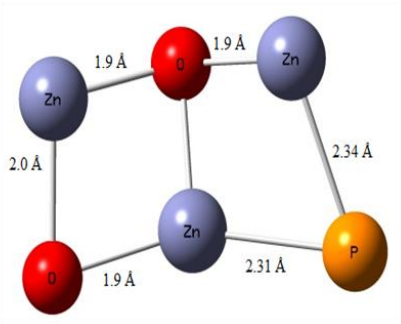

Fig.6.2(c): B3LYP/6-31G optimized geometrical structure of Zn_3O_2P 3D clusters

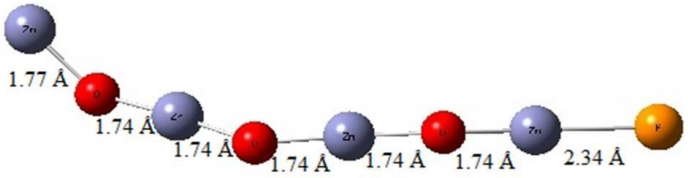

Figure 6.3. (a): B3LYP/6-31G optimized geometrical structure of Zn_4O_3P linear clusters.

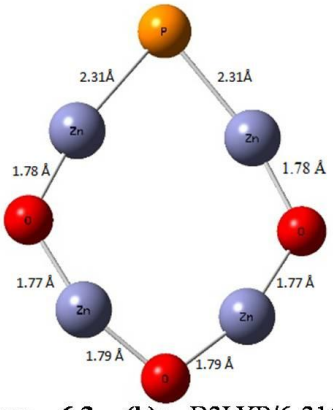

Figure 6.3. (b): B3LYP/6-31G optimized geometrical structure of Zn_4O_3P Ring clusters.

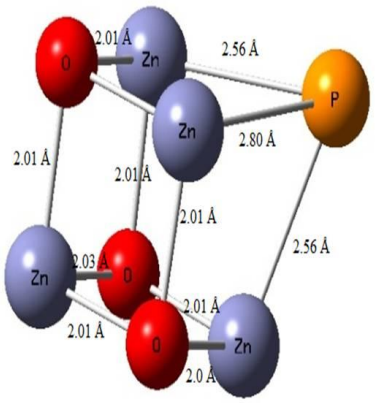

Figure 6.3. (c): B3LYP/6-31G optimized geometrical structure of Zn_4O_3P 3D clusters.

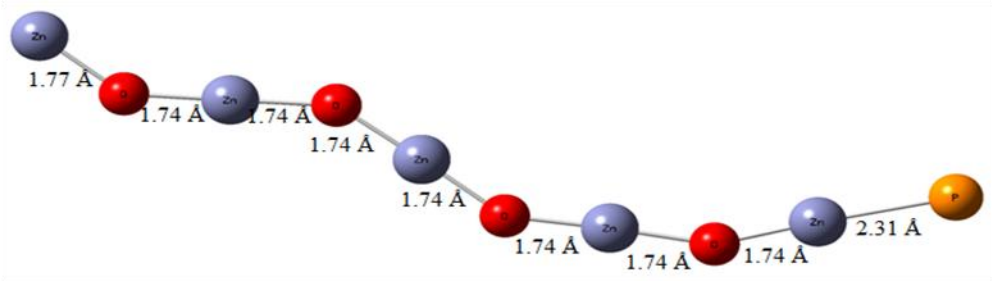

Figure 6.4 (a): B3LYP/6-31G optimized geometrical structure of Zn_5O_4P linear clusters.

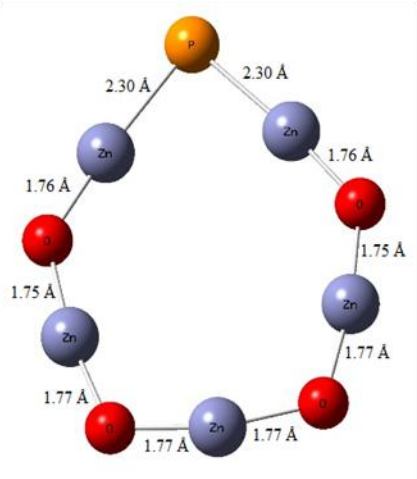

Figure 6.4 (b): B3LYP/6-31G optimized geometrical structure of Zn_5O_4P Ring clusters.

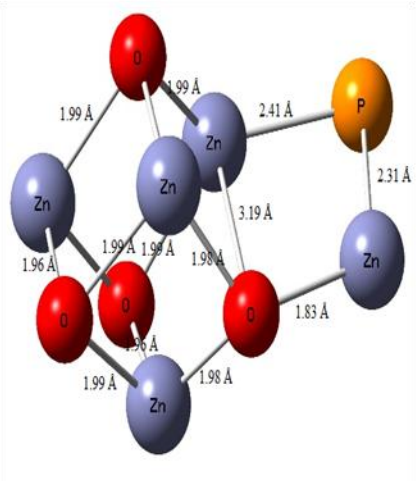

Figure 6.4 (c): B3LYP/6-31G optimized geometrical structure of Zn_5O_4P 3D clusters

Figure 6.1- 6.4: Depicts the various optimized geometries of $Zn_xO_{x-1}P$ clusters.

There are three possible isomers constructed for Zn_3O_2P clusters shown in Figure 6.2(a) – Figure 6.2(c). The optimized bond length for Zn-P and Zn-O is about 2.31 Å and 1.74Å. For linear and 3D structures it is 2.31 Å and 1.9 Å respectively. In the case of ring structure, the bond length between Zn-P for the optimized geometry is 2.35 Å. The Zn_4O_3P structures show three different isomers, among which the linear structure has least energy. The energy difference between linear and 3D is about 0.00593 Hartrees with equal bond lengths. In ring structure the bond length between Zn-O and

Zn-P is 1.78 Å and 2.31Å respectively and the angle between O-Zn-P is about 167^0. The Zn_5O_4P cluster also exhibits three structures, among these; the ring structure has higher stability than the linear and 3D structures with the energy difference of 0.0789 Hartrees and 0.0199 Hartrees respectively.

The dipole moment obtained for $Zn_xO_{x-1}P$ (x=2-5) clusters shows that the ring structure has lesser values due to neutralization of charges in the atoms since it has closed structure. In 3D structures, Zn_3O_2P has the least value because it has completely closed cubic structure. The dipole moment variation in the linear structure is due to the positioning of the atoms. The point group of linear structure for x=2, 3 and 5 is C_s which has high order of symmetry due to the position of atoms in the clusters. For linear structure, there are two possible the point group i.e. C_s or C_1. Due to the closed ring the point group for all the clusters in this group is C_s. However, in the case of 3D structure the point group is C_1, for 3D structures the dipole moment varies randomly due to unequal charge present in the cluster and it shows an increasing trend due to the cluster size.

6.3.2 Binding energy of $Zn_xO_{x-1}P$ clusters

The stabilities of $Zn_xO_{x-1}P$ (x=2-5) clusters are determined based on the binding energy per atom in the cluster by using the formula

$$E_{BE} = \frac{(n \times E(Zn) + m \times E(O) + E(P)) - E(Zn_nO_mP)}{(n+m+1)}$$

where, n is the number of Zn atom and m is the number of O atom. The calculated binding energies of $Zn_xO_{x-1}P$ are tabulated in Table 6.2. From the calculated E_{BE} values it is observed that on comparing linear and 3D structures, the ring structure is more stable since it has higher binding energy. It may be due to the position of the

atom in the cluster. The random variation in the binding energies of all the structures depend upon the placement of atoms in the clusters. Among all the clusters, Zn_5O_4P has highest binding energy value of 3.96 eV since the bond lengths are almost equal.

Table 6.2: Binding energy of $Zn_xO_{x-1}P$ (x=2-5) micro clusters.

Cluster size	Linear (eV)	Ring (eV)	3D (eV)
2	2.73	2.71	-
3	3.30	3.49	3.50
4	3.59	3.81	3.61
5	3.76	3.96	3.90

6.3.3 HOMO and LUMO analysis

The change in the chemical reaction will depend on the HOMO-LUMO energy gap. When the cluster size increases the energy gap increases in the cluster. Comparing the energy gap of all the structures, for ring structures there is a consistent increase in the gap with cluster size and has more energy gap in linear and 3D structure than in ring structure. The density of states (DOS) spectrum and HOMO-LUMO energies of Zn_5O_4P structures for linear, ring and 3D structure are shown in the Figure 6.5(a), (b) and (c) respectively.

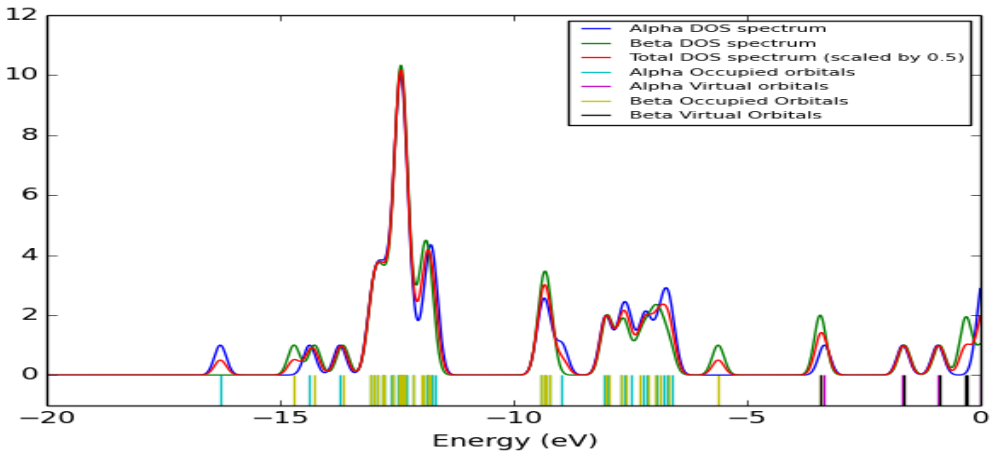

Figure 6.5 (a): HOMO-LUMO, DOS spectrum of Zn_5O_4P micro cluster linear structure.

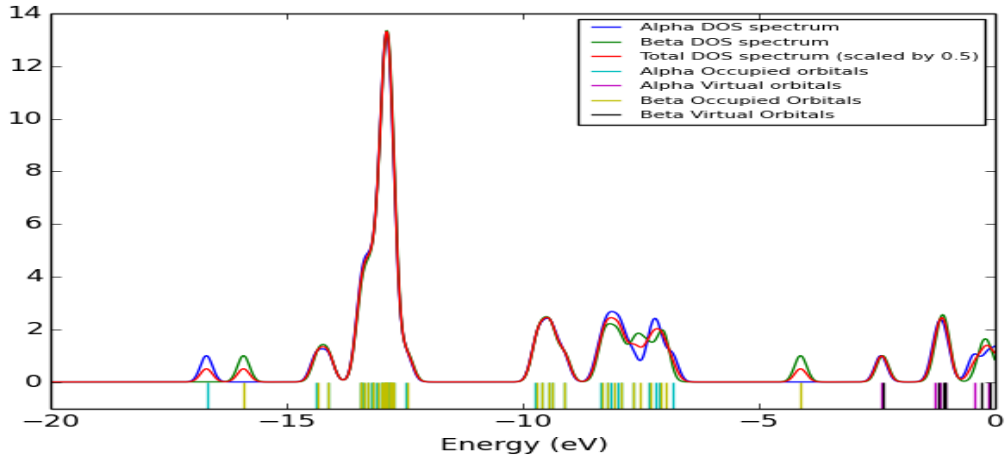

Figure 6.5 (b): HOMO-LUMO, DOS spectrum of Zn_5O_4P micro cluster ring structure

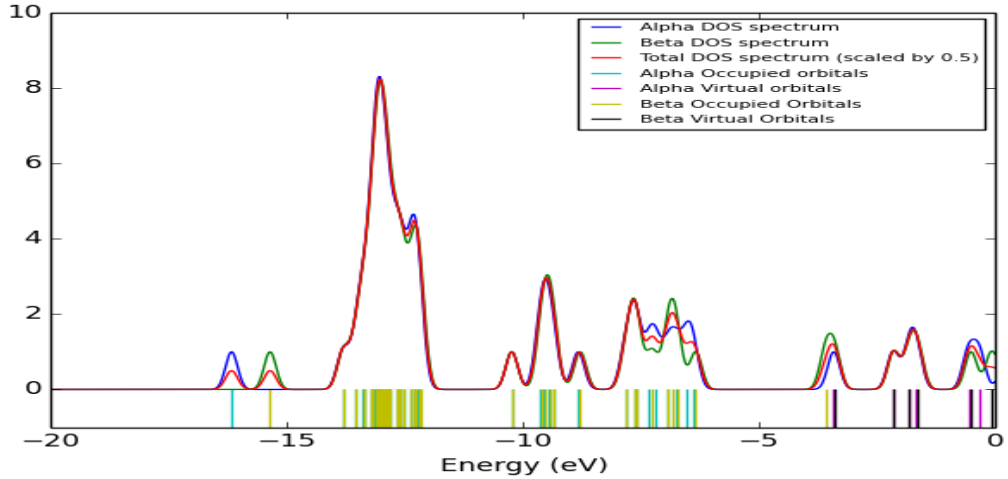

Figure 6.5(c): HOMO-LUMO, DOS spectrum of Zn_5O_4P micro cluster 3D structure

The DOS spectrum of Zn_5O_4P for linear, ring and 3D structures are shown in Figure. 6.5(a), 6.5(b) and 6.5(c). It is shown that the accepter level is very low in the linear structure as compared to the other structures (ring and 3D). It indicates that for closed structures of Phosphorus doped ZnO, the accepter level is more than expected for the stable p-type conductivity. The HOMO-LUMO visualisation is shown in Table 6.4.

Table 6. 3: HOMO-LUMO gap of $Zn_xO_{x-1}P$ (x=2-5).

Structure	Size	HOMO Alpha (eV)	LUMO Alpha (eV)	Gap (eV)	HOMO Beta (eV)	LUMO Beta (eV)	Gap (eV)
Linear	2	6.64	3.39	3.25	5.62	3.36	2.26
	3	6.63	3.42	3.21	5.64	3.38	2.26
	4	6.66	3.37	3.29	5.65	3.42	2.23
	5	6.60	3.34	3.26	5.61	3.43	2.19
Ring	2	6.22	3.28	2.94	6.02	3.65	2.37
	3	6.86	2.62	4.24	6.86	4.08	2.76
	4	6.79	2.41	4.39	6.89	4.12	2.77
	5	6.83	2.41	4.42	6.98	4.11	2.87
3D	3	5.35	3.12	2.23	5.27	3.63	1.64
	4	6.47	3.35	3.12	6.17	4.63	1.54
	5	6.39	3.41	2.99	6.33	3.57	2.76

Table 6.4: HOMO-LUMO visualization and spin states of $Zn_xO_{x-1}P$ micro clusters.

Cluster	Spin state	HOMO	LUMO
Zn_2O_1P Linear	Doublet	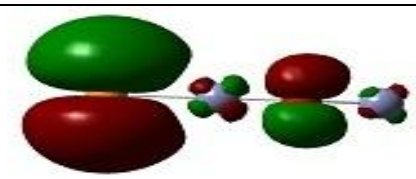	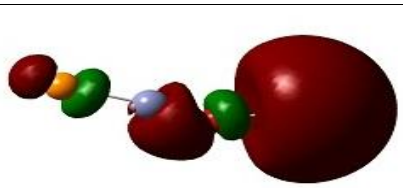
Zn_2O_1P Ring	Doublet	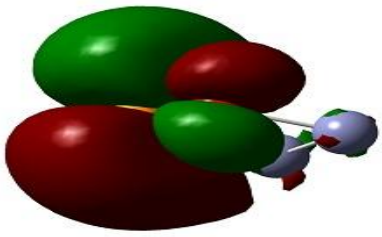	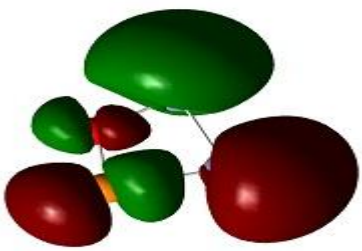
Zn_3O_2P Linear	Doublet	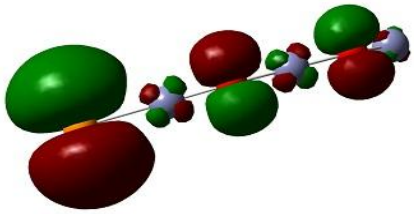	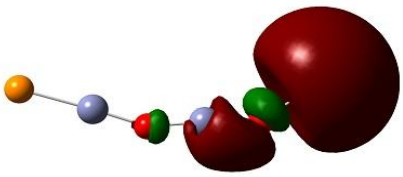
Zn_3O_2P Ring	Doublet	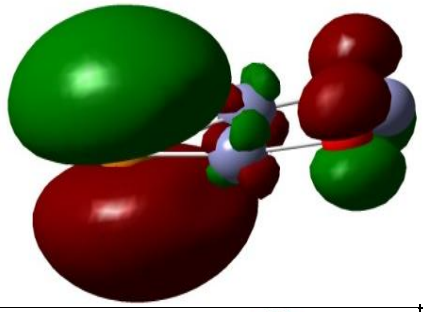	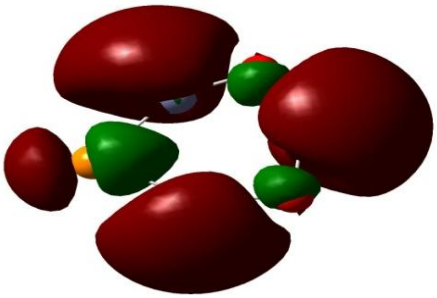
Zn_3O_2P 3D	Doublet	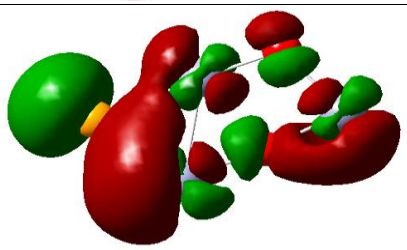	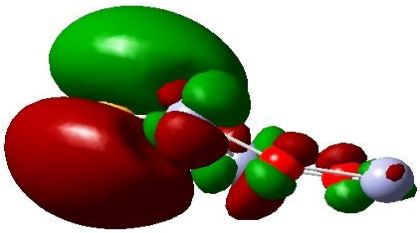
Zn_4O_3P Linear	Doublet	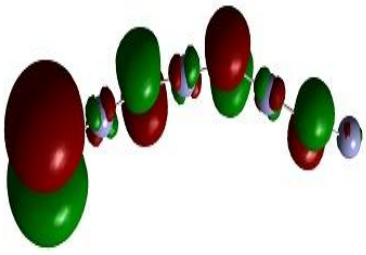	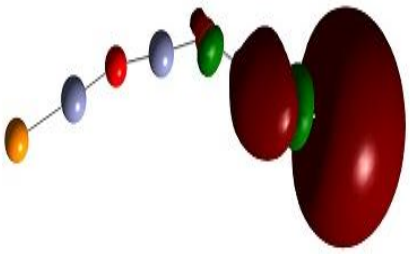

Zn_4O_3P Ring	Doublet	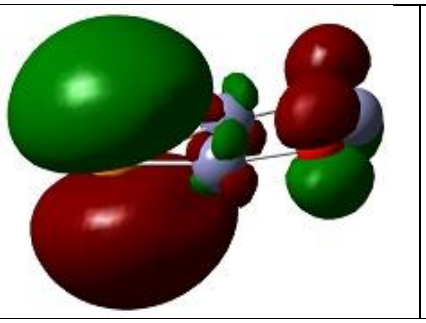	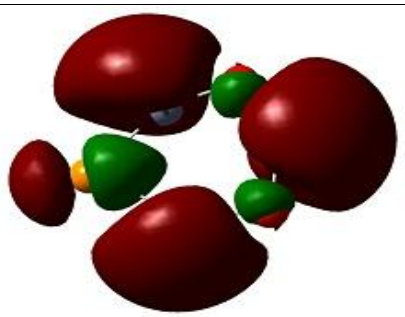
Zn_4O_3P 3D	Doublet	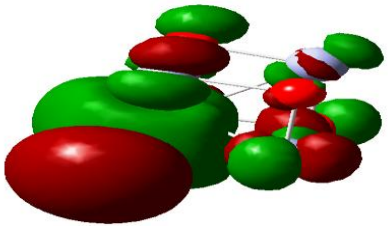	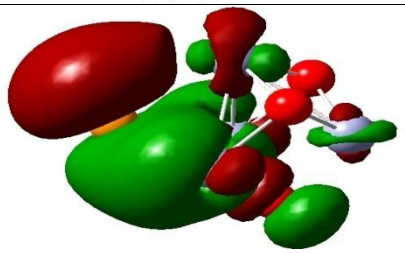
Zn_5O_4P Linear	Singlet	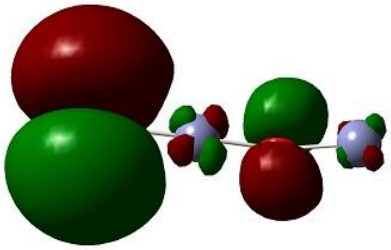	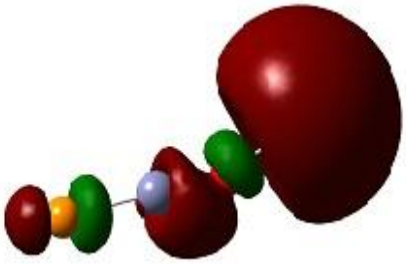
Zn_5O_4P Ring	Singlet	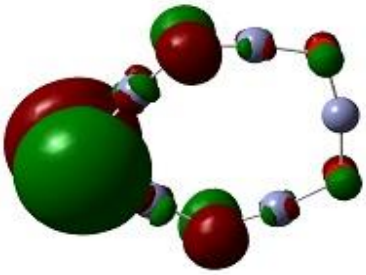	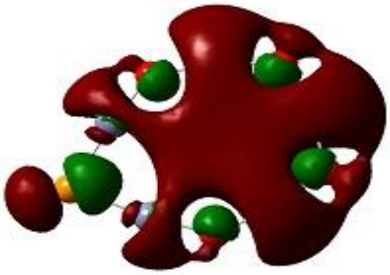
Zn_5O_4P 3D	Singlet	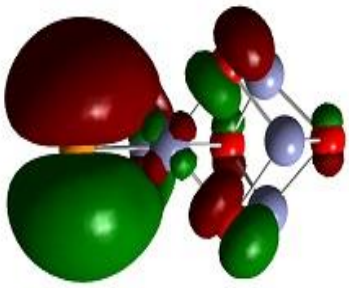	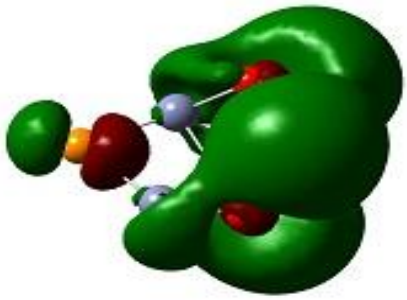

6.3.4 Ionization and Electron Affinity

The study of ionization potential (IP) and electron affinity (EA) are very important for micro clusters since they indicate the electronic structure of the cluster and also serves as a measuring tool for individual atomic to bulk behaviour change.[20] Ionization

potential and electron affinity of different isomers provide important clues for identifying various low energy isomers. The IP and EA values for $Zn_xO_{x-1}P$ clusters are calculated from their orbital energies. The variation of ionization potential and electron affinities of linear, ring and 3D structures with cluster size is shown in Figure 6.6(a), (b) and (c), respectively.

For linear structure, the ionization potential for $Zn_xO_{x-1}P$, x= 2, 3, and 5, is found to be almost same. Whereas for x=4 the ionization potential is less than other clusters. And the electron affinity (EA) values are found to be almost same since all the atoms are connected as a chain and are having an energy difference of approximately 0.2 eV. In the case of ring structure the ionization potential (IP) is found to be almost same whereas the electron affinity (EA) has very zig-zag path, due to closed structure. In the case of 3D clusters, the trend is almost the same for the ionization potential and electron affinity. The cluster with high electron affinity is more preferable for chemical sensor. Among all the clusters, EA values is high about 4.04 eV for ring structured Zn_4O_3P. The large value of electron affinity infers that it is more chemically reactive. Interestingly, the electron affinity for ring structure is observed to be high, which is more chemically reactive than two structures namely linear and 3D structures.

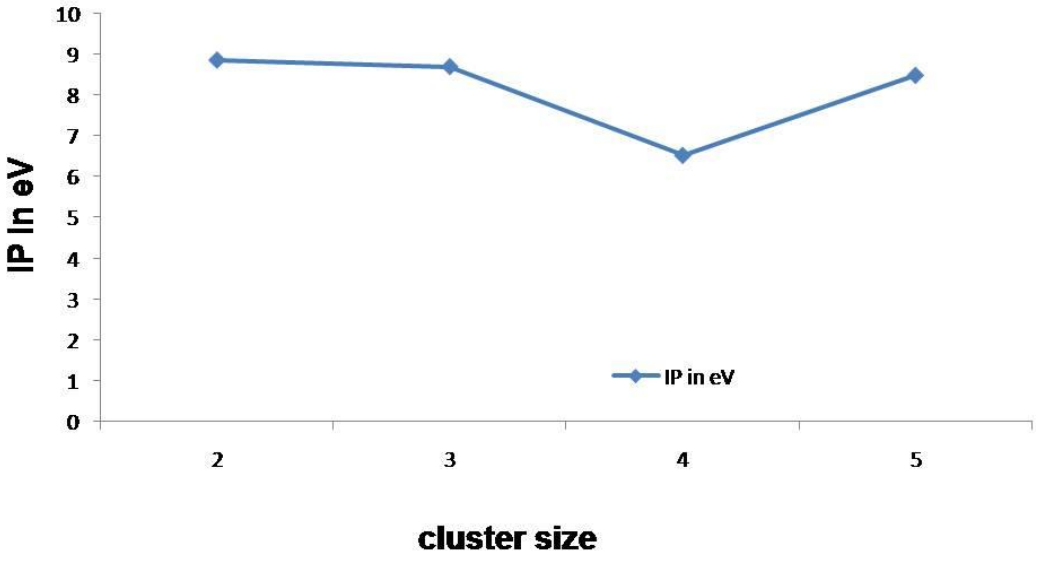

(a) Linear Structure

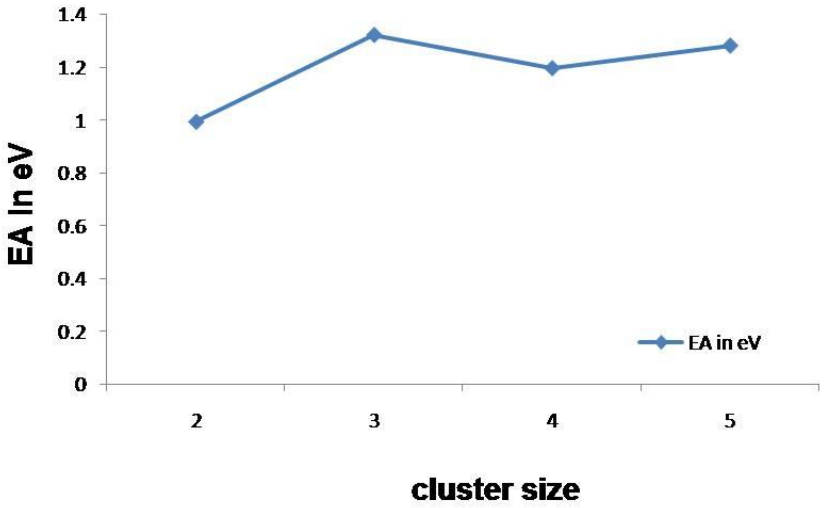

(b) Ring Structure

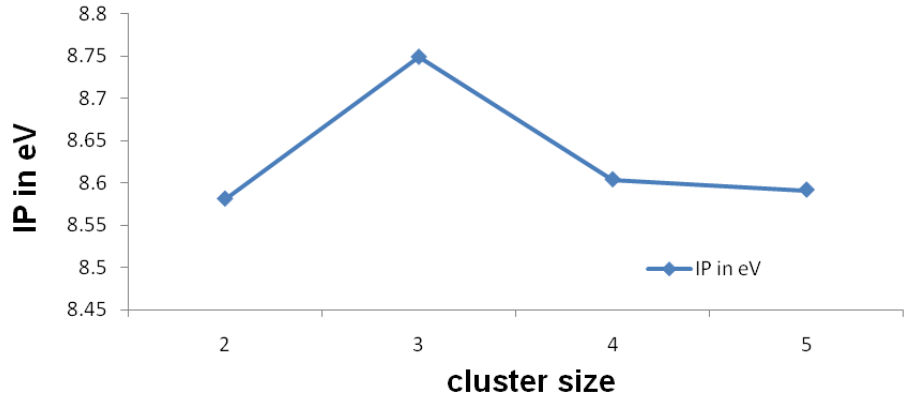

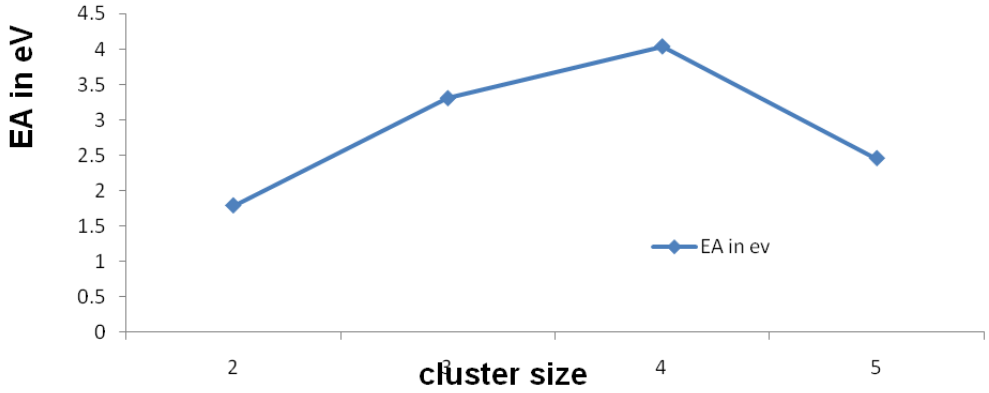

(c) 3D Structure

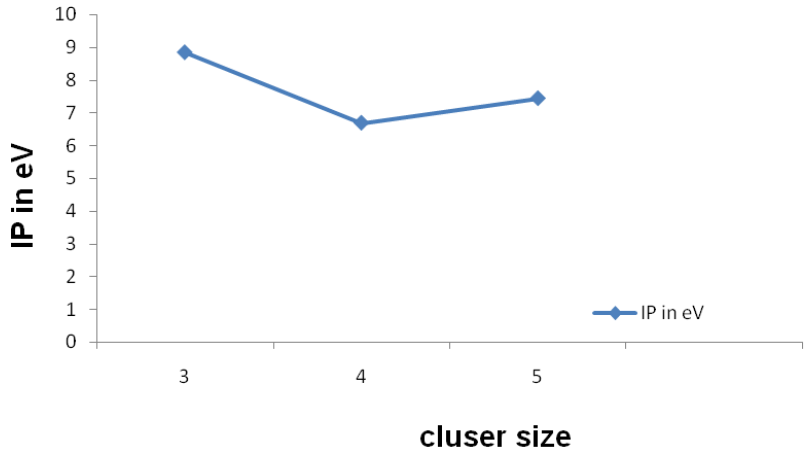

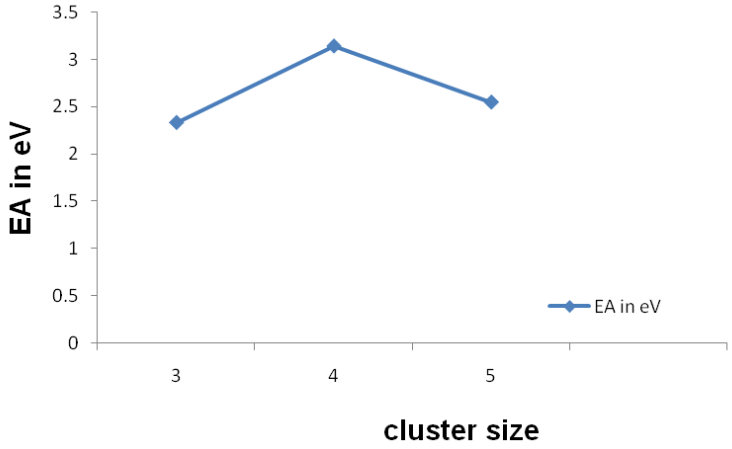

Figure 6.6 (a) IP and EA of $Zn_xO_{x-1}P$ clusters-linear Structure **(b)** IP and EA of $Zn_xO_{x-1}P$ clusters-ring structure, and **(c)** IP and EA of $Zn_xO_{x-1}P$ clusters-3D structure.

6.4. Conclusion

The Phosphorus doped ZnO clusters have been optimized with the B3LYP/6-31 G basis set. The results show that the closed ring structures are more stable than the other two studied structures. The stability of clusters increases with increasing the cluster size. The dipole moment of different structures depend on the position of the atoms in the cluster. The calculated binding energy also shows that the ring structured isomers are more stable than the other two structures. The ionization potential for linear structure is high, hence chemical reactivity and electron affinity for all the clusters have almost the same value as expected for ring structured Zn_4O_3P. The HOMO-LUMO energy gap reveals that when the atoms in the cluster is increased, the energy gap decreases which reflects overlapping of the orbitals due to increases in the number of atoms. The findings of the present work provide useful insights to experimentalist for tailoring new materials for the development of Phosphorus p-type ZnO with doped.

References

1. S. A. Fischer, A. M. Crotty, S. V. Kilina, S. A. Ivanov, S. Tretiak, *Nanoscale*,**4,** 904 (2012).
2. J. Sun, Q. Feng J. Bian D. Yu , M. Li, C. Li , H. Liang, J. Zhao H. Qiu , G. Du , *J. Lumin.,* **131,** 825 (2011).
3. Q. Qiao , B. H. Li , C.X. Shan , J.S. Liu , J. Yu , X.H. Xie , Zhang, T.B. Ji , Y. Jia , D.Z. Shen, *Mater. Lett.,* **74,** 104 (2012).
4. J.H. Jun, H. Seong , K. Cho , B.M. Moon , S. Kim, *Ceramics International,* **35** 2797 (2009).
5. Wan-Yu Wu, Jyh-Ming Ting, Po-Jung Huang *Nanoscale Res. Lett.,* **4,** 513 (2009).
6. X. Sheng , Y. Zhaoj , J. Zhai , L. Jiang , D. Zhu, *Appl. Phys. A,* **87,** 715 (2007).
7. R. Raza, Q. Liu, J. Nisar, X. Wang, Y. Ma, B. Zhu, *Electrochem. Commun.,* **13**, 917 (2011).
8. J. J. Yang , Y. F. Yuan , H. M. Wu, Y. Li , Y.B. Chen , S. Y. Guo, *Electrochim. Acta*, **55**, 7050 (2011).
9. G. Xian-ji, L. Li-min, L. Shu-min, B. Gai-ling, H. Wen-hua, *J. Fuel Chem. Technol.,* **35(3)**, 329 (2007).
10. Z. W. Pan, Z. R. Dai, Z. L. Wang, *Science,* **291**, 1947 (2001).
11. X. Y. Kong, Y. Ding, R. Yang, Z. L. Wang, *Science,* **303**, 1348 (2004).
12. X. Y. Kong, Z. L. Wang, *Nano. Lett.,* **3,** 1625 (2003).
13. P. X. Gao, Z. L.Wang, *J. Am. Chem. Soc.,***125**, 11299 (2003).
14. P. Schroer, P. Kruger, J. Pollmann, *Phys. Rev. B,* **47,** 6971 (1993).
15. D. Vogel, P. Kruger, J. Pollmann, *Phys. Rev. B,* **52,** R14316 (1995).
16. M. Usuda, N. Hamada, T. Kotani , M. V. Schilfgaarde, *Phys. Rev. B,* **66,** 125101 (2002).
17. K.C. Barick, S. Singh , M. Aslam, D. Bahadur, **134,** 195 (2010).
18. I. Ozerov, F. Chabre , W. Marine, *Mater. Sci. Eng. C,* **25**, 614 (2005).
19. J. H. Li, D. Z. Shen, J. Y. Zhang, D. X. Zhao, B. S. Li, Y. M. Lua. Y. C. Liu, X. W. Fan, *J. Magn. Magn. Mater*, **302**, 118 (2006).
20. D.W. Bahnemann, C. Kormann, M. R. Hoffmann, *J. Phys. Chem.*, **91,** 3789 (1987).
21. V. A. Fonoberov, A. A. Balandin, *Nano Structures and Nanodevices,* **4,** 119

(2005).

22. W. R. L. Lambrecht, A. V. Rodine, S. Limpijumnong, B. Segall, B. K. Meyer, *Phys. Rev. B,* **65,** 075207 (2002).
23. M.A.F. Hidalgo, D. B. Jimenez, D. G. Mitnik, *J. Mol. Struct. (THEOCHEM),* **957,** 100 (2010).
24. V. Ozgar, Y. I. Alivov, C. Liu , A. Teke , M.A. Reshehikov, S. Dogan , V. Avrutin, S. Cho, H. J. Markoe, *Appl. Phys.*, **98,** 041301 (2005).
25. S. J. Pearton, D. P. Norton, K. Ip, Y. Heo, W.I. Steiner, *J. Prog. Mater. Sci.*, **50,** 293 (2005).
26. A. Becheri, M. Durr, P. L. Nostro, P. J. Baglioni, *Nano Particle Res.*,**10,** 679 (2008).
27. D.C. Look, B. Claflin, *Phys. Status solid B,* **241,** 624 (2004).
28. I. Sheikhshoaie, H. Stoeckli-Evans, A. Akbari, S. Ali Yasrebi, S. Yousef brahimipour, *Arab. J. Chem*., **5,** 173 (2012).
29. M. Polini, A. Tomadin, R. Asgari, A. H. MacDonald, *Phys. Rev. B,* **78,** 115426 (2008).
30. J. G. Lu, Z. Z Ye, F. Zhuge, J. Y. Zeng, B. H. Zhao, L.P. Zha, *Appl. Phys. Lett.*,**85**,3134 (2004).
31. B. Xiang, W.P. Wang, X. Z. Zhang, S. A. Dayeh, D. P. Aplin, C. Soci , D. P. Yu, D. L.Wang, *Nano Lett.*, **7**, 323 (2007).
32. M. J. Frisch, G. W. Trucks, H. B. Schlegel, G. E. Scuseria, M. A. Robb, J. R. Cheeseman, G. Scalmani, V. Barone, B. Mennucci, G. A. Petersson, H. Nakatsuji, M. Caricato, X. Li, H. P. Hratchian, A. F. Izmaylov, J. Bloino, G. Zheng, J. L. Sonnenberg, M. Hada, M. Ehara, K. Toyota, R. Fukuda, J. Hasegawa, M. Ishida, T. Nakajima, Y. Honda, O. Kitao, H. Nakai, T. Vreven, J. A. Montgomery, Jr., J. E. Peralta, F. Ogliaro, M. Bearpark, J. J. Heyd, E. Brothers, K. N. Kudin, V. N. Staroverov, R. Kobayashi, J. Normand, K. Raghavachari, A. Rendell, J. C. Burant, S. S. Iyengar, J. Tomasi, M. Cossi, N. Rega, J. M. Millam, M. Klene, J. E. Knox, J. B. Cross, V. Bakken, C. Adamo, J. Jaramillo, R. Gomperts, R. E. Stratmann, O. Yazyev, A. J. Austin, R. Cammi, C. Pomelli, J. W. Ochterski, R. L. Martin, K. Morokuma, V. G. Zakrzewski, G. A. Voth, P. Salvador, J. J. Dannenberg, S. Dapprich, A. D. Daniels, Ö. Farkas, J. B. Foresman, J. V. Ortiz, J. Cioslowski, and D. J. Fox, *Gaussian 09* (Gaussian, Inc.,

Wallingford CT, (2009).

33. R. Srinivasaraghavan, R. Chandiramouli, B. G. Jeyaprakash, S. Seshadri, *Spectrochim. Acta, Part A,* **102**, 242 (2013).
34. M. Mihit, K. Laarej, E. L. Abou, H. Makarim, L. Bazzi, R. Salghi, B. Hammouti *Arab. J. Chem*., **3**, 55 (2010).
35. M. Bouklah, H. Harek , R. Touzani , B. Hammouti, Y. Harek, *Arab. J. Chem*.**, 5**, 163 (2012).

CHAPTER 7

CONCLUSIONS

The work done in this thesis highlights following general conclusions:

A. Technological advantage and recent development in theory have enabled evolution of highly accurate, efficient and inexpensive methods that are applicable in the field of material science. In order to determine the stability of cluster, the use of the cohesive energy, energy change in a modal reaction, energy gap in electronic structure are studied. These parameters can be accurately computed with the help of DFT methods.

B. The variation of bond length and the number of atoms consisting of Ga_xAs_x (x=10, 13, 15, 18, 20, 25, 30) clusters was studied in detail. The other important parameters like binding energy, HOMO LUMO gap confirms the stability of the studied clusters. The optical activity is also discussed in detail.

C. Theoretical electronic structure techniques have become an indispensible and powerful means for predicting molecular properties and designing new materials. The density functional approach provides evidence for some specific fullerene-like cage molecules of semiconductor materials which exhibit high energetic stability and point group symmetry of Ga_xAs_x fullerene like clusters.

D. The principle of electrical properties is applied in the case of clusters by visiting some of the most influential studies. It is the main objectives of the study to explore the stability of GaN clusters using the DFT.

E. The study of atomic structure and stability of $Cd_xS_{x\pm4}$ fullerenes like semiconductor cluster is done by using B3LYP method. It is found that the hollow fullerenes like clusters are stable when the pentagon edges are shared to reduce the number of homo-nuclear bonds. The energetic and the energy gap in electronic structure are indicators for the stability of cluster. The study predicts that these clusters are stable. The stability of the cluster increases when the number of homo-nuclear bonds in the cluster is less.

The coefficients and different parameters used in different proposed theoretical model for semiconductor cluster can be easily computed by using computational quantum mechanical tools.

Experimental studies require a lot of resources like instruments, materials, environments etc. The computational techniques at molecular level through computational quantum mechanical tools help to propose specific type of molecule for designing and improve the electrical and optical properties of cluster.

JACS
JOURNAL OF THE AMERICAN CHEMICAL SOCIETY
Article
Cite This: J. Am. Chem. Soc. 2017, 139, 18328–18338
pubs.acs.org/JACS

Keto–Enol Tautomerization Triggers an Electrophilic Aldehyde Deformylation Reaction by a Nonheme Manganese(III)-Peroxo Complex

Fabián G. Cantú Reinhard,[†] Prasenjit Barman,[‡] Gourab Mukherjee,[‡] Jitendra Kumar,[§] Deep Kumar,[§] Devesh Kumar,[§] Chivukula V. Sastri,*[,‡] and Sam P. de Visser*[,†]

[†]The Manchester Institute of Biotechnology and School of Chemical Engineering and Analytical Science, The University of Manchester, 131 Princess Street, Manchester M1 7DN, United Kingdom

[‡]Department of Chemistry, Indian Institute of Technology Guwahati 781039, Assam, India

[§]Department of Applied Physics, School for Physical Sciences, Babasaheb Bhimrao Ambedkar University, Lucknow 226025, UP, India

Supporting Information

ABSTRACT: Oxygen atom transfer by high-valent enzymatic intermediates remains an enigma in chemical catalysis. In particular, manganese is an important first-row metal involved in key biochemical processes, including the biosynthesis of molecular oxygen (through the photosystem II complex) and biodegradation of toxic superoxide to hydrogen peroxide by superoxide dismutase. Biomimetic models of these biological systems have been developed to gain understanding on the structure and properties of short-lived intermediates but also with the aim to create environmentally benign oxidants. In this work, we report a combined spectroscopy, kinetics and computational study on aldehyde deformylation by two side-on manganese(III)-peroxo complexes with bispidine ligands. Both manganese(III)-peroxo complexes are characterized by UV–vis and mass spectrometry techniques, and their reactivity patterns with aldehydes was investigated. We find a novel mechanism for the reaction that is initiated by a hydrogen atom abstraction reaction, which enables a keto–enol tautomerization in the substrate. This is an essential step in the mechanism that makes an electrophilic attack on the olefin bond possible as the attack on the aldehyde carbonyl is too high in energy. Kinetics studies determine a large kinetic isotope effect for the replacement of the transferring hydrogen atom by deuterium, while replacing the transferring hydrogen atom by a methyl group makes the substrate inactive and hence confirm the hypothesized mechanism. Our new mechanism is confirmed with density functional theory modeling on the full mechanism and rationalized through valence bond and thermochemical cycles. Our unprecedented new mechanism may have relevance to biological and biomimetic chemistry processes in general and gives insight into the reactivity patterns of metal-peroxo and metal-hydroperoxo intermediates in general.

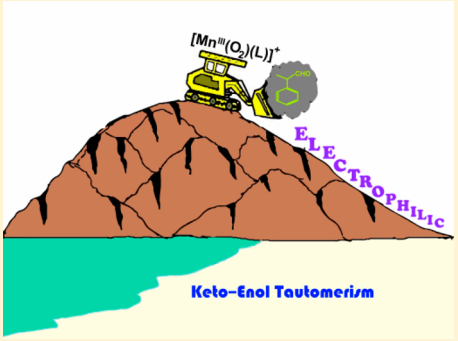

INTRODUCTION

Metalloenzymes are powerful oxidants in nature that catalyze important reactions for Biosystems.[1] Most of these metalloenzymes utilize iron as their central cofactor, due to its high natural abundance. Another transition metal in relatively large abundance in the Earth Crust is manganese and, as such, nature has found key uses of it in various biological transformations.[2] Thus, manganese complexes are strong oxidizers, and consequently, the active site of superoxide dismutase (SOD) contains a central Mn atom.[3] SOD is involved in the biodegradation of superoxide radicals and converts them on a manganese center to hydrogen peroxide. Often SOD enzymes are anchored to a catalase enzyme that react and detoxify hydrogen peroxide. Another biological system with manganese coordination is the Photosystem II (PSII) active cluster, which contains four manganese atoms held together with bridging oxygen atoms and a dangling Ca^{2+} ion in a cubane-type Mn_4O_5Ca cluster.[4] This cluster binds water molecules and reacts them to one molecule of molecular oxygen with the release of four protons.

In biomimetic chemistry, synthetic manganese containing models of SOD and PSII have been created and studied for their chemical properties and reactivity.[5] In several of these studies a manganese-peroxo was investigated and the spectroscopic features of the complexes was established with UV–vis, resonance Raman, infrared absorption and electron paramagnetic resonance (EPR) spectroscopy.[6,7] Furthermore, the reactivity of manganese-peroxo with respect to substrates was investigated and efficient conversion to aldehyde products via deformylation was obtained.[8] However, the exact details of the mechanism remain a mystery. Therefore, manganese(III)-peroxo shows interesting reactivity patterns with substrates that are still poorly understood.

Received: September 23, 2017
Published: November 17, 2017

DOI: 10.1021/jacs.7b10033
J. Am. Chem. Soc. 2017, 139, 18328–18338

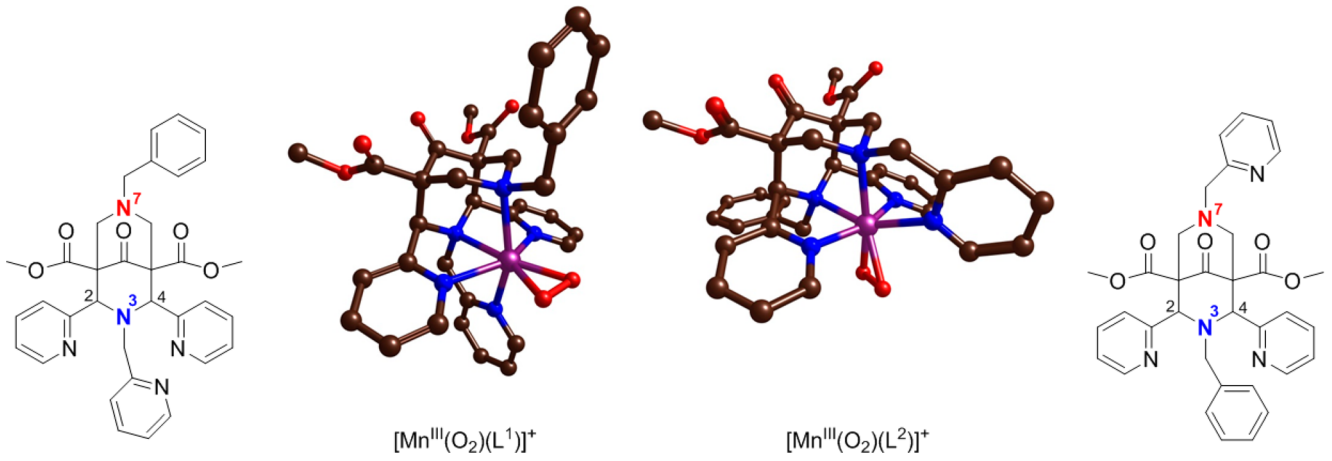

Figure 1. Manganese(III)-peroxo complexes investigated in this work.

Recently, our groups have shown that bispidine ligated manganese(III)-peroxo reacts with aldehydes through a rate-determining hydrogen atom abstraction reaction as evidenced from a large kinetic isotope effect (KIE) for the replacement of the α-hydrogen atom by deuterium.[9] Radical trapping experiments and density functional theory calculations further confirmed the rate-determining hydrogen atom abstraction and rationalized that this is originating from a more feasible electron transfer from peroxo to Mn as compared to substrate carbonyl. The question, therefore, is how the ligand system of the metal influences the bifurcation pathways between hydrogen atom abstraction (i.e., the electrophilic pathway) versus a nucleophilic pathway.

To test the ligand effect on the bifurcation pathways, we followed our previous work up with a detailed study on two functionally isomeric pentadentate manganese(III)-peroxo complexes, resulting in different orientations of two pyridine groups with respect to N^3 nitrogen of the bispidine backbone. In particular, we synthesized manganese(III)-peroxo complexes with bispidine ligand systems (see Figure 1), namely $[Mn^{III}(O_2)(L^1)]^+$ (**1**) and $[Mn^{III}(O_2)(L^2)]^+$ (**2**) with L^1 = dimethyl-2,4-di(2-pyridyl)3-(pyridin-2-ylmethyl)-7-benzyl-3,7-diaza-bicyclo[3.3.1] nonan-9-one-1,5-dicarboxylate) and L^2 = dimethyl 2,4-di(2-pyridyl)-3-benzyl-7-(pyridin-2-ylmethyl)-3,7-diazabicyclo[3.3.1] nonan-9-one-1,5-dicarboxylate). Thus, ligand L^1 has three pyridine groups pointing upward (i.e., along the molecular *z*-axis with the ortho-C−H groups in hydrogen bonding distance to the sixth ligand), whereas in ligand L^2 only one of those points upward and the other two are aligned with the *xy*-plane. Our combined experimental and computational study gives evidence of a novel reaction mechanism starting with a rate-determining hydrogen atom abstraction reaction and followed by a reshuttle of the hydrogen atom through a keto−enol tautomerization to set up a low-energy nucleophilic attack of peroxo on an olefin bond of the substrate. Alternative reaction mechanisms were tested and ruled out. Our observations are confirmed with computational modeling that rationalize the reaction mechanism with valence bond and thermochemical cycles.

METHODS

Experimental Procedures. Our procedures are similar to previous studies of our groups and will be summarized briefly here.[10] All reagents were obtained from Aldrich Chemical Co. and obtained at the best available purity and used without further purification unless otherwise indicated. Solvents were dried according to published procedures and distilled under argon prior to use.[11] The piperidone backbone of the ligands L^1 and L^2 were prepared according to a literature protocol[12] and used to generate the $[Mn^{II}(L^1)](ClO_4)_2$ and $[Mn^{II}(L^2)](ClO_4)_2$ complexes. Subsequently, the manganese(III)-peroxo complexes were prepared by reacting their corresponding Mn^{II} systems with 10 equiv of H_2O_2 and 2.5 equiv of triethylamine (TEA) in acetonitrile (2 mL) at 15 °C.

2-Methyl-2-phenylpropionaldehyde (2-Me-PPA) was synthesized in our laboratory according to a literature procedure,[13] while α-[D_1]-2-phenylpropionaldehyde (α-[D_1]-PPA, ∼90%, D enriched) was purchased from RVL Scientific & Engineering Pvt. Ltd. (Lucknow, India) and the purity of the compound was confirmed by NMR. All NMR spectra were recorded in $CDCl_3$.

Syntheses and Characterization. Bispidine ligands (0.17 mmol) were dissolved in acetonitrile and mixed with $Mn^{II}(ClO_4)_2{\cdot}2CH_3CN$ salt (0.22 mmol in CH_3CN) under inert conditions. The pale yellow solution was refluxed overnight and filtered through a 0.2 μm syringe filter and layered with diethylether to obtain a white crystal suitable for X-ray diffraction. The cif file of the complexes is deposited at the Cambridge Crystallographic Data Centre (CCDC) with the following deposition numbers: CCDC 1022749 and 1022750. Caution! Metal perchlorate salts are potentially explosive and should be handled with excessive care.

Instrumentation. NMR (^{1}H and ^{13}C) spectra were recorded with a Bruker 600/150 MHz spectrometer. UV−vis spectra and kinetic measurements were performed with a Hewlett-Packard 8453 spectrophotometer equipped with either a constant temperature circulating water bath or a liquid nitrogen cryostat (Unisoku) with a temperature controller. High-resolution electrospray ionization mass spectra (ESI-MS) of $[Mn^{III}(O_2)(L^1)]^+$ and $[Mn^{III}(O_2)(L^2)]^+$ were recorded on a Waters (Micromass MS Technologies) Q-TOF Premier mass spectrometer by infusing precooled samples directly into the source at 15 μL min^{-1} using a syringe pump. The spray voltage was set at 2 kV and the capillary temperature at 80 °C.

Reactivity Studies. The chemical reactions were monitored in a 10 mm path length cuvette by measuring the UV−vis spectral changes of the reaction solutions as a function of time. The rate constants were determined by fitting the changes in absorbance of the intermediates as a function of time under study. The rate constants were averaged from three individual experiments and resulted in a standard deviation of less than 10% of the given values.

Product Analysis. Product analysis was performed on a WATERS ACQUITY UPLC equipped with a variable wavelength UV-200 detector. Products were separated on a Waters Symmetry C18 reverse phase column (4.6 × 250 mm) and detection was made at 215 and 254 nm. Product yields were determined by comparison with standard curves of known authentic samples. All experiments were done at least in triplicate.

DOI: 10.1021/jacs.7b10033
J. Am. Chem. Soc. 2017, 139, 18328−18338

Computational Procedures. Density functional theory (DFT) calculations were performed on the catalytic reaction mechanism of deformylation of 2-phenylpropionaldehyde (2-PPA) by $[Mn^{III}(O_2)(L^1)]^+$ and $[Mn^{III}(O_2)(L^2)]^+$ following previously tested and benchmarked procedures.[14] We took initial structures from our previous study[9] but reoptimized all geometries in Gaussian-09 with a full solvent model as mimicked by a polarized continuum model (PCM) with a dielectric constant of 37.5 mimicking acetonitrile.[15,16] These geometry optimizations utilized the unrestricted B3LYP hybrid density functional method in combination with an LACVP basis set with core potential on Mn and 6-31G* on the rest of the atoms (basis set BS1).[17,18] The nature of the stationary points was confirmed through a frequency calculation also under solution conditions calculated with the PCM model. All local minima had real frequencies only, while the transition states were characterized by a single imaginary mode for the correct transition. To improve the energetics, single-point calculations using an LACV3P+ basis set with core potential on Mn and 6-311+G* on the rest of the atoms was performed: basis set BS2. Previously, we showed that little changes in structure and energetics are obtained for UB3LYP/BS1 versus UB3LYP/BS2 geometry optimizations.[19] Furthermore, the spin state ordering and relative energies of related manganese complexes were tested using a range of alternative DFT and ab initio methods.[20] On the basis of the fact that manganese(III)-peroxo has a high-spin ground state, we selected B3LYP as computational method and the results reproduce the experimental trends well.

Kinetic isotope effects (KIE) were evaluated computationally by reevaluating the free energy and vibrational frequencies of the structures, whereby one or more hydrogen atom is replaced by deuterium.[21] The Eyring kinetic isotope effect (KIE_{Eyring}) is determined from the change in free energy of activation ($\Delta G^{\ddagger}$) between the system with hydrogen and deuterium atoms, eq 1, with R representing the gas constant and T the temperature (298 K).

$$KIE_{Eyring} = \exp\{(\Delta G^{\ddagger}_{D} - \Delta G^{\ddagger}_{H})/RT\} \quad (1)$$

In addition, we estimated the Wigner kinetic isotope effect (KIE_{Wigner}), which corrects KIE_{Eyring} with tunneling corrections Q_t for the hydrogen and deuterium reactions through eqs 2 and 3. These equations contain Planck's constant (h), Boltzmann's constant (k_B), and the imaginary frequency in the transition state (ν).

$$KIE_{Wigner} = KIE_{Eyring} \times Q_{t,H}/Q_{t,D} \quad (2)$$

$$Q_t = 1 + (h\nu/k_BT)^2/24 \quad (3)$$

RESULTS

In this work, we describe the synthesis, characterization and reactivity patterns of two novel side-on manganese(III)-peroxo complexes with a pentadentate bispidine N5 ligand {i.e., $[Mn^{III}(O_2)(L^1)]^+$ (**1**) and $[Mn^{III}(O_2)(L^2)]^+$ (**2**)}, Figure 1. These two ligand systems have their equatorial pyridine groups either axial or equatorial to the manganese(III)-peroxo group and, hence, interact differently with an approaching substrate. The weak intermolecular interactions separating the two complexes may incur in functional differences due to the way substrate can approach to the catalytic center and/or the stability of the reactant complex. Therefore, these models may give insight into the properties and functions of enzymatic catalysts where substrate approach is often tightly controlled.[22]

Upon addition of 10 equiv of H_2O_2 to $[Mn^{II}(L^2)(ClO_4)_2]^{2+}$ in the presence of 2.5 equiv of TEA, a brown intermediate is formed with distinctive absorption features, Figure S2. The ESI mass spectra of **1** and **2** exhibit prominent peaks with m/z 678 and an isotope pattern that identify them as $[Mn^{III}(O_2)(L^1)]^+$ and $[Mn^{III}(O_2)(L^2)]^+$. When $H_2{}^{16}O_2$ was replaced by $H_2{}^{18}O_2$ in the reaction mixture, the mass of the parent ion increased with four units indicative of a dioxygen-bound complex. We attempted to resolve the resonance Raman spectrum of **1** and **2**, but due to degradation of the manganese complexes caused by scattering, all our efforts failed.

Subsequently, we investigated the deformylation behavior of compounds **1** and **2** in a reaction with 2-phenylpropionaldehyde (2-PPA). This was done by monitoring the change in UV−vis absorption spectra as a function of time after the addition of substrate. In particular, the aldehyde deformylation reaction and the mechanism of substrate activation by side-on manganese(III)-peroxo was investigated from the reactivity of $[Mn^{III}(O_2)(L^1)]^+$ and $[Mn^{III}(O_2)(L^2)]^+$ with 2-PPA under the same experimental reaction conditions (Figure 2). Addition of 2-PPA to **2** in acetonitrile at 15 °C led to immediate decay of the intermediate and the formation of acetophenone product as

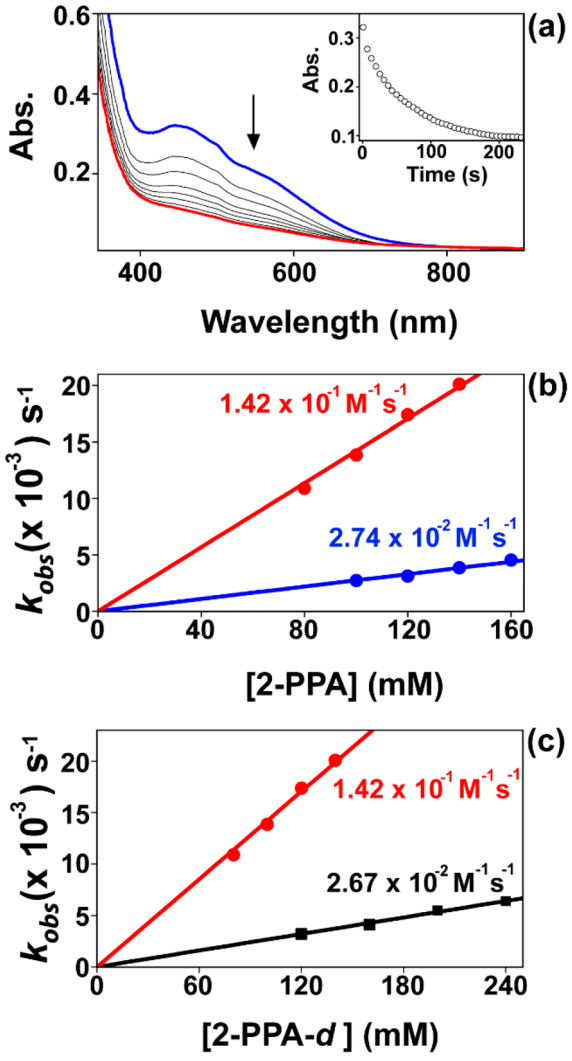

Figure 2. Kinetics of the reaction of **2** with 2-PPA. (a) UV−vis spectral changes of **2** (2 mM) upon addition of 2-PPA (120 mM) in the presence of TEA (5 mM) and hydrogen peroxide (20 mM) in CH_3CN at 15 °C. The inset shows the time course of the absorbance at 450 nm. (b) Plot of k_{obs} against the concentration of 2-PPA and the derived second-order rate constant for the reaction of 2 mM **1** and **2** with 2-PPA at various concentrations in CH_3CN at 15 °C [data for **2** (red •) and **1** (blue •) are given]. (c) Plot of k_{obs} against the concentration of α-[D_1]-PPA (~90%, D enriched, ■) with **2** in CH_3CN at 15 °C.

DOI: 10.1021/jacs.7b10033
J. Am. Chem. Soc. 2017, 139, 18328−18338

identified by NMR. The pseudo first-order rate constant for the decay of **2** increased linearly with increasing concentration of 2-PPA and enabled us to measure the second-order rate constant: $k_2 = 1.42 \times 10^{-1}$ M^{-1} s^{-1}. For comparison, the second-order rate constant for the reaction of $[Mn^{III}(O_2)(L^1)]^+$ with 2-PPA was 2.74×10^{-2} M^{-1} s^{-1}.[9] Therefore, it appears that $[Mn^{III}(O_2)(L^2)]^+$ reacts with 2-PPA about five times faster than the isomeric oxidant with ligand L^1. These results were in fact in opposite trend to those obtained in the reactivity of the corresponding manganese(IV)-oxo complexes $[Mn^{IV}(O)(L^1)]^{2+}$ and $[Mn^{IV}(O)(L^2)]^{2+}$.[12d] A possible reason for the change in rate constant ordering is the shape of the ligand system, whereby the L^1 ligand (see Figure 1) has protons pointing upward toward the peroxo group, whereas in the L^2 ligand the pyridine moieties are in the *xy*-plane and will not interact with the approaching substrate.

To understand the details of the rate-determining step for the reaction of $[Mn^{III}(O_2)(L^1)]^+$ and $[Mn^{III}(O_2)(L^2)]^+$ with 2-PPA, we decided to investigate the kinetic isotope effect (KIE) for replacing the α-hydrogen atom with deuterium (Figure 2c). Thus, upon addition of α-$[D_1]$-PPA (~90%, D-enriched) to **2** in acetonitrile at 15 °C, the absorption of the intermediates shows decay from which we determined a second-order rate constant of $k_2 = 2.67 \times 10^{-2}$ M^{-1} s^{-1}. Hence, the reaction between **2** and 2-PPA proceeds with a KIE = 5.3, and it can be concluded that the reaction has a rate-determining hydrogen atom abstraction step. A comparable KIE value of 5.4 was determined for the reactivity difference of **1** with 2-PPA/α-$[D_1]$-PPA.[9] Consequently, both $[Mn^{III}(O_2)(L^1)]^+$ and $[Mn^{III}(O_2)(L^2)]^+$ react with 2-PPA through a rate-determining hydrogen atom abstraction and a KIE that deviates from unity and most likely their reaction mechanisms will be similar.

To further ascertain that hydrogen atom abstraction from the α-position is key to the reaction mechanism, we used a mechanistic probe, namely 2-methyl-2-phenyl propionaldehyde (2-Me-PPA), Scheme 1. Lack of reactivity with this probe

Scheme 1. Reaction of $[Mn^{III}(O_2)(L^2)]^+$ with Substrates

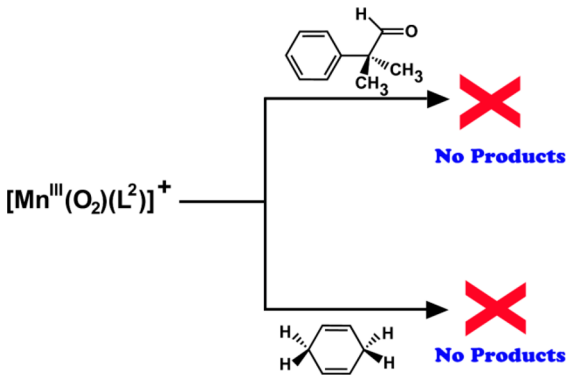

would confirm that the rate-determining step is indeed α-hydrogen atom abstraction and no nucleophilic pathway is possible. When we add 2-Me-PPA to **2** at 15 °C, however, no reaction products are observed and only natural decay profiles back to $[Mn^{II}(L^2)]^{2+}$ are seen due to the short lifetime of the parent complex in solution ($t_{1/2}$ ~ 45 min). After analyzing the reaction solution with ESI-MS, we do not find any evidence of deformylated products. Consequently, the reactivity study with 2-Me-PPA as a mechanistic probe confirms that the reaction of **2** with 2-PPA does not proceed through a rate-determining nucleophilic attack on the carbonyl group but is initiated by activation of the α-hydrogen atom instead.

To test whether the manganese(III)-peroxo can react efficiently through hydrogen atom abstraction, we decided to test alternative substrates with weak C–H bonds. Addition of 1,4-cyclohexadiene to either **1** or **2** did not lead to decay of the spectroscopic features of the manganese(III)-peroxo structures, Scheme 1, hence $[Mn^{III}(O_2)(L^1)]^+$ and $[Mn^{III}(O_2)(L^2)]^+$ are unable to react via desaturation pathways. This is surprising as the deformylation reaction described above appears to have a rate-determining hydrogen atom abstraction step from 2-PPA to $[Mn^{III}(O_2)(L^2)]^+$. Moreover, the mechanistic probes ruled out the more commonly seen nucleophilic attack on the carbonyl group. Computational modeling, vide infra, established the reasons behind the lack of reactivity toward cyclohexadiene as resulting from an energetically high second hydrogen atom abstraction.

Finally, a radical trapping experiment with bromotrichloromethane was performed to establish that the reaction mechanism of manganese(III)-peroxo with aldehydes proceeds through a radical intermediate species.[9,23] Addition of 2-PPA to intermediate **2** in the presence of excess $CBrCl_3$ or CBr_4 in acetonitrile at 15 °C leads to the formation of α-brominated product of the 2-PPA exclusively, Scheme 2, which was

Scheme 2. Reaction of $[Mn^{III}(O_2)(L^2)]^+$ with Radical Trapping Substrates

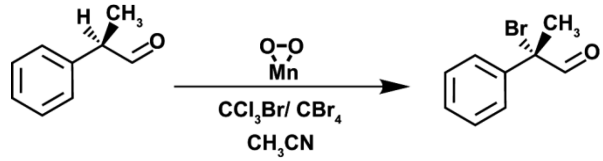

confirmed by NMR analysis (see Figure S4). Consequently, our radical trapping experiment confirms a radical mechanism that most likely starts with hydrogen atom abstraction from the α-position of 2-PPA.

In conclusion, experimental kinetics studies find that aldehyde deformylation starts with a rate-determining hydrogen atom abstraction from the α-position of 2-PPA leading to a radical intermediate. On the other hand, no reactivity is observed between $[Mn^{III}(O_2)(L^2)]^+$ and substrates with weak C–H bonds such as cyclohexadiene. To understand the reaction mechanisms and explain the reactivity patterns of side-on manganese(III)-peroxo with substrates, a computational study was performed.

Computational Modeling. To explain the experimentally obtained results on the reactivity of side-on manganese(III)-peroxo with aldehydes, we embarked on a density functional theory study on the possible reaction mechanisms leading to aldehyde deformylation by these complexes. Although we tested many possible mechanisms and spin states (vide infra), our lowest-energy pathway leading to the first oxygen atom transfer is on a quintet spin state, Figure 3. The reaction starts with a hydrogen atom abstraction via transition state TS_{HAT1} and forms a manganese(II)-hydroperoxo with a radical intermediate I_1.

In the quintet spin state, the barrier is 19.2 kcal mol^{-1} and the reaction is endothermic by 7.0 kcal mol^{-1}. Rather than radical rebound, however, as is common in typical hydrogen atom abstraction reactions,[24] actually the hydrogen atom is bounced back to substrate to give the enol form of the substrate

DOI: 10.1021/jacs.7b10033
J. Am. Chem. Soc. 2017, 139, 18328–18338

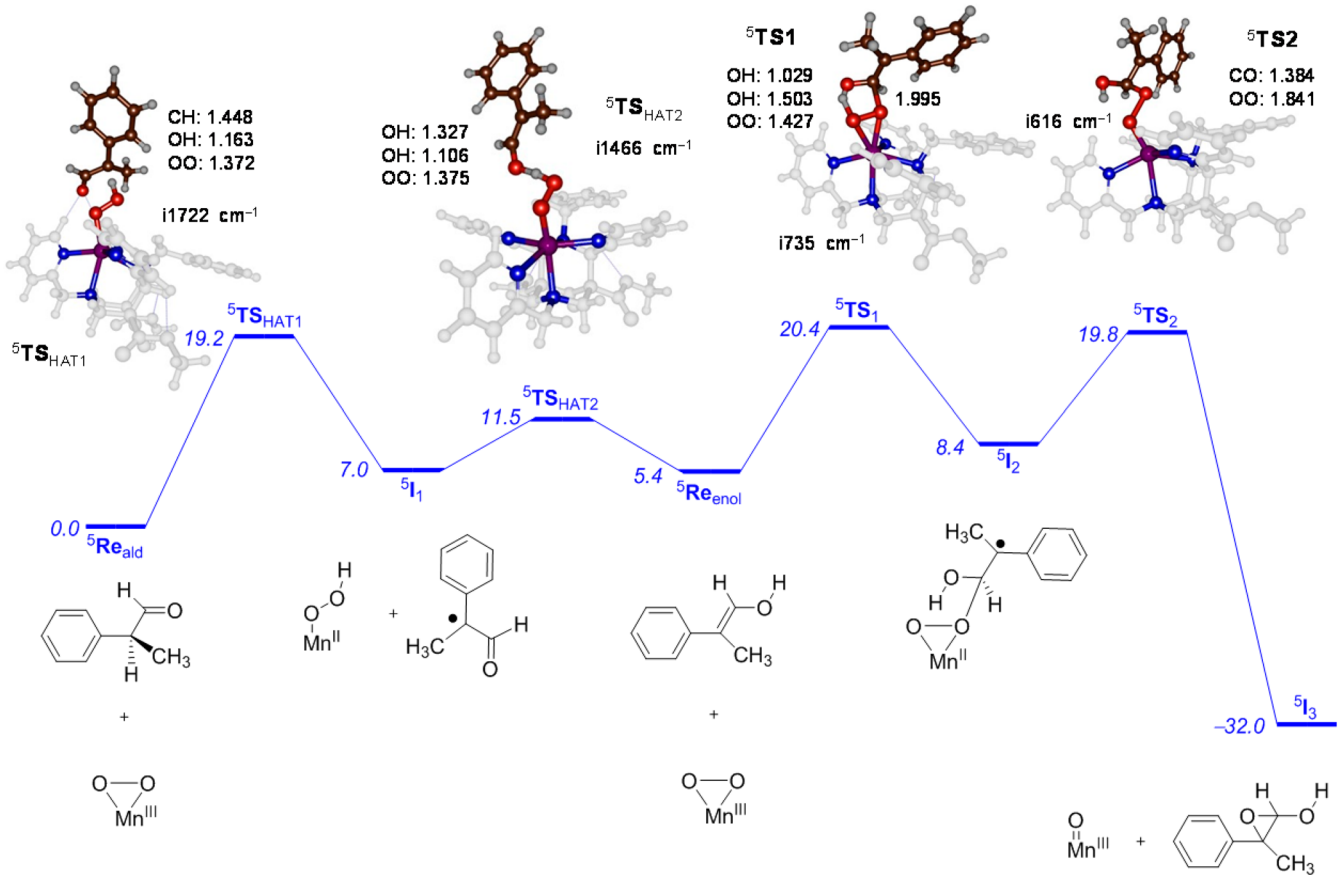

Figure 3. Potential energy profile (UB3LYP/BS2//UB3LYP/BS1+ZPE) for oxygen atom transfer from $[Mn^{III}(O_2)(L^2)]^+$ to 2-PPA with energies in kcal mol^{-1}. Transition state structures give distances in angstroms and the imaginary frequency in cm^{-1}.

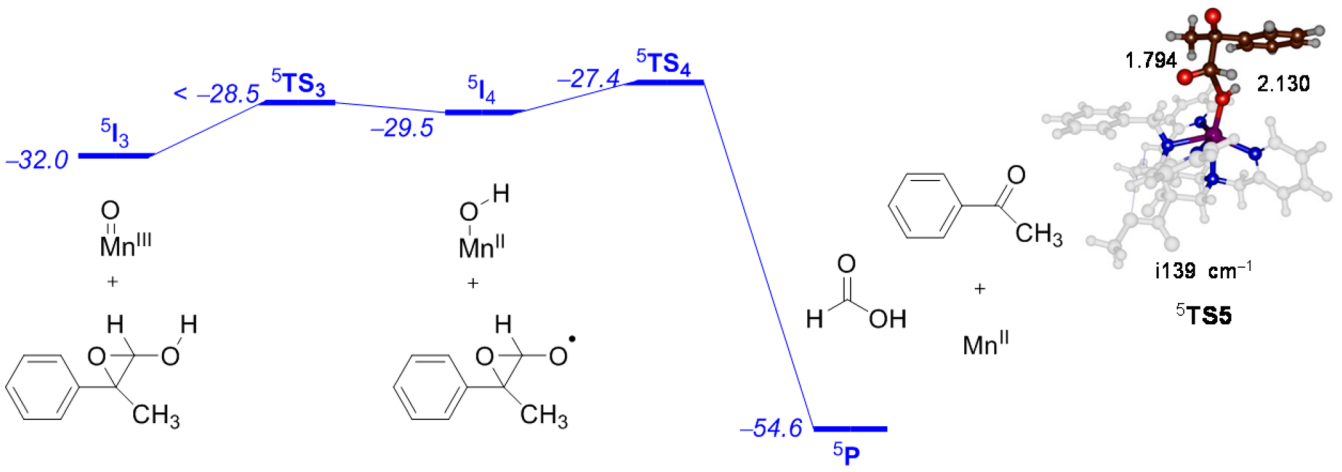

Figure 4. Potential energy profile (UB3LYP/BS2//UB3LYP/BS1+ZPE) for oxygen atom transfer from $^5\mathbf{I}_3$ leading to products with energies in kcal mol^{-1}. Transition state structure gives distances in angstroms and the imaginary frequency in cm^{-1}.

and manganese(III)-peroxo via a subsequent barrier $\mathbf{TS}_{HAT2}$ of 4.5 kcal mol^{-1}. The enol form of the reactant ($^5\mathbf{Re}_{enol}$) is slightly lesser stable than the keto form (by 5.4 kcal mol^{-1}). Once the reactant is in the enol-form, the manganese(III)-peroxo part of the reactant complex attacks the substrate olefin bond via a nucleophilic transition state ^{5}**TS1** of 20.4 kcal mol^{-1} to form the radical intermediate $^5\mathbf{I}_2$. Energetically, $^5\mathbf{I}_2$ is close in energy to $^5\mathbf{I}_1$ and $^5\mathbf{Re}_{enol}$ and will react via an O−O cleavage barrier (^{5}**TS2**) to form a manganese(III)-oxo complex and an epoxide ($^5\mathbf{I}_3$) in a highly exothermic process. As such, the computational studies implicate that probably the first steps in the reaction mechanism will be reversible, but the step from $^5\mathbf{I}_2$ to $^5\mathbf{I}_3$ will be irreversible. We also tested the triplet spin pathway but found it at least 20 kcal mol^{-1} higher in energy along the full profile (see the Supporting Information).

Geometrically, $^5\mathbf{TS}_{HAT1}$ and $^5\mathbf{TS}_{HAT2}$ have features typical of hydrogen atom abstraction barriers seen before for the reaction of heme and nonheme iron(IV)-oxo with aliphatic substrates.[25] Both barriers have a large imaginary frequency, which implies that substitution of the transferring hydrogen atom by

DOI: 10.1021/jacs.7b10033
J. Am. Chem. Soc. 2017, 139, 18328−18338

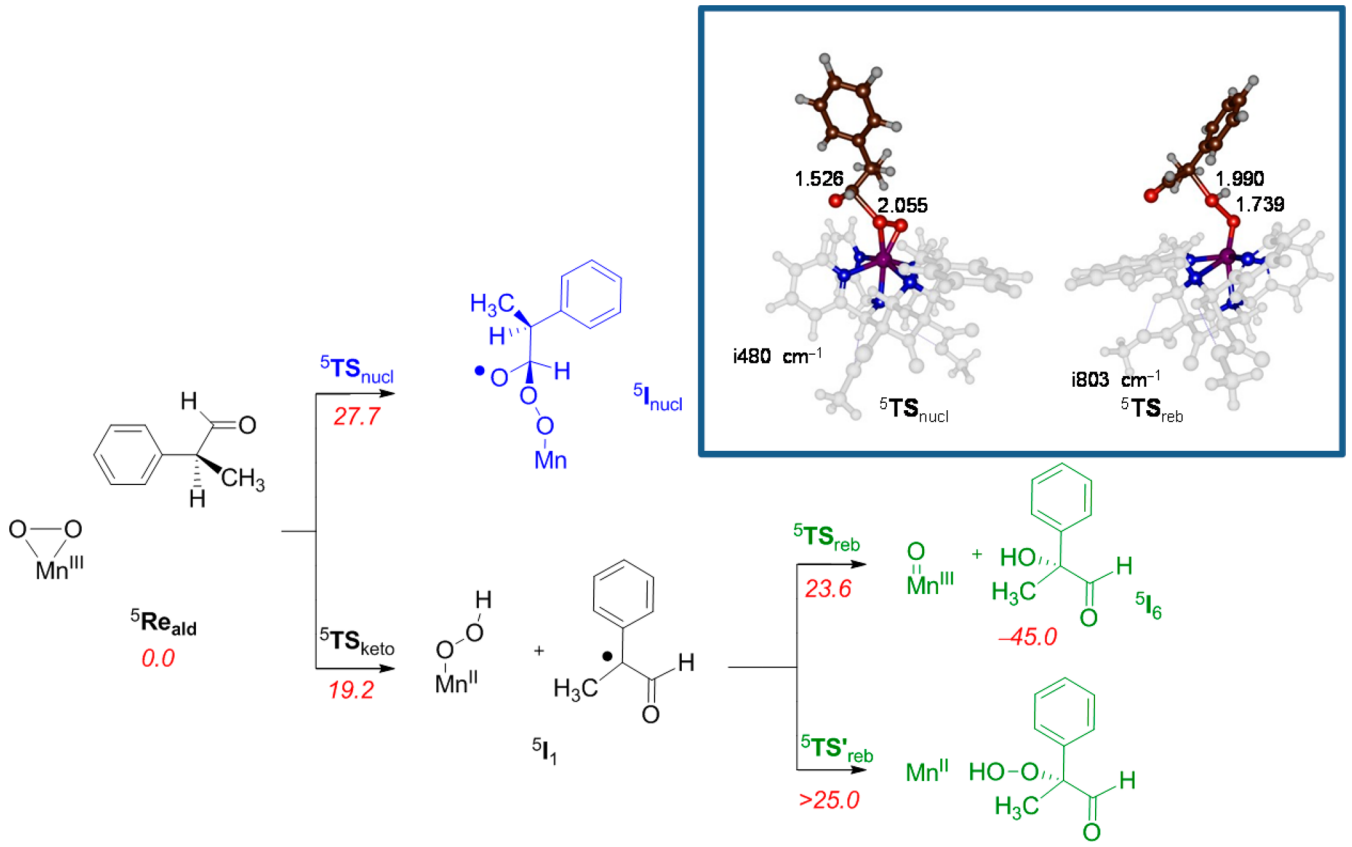

Figure 5. Alternative nucleophilic transition states along the pathway of aldehyde deformylation by side-on manganese(III)-peroxo as calculated at the UB3LYP/BS2//UB3LYP/BS1+ZPE level of theory. Energies are in kcal mol^{-1}. Transition state structures give distances in angstroms and the imaginary frequency in cm^{-1}.

deuterium should give a major change in the value of the free energy of activation and, hence, a large kinetic isotope effect,[26] as indeed observed experimentally and reported above in Figure 2. Moreover, the transition states are late with long C−H and short O−H distances for ^{5}**TS**$_{HAT1}$ (1.448 and 1.163 Å, respectively), while the transferring hydrogen atom in ^{5}**TS**$_{HAT2}$ is closer to the donor hydroperoxo group (1.106 Å) than the accepting alcohol oxygen atom (1.327 Å).

In the enol-form, a nucleophilic attack takes the place of the manganese(III)-peroxo group on the double bond through a C−O bond formation via ^{5}**TS1**. This transition state has a relatively large imaginary frequency of i735 cm^{-1} due to the simultaneous C−O bond formation and proton transfer from enol to peroxo. Thus, the peroxo bond weakens to 1.427 Å, and a C−O interaction of 1.995 Å is formed.

After the transition state, the system relaxes to a local minimum that has a single bond for the C−O interaction and a radical on the neighboring carbon atom. In addition, the dioxygen moiety moves from a side-on to an end-on conformation. The dioxygen bond cleaves in ^{5}**TS2** at an energetic cost of 19.8 kcal mol^{-1}. In this step, simultaneous to the O−O bond breaking, an epoxide ring is formed to give a low-energy manganese(III)-oxo species. The imaginary mode in the transition state indeed reflects the O−O bond cleavage on the one hand with the epoxide ring-closure on the other hand.

The next stage in the mechanism from epoxide to final deformylation products is given in Figure 4. Thus, the manganese(III)-oxo group abstracts a hydrogen atom in ^{5}**I**$_3$ from the alcohol position of substrate, which breaks the epoxide ring to form a complex between manganese(II)-hydroxo and a radical (^{5}**I**$_4$). This step has an almost barrierless reaction pathway via ^{5}**TS3**, and hence the ^{5}**TS3** structure could not be properly characterized. An estimate from the geometry scan predicts it to be less than 1 kcal mol^{-1} in energy above the value of ^{5}**I**$_4$. The subsequent OH rebound leads to simultaneous epoxide ring-opening, C−C bond cleavage and the formation of formic acid and methylphenylketone products via transition state ^{5}**TS4**. The imaginary frequency of i139 cm^{-1} indeed reflects the C−C bond breaking and the dissociation of methylphenylketone from the complex. At the same time the OH rebound to the HCO leaving group results in formic acid as the second product. The overall reaction mechanism has two highly exothermic reaction steps, namely the formation of the manganese(III)-oxo species (^{5}**I**$_3$) and the final reaction step leading to methylphenylketone and formic acid products. These two steps will be irreversible, although other reactions steps may be reversible.

In summary, the lowest-energy pathway for aldehyde deformylation by side-on manganese(III)-peroxide of 2-PPA is α-hydrogen atom abstraction followed by reshuttle and tautomerization to form the enol form and nucleophilic attack on the olefin bond. Oxygen atom transfer then gives epoxide that through a low-barrier hydrogen atom transfer gives formic acid and methylphenylketone products.

Alternative Mechanisms. Several alternative pathways for aldehyde deformylation by side-on manganese(III)-peroxo complexes were considered, as shown in Figure 5. First, a direct nucleophilic attack on the carbonyl group of 2-PPA was considered by side-on manganese(III)-peroxo. The nucleo-

DOI: 10.1021/jacs.7b10033
J. Am. Chem. Soc. 2017, 139, 18328−18338

philic pathway proceeds via a transition state ^{5}**TS**$_{nucl}$ to form the nucleophilic addition intermediate ^{5}**I**$_{nucl}$ (Figure 5). Similarly to the results reported previously,[9] this is a high-energy pathway with a barrier of $\Delta E^{\ddagger}$ + ZPE = 27.7 kcal mol^{-1}. The transition state has an imaginary frequency of i480 cm^{-1}, which reflects the C−O bond formation between peroxo and carbonyl moieties and simultaneously the peroxo moves from side-on to end-on. Clearly, the direct nucleophilic addition from side-on peroxo is well higher in energy than the hydrogen atom abstraction reported above in Figure 4 by at least 8.5 kcal mol^{-1} and hence will not be competitive.

We also investigated mechanisms starting from the manganese(III)-hydroperoxo intermediate ^{5}**I**$_1$ and, in particular, looked at OH rebound to form manganese(III)-oxo and 2-hydroxo-2-phenyl-propionaldehyde (^{5}**I**$_6$). Although, ^{5}**I**$_6$ is considerably more stable than the epoxide intermediate ^{5}**I**$_3$ reported above. Actually, its formation barrier is considerably higher in energy. Therefore, despite the fact that ^{5}**I**$_6$ is a more stable intermediate than ^{5}**I**$_3$, the preferred reaction intermediate leading to aldehyde deformylation will pass ^{5}**I**$_3$. The OH rebound transition state (^{5}**TS**$_{reb}$) has typical features seen before for OH transfer from iron(III)-hydroperoxo complexes,[27] with simultaneous O−O cleavage and C−O bond formation in a concerted reaction step. The OH group is located midway between donor and acceptor groups through long interactions of 1.990 and 1.739 Å.

Additionally, various other pathways were tested (see Supporting Information), including rebound of the OH group to the aldehyde carbon atom. However, this OH rebound pathway formed a biradical species that is very high in energy (>50 kcal mol^{-1}). Also, OOH transfer from the manganese(II)-hydroperoxo intermediate (^{5}**I**$_1$) to the radical gave a barrier (^{5}**TS'**$_{reb}$) of well over 25 kcal mol^{-1} in energy. Unfortunately, no subsequent pathways leading to aldehyde deformylation products could be identified, and therefore, the mechanism was ruled out. Finally, a mechanism was considered for nucleophilic attack of manganese(III)-peroxo on the secondary carbon atom of the enol form of 2-PPA. The intermediate formed through this pathway is high in energy (>40 kcal mol^{-1} with respect to ^{5}**Re**$_{ald}$), and consequently, the pathway is ruled out as a viable reaction mechanism.

In conclusion, the lowest-energy reaction mechanism for aldehyde deformylation by manganese(III)-peroxo complexes we have identified starts with hydrogen atom abstraction from the α-position followed by a reshuttle, whereby the aldehyde is converted into an enol that can efficiently react via nucleophilic addition with the side-on manganese(III)-peroxo.

DISCUSSION

To understand the unusual mechanism found for aldehyde deformylation by manganese(III)-peroxo complexes, we analyzed the structure and electronic configuration of all species in detail and set up valence bond and thermo-chemical cycles to explain the mechanism and rationalize the observed reactivities.

Thermochemical Modeling. Let us first try to predict the hydrogen atom abstraction barriers for the keto and enol form of 2-PPA by side-on manganese(III)-peroxo complexes. The driving force for the hydrogen atom abstraction can be written as the difference in energy between the C−H/O−H bond that is broken and the O−H bond formed to give the manganese-(II)-hydroperoxo, which in general terms using substrate SubH is given in eq 4.

$$[Mn^{III}(O_2)(L^2)]^+ + SubH \rightarrow [Mn^{II}OOH(L^2)]^+ + Sub^{\bullet} \quad (4)$$

The overall reaction (eq 4) has an energy corresponding to the driving force ΔE_{rp} and can be written as the difference between two bond dissociation free energies (BDFEs) of the bonds that are formed and broken as defined in eqs 5−7. Thus, the BDFE values for the substrate C−H bond of the aldehyde from 2-PPA and the O−H bond of the enol form of 2-PPA are defined as through eq 5 as BDFE$_{CH}$(2-PPA) and BDFE$_{OH}$(2-PPA). Values were calculated from a full geometry optimization of 2-PPA and 2-PPA with the transferring hydrogen atom removed (Sub$^{\bullet}$) and the free energy difference obtained from eq 5. Subsequently, we calculated the BDFE$_{OH}$ value of the manganese(II)-hydroperoxo species from its free energy difference with the manganese(III)-peroxo and a hydrogen atom (eq 6) as defined as BDFE$_{OH}$(Ox).

$$SubH \rightarrow Sub^{\bullet} + H^{\bullet} + BDFE_{AH}(SubH) \quad (5)$$

$$[Mn^{II}OOH(L^2)]^+ \rightarrow [Mn^{III}(O_2)(L^2)]^+ + H^{\bullet} + BDFE_{OH}(Ox) \quad (6)$$

$$\Delta G_{rp} = BDFE_{AH}(SubH) - BDFE_{OH}(Ox) \quad (7)$$

Therefore, the free energy driving force for the hydrogen atom abstraction from substrate (ΔG_{rp}), be it in the keto or enol form, by $[Mn^{III}(O_2)(L^2)]^+$ can be written in terms of BDFE of donor and acceptor groups, eq 7. We calculate BDFE values of 66.1 and 55.9 kcal mol^{-1} for hydrogen atom abstraction from the keto and enol forms of 2-PPA, respectively. In agreement with the potential energy landscape in Figure 4 above, these BDFE$_{CH}$ values implicate that it is easier to abstract a hydrogen atom from the enol form of substrate than from the α-position of the aldehyde.

Furthermore, BDFE$_{OH}$ values of 56.6 and 61.1 kcal mol^{-1} were obtained for $[Mn^{II}OOH(L^1)]^+$ and $[Mn^{II}OOH(L^2)]^+$, respectively. Consequently, the driving forces for hydrogen atom abstraction of $[Mn^{III}(O_2)(L^2)]^+$ from 2-PPA in its keto form is ΔG = 5.0 kcal mol^{-1}, which is in excellent agreement with the reaction free energy from ^{5}**Re**$_{ald}$ to ^{5}**I**$_1$ of 6.2 kcal mol^{-1} (Table S3). Similarly, the driving force from hydrogen atom abstraction of the enol form of 2-PPA by $[Mn^{III}(O_2)(L^2)]^+$ of ΔG = −5.2 kcal mol^{-1} matches the free-energy difference between ^{5}**Re**$_{enol}$ and ^{5}**I**$_1$ reasonably well.

To compare the BDFE$_{CH}$ of 2-PPA with typical substrates used in hydrogen atom transfer reactions, we calculated the BDFE$_{CH}$ of 1,4-cyclohexadiene. Interestingly, the BDFE$_{CH}$ of 1,4-cyclohexadiene is 61.9 kcal mol^{-1}, which is midway in between the values for breaking the C−H bond of the keto-form of 2-PPA and the O−H bond of the enol form. Therefore, theory would expect the first aliphatic hydrogen atom abstraction of 1,4-cyclohexadiene by side-on manganese(III)-peroxo to proceed with similar rate constants as 2-PPA. However, no benzene products are obtained, which probably means that the subsequent reaction step between manganese-(II)-hydroperoxo and the C_6H_7 radical does not lead to products, and a further hydrogen atom abstraction is hampered. As side-on manganese(III)-peroxo can abstract a hydrogen atom from 2-PPA, this implies that the cyclohexadiene reaction is prevented due to an energetically unfavorable second hydrogen atom abstraction performed by the manganese(II)-hydroperoxo species. Thus, side-on manganese(III)-peroxo will

DOI: 10.1021/jacs.7b10033
J. Am. Chem. Soc. 2017, 139, 18328−18338

not react with aliphatic C−H bonds through substrate hydroxylation.

To test this hypothesis, we calculated the hydrogen atom abstraction energy by $[Mn^{II}OOH(L^2)]^+$ at either the distal or proximal oxygen atom, Scheme 3. In particular, we calculated

Scheme 3. Reactivity Channels of $[Mn^{II}(OOH)(L^2)]^+$ through Hydrogen Atom Abstraction (top) or O−O Bond Cleavage (Bottom)

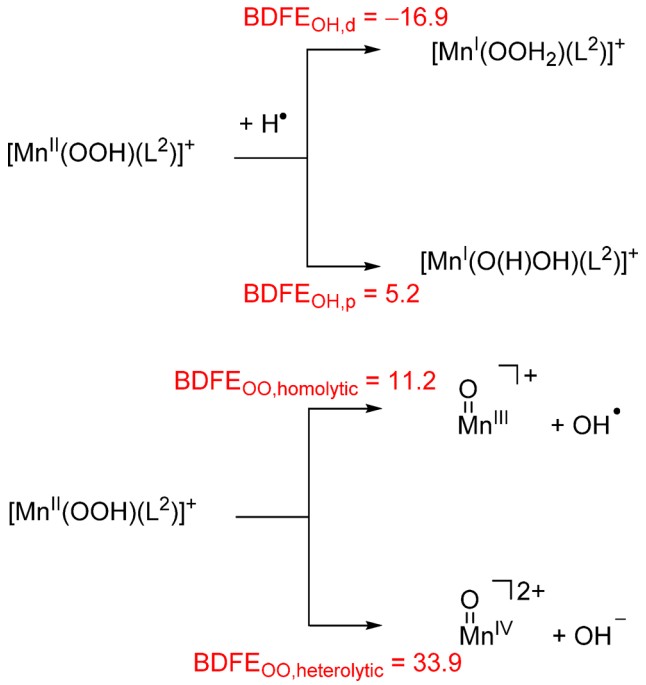

the diabatic hydrogen atom abstraction energy by the manganese(II)-hydroperoxo species as a full geometry optimization of either $[Mn^I(OOH_2)(L^2)]^+$ or $[Mn^I(O(H)OH)(L^2)]^+$, which led to dissociation of both complexes. Proximal donation of a hydrogen atom has a driving force of only 5.2 kcal mol^{-1}, whereas distal donation gives an endothermic BDFE value. Consequently, despite the fact that manganese(III)-peroxo is able to abstract hydrogen atoms from weak aliphatic C−H bonds, the resulting manganese(II)-hydroperoxo is inactive and thermodynamically unable to react further to give either alcohols or a dehydrogenation of the substrate.

To find out, whether the manganese(II)-hydroperoxo has other catalytic abilities, we calculated its homolytic and heterolytic O−O bond cleavage free energies, see bottom part of Scheme 3. Similar to that seen for nonheme iron(III)-hydroperoxo complexes,[28] also here the heterolytic cleavage is high in free energy (>30 kcal mol^{-1}) and can be ruled out. Homolytic cleavage is endothermic by 11.2 kcal mol^{-1} and, therefore, although a slow process, may be feasible. As such, the only probable reaction pathway for manganese(II)-hydroperoxo is homolytic cleavage of the O−O bond but will only be possible if the bond that is subsequently formed is strong enough to balance the energetic cost of the O−O bond breaking mechanism.

Valence Bond Rationalization of the Mechanism. Figure 6 gives the electronic delineation of the properties a rate-determining reaction barrier should possess and how this links to the properties of reactants and products.[9,21,29] Thus, as

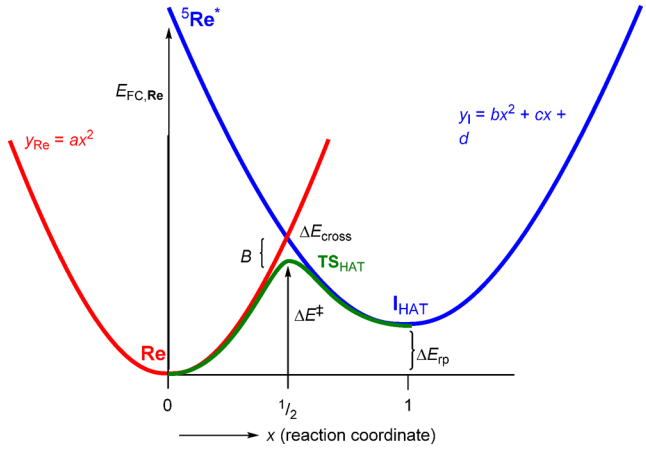

Figure 6. Definition of a reaction barrier and its connection to the vertical excitation energy in the reactants ($E_{FC,R}$) and the driving force for the reaction (ΔE_{rp}).

an example, we consider the hydrogen atom abstraction reaction from a reactant complex (*Re*) via a transition state ($\mathbf{TS}_{HAT}$) leading to a radical intermediate ($\mathbf{I}_{HAT}$). We now envisage the local minima to reside in a parabolic function (y, representing the potential energy) along the reaction coordinate axis (x) for the hydrogen atom abstraction with the reactants in the origin ($x = 0$) and the radical intermediate at the value $x = 1$. Mathematically, the potential energy functions for the reactant and intermediate states can then be described as shown in eqs 8 and 9 with a, b, c, and d some constants that determine the shape and curvature of the two parabolic functions.

$$y_{Re} = ax^2 \tag{8}$$

$$y_I = bx^2 + cx + d \tag{9}$$

It has been shown through valence bond modeling that the transition state connecting two local minima is located nearby the curve crossing of the valence bond (VB) curves of the reactant and product wave functions.[30] If we assume the crossing happens in $x = {}^1/_2$ then we can derive a function for the crossing point of the two curves as a function of two variables, namely the difference in energy between the two functions in $x = 0$ [i.e., the Franck−Condon energy in the reactants ($E_{FC,Re}$)] and the driving force for the hydrogen atom abstraction reaction (ΔE_{rp}), eq 10.

$$\Delta E_{cross} = 1/4E_{FC,Re} + 3/4\Delta E_{rp} \tag{10}$$

Further, it has been shown that the curve crossing energy is a fraction B (the resonance energy) above the actual transition state,[30] so that the height of the reaction barrier can be estimated from the Franck−Condon energy between the two states in the reactants, the driving force and the resonance energy. Previously, we used this procedure successfully to predict trends in aromatic hydroxylation reactions by iron(IV)-oxo porphyrin cation radical models and benchmarked the results against experimental rate constants.[31] In addition, we predicted regioselectivity ratios of aliphatic hydroxylation versus decarboxylation reactions in cytochrome P450 peroxygenase enzymes using VB models.[32]

Subsequently, we attempted to estimate the Franck−Condon energies ($E_{FC,Re}$) from electronic changes along the reaction mechanism for hydrogen atom abstraction (HAT) and

DOI: 10.1021/jacs.7b10033
J. Am. Chem. Soc. 2017, 139, 18328−18338

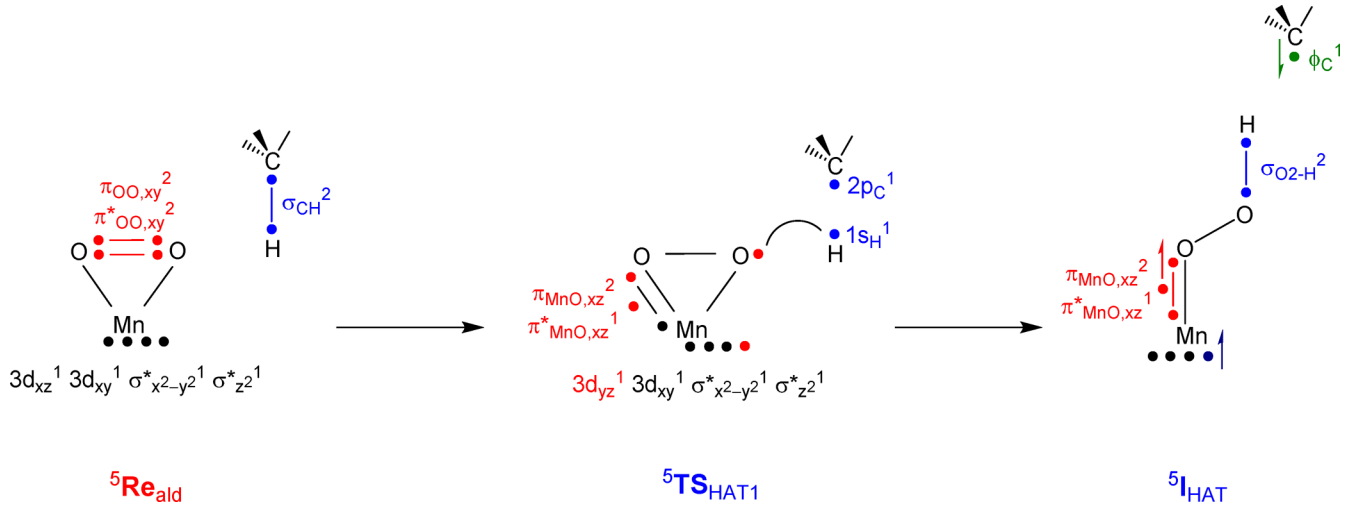

Figure 7. Electronic changes during the hydrogen atom abstraction from substrate by quintet spin side-on manganese(III)-peroxo. Dots represent electrons and lines between dots represent a bond orbital.

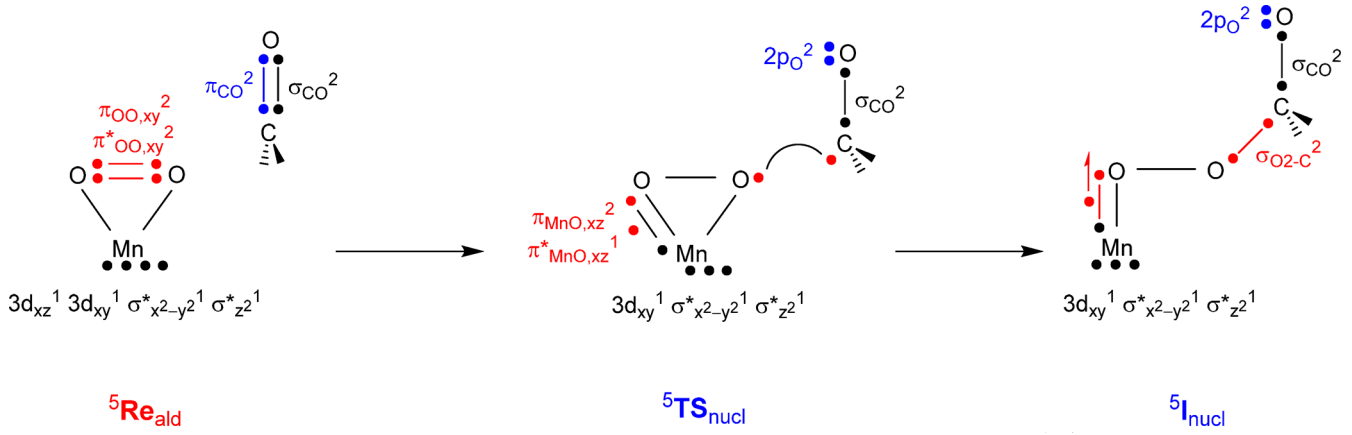

Figure 8. Electronic changes during the nucleophilic addition from substrate by quintet spin side-on manganese(III)-peroxo. Dots represent electrons and lines between dots a bond orbital.

nucleophilic addition (NA). Figure 7 displays the electronic changes during the hydrogen atom abstraction step between $^5[Mn^{III}(O_2)(L^2)]^+$ and substrate. Obviously, the hydrogen atom abstraction implies the breaking of a substrate C−H (or O−H in the case of the enol structure) bond orbital of the substrate (σ_{CH}) that splits into two atomic orbitals ($2p_C$ and $1s_H$ each with one electron). Therefore, the value of $E_{FC,Re}$ will contain the energy to break the σ_{CH} bond, $E_{\sigma(C-H)}$.

In addition, the peroxo double bond ($\pi_{OO,xy}/\pi^*_{OO,xy}$) breaks with energy $E_{\pi/\pi^*OO,xy}$, and the four electrons are redistributed over the manganese-peroxo system: two of those will pair up with the $3d_{xz}$ on manganese to form a three-electron MnO bond ($\pi_{MnO,xz}^2\ \pi^*_{MnO,xz}^1$), the third electron stays as a 2p on oxygen and will pair up with $1s_H$ to form the O−H orbital (σ_{O2-H}), while the fourth electron is promoted into the virtual $3d_{yz}$ orbital on manganese ($E_{exc,Mn}$). Consequently, the Franck−Condon energy should correlate with the breaking of the $\pi_{MnO,xz}$ orbitals, the formation of the O−H orbital, the breaking of the C−H orbital, and the electron transfer from peroxo to manganese, eq 11.

$$E_{FC,Re,HAT} = E_{\sigma(C-H)} + E_{\pi/\pi^*OO,xy} + E_{exc,Mn} \quad (11)$$

The $E_{\sigma(C-H)}$ was determined from the adiabatic values using eq 5 above as 82.6 kcal mol^{-1}. The $E_{\pi/\pi^*OO,xy}$ energy was determined from the orbital energy difference of the α-type $\pi_{OO,xy}$ and $\pi^*_{OO,xy}$ orbitals in the quintet spin reactant complex (78.2 kcal mol^{-1}), whereas $E_{exc,Mn}$ was taken as the energy difference between the $\pi^*_{OO,xy}$ and π^*_{yz} orbitals with β spin. These values gave us a prediction of $E_{FC,Re,HAT}$, whereas the energy difference of the BDE_{CH} of the substrate and the BDE_{OH} of $^6[MnOOH(L^2)]^+$ gave ΔE_{rp} = 8.0 kcal mol^{-1}. On the basis of eqs 10 and 11, we estimated the hydrogen atom abstraction barrier from the keto position as $\Delta E^{\ddagger}_{VB,HAT}$ = 18.5 kcal mol^{-1}. For comparison, using transition state theory, the experimental second-order rate constant of k_2 = 0.142 M^{-1} s^{-1} corresponds to a free energy of activation of $\Delta G^{\ddagger}_{2,exp}$ = 18.9 kcal mol^{-1} at 15 °C. Therefore, our DFT model predicts the hydrogen atom abstraction barrier perfectly and explains the contributions from orbital/bond breaking and forming processes.

Finally, we analyze the VB electronic configuration changes for the nucleophilic reaction of manganese(III)-peroxo with aldehyde in Figure 8. Similarly to the hydrogen atom abstraction step, the $\pi_{OO,xy}/\pi^*_{OO,xy}$ orbital couple is rehybridized and converted back into atomic orbitals, whereby again two of those electrons will form a new three-electron bond along the Mn−O axis ($\pi_{MnO,xz}^2\ \pi^*_{MnO,xz}^1$). The remaining two electrons originating from the $\pi_{OO,xy}/\pi^*_{OO,xy}$ orbitals are donated into the new σ-bond for the C−O interaction. This

DOI: 10.1021/jacs.7b10033
J. Am. Chem. Soc. 2017, 139, 18328−18338

results in the breaking of the π-bond of the carbonyl (in the keto-form) or olefin (in the enol-form) bond of the substrate.

To estimate the VB barrier for the nucleophilic attack, we again took the energy to break the $\pi_{OO,xy}/\pi^*_{OO,xy}$ orbitals ($E_{\pi/\pi^*oo,xy}$) as well as the energy to break the double bond ($E_{\pi,Sub}$), eq 12. The energy $E_{\pi,Sub}$ for the keto and enol forms of the substrate was determined from the singlet−triplet energy gap in the isolated forms as 83.1 and 77.5 kcal mol^{-1}, respectively. That way, we predict a nucleophilic barrier height of 24.8 kcal mol^{-1} for direct attack of aldehyde on side-on manganese(III)-peroxo. This value is in good quantitative agreement with the DFT barrier reported above and explains the electrostatic interactions relevant for the barrier height. It also shows that it will be easier for the enol form to react through nucleophilic addition then the keto form as the singlet−triplet energy gap in the double bond is much higher.

$$E_{FC,Re,NA} = E_{\pi,Sub} + E_{\pi/\pi^*OO,xy} \quad (12)$$

CONCLUSIONS

In this work, a combined experimental and computational study is reported on aldehyde deformylation by side-on manganese(III)-peroxo complexes. We identify a novel reaction mechanism that starts with a hydrogen atom abstraction and reshuttle to give a keto−enol tautomerization in the substrate as the rate-determining step. Subsequently, a nucleophilic attack on the olefin bond in the enol form leads to a low-energy mechanism to products. Alternative pathways were tested and ruled out. A detailed thermochemical and valence bond analysis of the structures of intermediates and reactants explains the need of the keto−enol tautomerization. Thus, in the enol form the olefin π-bond is easy to break, whereas breaking the carbonyl π-bond is more energetically demanding. As the reaction starts with a hydrogen atom abstraction from aldehyde, we also considered the manganese(III)-peroxo species as a general oxidant for substrate hydroxylation and desaturation reactions. Unfortunately, high reaction barriers for radical rebound are encountered and substrate hydroxylation and desaturation are unfeasible pathways at room temperature.

ASSOCIATED CONTENT

Supporting Information

The Supporting Information is available free of charge on the ACS Publications website at DOI: 10.1021/jacs.7b10033.

Mass, UV-vis, and NMR spectra; tables with energies, group spin densities, charges, and optimized geometries; Cartesian coordinates of all structures reported; and optimized structures (PDF)

AUTHOR INFORMATION

Corresponding Authors

*sam.devisser@manchester.ac.uk
*sastricv@iitg.ernet.in

ORCID

Prasenjit Barman: 0000-0002-4409-2782
Gourab Mukherjee: 0000-0002-7150-5570
Chivukula V. Sastri: 0000-0003-0477-7741
Sam P. de Visser: 0000-0002-2620-8788

Author Contributions

The manuscript was written through contributions of all authors. All authors have given approval to the final version of the manuscript.

Notes

The authors declare no competing financial interest.

ACKNOWLEDGMENTS

F.G.C.R. thanks the Conacyt (Mexico) for a studentship. D.K. and S.P.d.V. thank the University of Manchester for a Targeting GCRF Applications in Industrial Biotechnology: Enhancing International Collaborations award. Research support was provided by the Department of Science and Technology (SERB), India (EMR/2014/000279), to C.V.S. D.K. and J.K. acknowledge financial support from DBT, New Delhi (BT/PR14510/BID/07/334/2010).

REFERENCES

(1) See, for example: (a) Solomon, E. I.; Brunold, T. C.; Davis, M. I.; Kemsley, J. N.; Lee, S.-K.; Lehnert, N.; Neese, F.; Skulan, A. J.; Yang, Y.-S.; Zhou, J. *Chem. Rev.* **2000**, *100*, 235−349. (b) Bugg, T. D. H. *Curr. Opin. Chem. Biol.* **2001**, *5*, 550−555. (c) Ryle, M. J.; Hausinger, R. P. *Curr. Opin. Chem. Biol.* **2002**, *6*, 193−201. (d) Costas, M.; Mehn, M. P.; Jensen, M. P.; Que, L., Jr *Chem. Rev.* **2004**, *104*, 939−986. (e) Abu-Omar, M. M.; Loaiza, A.; Hontzeas, N. *Chem. Rev.* **2005**, *105*, 2227−2252. (f) Krebs, C.; Galonić Fujimori, D.; Walsh, C. T.; Bollinger, J. M., Jr *Acc. Chem. Res.* **2007**, *40*, 484−492. (g) Bruijnincx, P. C. A.; van Koten, G.; Klein Gebbink, R. J. M. *Chem. Soc. Rev.* **2008**, *37*, 2716−2744. (h) Solomon, E. I.; Light, K. M.; Liu, L. V.; Srnec, M.; Wong, S. D. *Acc. Chem. Res.* **2013**, *46*, 2725−2739. (i) McDonald, A. R.; Que, L., Jr *Coord. Chem. Rev.* **2013**, *257*, 414−428.

(2) (a) Zhu, W.; Richards, N. G. J. *Essays Biochem.* **2017**, *61*, 259−270. (b) Aguirre, J. D.; Culotta, V. C. *J. Biol. Chem.* **2012**, *287*, 13541−13548.

(3) (a) Jackson, T. A.; Brunold, T. C. *Acc. Chem. Res.* **2004**, *37*, 461−470. (b) Streit, B. R.; Blanc, B.; Lukat-Rodgers, G. S.; Rodgers, K.; Dubois, J. L. *J. Am. Chem. Soc.* **2010**, *132*, 5711−5724. (c) Hofbauer, S.; Gruber, C.; Pirker, K. F.; Sündermann, A.; Schaffner, I.; Jakopitsch, C.; Oostenbrink, C.; Furtmüller, P. G.; Obinger, C. *Biochemistry* **2014**, *53*, 3145−3157. (d) Grove, L. E.; Xie, J.; Yikilmaz, E.; Miller, A.-F.; Brunold, T. C. *Inorg. Chem.* **2008**, *47*, 3978−3992. (e) Kenkel, I.; Franke, A.; Dürr, M.; Zahl, A.; Dücker-Benfer, C.; Langer, J.; Filipović, M. R.; Yu, M.; Puchta, R.; Fiedler, S. R.; Shores, M. P.; Goldsmith, C. R.; Ivanović-Burmazović, I. *J. Am. Chem. Soc.* **2017**, *139*, 1472−1484. (f) Miller, A.-F. *FEBS Lett.* **2012**, *586*, 585−595. (g) Lee, A. Q.; Streit, B. R.; Zdilla, M. J.; Abu-Omar, M. M.; DuBois, J. L. *Proc. Natl. Acad. Sci. U. S. A.* **2008**, *105*, 15654−15659.

(4) (a) Vinyard, D. J.; Ananyev, G. M.; Dismukes, G. C. *Annu. Rev. Biochem.* **2013**, *82*, 577−606. (b) Renger, G.; Renger, T. *Photosynth. Res.* **2008**, *98*, 53−80. (c) Barber, J. *Q. Rev. Biophys.* **2003**, *36*, 71−89. (d) Siegbahn, P. E. M. *Chem. - Eur. J.* **2008**, *14*, 8290−8302.

(5) (a) Kryatov, S. V.; Rybak-Akimova, E. V.; Schindler, S. *Chem. Rev.* **2005**, *105*, 2175−2226. (b) Nam, W. *Acc. Chem. Res.* **2007**, *40*, 522−531. (c) Sahu, S.; Goldberg, D. P. *J. Am. Chem. Soc.* **2016**, *138*, 11410−11428. (d) Saisaha, P.; de Boer, J. W.; Browne, W. R. *Chem. Soc. Rev.* **2013**, *42*, 2059−2074.

(6) (a) Roelfes, G.; Vrajmasu, V.; Chen, K.; Ho, R. Y. N.; Rohde, J.-U.; Zondervan, C.; la Crois, R. M.; Schudde, E. P.; Lutz, M.; Spek, A. L.; Hage, R.; Feringa, B. L.; Münck, E.; Que, L., Jr *Inorg. Chem.* **2003**, *42*, 2639−2653. (b) Annaraj, J.; Suh, Y.; Seo, M. S.; Kim, S. O.; Nam, W. *Chem. Commun.* **2005**, 4529−4531. (c) Thibon, A.; Bartoli, J.-F.; Bourcier, S.; Banse, F. *Dalton Trans.* **2009**, 9587−9584. (d) Mukherjee, A.; Cranswick, M. A.; Chakrabarti, M.; Paine, T. K.; Fujisawa, K.; Münck, E.; Que, L., Jr *Inorg. Chem.* **2010**, *49*, 3618−3628. (e) Cho, J.; Jeon, S.; Wilson, S. A.; Liu, L. V.; Kang, E. A.; Braymer, J. J.; Lim, M. H.; Hedman, B.; Hodgson, K. O.; Valentine, J. S.; Solomon, E. I.; Nam, W. *Nature* **2011**, *478*, 502−505.

DOI: 10.1021/jacs.7b10033
J. Am. Chem. Soc. 2017, 139, 18328−18338

(7) (a) Annaraj, J.; Cho, J.; Lee, Y.-M.; Kim, S. Y.; Latifi, R.; de Visser, S. P.; Nam, W. *Angew. Chem., Int. Ed.* **2009**, *48*, 4150−4153. (b) Leto, D. F.; Chattopadhyay, S.; Day, V. W.; Jackson, T. A. *Dalton Trans.* **2013**, *42*, 13014−13025. (c) Zlatar, M.; Gruden, M.; Vassilyeva, O. Y.; Buvaylo, E. A.; Ponomarev, A. N.; Zvyagin, S. A.; Wosnitza, J.; Krzystek, J.; Garcia-Fernandez, P.; Duboc, C. *Inorg. Chem.* **2016**, *55*, 1192−1201. (d) Lee, C.-M.; Chuo, C.-H.; Chen, C.-H.; Hu, C.-C.; Chiang, M.-H.; Tseng, Y.-J.; Hu, C.-H.; Lee, G.-H. *Angew. Chem., Int. Ed.* **2012**, *51*, 5427−5430. (e) Gennari, M.; Brazzolotto, D.; Pécaut, J.; Cherrier, M. V.; Pollock, C. J.; DeBeer, S.; Retegan, M.; Pantazis, D. A.; Neese, F.; Duboc, C. *J. Am. Chem. Soc.* **2015**, *137*, 8644−8653. (f) Brazzolotto, D.; Cantú Reinhard, F. G.; Smith-Jones, J.; Retegan, M.; Amidani, L.; Faponle, A. S.; Ray, K.; Philouze, C.; de Visser, S. P.; Gennari, M.; Duboc, C. *Angew. Chem., Int. Ed.* **2017**, *56*, 8211−8215.

(8) (a) Coggins, M. K.; Kovacs, J. A. *J. Am. Chem. Soc.* **2011**, *133*, 12470−12473. (b) Coggins, M. K.; Martin-Diaconescu, V.; DeBeer, S.; Kovacs, J. A. *J. Am. Chem. Soc.* **2013**, *135*, 4260−4272. (c) Colmer, H. E.; Howcroft, A. W.; Jackson, T. A. *Inorg. Chem.* **2016**, *55*, 2055−2069. (d) Cho, J.; Sarangi, R.; Nam, W. *Acc. Chem. Res.* **2012**, *45*, 1321−1330. (e) Zhang, Q.; Bell-Taylor, A.; Bronston, F. M.; Gorden, J. D.; Goldsmith, C. R. *Inorg. Chem.* **2017**, *56*, 773−782.

(9) Barman, P.; Upadhyay, P.; Faponle, A. S.; Kumar, J.; Nag, S. S.; Kumar, D.; Sastri, C. V.; de Visser, S. P. *Angew. Chem., Int. Ed.* **2016**, *55*, 11091−11095.

(10) (a) Vardhaman, A. K.; Barman, P.; Kumar, S.; Sastri, C. V.; Kumar, D.; de Visser, S. P. *Angew. Chem., Int. Ed.* **2013**, *52*, 12288−12292. (b) Kumar, S.; Faponle, A. S.; Barman, P.; Vardhaman, A. K.; Sastri, C. V.; Kumar, D.; de Visser, S. P. *J. Am. Chem. Soc.* **2014**, *136*, 17102−17115. (c) Barman, P.; Faponle, A. S.; Vardhaman, A. K.; Angelone, D.; Löhr, A.-M.; Browne, W. R.; Comba, P.; Sastri, C. V.; de Visser, S. P. *Inorg. Chem.* **2016**, *55*, 10170−10181.

(11) Armarego, W. L. F. In *Purification of Laboratory Chemicals*, Perrin, D. D., Ed.; Pergamon Press: Oxford, 1997.

(12) (a) Börzel, H.; Comba, P.; Hagen, K. S.; Lampeka, Y. D.; Lienke, A.; Linti, G.; Merz, M.; Pritzkow, H.; Tsymbal, L. V. *Inorg. Chim. Acta* **2002**, *337*, 407−419. (b) Comba, P.; Kuwata, S.; Linti, G.; Pritzkow, H.; Tarnai, M.; Wadepohl, H. *Chem. Commun.* **2006**, 2074−2076. (c) Comba, P.; Kanellakopulos, B.; Katsichtis, C.; Lienke, A.; Pritzkow, H.; Rominger, F. *J. Chem. Soc., Dalton Trans.* **1998**, 3997−4001. (d) Barman, P.; Vardhaman, A. K.; Martin, B.; Wörner, S. J.; Sastri, C. V.; Comba, P. *Angew. Chem., Int. Ed.* **2015**, *54*, 2095−2099.

(13) Goto, Y.; Wada, S.; Morishima, I.; Watanabe, Y. *J. Inorg. Biochem.* **1998**, *69*, 241−247.

(14) (a) de Visser, S. P.; Quesne, M. G.; Martin, B.; Comba, P.; Ryde, U. *Chem. Commun.* **2014**, *50*, 262−282. (b) Sainna, M. A.; Kumar, S.; Kumar, D.; Fornarini, S.; Crestoni, M. E.; de Visser, S. P. *Chem. Sci.* **2015**, *6*, 1516−1529.

(15) Frisch, M. J.; Trucks, G. W.; Schlegel, H. B.; Scuseria, G. E.; Robb, M. A.; Cheeseman, J. R.; Scalmani, G.; Barone, V.; Mennucci, B.; Petersson, G. A.; Nakatsuji, H.; Caricato, M.; Li, X.; Hratchian, H. P.; Izmaylov, A. F.; Bloino, J.; Zheng, G.; Sonnenberg, J. L.; Hada, M.; Ehara, M.; Toyota, K.; Fu-kuda, R.; Hasegawa, J.; Ishida, M.; Nakajima, T.; Honda, Y.; Kitao, O.; Nakai, H.; Vreven, T.; Montgomery, J. A., Jr.; Peralta, J. E.; Ogliaro, F.; Bearpark, M.; Heyd, J. J.; Brothers, E.; Kudin, K. N.; Staroverov, V. N.; Keith, T.; Kobayashi, R.; Normand, J.; Raghavachari, K.; Rendell, A.; Burant, J. C.; Iyengar, S. S.; Tomasi, J.; Cossi, M.; Re-ga, N.; Millam, J. M.; Klene, M.; Knox, J. E.; Cross, J. B.; Bakken, V.; Adamo, C.; Jaramillo, J.; Gomperts, R.; Stratmann, R. E.; Yazyev, O.; Austin, A. J.; Cammi, R.; Pomelli, C.; Ochterski, J. W.; Martin, R. L.; Morokuma, K.; Zakrzewski, V. G.; Voth, G. A.; Salvador, P.; Dannen-berg, J. J.; Dapprich, S.; Daniels, A. D.; Farkas, O.; Foresman, J. B.; Ortiz, J. V.; Cioslowski, J.; Fox, D. J. *Gaussian 09*, revision C.01; Gaussian, Inc.: Wallingford, CT, 2010.

(16) Tomasi, J.; Mennucci, B.; Cammi, R. *Chem. Rev.* **2005**, *105*, 2999−3093.

(17) (a) Becke, A. D. *J. Chem. Phys.* **1993**, *98*, 5648−5652. (b) Lee, C.; Yang, W.; Parr, R. G. *Phys. Rev. B: Condens. Matter Mater. Phys.* **1988**, *37*, 785−789.

(18) (a) Hay, P. J.; Wadt, W. R. *J. Chem. Phys.* **1985**, *82*, 270−283. (b) Hehre, W. J.; Ditchfield, R.; Pople, J. A. *J. Chem. Phys.* **1972**, *56*, 2257−2262.

(19) (a) de Visser, S. P. *J. Am. Chem. Soc.* **2010**, *132*, 1087−1097. (b) Quesne, M. G.; Senthilnathan, D.; Singh, D.; Kumar, D.; Maldivi, P.; Sorokin, A. B.; de Visser, S. P. *ACS Catal.* **2016**, *6*, 2230−2243.

(20) (a) Cantú Reinhard, F. G.; Faponle, A. S.; de Visser, S. P. *J. Phys. Chem. A* **2016**, *120*, 9805−9814. (b) Yang, T.; Quesne, M. G.; Neu, H. M.; Cantú Reinhard, F. G.; Goldberg, D. P.; de Visser, S. P. *J. Am. Chem. Soc.* **2016**, *138*, 12375−12386.

(21) (a) de Visser, S. P. *Chem. - Eur. J.* **2006**, *12*, 8168−8177. (b) Li, X.-X.; Postils, V.; Sun, W.; Faponle, A. S.; Solà, M.; Wang, Y.; Nam, W.; de Visser, S. P. *Chem. - Eur. J.* **2017**, *23*, 6406−6418.

(22) (a) Quesne, M. G.; Latifi, R.; Gonzalez-Ovalle, L. E.; Kumar, D.; de Visser, S. P. *Chem. - Eur. J.* **2014**, *20*, 435−446. (b) Timmins, A.; Saint-André, M.; de Visser, S. P. *J. Am. Chem. Soc.* **2017**, *139*, 9855−9866.

(23) (a) Groves, J. T.; Nemo, T. E. *J. Am. Chem. Soc.* **1983**, *105*, 6243−6248. (b) Rana, S.; Dey, A.; Maiti, D. *Chem. Commun.* **2015**, *51*, 14469−14472.

(24) (a) Yoshizawa, K.; Kamachi, T.; Shiota, Y. *J. Am. Chem. Soc.* **2001**, *123*, 9806−9816. (b) Shaik, S.; Kumar, D.; de Visser, S. P.; Altun, A.; Thiel, W. *Chem. Rev.* **2005**, *105*, 2279−2328. (c) Shaik, S.; Kumar, D.; de Visser, S. P. *J. Am. Chem. Soc.* **2008**, *130*, 10128−10140. (d) Li, D.; Wang, Y.; Han, K. *Coord. Chem. Rev.* **2012**, *256*, 1137−1150.

(25) (a) de Visser, S. P.; Kumar, D.; Cohen, S.; Shacham, R.; Shaik, S. *J. Am. Chem. Soc.* **2004**, *126*, 8362−8363. (b) Kumar, D.; Hirao, H.; Que, L., Jr.; Shaik, S. *J. Am. Chem. Soc.* **2005**, *127*, 8026−8027. (c) Geng, C. Y.; Ye, S. F.; Neese, F. *Angew. Chem., Int. Ed.* **2010**, *49*, 5717−5720. (d) Srnec, M.; Solomon, E. I. *J. Am. Chem. Soc.* **2017**, *139*, 2396−2407.

(26) Latifi, R.; Bagherzadeh, M.; de Visser, S. P. *Chem. - Eur. J.* **2009**, *15*, 6651−6662.

(27) Faponle, A. S.; Quesne, M. G.; Sastri, C. V.; Banse, F.; de Visser, S. P. *Chem. - Eur. J.* **2015**, *21*, 1221−1236.

(28) Faponle, A. S.; Banse, F.; de Visser, S. P. *JBIC, J. Biol. Inorg. Chem.* **2016**, *21*, 453−462.

(29) (a) Hernández-Ortega, A.; Quesne, M. G.; Bui, S.; Heyes, D. J.; Steiner, R. A.; Scrutton, N. S.; de Visser, S. P. *J. Am. Chem. Soc.* **2015**, *137*, 7474−7487. (b) Cantú Reinhard, F. G.; de Visser, S. P. *Chem. - Eur. J.* **2017**, *23*, 2935−2944.

(30) Shaik, S. *Phys. Chem. Chem. Phys.* **2010**, *12*, 8706−8720.

(31) Cantú Reinhard, F. G.; Sainna, M. A.; Upadhyay, P.; Balan, G. A.; Kumar, D.; Fornarini, S.; Crestoni, M. E.; de Visser, S. P. *Chem. - Eur. J.* **2016**, *22*, 18608−18619.

(32) Faponle, A. S.; Quesne, M. G.; de Visser, S. P. *Chem. - Eur. J.* **2016**, *22*, 5478−5483.

DOI: 10.1021/jacs.7b10033
J. Am. Chem. Soc. 2017, 139, 18328−18338

Advanced Materials Science

Research Article

Quantum mechanical study of Ga_xAs_x fullerene type Micro-Clusters for X=10, 13, 15, 18, 20, 25 and 30 atoms

Deep Kumar, Ankur Trivedi and Devesh Kumar*

Department of Applied Physics, Babasaheb Bhimrao Ambedkar Univesity, Lucknow, India

Abstract

The present paper presents electronic structure and optical properties of the Ga_xAs_x clusters for x= 10, 13, 15, 18, 20, 25 and 30 using density functional theory (DFT) method. The Ga-Ga bond length lies in range of 2.50-2.69 A^0, the As-As bond length lies in range 2.58-2.62 A^0 and Ga-As bonds length is in range 2.46-2.52 A^0. The variation of polarizability, which reflects optical activity, with increase cluster size is presented and the study suggests that Ga25As25 cluster has more optical activity in comparison with other studied clusters.

Introduction

Low-dimensional semi-conducting material is of great interest to researchers in Nano science [1-4]. Micro-clusters present a new phase of a solid with novel properties and are formed by aggregation of atoms or molecules, and also exhibit properties significantly different from that of the bulk solid state of the constituent molecules or atoms. The dependence of electronic structure of the micro-cluster on its physical size gives rise to new physical, optical [5] electronic [6] chemical as well as magnetic properties [7]. Since the properties of a micro-cluster depend on its composition so it enables to fine tune different properties of micro-clusters, particularly in case of semiconductor clusters, resulting in novel optical and electronic capabilities. Investigation of clusters also enables to study the emergence of bulk crystalline properties from atomic or molecular scale. In order to obtain some desired property from a cluster, a detailed study about the properties of the cluster and its flexibility to control its size. The present day computational resources and techniques have enabled to model and investigate these clusters with ease and accuracy.

Fullerenes that have a special structure which consists only of pentagonal and hexagonal rings with hollow cage like structure and belong to the class of micro-clusters. With all possible arrangement of collections of atom between these pentagon and hexagon many isomers can be constructed by varying the number of atoms [7]. After the discovery of Carbon fullerene the interest has now shifted towards the search of new fullerene like structures formed by other elements/combination of different elements because fullerene type structure offers several unique properties that can be used in different Nano-technology applications like synthesis of Nano-structured semiconducting magnets [6]. With the rapid increase in the density of the electrons with the reduced size of components in the electronic devices such as quantum dots and quantum clusters. Currently available technology has already made it possible to fabricate semiconductor clusters by using laser vaporization technique and mass spectroscopy. A great interest in the field of clusters has arisen because of the advancement in computational and theoretical techniques along with development of advanced spectroscopic techniques.

III – V group semiconductor materials have been the focus of numerous experiments [8-9]. Due to high electron mobility of III – V compounds such as GaAs, these have the capability of replacing Si in the electronics industry. GaAs is a direct band gap semiconductor with band gap energy of ~1.43 eV. In the recent years several experimental and theoretical investigations of GaAs clusters have been done. These studies have enabled to know more about the structural stability, reactivity and nature of bonding in these clusters. It is expect that gallium arsenide cluster may exhibit different bonding characteristics than their bulk because of their strong anion-anion bonds [10]. Investigations based on density functional techniques (DFT) have proved to be very useful for studying these type of micro-clusters. The DFT scheme is accurate enough to explain the physical properties of the cluster which depend on several parameters like the size, charge or the stoichiometric composition of the cluster [11-13].

The present work is focused on the structures, as well as electronic properties of fullerene type Ga_xAs_x micro-clusters for x=10, 13, 15, 18, 20, 25 and 30 atoms.

Computational method

The fullerene like Ga_xAs_x structures were generated using Gauss View 5.0The optimization and study of the structures and characteristics of these clusters has been carried out by using the DFT with unrestricted B3LYP exchange-correlation potential as implemented in Guassion 09 program [14-15]. For describing the good geometrical and bonding feature for heavy atom, the basis set with effective core potential, LanL2DZ [16] is used for Gallium (Ga) and Arsenic(As) atoms. The basis set LanL2DZ describes the outermost electrons of $3s^2$ $3p^6$ $4s^2$ $3d^{10}$ $4p^1$for Ga and As atoms. The interaction between core and valence electron was handled by Torullier-Martins norm conserving pseudo

Correspondence to: Devesh Kumar, Department of Applied Physics, Babasaheb Bhimrao Ambedkar Univesity, Vidya Vihar, Raibareli Raod, Lucknow, Uttar Pradesh., India, E-mail: dkclcre@yahoo.co.in

Key words: *density functional theory, micro-cluster, GaAs clusters*

Received: June 12, 2017; **Accepted:** July 24, 2017; **Published:** July 21, 2017

potential in their fully separable form and the pseudo potential also includes d orbitals in the valance configuration [17,18].

Optimized geometries were obtained without any symmetry constraints and continued until the force components on each atom are less than 0.01 eV/Å using a conjugated gradient algorithm. These optimized geometries were subsequently verified by frequency calculations. The presence of real imaginary frequencies confirms the stability of obtained geometries. The gap between energy of the highest occupied molecular orbital and lowest unoccupied molecular orbital levels and the binding energy is also used to determine the stability of the micro-clusters. The method and the basis set used are well established for the similar type study metal clusters [19].

Results and discussion

The optimized structures for gallium arsenide fullerenes (Ga_XAs_X) are presented in Figure 1 for X= 10, 13, 15, 18, 20, 25 and 30, the dark red colours represent the Ga atom and violet colours represent the As atoms. In each structure has 12 pentagons and six edges are shared by adjacent pentagons. Common edges of pentagons consist of Ga-Ga and As-As homo nuclear bonds. The Ga-Ga bond length lies in range of 2.50-2.69 A^0, the As-As bond length lies in range 2.58-2.62 A^0 and Ga-As bonds length is in range 2.46-2.52 A^0. The variation of bond lengths for Ga-Ga, As-As and Ga-As is shown Figure 2. The figure 2 clearly indicates that the dependency bond lengths in clusters are insignificant of cluster size. The homo-nuclear Ga-Ga and As-As bonds are almost constant, except for Ga-Ga bond in case of $Ga_{10}As_{10}$, which confirms their bonding. The Ga-As-Ga bond angle is 100^0-109^0 but the As-Ga-As bond angles tends to have larger values 113^0-130^0. The As-Ga-Ga bond angle at the shared pentagon edge is $\approx 111^0$ and Ga-As-As bond angles at shared pentagon edge is $\approx 98^0$ but lies between the above bond angle ranges.

The variation of formation energy in eV for Ga_xAs_x clusters for X=10, 13, 15, 18, 20, 25 and 30 is shown in Figure 3. The formation energy of the clusters lies between 0.1078-0.114976 eV. The binding energy in eV for Ga_xAs_x clusters for X=10, 13, 15, 18, 20, 25 and 30 is shown in Figure 4. The binding energy increases monotonically with increase in cluster size.

The energetic of possible reaction from reactants Ga and As to the products i.e. cluster depending on the stoichiometric the clusters are obtained by the reaction

$$x(GaAs) \rightarrow Ga_xAs_x$$

The binding energy change ΔE shown in figure 4 is a function of total number of atoms X+X in Ga_xAs_x. It is obvious from figure 4 that the binding energy increases as the cluster size increases.

Electronic structure of the gallium arsenide fullerenes

The energy gap E_g is considered as the difference between energy highest occupied orbital (HOMO) and energy of lowest unoccupied orbital (LUMO), this also represents the chemical stability of clusters. The E_g of Ga_xAs_x clusters are lie between 2.20-2.50 eV. The variation of E_g of GaxAsx cluster for x = 10, 13, 15, 18, 20, 25 and 30 is shown in Figure 5. The optical activity of a cluster is related to its corresponding polarizabillity. The variation of polarizability in au for Ga_xAs_x clusters for x= 10, 13, 15, 18, 20, 25 and 30 is presented in Figure 6. The polarizabilty increase gradually till x=25 in Ga_xAs_x cluster and it falls for $Ga_{30}As_{30}$. From figure 6 is clear that Ga25As25 is higher than other studied clusters.

Conclusions

The electronic structure and optical properties of the Ga_xAs_x clusters for x=10, 13, 15, 18, 20, 25 and 30 were studied using DFT method. The binding energy and HOMO-LUMO gap (Eg) confirms the stability of the clusters. The variation of polarizability, which reflects optical activity, with increase cluster size is presented and the study suggests that Ga25As25 cluster has more optical activity in comparison with other studied clusters.

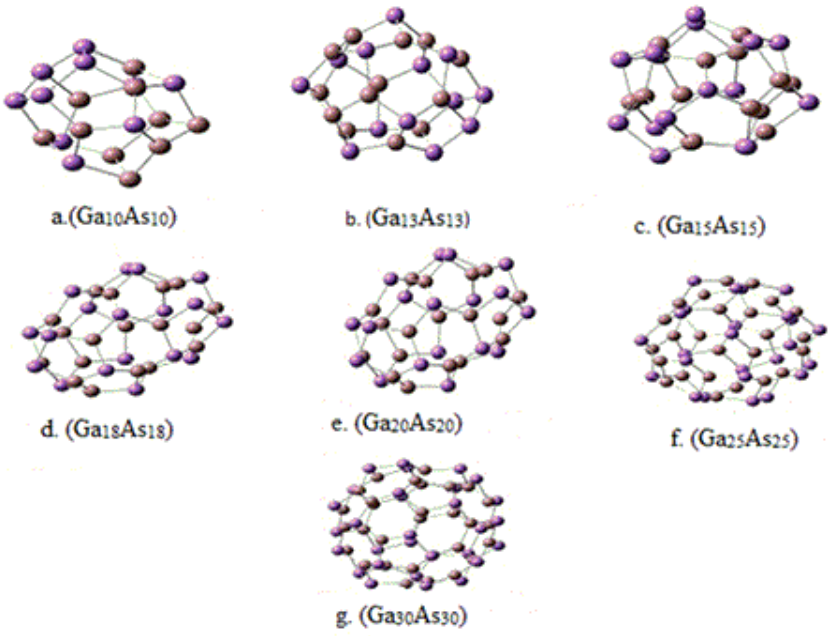

Figure 1. The optimized structures Ga_xAs_x micro-clusters for x= 10, 13, 15, 18, 20, 25 and 30.

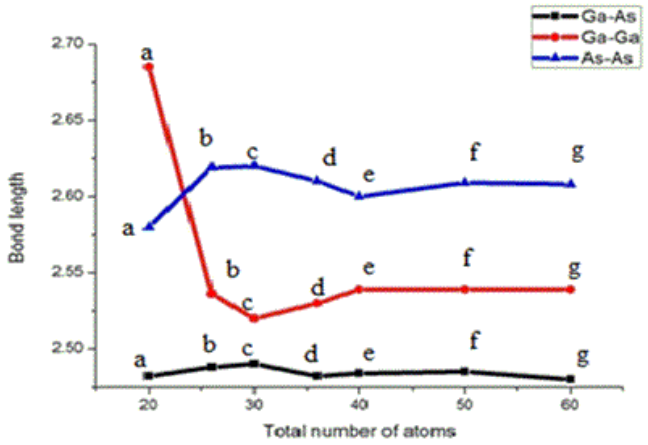

Figure 2. Variation of bond lengths in Å the Ga_xAs_x clusters for x = 10, 13, 15, 18, 20, 25 and 30.

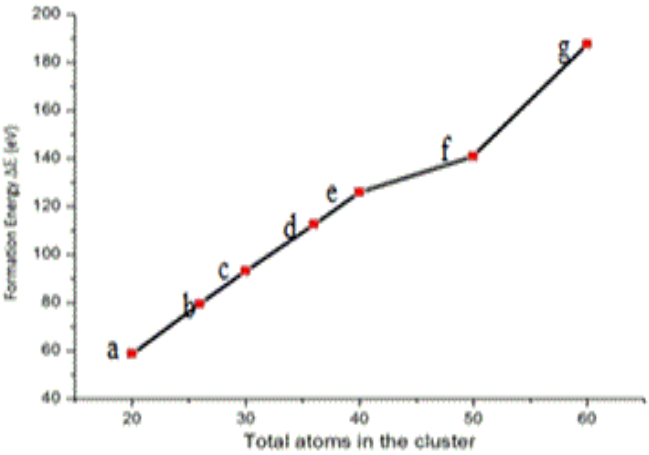

Figure 3. Variation of formation energy in eV for Ga_xAs_x clusters for x = 10, 13, 15, 18, 20, 25 and 30.

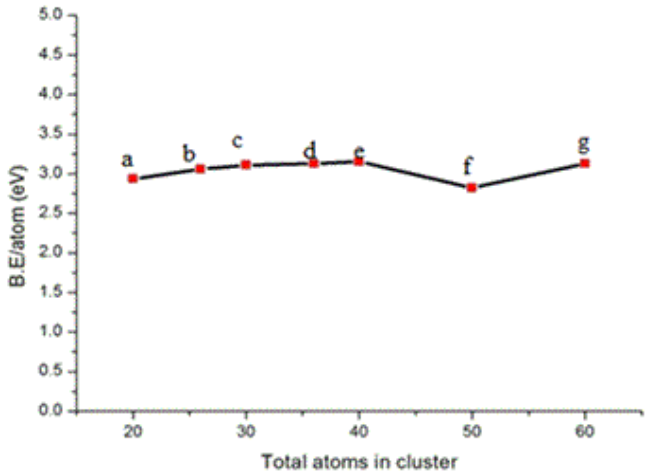

Figure 4. The Variation of binding energy in eV for Ga_xAs_x clusters for x = 10, 13, 15, 18, 20, 25 and 30.

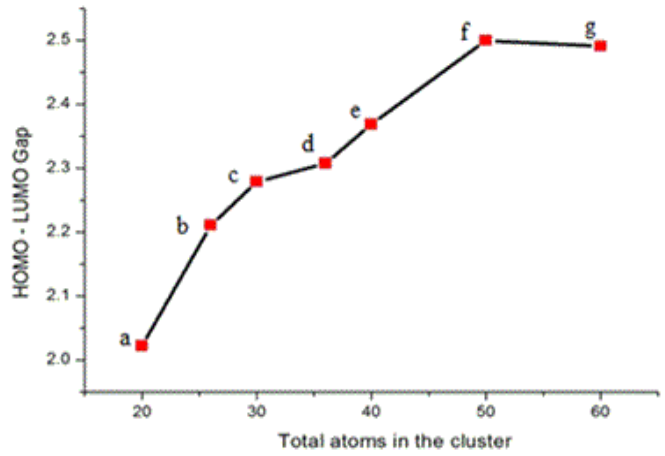

Figure 5. The variation of homo-lumo gap (E_g) in eV for Ga_xAs_x clusters for x = 10, 13, 15, 18, 20, 25 and 30.

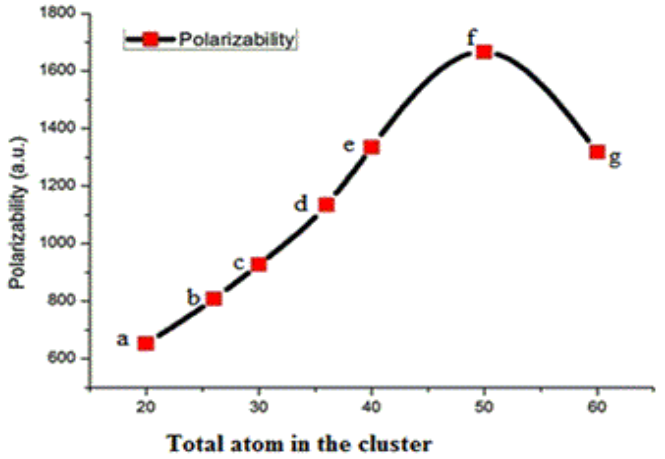

Figure 6. The variation of polarizability in au for Ga_xAs_x clusters for x= 10, 13, 15, 18, 20, 25 and 30.

References

1. Dobwolski W, Kossut J, Story T (2003) II–VI and IV–VI Diluted Magnetic Semiconductors – New Bulk Materials and Low-Dimensional Quantum Structures. *Handb Magn Mater* 15: 289-377.
2. Kamat PV (1993) Photochemistry on nonreactive and reactive (semiconductor) surfaces. *Chem Rev* 93: 267-300.
3. Wang Y, Herron N (1988) Photoluminescence and relaxation dynamics of cadmium sulfide superclusters in zeolites. *J Phys Chem* 92: 4988-4994.
4. Cox SD, Gier TE, Stucky GD, Bierlein J (1988) Inclusion tuning of nonlinear optical materials: switching the SHG of p-nitroaniline and 2-methyl-p-nitroaniline with molecular sieve hosts. *J Am Chem Soc* 110: 2986-2987.
5. Javan MB (2013) Optical properties of GaAs nanocrystals: influence of an electric field. *J Mol Model* 19: 2273-2283. [Crossref]
6. Li-Ren L, Heng-Jiang Z, Zhi-Feng L, Peng W (2012) Structures, stabilities, and electronic properties of GaAs tubelike clusters and single-walled GaAs nanotubes. *Chin Phy B* 21: 123601.
7. Galica M, Buczko R (2013) Physica status solidi B-basic solid state. *Physics* pp: 739.
8. Sabirov DS, ÅŒsawa E (2015) Information Entropy of Fullerenes. *J Chem Inf Model* 55: 1576-1584. [Crossref]

9. Obrien SC, Liu Y, Zhang Q (1986) Supersonic cluster beams of III–V semiconductors: GaxAsy. *J Chem Phys* 84: 4074.

10. Schäfer R, Becker JA (1996) Photoabsorption spectroscopy on isolated GaNAsM clusters. *Phys Rev B Condens Matter* 54: 10296-10299. [Crossref]

11. Wang L, Chibante LPF, Tittel FK (1990) Ammonia chemisorption on gallium arsenide clusters. *Chem Phy Lett* 172: 335-340.

12. Sarkar P, Springborg M (2003) Density-functional study of size-dependent properties of CdmSen clusters. *Phys Rev B* 68: 235409.

13. Ghosh C, Pal S, Goswami B (2005) Theoretical studies on size-dependent properties of GanAsn clusters. *Chem Phys Lett* 407: 498-503.

14. Brena B, Ojamae L (2008) Surface Effects and Quantum Confinement in Nanosized GaN Clusters: Theoretical Predictions. *J Phys Chem C* 112: 13516-13523.

15. Becke AD (1988) Density-functional exchange-energy approximation with correct asymptotic behavior. *Phys Rev A Gen Phys* 38: 3098-3100. [Crossref]

16. Lee C, Yang W, Parr RG (1988) Development of the Colle-Salvetti correlation-energy formula into a functional of the electron density. *Phys Rev B Condens Matter* 37: 785-789. [Crossref]

17. Wadt RW, Hay JP (1985) Ab initio effective core potentials for molecular calculations. Potentials for main group elements Na to Bi. *J Chem Phys* 82: 284.

18. Fowler PW, Rogers KM, Seifert G (1999) Pentagonal rings and nitrogen excess in fullerene-based BN cages and nanotube caps. *Chem Phys lett* 299: 359-367.

19. de Visser SP, Kumar D, Danovich M, Nevo N, Danovich D, et al. (2006) Ferromagnetic bonding: high spin copper clusters (n+1)Cu(n); n = 2-14) devoid of electron pairs but possessing strong bonding. *J Phys Chem A* 110: 8510-8518. [Crossref]

Article

Advanced Science, Engineering and Medicine
Vol. 10, 1–5, 2018
www.aspbs.com/asem

Structural Stability and Electronic Properties of $(Ga_nN_n)_m$ Micro Cluster by Using *Ab-Initio* and Tight-Binding Study

Deep Kumar, Asheesh Kumar, Jitendra Kumar, and Devesh Kumar*

Department of Applied Physics, School of Physical Sciences, Babasaheb Bhimrao Ambedkar University, Vidya Vihar, Lucknow, UP, India

First principle calculations were performed to investigate the electronic properties and structural stability of 1-D condensed cluster. The stability of $(Ga_nN_n)_m$ where $n = 1-4$ and $m = 1-6$ micro cluster is calculated. Due to the linear stacking of these stable isomers, the condensed clusters, $(Ga_nN_n)_m$ where $n = 1-4$ and $m = 1-6$ were modeled. The structural stability of clusters and their building blocks were obtained from the electronic density of states, and it infers that *s–p* hybridization plays a key role in microcluster stabilization. The various calculation shows that the $(Ga_3N_3)_m$ clusters are energetically more stable as compared with other sized condensed cluster but such microclusters can be fragmented into two micro clusters by providing external temperature.

Keywords: Micro-Clusters, Density Functional Theory, Gallium Nitrate, Binding Energy, Carbon Nanotube.

1. INTRODUCTION

The one dimension carbon nanotubes (CNT) is studied by several research groups all across the globe. The potential application of CNT was due to their high mechanical strength, ballistic transport and other novel properties[1] explored such as one-dimensional system of inorganic compounds. The carbon nanotubes and nanowires from Mo–S compound have been extensively studied.[2, 3] Synthesis with ultimate structural and electronic properties and the ability to advance tune their properties by adding dopants is also performed.[4] CdS compounds have attracted the attention as a result of which the synthesis of nanowires[5, 6] nanotubes[7] and nanorods[8–10] with controlled dimensions is performed.

In the recent past the low dimensional semiconductor material has become of great interest in the research field of nanoscience.[11–13] The materials of III–V group semiconductor compound due to their paramount technological potential applications such as photoelectronic devices, photonic integrations, ultrahigh frequency microwave and photovoltaic solar cells are studied predominantly. Gallium nitride (GaN) is an important semiconducting material that exhibits a broad range of potential applications for optoelectronics and high power electronic devices. Light emitting diodes have made a boom in the market with its appearance in the recent past year.[14] The high thermal conductivity provides new routes in high-temperature and high–power electronic devices[15, 16] such as metal semiconductor field effect transistor (MESFETs), high electron mobility transistor (HEMTs) and heterojunction bipolar transistor (HBTs).[17, 18] Furthermore high Curie temperature and room temperature ferromagnetic has been predicted in GaN-doped with transition metal (MT) element.[19–21] GaN nanotubes with inner diameters of 30–200 nm and wall thickness of 5–50 nm were also synthesized.[22] Single-walled GaN nanotube was examined computationally by using first-principle methods.[23] Several theoretical studies on Ga_nN_n clusters up to $n = 4-6$ by BelBruno,[24] Kandallam et al.[25–28] and Song et al.[29–31] are also investigated. To predict the lowest energy of $(Ga_nN_n)_x$ clusters, a number of possible structure isomers were considered for the study. These structures were adopted from those previously proposed for the III–V semiconductor compound cluster such as BN,[32–34] AlN and GaAs.

2. COMPUTATIONAL METHOD

Density functional theory has been used for the optimization of GaN condensed nanocluster and to calculate their ground and excited state properties. Geometrical optimizations have been performed without any constraints imposed on the nanocluster structures. Various possible structures for each GaN cluster were drawn using Gauss

*Author to whom correspondence should be addressed.

View 0.5. For geometry optimization, B3LYP method DFT method, Beck's three parameters with correlation function (Lee-Yang-Parr), and relativistic effective core potential with double zeta basis set, LANL2DZ as implemented in Gaussian 09 programme suit were used. For the evaluation of density of states (DOS) spectrum Gauss Sum 3.0 has been used.

The binding energy per atom (BE) of a cluster is calculated using the formula

$$\mathrm{BE} = \frac{nE(\mathrm{Ga}) + nE(\mathrm{N}) - E(\mathrm{Ga}_n\mathrm{N}_n)}{2n}$$

Where $E(\mathrm{Ga})$, $E(\mathrm{N})$, and $E(\mathrm{Ga}_n\mathrm{N}_n)$ are total energy of a single Ga atom, a single N atom, and Ga_nN_n clusters, respectively and n is the number of Ga or N atoms. Similar calculations were performed using the first principle calculations on optimized Ga_nN_n nanowires with $n = 1-4$ in order to perform the comparison.

3. RESULTS AND DISCUSSION

3.1. Atomic Structure of Ga_nN_n Cluster

First principle calculations on the various Ga_nN_n ($n = 1-4$) clusters, were performed to obtain the stable structure which acts as a fundamental building block of condensed cluster or nano assemblies. Optimized structures are shown in Figure 1 with the BE, HOMO–LUMO gap and Ga–N bond distance of stable isomers are reported in Table I(a)–(c). The stable isomers of Ga_nN_n clusters from $n = 4$ to 12 possesses ring and cage (37) geometries respectively, which is quite comparable to earlier reports.

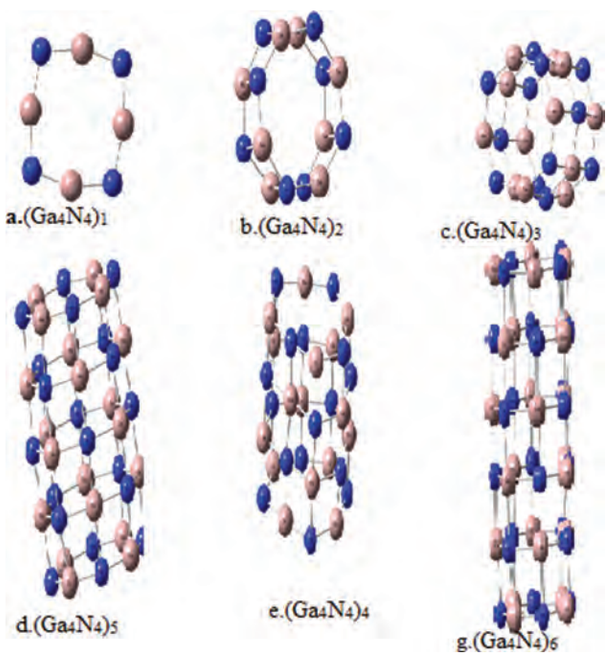

Figure 1. Illustrates the optimized structures of $(Ga_4N_4)_m$ micro cluster.

Table I. The Binding energy, band gap and bond distance $(Ga_2N_2)_n$ where $n = 1-6$.

Atoms	Binding energy/atom (eV)	Band gap (eV)	Bond distance (Å)
	(a)		
$(Ga_2N_2)_1$	10.34	1.49	1.92
$(Ga_2N_2)_2$	10.81	0.84	1.91
$(Ga_2N_2)_3$	11.29	1.30	1.93
$(Ga_2N_2)_4$	11.48	1.33	1.92
$(Ga_2N_2)_5$	11.60	1.54	1.90
$(Ga_2N_2)_6$	11.61	2.43	1.91
	(b)		
$(Ga_3N_3)_1$	10.92	2.11	1.87
$(Ga_3N_3)_2$	11.54	1.60	1.90
$(Ga_3N_3)_3$	11.83	2.12	1.92
$(Ga_3N_3)_4$	11.96	2.32	1.93
$(Ga_3N_3)_5$	12.05	2.39	1.92
$(Ga_3N_3)_6$	12.10	2.49	1.92
	(c)		
$(Ga_4N_4)_1$	11.15	2.65	1.77
$(Ga_4N_4)_2$	11.61	2.35	1.83
$(Ga_4N_4)_3$	11.83	2.52	1.91
$(Ga_4N_4)_4$	11.88	2.43	1.89
$(Ga_4N_4)_5$	12.00	2.69	1.89
$(Ga_4N_4)_6$	11.99	2.42	1.90

3.2. Condensed Clusters

With an understanding of stable isomers of Ga_nN_n with different geometries, condensed cluster of $(Ga_nN_n)_m$ are obtained by linear stacking of m up to 7 units of stable Ga_nN_n isomers ($n = 1-4$). The optimized structure of condensed clusters are shown in Figure 1, the $(Ga_nN_n)_2$ cluster is obtained by condensing one planar Ga_3N_3 isomer at the top while another isomer at the bottom thus increasing the number of Ga–N bonds in the cluster. Similarly, $(Ga_3N_3)_4$ and other condensed clusters, $(Ga_nN_n)_m$ were obtained and optimized structure are shown in Figures 1(b)–(g) further, other–sized $(Ga_nN_n)_2$ cluster are stacked from their basic units of Ga_nN_n.

The Binding Energy and HOMO–LUMO gap of all the condensed (Ga_nN_n) clusters are calculated and the results are shown in Figure 2 along with the cohesive energy per atom and band gap of infinite Ga_nN_n nanowires. As expected, the BE of condensed cluster increases linearly with m and slowly achieves the cohesive energy per atom and band gap of infinite nano wires, as shown in Figure 2(a). In the inset, the BEs, of $(Ga_nN_n)_m$ condensed cluster with respect to the diameter (in terms of n) are shown. Even though the diameter of the $(Ga_3N_3)_m$ condensed clusters is smaller than that of the $(Ga_4N_4)_m$ cluster, beyond $m = 3$. The BE of the cluster is almost equal with that of the latter. The BEs of $(Ga_3N_3)_5$ and $(Ga_4N_4)_5$ are 12.05 and 12.00 eV/atom, respectively. Hence it can be concluded that $(Ga_4N_4)_m$ condensed cluster are more stable as compared to other-sized condensed cluster and preferably this cluster could be extended to

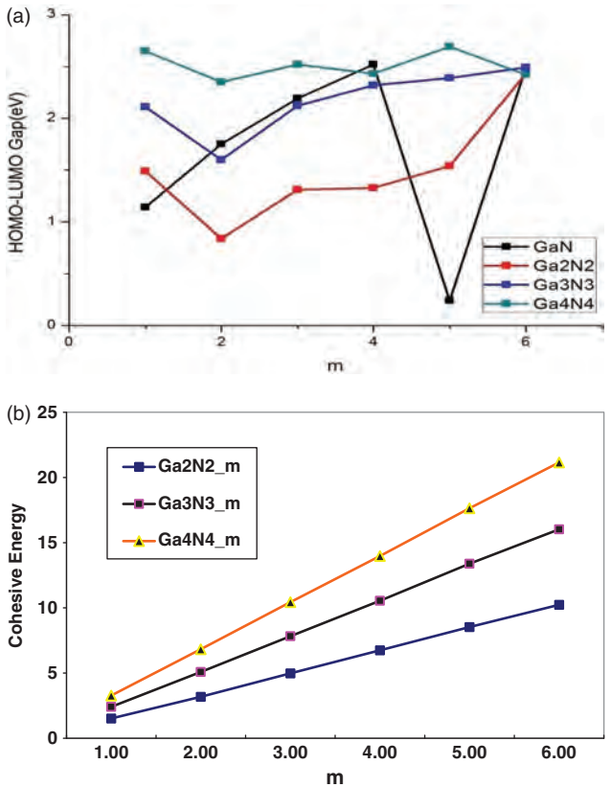

Figure 2. (a) Cohesive energy and (b) HOMO–LUMO gap of $(Ga_nN_n)_m$ are shown. In the inset, BEs of $(Ga_nN_n)_m$ are shown for various n. The band gap shown in figure is less than the bad gap of bulk GaN, which is obtained from the calculation.

nanorod and nanowires. Even our calculations on infinite nanowires support this conclusion as the cohesive energies of $(Ga_3N_3)_3$ and $(Ga_4N_4)_3$ infinite nanowires are almost same (11.83 eV/atom).

Figure 2(b) describes the variation of the HOMO–LUMO gap of the cluster. For $n = 2$, 3 the HOMO–LUMO gap increases as m values increases, and for $n = 4$ its lies between 2.35 to 2.69 eV. The HOMO–LUMO gap for $(Ga_4N_4)_m$ condensed clusters is significantly higher than that of another condensed cluster. This supports our previous statement that $(Ga_4N_4)_m$ condensed clusters are more stable among all the clusters. Further, it may also be noted in Figure 2 that beyond $m = 2$, the HOMO–LUMO gap of $(Ga_1N_1)_m$ atomic wire is less than that of another condensed cluster. It is a consequence of the increase in the number of nonbonding states with the increase in the length of the atomic wire. The HOMO–LUMO gap of all $(Ga_nN_n)_m$ clusters is comparatively less than the band gap of the bulk GaN compound.

3.3. Electronic Structure

To study the structural stability of $(Ga_3N_3)_m$ cluster, total and partial density of states (DOS) of the cluster with $m = 2, 3$ and 4 as shown in Figure 3. The DOS states are

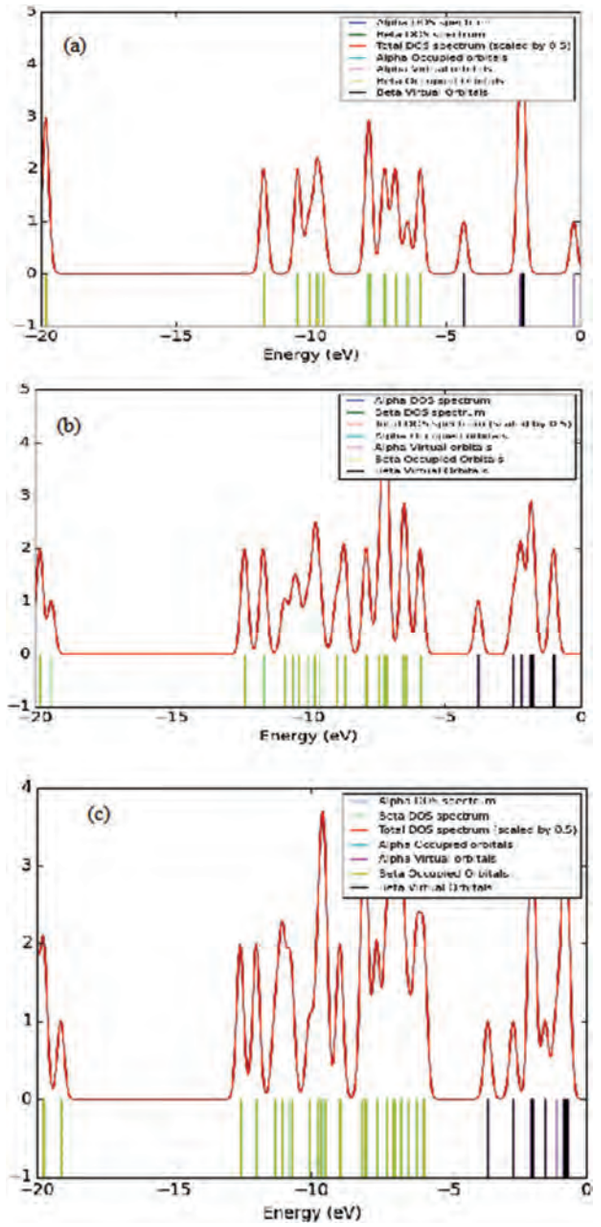

Figure 3. Total and partial DOS of $(Ga_3N_3)_m$ cluster with $m = 2$ (a), $m = 3$ (b), and $m = 4$ (c).

located in the energy range from −13.0 to −0.0 eV. While Ga (S P) states are distributed in the unoccupied region these clusters can be understood on the structural stability of the molecular orbital theory.

3.4. Fragmentation of Condensed Cluster

We also effort the possibility of fragmentation of condensed $(Ga_4N_4)_m$ cluster into smaller units to be aware of their expansion stability for example, that $(Ga_4N_4)_4$ nano wire can fragment into two part of a set of that $(Ga_4N_4)_2$ cluster or that (Ga_4N_4) and that $(Ga_4N_4)_3$

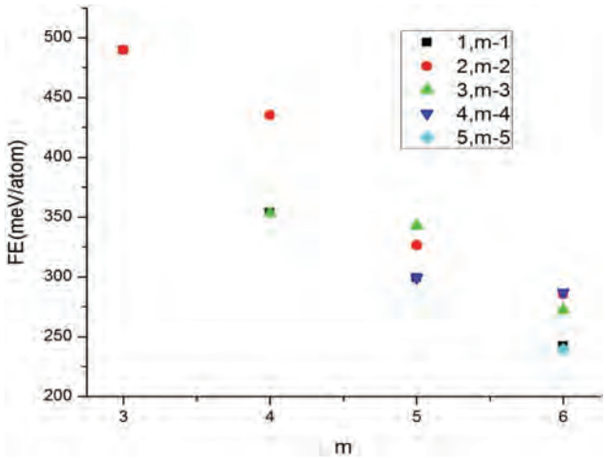

Figure 4. FE versus m of $(Ga_nN_n)_m$ of various possible fragments.

clusters. The fragmentation energy per atom (FE) is calculated from.

$$\mathrm{FE} = \frac{E[(Ga_3N_3)_n] + E[(Ga_3N_3)_{m-n}] - E[(Ga_3N_3)_m]}{6m}$$

Every $(Ga_3N_3)_m$ may be divided into the following two pieces of a possible cluster: $(1, m-1)$, $(2, m-2)$, $(3-m-3)$, $(4, m-4)$. FE is calculated and shown in Figure 4.

Figure 4 shows that when a cluster FE decreases, m values increases. This infers that the condensed clusters under the influence of temperature breaks into smaller units on the order of 450 k. Although the diameter of the condensed cluster as well nanorod-below this temperature can be synthesized.

We condensed the second derivative of the total energy $(\Delta^2 E)$ of the cluster and the cluster understands the structural stability and it is reported in Figure 5. Our calculations conclude that the $\Delta^2 E$ of $(Ga_3N_3)_3$ cluster shows the maximum value and high structural stability of this cluster.

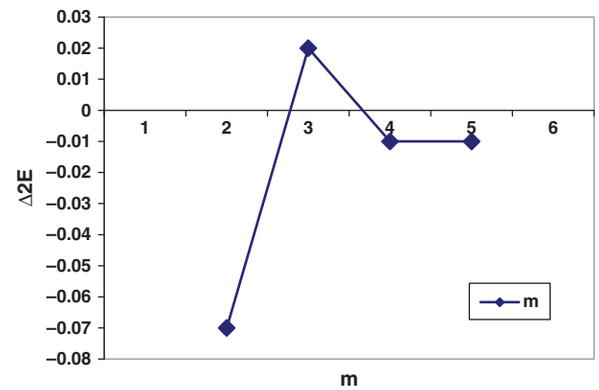

Figure 5. The second derivative of energy of $(Ga_3N_3)_m$ cluster with respect to m. The calculated value by using the formula $\Delta^2 E = E(m+1) + E(m-1) - 2E(m)$.

4. CONCLUSION

The structural stability and electronic properties of $(Ga_nN_n)_m$ $(n = 1-4,\ m = 1-6)$ cluster by implementing first principle calculations is studied in detail. The stability of cluster is explained by the DOS. It is estimated that it creates stability due to *sp*-hybridization along with the different-sized condensed clusters $(Ga_3N_3)_m$ that are found to be more stable. Further, the electronic properties of the cluster are shown to have lower energy gap as compared to the bulk GaN system. It could be used as an interesting photo-catalytic application. Our calculations also revealed that more concentrated clusters have structural stability equivalent to 1-D nanorods obtained from the bulk which are comparable.

Acknowledgments: The author is thankful to the UGC for the financial support and also acknowledges the computing facility provided by the Department of Applied Physics, Babasaheb Bhimrao Ambedkar University, Lucknow without whose support this work would not have been in the present form.

References and Notes

1. G. Dresselhaus, M. S. Dresselhaus, and P. Eklund, Science of Fullerenes and Carbon Nanotubes, Academic Press, San Diego, CA (**1995**).
2. Y. Feldman, E. Wasserman, D. J. Srolovitz, and R. Tenne, *R. Science* 267, 222 (**1995**).
3. V. Nicolosi, P. D Nellist, S. Sanvito, E. C. Cosgriff, S. Krishnamurthy, W. J. Blau, M. L. H. Green, D. Vengust, D. Dvorsek, D. Mihailovic, G. Compagnini, J. Sloan, V. Stolojan, J. D. Carey, S. J. Pennycook, and J. N. Coleman, *Advanced Materials* 19, 543 (**2007**).
4. Iflah Laraib, J. Karthikeyan, and P. Murugan, *Physical Chemistry Chemical Physics* 5471 (**2014**).
5. J. H. Zhan, X. G. Yang, W. X. Zhang, D. W. Wang, Y. Xie, and Y. T. Qian, *Journal of Materials Research* 03, 629 (**2015**).
6. J. Xu, X. Zhuang, P. Guo, Q. Zhang, W. Huang, Q. Wan, W. Hu, X. Wang, X. Zhu, C. Fan, Z. Yang, L. Tong, X. Duan, and A. Pan, *Nano Lett.* 12, 5007 (**2012**).
7. H. Zhang, D. Yang, Y. Ji, X. Ma, J. Xu, and D. Que, *ACS Nano* 4, 98 (**2010**).
8. H. Zhang, X. Y. Ma, J. Xu, and D. R. Yang, *J. Cryst. Growth* 263, 372 (**2004**).
9. A. E. Saunders, A. Ghezelbash, P. Sood, and B. Korgel, *Langmuir* 24, 9043 (**2008**).
10. A. S. Barnard and H. Xu, *J. Phys. Chem. C* 111, 18112 (**2007**).
11. S. Nakamura and G. Fasol, The Blue Laser Diode, Springer, Berlin (**1997**).
12. S. Nakamura, M. Senoh, N. Iwasa, and S. Nagahama, *Appl. Phys. Lett.* 67, 1868 (**1995**).
13. H. Bar-Ilan, S. Zamir, O. Katz, B. Meyler, and J. Salzman, *Materials Science and Engineering A* 14, 30 (**2001**).
14. R. J. Trew, M. W. Shin, and V. Gatto, *Solid-State Electronics* 41, 1561 (**1997**).
15. S. J. Pearton, F. Ren, A. P. Zhang, and K. P. Lee, *Materials Science and Engineering: R. Reports* 3, 55 (**2000**).
16. R. D. Paiva, J. L. A. Alves, R. A. Nogueira, J. R. Leite, and L. M. R. Scolfaro, *Brazilian Journal of Physics* 34, 647 (**2004**).
17. T. Dietl, H. Ohno, F. Matsukura, J. Cibert, and D. Ferrand, *Science* 287, 1019 (**2000**).

18. T. Jungwirth, J. Sinova, J. Masek, J. Kucera, and A. H. Mac-Donald, *Rev. Mod. Phys.* 78, 809 **(2006)**.
19. J. Goldberger, R. He, Y. Zhang, S. Lee, H. Yan, H. J. Choi, and P. Yang, *Nature* 422, 599 **(2003)**.
20. S. M. Lee, Y. H. Lee, Y. G. Hwang, J. Elsner, D. Porezag, and T. Frauenheim, *Phys. Rev. B* 60, 7788 **(1999)**.
21. J. J. BelBruno, *Chem. Rev.* 11, 281 **(2000)**.
22. A. K. Kandalam, R. Pandy, M. A. Blanco, A. Costales, J. M. Recio, and J. M. Newsam, *J. Phys. Chem. B* 104, 4361 **(2000)**.
23. A. K. Kandalam, M. A. Blanco, and R. Pandy, *J. Phys. Chem. B* 105, 6080 **(2001)**.
24. A. K. Kandalam, M. A. Blanco, and R. Pandy, *J. Phys. Chem. B* 106, 1945 **(2002)**.
25. A. K. Kandalam, M. A. Blanco, and R. Pandy, *J. Phys. Chem. B* 107, 4508 **(2003)**.
26. B. Song and P. L. Cao, *Phys. Lett. A* 300, 485 **(2002)**.
27. B. Song, P. L. Cao, and B. X. Li, *Phys. Lett. A* 315, 308 **(2003)**.
28. D. L. Strout, *J. Phys. Chem. A* 104, 3364 **(2000)**.
29. D. L. Strout, *J. Phys. Chem. A* 105, 261 **(2001)**.
30. J. M. Matxain, J. M. Ugalde, M. D. Towler, and R. J. Needs, *J. Phys. Chem. A* 107, 10004 **(2003)**.
31. Ch. Chang, A. B. C. Patzer, E. Sedlmayr, T. Steinke, and D. Sulzle, *Chem. Phys. Lett.* 350, 399 **(2001)**.
32. H. S. Wu, F. Q. Zhang, X. H. Xu, C. J. Zhang, and H. J. Jiao, *J. Phys. Chem. A* 107, 204 **(2003)**.
33. J. Zhao, B. Wang, X. Zhou, and X. Chen, *Chem. Phys. Lett.* 422, 170 **(2006)**.
34. R. Hoffmann, Soli and Surface: A Chemiet's View on Bonding in Extended Structures, VHC Publisher, New York **(1988)**.

Received: 25 July 2017. Accepted: 20 December 2017.

ISSN (Online) 2393-8021
ISSN (Print) 2394-1588

International Advanced Research Journal in Science, Engineering and Technology
Vol. 2, Issue 11, November 2015

Structures Stabilities and Electronic Properties of GaAs Condensed Clusters

Deep Kumar[1], Rajkamal Shastri[2], Anil Kumar yadav[3], Devesh kumar[4]

Research Scholar, Dept of Applied Physics, School for Physical Sciences Babasaheb Bhimrao Ambedkar University, Lucknow, India[1, 2]

Assistant Professor, Dept of Applied Physics, School for Physical Sciences Babasaheb Bhimrao Ambedkar University, Lucknow, India[3]

Associate Professor, Dept of Applied Physics, School for Physical Sciences Babasaheb Bhimrao Ambedkar University, Lucknow, India[4]

Abstract: First-principal calculation are conceded out to appreciate the structural stability and electronic properties of nanotubes cluster and fundamental building blocks, Ga_nAs_n (n=1-3) small cluster by linear stacking of stable isomers, the condensed clusters, $(Ga_nAs_n)_m$ where n=1-3 and m =1-6 are modeled. The structure stability of condensed cluster their building blocks are achieved from the electron density of states. Electronic properties of all condensed cluster, with m≥4 are interesting in photo catalytic application as they have large energy gap than that of bulk. Our calculations also so that the $(Ga_3As_3)_m$ cluster are energetically more stable as compared with other condensed cluster.

Keyword: Carbon nanotubes, Density Functional Theory, Gallium arsenide.

I. INTRODUCTION

We are first going discussed carbon nano tubes (CNT) one dimension system gaining momentum with the invention of carbon nano tube (CNT). Appreciating that the potential application of CNT were due to their high mechanical strength ballistic transport and other novel properties (1) researches explored such as one dimensional system of inorganic compounds. For this above approach nanotubes and nanowires from Mo-S compound have been expansively studied and Even because of their many advantages for certain applications of CNTs has been suggested (2,3)as an alternative. Synthesis with unique structural and electronic properties and the ability to advance tune their properties by adding do pants (4). Recently, 1-D systems of CdS compounds have drawn much attention, leading to the synthesis of their nanowires,(5,6) nanotubes ,(7) and nanorods (8−10) with controlled dimensions.

As recently have proved that low dimensional semiconductor material have become a great interest to researcher in nanoscience among these material III-V group semiconductor compound have their paramount technological potential application such as photo electronic device, photonic integrations, ultrahigh frequency microwave and photovoltaic solar cells.

Gallium arsenide (GaAs) as substantial member of the III-V group semiconductor compounds has many distinctive properties as a low electronic effective mass high electron mobility and high saturation drift velocity which make it ideal for optoelectronic, low power and ultra high speed devices application more over it is an advantage material for making nanoscale devices because it surface Fermi level, pinning in the conduction band does not became an insulator due to depletion of carriers. Hence the post decades there have been a great number of studies investigating the chemical and physical properties of its nanostructure.

In the present work, we have investigated the atomic structure and electronic properties of condensed clusters and their infinite nanowires by first principles calculations within the construction of density functional theory.

II. COMPUTATIONAL

All GaAs and condensed clusters reported in this work are optimized by using the DFT with unrestricted B3LYP exchange-correlation potential. To superior describe the binding and geometrical feature of heavy atom, the basis set, effective core potential LanL2DZ, was adopted in this study for both arsenic (As) and gallium (Ga) atoms.. In this basis set the outermost electrons$3s^2\ 3p^6\ 4s^2\ 3d^{10}\ 4p^1$for Ga and $3s^2\ 3p^6\ 4s^2\ 3d^{10}\ 4p^1$ for As were described .the procedures of optimization were based on energy system convergence of energy was superior then10^{-6}(a.u. is atomic unit). In sequence to save time and improve efficiency the processes to optimize the structures with determined bond length ,bond angle, and dihedral angle of the initial value in the convergence criterion of 10^{-4}a.u. based on the optimized tube like clusters. All these calculation were implemented with the Gaussian 09 program package

The binding energy per atom (BE) of cluster is calculated from

$$\text{BE}=\frac{nE(Ga)+nE(As)-E(Ga_nAs_n)}{2n}$$

Where E(Ga), E(As)and $E(Ga_nAs_n)$ are the total energy of a single Ga atom, a single As atom and Ga_nAs_n clusters respectively and nis the number of Ga or As atoms.

ISSN (Online) 2393-8021
ISSN (Print) 2394-1588
International Advanced Research Journal in Science, Engineering and Technology
Vol. 2, Issue 11, November 2015

Similarly calucalation are extended to condensed cluster we also agreed out the firest principal calculation on infinite Ga_nAs_n nanowires with n=1-3 for the sake of comparision

III. RESULTS AND DISCUSSION

We conceded out first principal calculations on various Ga_nAs_n (n=1-4) cluster, to obtained the stable isomers in each size range, which act as building blocks of condensed cluster . The optimized structure are shown in fig. and the BE, HOMO-LUMO gap, Cd−S bond distance, and bond angle of stable isomers are reported in Table 1

Condensed Clusters With a information of stable isomers of Ga_nAs_n in each size range, condensed clusters of $(Ga_nAs_n)_m$ are achieved by linear stacking of m (up to 6) units of stable Ga_nAs_n isomers (n = 1−3). We also effort the condensed of the stable isomer of Ga_5As_5 but the significant structural distortion observed due to a larger cavity in the center of the ring. Hence we did not progress further.

The optimized structures of condensed clusters are shown in fig 1. the $(Ga_3As_3)_2$ clusters is obtained by condensing a planer Ga_3As_3 cluster at the top and another cluster at the bottom, thus increasing the number Ga-As bonds in the cluster. In a similar way $(Ga_3As_3)_4$ and other condensed cluster, $(Ga_nAs_n)_m$ are obtained and optimized structures are shown in figure.

We calculate the BE and HOMO-LUMO gap of all condensed $(Ga_nAs_n)_m$ cluster, and the results are shown in table1. Along with the cohesive energy per atom and band gap of infinite Ga_nAs_n nanowires. As estimated the BE of condensed cluster increases with m and slowly reaches the cohesive energy of the corresponding infinite nanowires, as seen in table 1. Nanorods and infinite nanowires.

In the inset the Bes of condensed cluster with respect to the diameter (in terms of n) are shown. Hence it conclusion that the $(Ga_3As_3)_m$ condensed clusters are more stable as compared to other-sized condensed clusters and this cluster could preferably extend to the HOMO−LUMO gap decreases, beyond m = 2.

Table 1 showing HOMO-LUMO gap, Bond length (Ga-As) and binding energy of the cluster. **(a)** $(GaAs)_m$ cluster, **(b)** $(Ga_2As_2)_m$ cluster, **(c)** $(Ga_3As_3)_m$ cluster

(a)

Structure	Energy Gap eV	Bond length (Ga-As) A^0	Binding energy (eV)
(GaAs)2	1.89	2.39-2.51	2.10
(GaAs)3	0.56	2.49-2.52	2.01
(GaAs)4	0.53	2.38-2.52	2.36
(GaAs)5	0.40	2.36-2.39	2.40
(GaAs)6	0.53	2.38-2.51	2.43

(b)

Structure	Energy Gap eV	Bond length (Ga-As)	Binding energy (eV)
$(Ga_2As_2)_2$	2.05	2.54-2.71	2.60
$(Ga_2As_2)_3$	2.30	2.41-2.55	2.78
$(Ga_2As_2)_4$	1.39	2.53-2.58	2.82
$(Ga_2As_2)_5$	1.09	2.52-2.59	2.87
$(Ga_2As_2)_6$	0.57	2.53-2.62	2.56

(c)

Structure	Energy Gap eV	Bond length (Ga-As)	Binding energy (eV)
$(Ga_3As_3)_2$	1.48	2.53-2.58	2.85
$(Ga_3As_3)_3$	1.46	2.53-2.62	2.86
$(Ga_3As_3)_4$	1.11	2.53-2.56	2.88
$(Ga_3As_3)_5$	1.94	2.48-2.54	3.00
$(Ga_3As_3)_6$	1.12	2.57-2.59	2.90

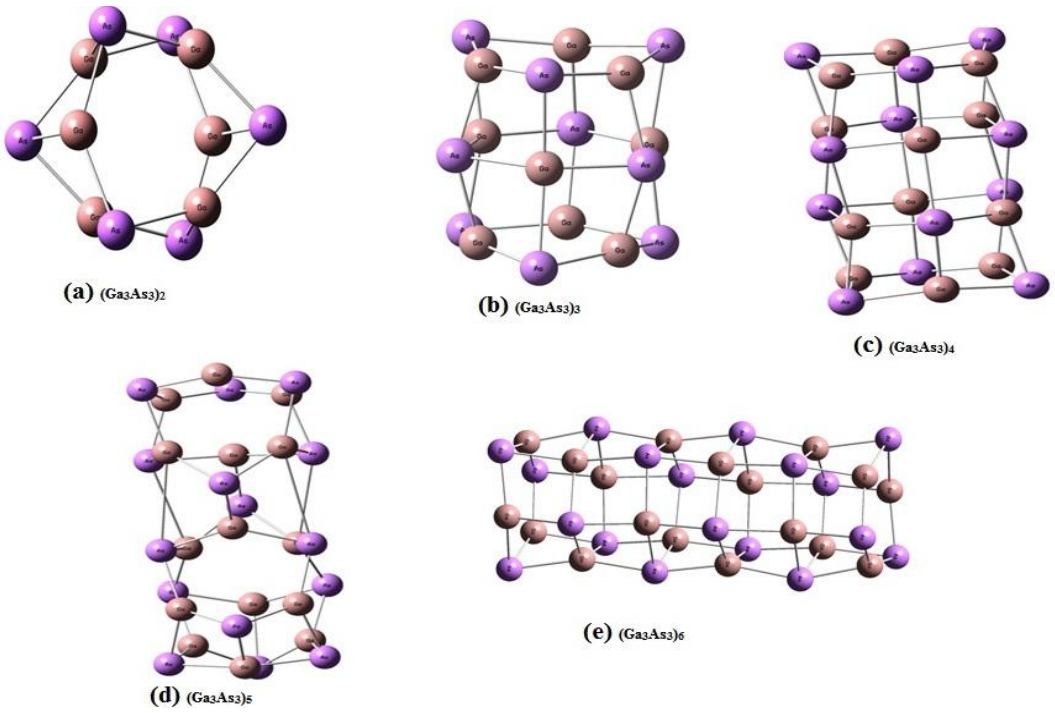

Fig.1 The optimized structure of $(Ga_3As_3)_m$ condensed clusters. (a) $(Ga_3As_3)_2$ (b) $(Ga_3As_3)_m$ (c) $(Ga_3As_3)_m$ (d) $(Ga_3As_3)_m$ (e) $(Ga_3As_3)_m$ are shown.

DOI 10.17148/IARJSET.2015.21121

ISSN (Online) 2393-8021
ISSN (Print) 2394-1588
International Advanced Research Journal in Science, Engineering and Technology
Vol. 2, Issue 11, November 2015

Figure 2 shows the variation of the HUMO−LUMO gaps of the condensed clusters. For the $(Ga1As1)_m$ atomic wire, We find that the decrease in the gap is mainly due to variation in the LUMO of atomic wires, which is quite similar to a linear polyene system. Similarly, for n = 2, 3, and 4, the HOMO−LUMO gap decreases as the m value increases. It is interesting to observe that, beyond m = 4, the HOMO−LUMO gap for $(Ga_3As_3)_m$ condensed clusters is significantly higher than that of other condensed clusters (including infinite nanowires). This supports our earlier statement that $(Ga_3As_3)_m$ condensed clusters are the most stable among all other clusters. Further, we also noted in Figure 2 that, beyond m = 5, the HOMO− LUMO gap of the $(Ga1As1)_m$ atomic wire is less than that of other condensed clusters. It is a consequence of the increase in the number of nonbonding states with the increase in the length of the atomic wire. Overall, the HOMO−LUMO gap of all $(Ga_nAs_n)_m$ condensed clusters, beyond m = 4, is less than the band gap of the bulk GaAs compound. Hence, the photo catalytic activity of these clusters is expected to be higher when compared with that of the bulk.

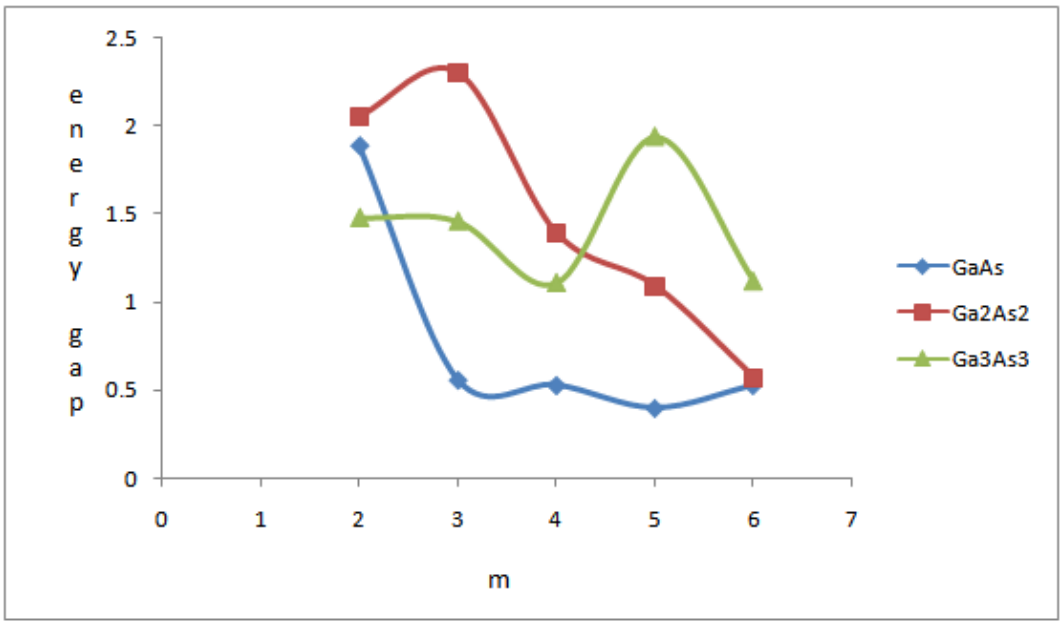

Fig.2. showing HOMO-LUMO gap of $(Ga_nAs_n)_m$ are shown.

IV. CONCLUSION

We studies the structure stablity and electronic properties of $(Ga_nAs_n)_m$ (n=1-3,m=1-6) condensed cluster and their building block from firest-principal calculation . the structual stablity of cluster is explain by the HOMO – LUMO gap and Bes. Further, electronic properties of condensed clusters with m > 4 show a lower energy gap as compared with the bulk GaAs system, and it would be interesting in photo catalytic applications. Our calculations also reveal that the condensed clusters have more structural stability as compared to 1-D nanorods obtained from the bulk in this dimension.

REFERENCES

1. G Dresselhaus, M S Dresselhaus, P Eklund, Science of Fullerenes and Carbon Nanotubes; Academic Press: San Diego, CA, 1995.
2. Y Feldman , E Wasserman, D J Srolovitz, R Tenne High-Rate, Gas-Phase Growth of MoS2 Nested Inorganic Fullerenes and Nanotubes. R. Science 1995, 267, 222−225
3. V. Nicolosi, P. D Nellist, S. Sanvito, E. C. Cosgriff, S. Krishnamurthy, W. J. Blau, M. L. H. Green, D. Vengust, D. Dvorsek, D. Mihailovic, G. Compagnini, J. Sloan, V. Stolojan, J. D Carey, S. J Pennycook And J. N. Coleman, Aberration Corrected Electron Microscopy Reveals van der Waals Driven Self-Assembly Of MoSI Nanowires into A Low Symmetry Structure", in Advanced Materials, 2007, 19, 543 – 547.
4. P Murugan, V Kumar, Y Kawazoe, N Ota Ab initio study of structural stability of Mo-S clusters and size specific stoichiometries of magic clusters, Physical Chemistry A 111 (14), 2778-2782.
5. JH Zhan, XG Yang, WX Zhang, DW Wang, Y Xie, YT Qian, A solvothermal route to wurtzite ZnSe nanoparticles Journal of Materials Research 2015 (03), 629-632.
6. Jinyou Xu, Xiujuan Zhuang, Pengfei Guo, Qinglin Zhang, Weiqing Huang, Qiang Wan, Wei Hu,Xiaoxia Wang, Xiaoli Zhu, Changzeng Fan, Zongyin Yang, Limin Tong, Xiangfeng Duan, and Anlian Pan, Wavelength-Converted/Selective Waveguiding Based on Composition-Graded Semiconductor Nanowires Nano Lett. 2012, 12, 5003−5007.
7. Hui Zhang, Deren Yang, Yujie Ji, Xiangyang Ma, Jin Xu, and Duanlin Que Low Temperature Synthesis of Flowerlike ZnO Nanostructures by Cetyltrimethylammonium Bromide-Assisted Hydrothermal Process ACS Nano 2010, 4, 91−98
8. Zhang, H.; Ma, X. Y.; Xu, J.; Yang, D. R Synthesis and Characterization of CdS, ZnS and CdZnS Nanoparticles Embedded in Polystyrene, j. Cryst. Growth 2004, 263, 372−376.
9. A.E Saunders,A Ghezelbash, P Sood, B Korgel, Synthesis of high aspect ratio quantum-size CdS nanorods and their surface-dependent photoluminescence. A. Langmuir2008, 24, 9043−9049.
10. A S Barnard, Xu, H. Modelling polar wurtzite ZnS nanoparticles: the effect of sulphur supersaturation on size- and shape-dependent phase transformations J. Phys. Chem. C 2007, 111, 18112− 18117

RESEARCH ARTICLE

International Journal of Science, Technology and Society
Vol 3, No. 1 (2017) : 16-20

Study of absorption spectra of organic light emitting materials (triphenyl derivatives of amine): A quantum mechanical study

Jitendra Kumar, Ankur Trivedi, Deep Kumar, Devesh Kumar*

Department of Applied Physics, School for Physical Sciences, Babasaheb Bhimrao Ambedkar University, Vidya Vihar, Rae Bareilly Road, Lucknow (U. P.) 226 025 INDIA

Publication Info

Article history:
Received : 31.07.2017
Accepted : 29.08.2017
DOI:

Key words:
OLED, TPBB, HOMO - LUMO, GAUSSIAN, TD-DFT

****Corresponding author:***
Devesh Kumar

Email:
dkclcre@yahoo.com

ABSTRACT

Density Functional theory (DFT) is used to study the effect of substituents on the electronic and optical property of organic light emitting material 1,3,5-tris(4'-(1''- phenyl-benzimidazol-2''-yl)phenyl) amine (TPBB) and its derivatives (MeO-TPBB, Br-TPBB and Bu-TPBB). TD – DFT has been used to study the absorption spectra of these molecules. This study suggests that each derivative of TPBB shows a UV – VIS spectra at slightly different frequency.

INTRODUCTION

Organic molecules are generally considered to be insulators but the discovery of conducting polymers in 1970s brought about a new era in the field of organic opto – electronics. Since then organic luminescent materials have received an increased attention due to their potential application as organic light – emitting devices (OLEDs) (Minaev et al. 2014; Xio et al. 2011). Tang and VanSlyke (Tang et al. 1987) in 1987 found the emission from a semiconducting organic molecule under the application of an electric field. In the year 1990, Conjugated organic polymers were also found to emit yellow green light under an electric field (Brroughes et al. 1990). At present organic light emitting devices have already been commercialized. In order to make these devices more practical, devices based on new mechanisms such as thermally activated delayed fluorescence (TADF) (Adachi et al. 2014) are being looked into. The phenomenon of electroluminescence in OLED is either fluorescence or phosphorescence, further a high efficiency and long life time can be achieved by these organic materials if they are stacked in a proper manner (Karzai et al. 2001, 2003; Kukarni et al. 2004; Hung et al. 2002). An OLED emits light when it is provided a proper external voltage (less than 5eV). The low operating voltage leads to less power consumption (Peumans et al. 2003; Karzazi et al. 2014; Blochwitz et al. 1998; Miyata et al. 1997). The photo – physical and electronic properties of organic materials depends on the nature of substituent (Detert et al. 2000; Park et al. 2008). These properties of luminescent molecules can be altered by the presence of substituent, therefore several derivatives of these molecules have been synthesized, for e.g. by Huang *et al*. (Xia et al. 2000). The effect of the nature of substituent, i.e. electron donating or withdrawing, has also been investigated by Urch *et al. 2001*.

Computational techniques such as DFT and TD – DFT (Runge et al. 1984) have enabled systematic calculations and study of the properties and structure of OLED materials both in ground and excited states providing valuable knowledge for photo absorption, emission and charge carrier mobility (Hwang et al. 2011). It is known that the optical and electronic properties of organic luminescent materials depend on the nature of substituents. The present work reports electronic structures of four TPBB derivatives and their excited state absorption spectra in UV-visible range. These materials were observed to have very useful emission properties (Kim et al. 2010). Theoretical study of TPBB and its derivatives (with different substituents) using Time dependant – Density Function Theory (TD – DFT) with singlet excitation method is done to calculate the absorption spectra of TPBB and its derivatives.

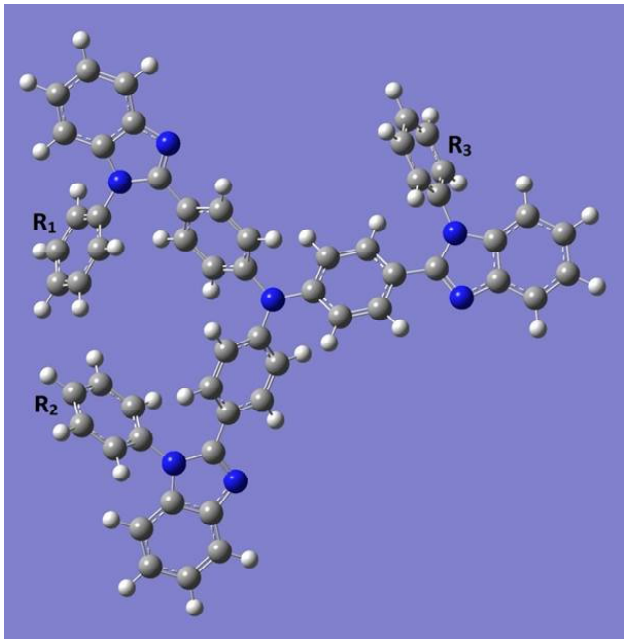

Fig. 1. Optimized Geometry of TPBB

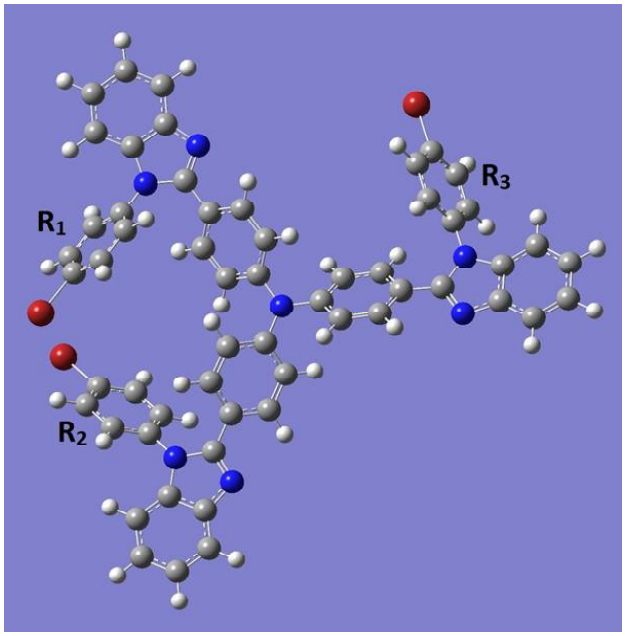

Fig. 3. Optimized Geometry of Br-TPBB

Theoretical methodology

DFT calculations for TPBB and its derivatives were performed. A uniform strategy is adopted for the study of these molecules. After generating the molecular structure using Gauss view, geometry optimization has been carried out without any constraints and checked for imaginary frequencies using M06 (Zhao yet al. 2008) method with 6-31G** (Hay et al. 1985) basis set (i.e. split valence –shell augmented by d polarization function on hydrogen atom as well as diffuse function for both hydrogen and heavy atom was used) (Ku et al. 2009; Hwang et al. 2009; Hehre et al. 1972; Kim et al. 2003). The above basis set has been

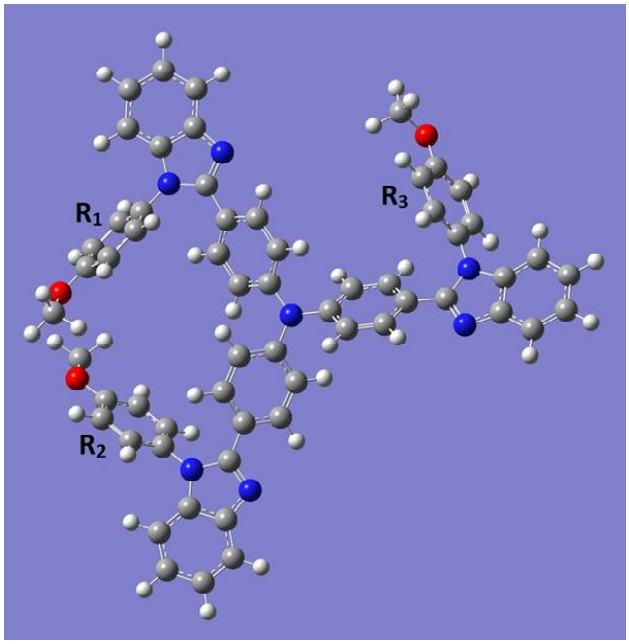

Fig. 2. Optimized Geometry of MeO-TPBB

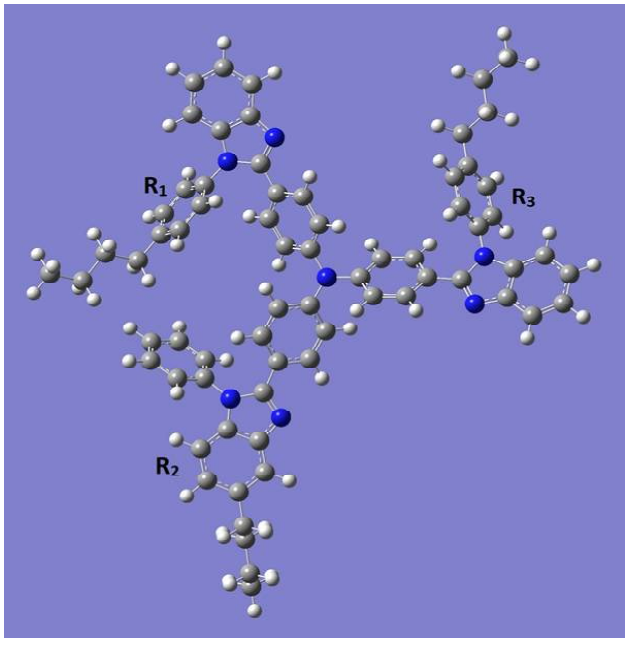

Fig. 4. Optimized Geometry of Bu-TPBB

Table 1. Optimized Geometry parameters of TPBB and its derivatives

Derivative	substituent group	bond length between substituent group and benzene rings (Å)		Mullikan charge on substituent group
		Ring	Bond Length	
TPBB	**H**	R1	1.088	0.114086
		R2	1.088	0.113276
		R3	1.087	0.130698
Bu - TPBB	**Bu**	R1	1.500	-0.021456
		R2	1.503	-0.011708
		R3	1.500	-0.035824
Br - TPBB	**Br**	R1	1.892	-0.137
		R2	1.893	-0.138
		R3	1.891	-0.127
MeO -TPBB	**Meo**	R1	1.352	-0.237875
		R2	1.352	-0.241268
		R3	1.351	-0.233352

R1, R2, R3 are the rings as shown in figures.

employed on Gaussian 09 package (Frisch et al. 2010) for this purpose and TD – DFT calculation was also done using the same method.

RESULT AND DISCUSSION

The Figures 1-4 present optimized geometry of TPBB, MeO-TPBB, Br-TPBB, and Bu-TPBB. From figures it is clear that in case Bu-TPBB, because of long alkyl chain there is a rotation in benzene ring and all three Butyl group are away from each other. In all other cases two substituent groups are interacting with each other non-covalently. The geometry parameters after optimization are listed in Table 1. The parameters include the Mullikan charge on the substituent group present in each molecule along with the bond length between the substituent and the benzene rings R_1 , R_2 , R_3 as shown in figures 1 – 4.

The molecular orbital analysis of (HOMO and LUMO) of molecules 1-4 provides a reasonable qualitative indication of the excitation properties and the electron transport because of the relative order of these orbitals. The HOMO and LUMO energy of TPBB and its derivatives computed using the TD-DFT/6-31G** method, are shown in Table 2. The calculated HOMO-LUMO gap is usually considered as representation of the emission characteristics of the molecule. The TPBB derivatives showed almost the same HOMO and LUMO energy values without reference to the substituent.

The computed results in Table 2 suggest that there is not much effect on HOMO – LUMO gap and in vertical excitation with substitution. Table 3 gives the prominent excitations in these molecules along with their oscillator strengths and absorption wavelengths. Figures 5 – 8 give the UV – VIS spectra of TPBB and its derivatives.

CONCLUSION

The M06/6-31G** method is good for the analysis of structural and electronic properties of TPBB and its derivatives. The TPBB derivatives with substituent Br, Bu and MeO group show improvement in light absorption. The Br, Bu, and MeO substituent could hardly alter the energy levels of TPBB although they have different electron donating ability. The slight variations in the absorption wavelengths can be attributed to the variations of conjugation present in these molecule due to different

Table 2. HOMO and LUMO values for TPBB and its derivatives

Derivative	HOMO (eV)	LUMO (eV)	LUMO + 1 (eV)
TPBB	-5.308290312	-1.269112304	-1.170933587
Bu-TPBB	-5.254983187	-1.153572716	-1.131776388
Br-TPBB	-5.472130128	-1.340895967	-1.099394827
MeO - TPBB	-5.275201254	-1.148701876	-1.282636368

Table 3. Details of major transitions in TPBB and its Derivatives

Derivative	Major Transition	Absorption Wavelength (λ_{abs})	Oscillator Strength (f)
TPBB	HOMO → LUMO	377.91 nm	0.6586
	HOMO → LUMO + 1	367.55 nm	1.1684
Bu-TPBB	HOMO → LUMO	372.61 nm	1.0049
	HOMO → LUMO + 1	369.70 nm	0.8519
Br-TPBB	HOMO → LUMO	369.23 nm	0.8908
	HOMO → LUMO + 1	364.62 nm	0.7630
MeO-TPBB	HOMO → LUMO	370.02 nm	0.8112
	HOMO → LUMO + 1	365.34 nm	0.9538

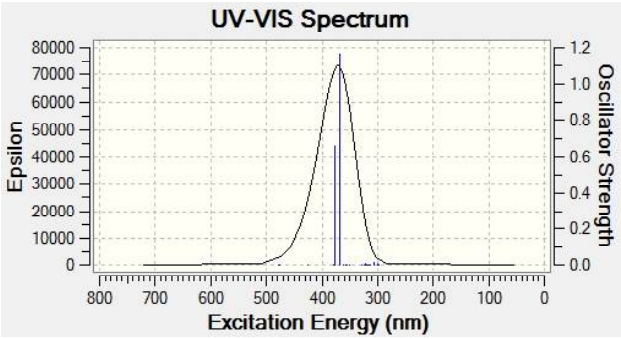

Fig. 5. Absorption Spectra for TPBB.

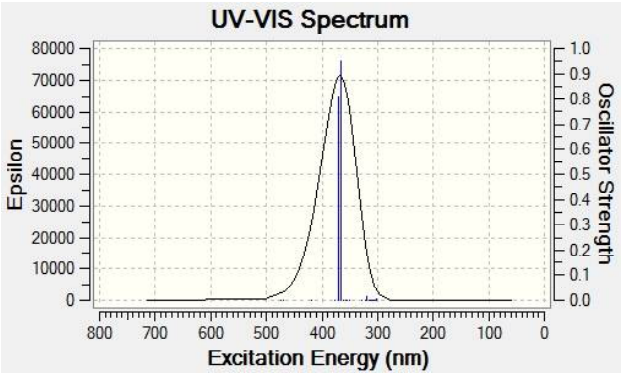

Fig. 6. Absorption Spectra for MeO-TPBB

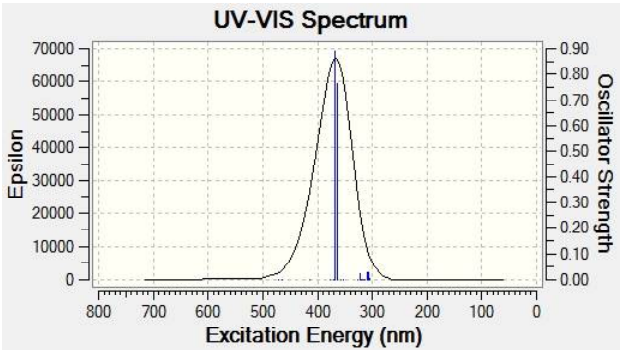

Fig. 7. Absorption Spectra for Br-TPBB

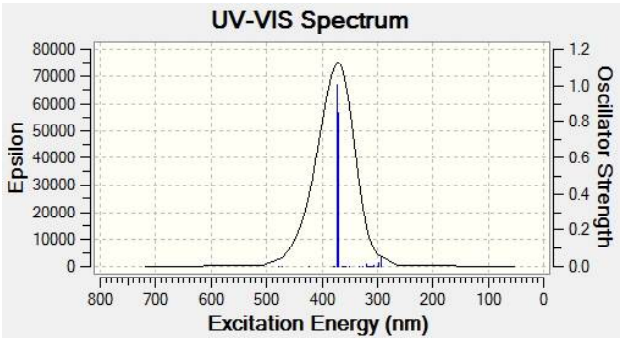

Fig. 8. Absorption Spectra for Bu-TPBB.

substituents. This result suggests that derivatives of TBPP can also be effectively used for fabrication of a practical OLED.

REFERENCES

Adachi, C. (2014). Third-generation organic electroluminescence materials. *Jpn. J. Appl. Phys.*, 53:060101-12.

Blochwitz, J., Pfeiffer, M., Fritz, T., & Leo, K. *(1998). Appl. Phys. Lett., 73,* 729.

Burroughes, J.H., Bradley,D.D.C, Brown, A.R., Marks, R.N., Mackay, K., Friend, R.H., Burns, P.L., Holmes, A.B. (1990). Light-emitting diodes based on conjugated polymers. *Nature*, *347*:539-541.

Detert, H. & Sugiono, E. (2000). Soluble oligo(phenylenevinylene)s with electron withdrawing substituents for the use in light emitting diodes. *Synthetic Metals, 115:*89-92.

Frisch, M. J., Trucks, G. W., Schlegel, H. B., Scuseria, G. E., Robb, M. A., Cheeseman, J. R., Scalmani, G., Barone, V., Mennucci, B., Petersson, G. A., Nakatsuji, H., Caricato, M., Li, X., Hratchian, H. P., Izmaylov, A. F., Bloino, J., Zheng, G., Sonnenberg, J. L., Hada, M., Ehara, M., Toyota, K., Fukuda, R., Hasegawa, J., Ishida, M., Nakajima, T., Honda, Y., Kitao, O., Nakai, H., Vreven, T., Montgomery Jr., J. A., Peralta, J. E., Ogliaro, F., Bearpark, M., Heyd, J.

J., Brothers, E., Kudin, K. N., Staroverov, V. N., Keith, T., Kobayashi, R., Normand, J., Raghavachari, K., Rendell, A., Burant, J. C., Iyengar, S. S., Tomasi, J., Cossi, M., Rega, N., Millam, J. M., Klene, M., Knox, J. E., Cross, J. B., Bakken, V., Adamo, C., Jaramillo, J., Gomperts, R., Stratmann, R. E., Yazyev, O., Austin, A. J., Cammi, R., Pomelli, C., Ochterski, J. W., Martin, R. L., Morokuma, K., Zakrzewski, V. G., Voth, G. A., Salvador, P., Dannenberg, J. J., Dapprich, S., Daniels, A. D., Farkas, O., Foresman, J. B., Ortiz, J. V., Cioslowski, J. & Fox, D. J., Gaussian, Inc. (2010). *Gaussian-09, Revision B.01,* Wallingford CT.

Hay, P. J., & Wadt, W. R. (1985). Ab initio effective core potentials for molecular calculations. Potentials for the transition metal atoms Sc to Hg. *J. Chem. Phys*., *82*:270.

Hehre, W. J., Ditchfield, R. & Pople, J.A. (1972). Self—Consistent Molecular Orbital Methods. XII. Further Extensions of Gaussian—Type Basis Sets for Use in Molecular Orbital Studies of Organic Molecules. *J. Chem. Phys., 56:*2257.

Hung, L. S. & Chen, C.H. (2002). Recent progress of molecular organic electroluminescent materials and devices. *Mater. Sc. Eng., R 39:*143-222.

Hunter, C. A., Lawson, K. R., Perkins, J. & Urch, C. J. (2001). Aromatic interactions. *J. Chem. Soc., Perkin Trans. 2, 2,* 651-669.

Hwang, K. Y., Kim, H., Lee, Y. S., Lee, M. H. & Do, Y. (2009). *Chem. Eur. J., 15.*

Hwang, T.K., Kim, J.Y. & Lee, S. (2011). Quantum Chemical Study of the OLED Materials Tris[4'-(1"-phenylbenzimidazol-2"-yl)phenyl] Derivatives of Amine and Benzene. *Bull. Korean Chem. Soc., 32(5):*1733-1736.

Karzai, Y., Cornil, J. & Bredas, J.L. (2001). Negative Differential Resistance Behavior in Conjugated Molecular Wires Incorporating Spacers: A Quantum-Chemical Description. *J. Am. Chem. Soc., 123:*10076-10084.

Karzai, Y., Cornil, J. & Bredas, J.L. (2003). Theoretical investigation of the origin of negative differential resistance in substituted phenylene ethynylene oligomers. *Nanotechnolgy, 14:*165-171.

Karzazi, Y. (2014). Synthesis and Anticorrosion for X70 Steel of Propynol Derivatives in Acid Medium. *J. Matter. Environ. Sci.5 (1):1-12.*

Kim *et al*, (2010). Effect of Intermolecular Interaction on the Characteristics of Organic Light Emitting Diodes with TPBB Derivatives *Mol. Cryst. Liq. Cryst.*, Vol, 520: 28/[304]- 35/[311].

Kim, H., & Lee, Y.S. (2003). Quantum chemical analysis of salen–aluminum complexes for organic light emitting diodes. *J. Chem. Phys. Let.* **585**:143-148.

Ku, Y., Chi, L.C., Hung, W. Y., Yang, S. W., Tsai, T. C., Wong, K. T., Chin, Y.H. &Wu, C. I. (2009). High-luminescence non-doped green OLEDs based on a 9,9-diarylfluorene-terminated 2,1,3-benzothiadiazole derivative. *J. mater. chem., 19:*773-780.

Kulkarni, A. P., Tanzola, C.J., Babel, A. & Jenekhe, S. A. (2004). Electron Transport Materials for Organic Light-Emitting Diodes. *Chemi. Mater., 16:*4556-4573.

Minaev, B., Baryshnikov, G., Agren, H. (2014). Principles of phosphorescent organic light emitting devices. *Phys. Chem. Chem. Phys.,* 16:1719-1758.

Miyata, S. & Nalwa, H.S. (1997). *Organic Electroluminescent Materials and Devices*, Gordon and Breach: Amsterdam.

Park, J. W., Kim, Y. H., Jung, S. Y., Byeon, K. N., Jang, S. H., Lee, S. K., Shin, S. C. & Kwon, S. K. (2008). Efficient and stable blue organic light-emitting diode based on an anthracene derivative. *Thin Solid Films, 561:*8381–8385.

Peumans, P., Yakimov, A., & Forrest, S.R. (2003). Small molecular weight organic thin-film photodetectors and solar cells. *J. Appl. Phys.:93,* 3693-3723.

Runge, E. & Gross, E. K. U. (1984). Density-Functional Theory for Time-Dependent Systems. *Phys. Rev. Lett.* ***52*** *(12):* 997–1000.

Tang, C.W., Vanslyke, S.A. (1987). Organic electroluminescent diodes. *Appl. Phys. Lett., 51:*913-915.

Xia, C., Wang, X., Lin, J., Jiang, W., Ni, Y. & Huang, W. (2009). Organic light-emitting devices (OLED) based on new triphenylamine derivatives. *Synthetic Metals, 159:*194-200.

Xiao, L., Kido, J., et al. (2011). Recent Progresses on Materials for Electrophosphorescent Organic Light-Emitting Devices. *Adv. Mater.,* 23:926-952.

Zhao, Y. & Truhlar, D. G. (2008). The M06 suite of density functionals for main group thermochemistry, thermochemical kinetics, noncovalent interactions, excited states, and transition elements: two new functionals and systematic testing of four M06-class functionals and 12 other functional. *Theor. Chem. Acc., 120*:215-241.

REVIEW ARTICLE

International Journal of Science, Technology and Society
Vol 3, No. 2 (2017) : 01-10

A review on QM/MM studies of nucleic bases interactions with graphene and carbon nanotubes

Asheesh Kumar, Ruchi Mishra, Deep Kumar, Devesh Kumar*

Department of Physics, School of Physical and Decision Sciences, Babasaheb Bhimrao Ambedkar University, Vidya Vihar, Rae Bareilly Road, Lucknow-226 025, India.

Publication Info

Article history:
Received : 10.12.2017
Accepted : 22.12.2017
DOI: https://doi.org/10.18091/ijsts.v3i02.11404

Key words:
Nucleic Acid (NA), Carbon nanotube (CNT), Graphene, Binding Energy, Initial Configurations (IC), QM (Quantum Mechanics) / MM (Molecular Mechanics).

Corresponding author:
Devesh Kumar

Email:
*dkclcre@yahoo.com

ABSTRACT

Nucleic bases interaction with carbonaceous materials finds significant attention due to their application in various fields such as DNA sequencing, DNA sensing and drug delivery. Nucleic bases, building blocks of nucleic acids interact with carbon nanotube and contribute significantly to the stability of the nucleic bases, carbon nanotube hybrids and their properties. In the present work, a thorough review of previous studies on the binding of nucleic bases with graphene and CNT is presented, with a focus on the simulation works that attempted to evaluate the structure and strength of binding. Dissimilitude among these works is noticed and factors that might contribute to such discrepancies are discussed in detail.

INTRODUCTION

Graphene and carbon-nanotubes have different applications for many reasons, but the differences can be ultimately attributed to the difference between one-dimensional materials and two dimensional materials. For example, a single walled carbon nanotube can be regarded as a single crystal with a high length–diameter ratio. However, the current synthesis and assembly technology cannot prepare the carbon nanotube crystals on a macroscopic scale, which limits their applications. While, graphene may be considered as a two-dimensional crystal structure, and its strength, conductivity and thermal conductivity are seen to be the best in two-dimensional crystal materials. It has a broad range of applications because of its ability to have a large area of continuous growth.

Graphene, is a planar form of carbon atoms designed in a two-dimensional hexagonal lattice fashion. It has emerged as the most dominating allotropes of carbon during the last few years. Its extended honeycomb network is the basic building block of other important allotropes such as 3D graphite formed by the stacking of several layers of graphene; 1D nanotube, obtained by rolling the graphene and the 0D fullerene prepared by wrapped graphenes (J. Allen Matthew *et al.,* 2010). Graphene is being used in the designing of new nanomaterials for energy storage devices, fuel cells and biosensors owing to its high stability, elasticity and electromechanical modulation (Stoller Meryl D *et al.*, 2008, Si Yongchao and T Samulski Edward, 2008, Pumera Martin *et al.,* 2010). Also, graphene exhibits extraordinary electronic properties in comparison to many of the conventional materials; the highly conductive graphene becomes an insulator after hydrogenation. This hydrogenation of graphene is highly reversible; the intrinsic conductivity as well as the structure of graphene can be restored on annealing (Chen Liang *et al., 2007;* Denis Pablo A *et al.,* 2009; Rubes Miroslav *et al.,* 2009). Graphene is also an important material in nanoscale electronics due to its compatibility with industry standard lithographic processing. The electron mobilities is up to 150 times greater than Si, and the thermal conductivity is approximately twice that of diamond (Ritter Kyle A *et al.,* 2009). Thus one can say that graphene has revolutionalized the technology.

Graphene sensors have emerged as another area of recent interest. The chemical and physical properties of graphene make it a promising candidate that can be used as a sensor to detect different gases such as H_2, NO_2, and NH_3. Schedin *et* al., in their experimental results, illustrated that graphene based sensors allow the sensitivity levels such that the adsorption of individual gas molecules could be detected accurately (Rao, C. N. R. *et al.,* 2009; Schedin F *et al.,* 2007). Graphene-polyaniline nanocomposite is found to be a good sensor for H_2 gas while nitrogen doped graphene find its application in electrochemical biosensing (Al-Mashat Laith *et al.,* 2010). It is also shown that, through functionalization, properties of graphene can be modified. The functionalization of graphene with hydrogen, oxygen, or other chemical groups is of prime importance as a way to engineer the different properties of graphene. A recent study reveals that with controlled epoxide functionalization, graphene can be used as a starting material for diverse chemical functionalization by chemical modification of the epoxide group. The functionalization of graphene and single-walled carbon nanotubes with individual 3d transition metal atoms were also modeled using density functional theory calculations.(Lee Geunsik *et al.,* 2009; Hubert Valencia *et al.,* 2010; Ghaderi Nahid *et al.,* 2010;Park Sungjin *et al.,*2008; Wang Donghai *et al.,2010;* Quintana Mildred *et al.*, 2010; Tachikawa Hirotoet *al.,* 2010; Al-Aqtash Nabil *et al.,* 2009).

The capability to detect single bio-molecules with high accuracy and efficiency is of prime importance in many areas of environmental science, biology, and chemistry (Lim Sung H. *et al.,* 2009; Bano Fouzia *et al.,* 2009; Zwolak Michael *et al.,* 2008; Fredlake P. Christopher *et al.,* 2006; Jonkheijm Pascal *et al.,* 2008; Patolsky Fernando *et al.,* 2006; Vidic Jasmina *et al.,* 2006). Efficient bio-sensors are expected to contribute to the improvement of medicine and medical treatment (Zwolak Michael, 2008). It is, quite uncertain whether traditional chemical techniques can be simultaneously fast and inexpensive which is another very important aspect that needs to be taken care of (Fredlake P. Christopher *et al.,* 2006). Nano-materials, due to their extreme sensitivity of the electron-transport properties in confined materials to external perturbations, form an excellent technological platform for single-molecule recognition (Zhang Guangyu *et al.,* 2006; Meyer Jannik C *et al.,* 2007; Shapir Errez *et al.,* 2008; N Kang *et al.,* 2007). Recently, graphene nano-ribbon (GNR) has emerged as a suitable candidate for making sensors for single small molecules, such as H_2, H_2O, and NO. This concept is based on measuring a variation in the source-drain current of a GNR based field-effect transistor originating from the covalent bond formed between the molecule to be detected and a defect (or an edge) of GNR. However, few reports exist on the use of GNRs as bio-sensors. One of the main reasons is that the biomolecules do not usually bind GNR via covalent bonds as a result of which the electrical perturbation induced by a biomolecule on a GNR is too weak to be detected. However the GNR is proposed to be used for the DNA sequence via π-π stacking in many reports.

Relevance of DNA bases and graphene/carbon nanotube interaction

The interaction of the biomolecules such as nucleic bases on the surface of GNR and CNT has attracted many researchers. In particular, the DNA-CNT interaction has cast its spell in the research community due to its application in various fields such as DNA sensing, DNA sequencing, and drug delivery (Zhao Xiongce 2011; Paul Ambarish 2010; Liu Zhuang *et al.,* 2011; Yarotski Dzmitry A *et al.,* 2009). It has also been found that the determination of a patient's DNA sequence can even reveal his risk of falling ill with particular diseases and it also helps to design "personalized medicine", and it is therefore the DNA sequencing that appears to be one of the most potential applications for the carbon nanostructures (Sanchez Jimenez Gerardo *et al.,* 2001; Nelson Tammie *et al.,* 2010; Prasongkit Jariyanee *et al.,* 2011). Sensors for amplified detection methods based on CNT-biomolecule composites is an area of recent interest, and such sensors can be efficiently used to detect various carbon nanostructures as well as different biomaterials such as DNA, protein, and so on (Barone Paul W *et al.*, 2005). Also, DNA-functionalized carbon nanotubes form the basis for not only a new class of chemical sensors but also for the molecular electronic devices. An ultrasensitive graphene-embedded nano channel device which effectively controls the motion of nucleobases via π-π interaction was also reported (Min Seung Kyu *et al.,* 2011).Weizmann *et al.,* 2011, recently reported that DNA-CNT nanowire networks can be used for DNA detection and Zheng Y*et al.,* 2009, constructed a carbon nanotube-based DNA biosensor for sensing the phenolic pollutants. Beside biomedical applications, comprehending the DNA-CNT interaction can also be used in the separation of carbon nanotubes as it has been shown that single-stranded DNA can be effectively used for the dispersion and separation of single-walled carbon nanotubes (Zheng M *et al.,* 2003). Some of the important conclusions can also be drawn from the studies (Wang X et al., (2011); Lu G et al.,(2009) ; Li J et al.,(2003)). Many research groups have focused on

determining the DNA-CNT interaction and tried to explore the strength of binding of different nucleosides, nucleobases, and nucleobases pairs on the carbon nanotubes and graphene, in both experimental and computational studies (Chen Robert J. *et al.,* 2003; Stepanian S.G. *et al.,* 2008; Shtogun Yaroslav V. *et al.,* 2007; Wang Hongming *et al.,* 2009; Wang Po *et al.,* 2011). The different binding energy orders for different studies are found in many experimental studies and it is understood that this may be due to the different experimental conditions applied. For most cases, in computational studies, the order is G > A > T > C > U, and in some cases, were found to be in the order as G~A~T~C > U. There are a number of theoretical and experimental studies on the nucleobases interaction with carbon nanotube and graphene surfaces as shown below:

Table 1. BE (kJ/mol) of nucleobases with SWCNT and graphene in theoretical and experimental studies.

Nucleic bases interaction with different Carbon nanomaterials			
Type	**Order**	**Method**	**Ref.**
SWCNT	T A ~C	Exp.	100
CNT(5,0)	G A T C U	Comp.	23
CNT(7,0)	G A ~T ~C U	Comp.	65
CNT (5,5), CNT(10,0)	G A T C	Comp.	86
GNR	G A ~T ~C U	Comp.	22

The binding energy of all the considered complexes illustrates that the binding energy increases as the curvature of SWCNT (single walled carbon nanotube) decreases and reaches the maximum for graphene. In general, the nucleobases tend to have π-π stacking (Zheng Y *et al.,* 2009) type of interaction with the carbon nanostructures. Hence, as the curvature of SWCNT decreases, there will be more efficient stacking between the carbon nanotube and the nucleobases surface, resulting in an increase in the binding energy of the complexes. The effect of size and curvature generally plays an important role in the non-bonded interactions (Zheng Ming *et al.,* 2003; Chen Robert J. *et al.,* 2003).

METHODS

First-Principles Methodology

In the QM methods, mostly DFT has been used in the computational chemistry and quantum physics due to their relatively low computational cost compared to high level *ab initio* methods and high accuracy in comparison to the semi- empirical methods.

The dispersion forces in the dispersion interaction are the most important interactions in molecular systems that are not addressed well in several DFT approaches. Efforts were made by the several research groups (Rutledge *et al.*, 2009; Rutledge and Wetmore, 2010; Johnson *et al.*, 2004, 2009; Dion *et al.*, 2004a; Zhao and Truhlar, 2005, 2011; Meijer and Sprik, 1996; Tkatchenko and Scheffler, 2009; Grimme, 2004, 2006; Grimme *et al.*, 2010, etc) to precisely incorporate dispersion in the correlation term of DFT. There were several studies of interaction of nucleic bases with CNT or graphene which however did not consider the dispersion interaction into account. Some early works based on LDA scheme of DFT, also lack dispersion correction. However the recent studies adopted either classical FF (force field) or dispersion corrected DFTs to consider the dispersion factor. It is believed that the π-π stacking plays a key role in the binding of nucleobase to graphene or CNT, dispersion therefore can play a significant role in determining the binding structure and BE (Binding Energy). So, one can precisely say that different approaches lead to different results. Therefore the past studies can be broadly classified into two categories: those performed with methods that consider dispersion, and those which do not consider dispersion-corrected methods.

Among the QM studies, there are also various methods with different levels of complexity and accuracy, including *ab initio* methods (HF, MP2 and CCSD (T)), DFT and semi-empirical methods. HF, originally named SCF method, is the first *ab initio* method and forms the basis of post- HF methods. Despite of having the correct description for the exchange energy, HF does not address the electron correlation precisely. Post-HF methods include MP2 (Møller and Plesset, 1934; Head- Gordon *et al.*, 1988), CI and CCSD (T) that were proposed to properly describe the correlation energy. These *ab initio* methods are usually employed for very small atomic systems due to their high computational cost. Semi-empirical QM methods are based on *ab initio* methods but include empirical parameters to speed up the calculations, examples include AM1 (Dewar *et al.*, 1985), PM3 (Stewart, 1989a,b, 1991) and PM6 (Stewart, 2007). In computational quantum chemistry and physics, DFT has been widely used, due to its relatively low computational cost compared with high level *ab initio* methods and high accuracy compared with semi-empirical methods. In 1964, Kohn and Hohenberg published the first paper on DFT in which they substituted the many electron wavefunction with the electron density and reduced the number of

variables. One year later, Kohn and Sham in 1965 improved the Hohenberg and Kohn's theory by introducing effective potential that included external potential, exchange and correlation interactions.

Methods lacking the dispersion correction

Gowtham *et al*., studied the adsorption of nucleobases (A, C, G, T and U) on graphene using MP2 and LDA (Gowtham *et al.*, 2007). Nucleobases in their work were attached to a methyl group. Plane wave basis set was used in the LDA calculations (Supercell approach), while in the MP2 calculations, 6-311++G(d,p) basis set was used with the graphene containing 28 carbon atoms terminated by hydrogen atoms at the edges. For each configuration of the nucleobase on the graphene, they initially performed a force relaxation to determine the preferred orientation and kept the bases at optimum separation distance. This was followed by a scan of the potential energy surface (PES) where the nucleobases were kept parallel to the graphene surface at a fixed distance. For each configuration, single point energy calculations were also performed and the minimum potential energy was determined. This configuration was subjected to a further optimization step in which all atoms were free to move and the final optimized structure was identified. Thereafter, BE was then calculated for the optimized structure using both MP2 and LDA. Table 2 shows the values of the obtained BEs. Among these two, MP2 predicted BE values that were almost doubled the LDA values. The BEs with respect to the different nucleobases almost remained in the same order: it was G>A=T=C>U using LDA and G>A>T>C>U using MP2. The final optimized nucleobases were found to be parallel to the graphene sheet with the separation distance being 3.5 Å.

Table 2. BE (kJ/mol) between nucleobases and graphene [Gowtham *et al.*, (2007)].

Nucleobase	LDA	MP2
G	58.86	103.24
A	47.28	90.70
T	47.28	80.08
C	47.28	77.19
U	42.25	71.40

In a later work, Gowtham *et al.,* also studied the adsorption of the same nucleobases on a (5,0) CNT (Gowtham *et al.,* 2008), using the same approach except that the BE calculation was only done with LDA only, and not with MP2. The order of the BE was found to be the same, i.e., G>A>T>C>U with the values being 47.28, 37.63, 32.81, 27.98 and 27.02 kJ/mol, respectively. Their results confirmed that the BEs for CNT were much smaller than those for graphene, that was attributed to the larger curvature of the CNT and resulting smaller area of contact.

Meng *et al.,* (Meng *et al.*, 2007a) first optimized the structures using CHARMM FF which includes an empirical description of dispersion interaction, but this dispersion was neglected again during the re-optimization step using LDA.

Meng *et al*., used a different approach (time-dependent LDA method) to study the binding between DNA nucleosides and a CNT (10,0) (Meng *et al.*, 2007b). From these simulations, the optical absorbance spectrum for DNA nucleosides were obtained, which were used to determine the preferred orientation of the nucleosides on the CNT. Optimized binding structures were also obtained using MM (CHARMM) calculations, and were found in good agreement between the MM results and LDA results. According to MM calculations, the order of the BE for the most stable structures was G>A>T>C with the BE values of 82.01, 78.15, 74.29 and 67.54 kJ/mol, respectively.

The dependence of BE on CNT chirality was studied by Wang and Ceulemans (Wang *et al.*, 2009) using LDA. They considered two connected adenosine-monophosphates with the phosphate groups terminated by H atoms. The resulting molecule was neutral and was taken to interact with different CNTs, including five (m,0) zigzag tubes with m = 7,8,9,10,17 and four (n,n) armchair tubes with n= 4,5,6,7. Periodic boundary condition using supercell approach and the linear combination of numerical atomic orbitals (LCAO) basis set with double-zeta polarizations were used.

In another work, Wang considered all four DNA nucleobases interacting with two types of CNTs: (5,5) and (10,0) (Wang, 2008). Same as his first work (Wang *et al.*, 2007), for each type of CNT, only a small part (C24H12) was made to interact with the nucleobases. Both DFT and MP2 methods were adopted in the simulations. The geometry optimization was carried out at MPWB1K/cc-pVDZ level where carbon and hydrogen atoms were kept frozen in the C24H12 fragments. The optimized structures were then subjected to a single point energy calculation at MP2/6-311++G(d,p) level. The BSSE-corrected BE for the C(5,5) CNT hybrid in vacuum was 46.46 kJ/mol which is quite different from Wang's former study (Wang *et al.*, 2007) in which the BE for the same system was determined to be 32.76 kJ/mol. The order of the BE between nucleobase and

CNT in the gas phase was found to be G>A>T>C for both CNTs. This is in agreement with the DFT studies of Gowtham *et al.,* on the interaction of nucleobases with graphene and (5,0) CNT (Gowtham *et al.*, 2007, 2008), and also with the MM results of Meng *et al.*, for the interaction of nucleosides with a (10,0) CNT.

The simulation works reviewed above are all based on methods that lack correction for dispersion interaction. With the pace of time and advancement in computational chemistry, more accurate dispersion corrected methods have been introduced.

Methods with dispersion-corrected methods

Recent works using dispersion-corrected DFT also gave rise to different results, possibly due to the difference in ways of incorporating dispersion interaction in these methods. The choice of basis sets can affect the BE evaluation, even with the same method (Shukla *et al.*, 2009). In addition, it is also found that BSSE can be large and has to be taken into account (Tournus *et al.*, 2005). Performance of simulation methods and basis set are still being widely evaluated in the computational chemistry community.

Though a large number of dispersion-corrected methods exist in literature however benchmarking has been performed by some of them (Johnson *et al.*, 2004; Dion *et al.*, 2004a; Hohenstein *et al*., 2008; Zhao *et al.*, 2008; Johnson *et al.*, 2009; Rutledge *et al.*, 2010; Zhao *et al.*, 2011; Grimme, 2011; Ehrlich *et al.*, 2013). Among these methods, Minnesota density functional developed by Truhlar's group, e.g., M05, M05-2X, M06, M06-L, M06-2X and M06-HF, are based on meta-GGA approximations (Zhao *et al.*, 2005, 2006; Zhao *et al.*, 2008, 2006 a,b). The exchange-correlation term in all Minnesota functionals depend on kinetic energy.

In the M06 family, M06-2X has shown good performance in several studies where vdW interaction played an important role (Rutledge *et al.*, 2010). Panigrahi *et al.*, employed dispersion-corrected DFT using wB97XD functional to study nucleobase-graphene binding (Panigrahi *et al.*, 2012). Nucleobases in their work were attached to a methyl group, similar to the study by Gowtham *et al.,* (Gowtham *et al.*, 2007). Each nucleobase was placed above a square graphene sheet with eight carbon rings in each direction and H atoms at the edges. The IC (initial configuration) of the base plane was parallel to the graphene surface with a separation distance of 4 Å, which was subjected to a full optimization at wB97XD/6-31G(d,p) level. The separation distance in the optimized structures was found to be around 3.5 Å. BSSE corrected BE was calculated at the same level and found to be 94.16, 85.03, 79.30, 77.04 and 68.41 kJ/mol respectively for G, A, C, T and U, i.e., G>A>C>T>U. Such order is identical to what was observed by Gowtham *et al.*, (Gowtham *et al.*, 2007) on the same system using LDA optimization accompanied by MP2 energy calculation. The BE values are also close to the MP2 results (Gowtham *et al.*, 2007) but almost double to those obtained using LDA alone.

Swathi and Chandra Shekar (with wB97XD functional) examined physisorption of nucleobases on coronene (C24H12) as a model of graphene (Chandra Shekar *et al.*, 2014). Different ICs were considered while the separation distance was considered to 3Å in all ICs. Geometry optimization was carried out at wB97XD/6-31G(d,p) level followed by a single point energy calculation at wB97XD/6-311+G (d,p). The order of the BSSE corrected BEs was determined to be G>T>A>C>U with the values of 75.73, 66.53, 65.27, 64.43 and 56.48 kJ/mol, respectively. BE values in this work were less than the ones obtained by Panigrahi *et al*., (Panigrahi *et al.*, 2012), which may be attributed to the smaller size of graphene in this study compared to that in Panigrahi *et al*. The separation distance in the optimized structures was found to be 3.24, 3.25, 3.30, 3.22 and 3.20 Å, respectively for G, T, A, C and U. These separation distances were also smaller than the ones obtained by Panigrahi *et al.,* (Panigrahi *et al.*, 2012).

Antony and Grimme studied the interaction of nucleobases with graphene in which four different sizes of graphene were considered, with 24 (C24H12), 54 (C54H18), 96 (C96H24) and 150 (C150H30) carbon atoms respectively (Antony *et al.*, 2010). Hybrids were fully optimized at B97-D/TZV(d,p) level. A three dimensional PES scan was also performed for the interaction of nucleobases with the C96H24 fragment, and no other minima was found except the one obtained from optimization. Nucleobases were attached to a methyl group and PBC was applied in their study. Full geometry optimization for the hybrid structures was also performed but no detailed explanations were given for the ICs.

Vovusha *et al.,* studied the interaction of nucleobases with graphene using M05-2X and M06-2X functional. Vovusha *et al.*, 2013 in their study of graphene model included 54 carbons with 18 hydrogen atoms capping the edge carbons. Geometry optimizations were all performed at M05-2X/6-31G(d) level and BEs were evaluated using both M05-2X and M06-2X methods with 6-31+G(d,p) and 6311++G(d,p) basis sets. The separation distance between nucleobases and graphene in the optimized structures was determined to be 3.2-3.5 Å that is close to previously reported results. Results obtained using M06-2X were considerably

larger than the ones obtained using M05-2X method. The order of the BE using M05- 2X was determined to be G>C=T>A>U and G>C>T>A>U respectively with 6-31+G(d,p) and 6-311++G(d,p) basis sets. When M06-2X was used for the BE calculation, the order was changed to G>T>A>C>U and G>T>C>A>U respectively using 6-31+G(d,p) and 6-311++G(d,p) basis sets. This demonstrates the great effect of method and basis set on the value and order of the BE. In most of the previous results on the BE between nucleobases and graphene, BE of A was only second to G, while this was not obtained by Vovusha *et al.*

Studies on semi-empirical and force-field methods

The studies of the binding of nucleobases with graphene or CNT at lower level methods involve classical MM or semi-empirical QM approaches. AM1 (Dewar *et al.*, 1985), PM3 (Stewart, 1989 a,b, 1991) and PM6 (Stewart, 2007) are the widely used semi-empirical methods. Non-bonded interactions including electrostatic and vdW forces that are implemented in classical FFs such as Amber (Cornell *et al.*, 1995) and CHARMM (MacKerel Jr. *et al.*, 1998). It has been shown that Amber FF can even be more accurate than some of the semi-empirical QM methods when evaluating the BE for biological systems (Rutledge *et al.*, 2009; Rutledge *et al.*, 2010).

Optimization process also plays a key role in BE calculation for these weakly bound systems where PES is expected to be near local minima. Direct optimization may lead system to nearby local minima, but not near the global minima. So, optimization is very sensitive to the IC chosen. The different IC result in different BE values and can even change the order of BE for different nucleobases (NB).

Umadevi *et al.*, brought to light the dependence of the curvature by considering the binding of nucleobases with graphene and a series of armchair (n,n) CNTs where n=3, 4 and 5 (Umadevi *et al.*, 2011). The graphene and CNTs were made using the Gaussian software package with H atoms at the edges was used to saturate the dangling bonds at the boundaries. Each system was optimized using ONIOM method at the (M06-2X/6-31G(d):AM1) level. Atoms of the nucleobases and the "reacting atoms" of CNTs were modeled as the high layer using M06-2X/6-31G(d). The atoms in CNT were considered as the low layer using semi-empirical AM1. Single point energy calculations were performed for the optimized structures using the dispersion-corrected B3LYP method (B3LYP-D) with the 6-31G(d) basis set. The BE was found to be graphene>CNT(5,5)> CNT(4,4)> CNT(3,3) for all nucleobases except T, for which the order was graphene>CNT(5,5)> CNT(3,3)>CNT(4,4). The BSSE-corrected BE was 30-51 kJ/mol for CNTs and 50-73 kJ/mol for graphene. The order of the BE with respect to different nucleobases was determined to be G>T>A>C>U for the CNTs and G>A>T>C>U for the graphene. In another work, using the M06-2X/6-311G**, Umadevi *et al*., found the order of binding for nucleobases with graphane in the order G > A > C > T > U (Umadevi *et al.*, 2015).

DISCUSSION AND FUTURE PERSPECTIVES

This paper presents a comprehensive review of past computational work, where three categories of methods have been used: (1) first-principles studies based on methods lacking dispersion correction, (2) first-principles studies based on dispersion corrected methods and (3) studies based on semi-empirical and FF methods. In nearly all studies reviewed above, the nucleobases were found to be parallel to the graphene or CNT with the separation distance being around 3 Å, which confirms the π-π stacking nature of the interaction. On the other hand, drastically different results have been reported for the BE.

Previous QM calculations on BE already illustrates some effects of CNT chirality (Akdim *et al.,* 2012), however it is not yet clear whether such effects are correlated with the electronic structure of the CNT. Finally, it can be noted that BE has been used as the main parameter for comparisons made in this review. Other properties such as charge transfer and density of states have only been reported in some

Table 3. BE (kJ/mol) between nucleobases and graphene [Vovusha *et al.*, (2013)].

	DFT level			
	M05-2X		M06-2X	
Nucleobase	6-31+G(d,p)	6-311++G(d,p)	6-31+G(d,p)	6-311++G(d,p
G	37.62	27.23	65.08	57.46
A	27.01	16.70	52.19	44.23
T	27.98	19.64	52.93	46.23
C	27.98	20.50	51.02	45.10
U	22.19	13.93	46.36	35.00

(<50%) of the cited works and hence are not suitable for systematic comparison. Also, the calculation of charge transfer does not only depend on the QM method but also on the charge distribution scheme (e.g., Mulliken, ESP, RESP, etc.). This makes the comparison among different studies more complicated.

CONCLUSION

In the present work, a thorough review on the theoretical studies, mainly at the QM level, on the binding of nucleobases (and in a few cases, nucleosides or nucleotides) with graphene or CNT has been performed. BE, as an indicator for the stability of the binding, is used to compare different studies. Due to the different simulated systems and procedure considered for the study, a large range of binding energy values were reported, and considerable discrepancies exist among the past investigations. So, the importance of using dispersion-corrected method and proper design of the optimization procedure plays a crucial role in understanding the interaction of the nucleobases with the CNTs or graphene.

ACKNOWLEDGEMENT

AK would like to acknowledge the UGC for the financial support.

REFERENCES

Akdim B, Pachter R, Day PN, Kim SS and Naik RR (2012). On modelling biomolecular-surface non-bonded interactions: application to nucleobase adsorption on single-wall carbon nanotube surfaces. Nanotechnology, 23: 165703(1-6).

Al-Aqtash N and Vasiliev I (2009). Ab Initio Study of Carboxylated Graphene. J. Phys. Chem. C, 113: 1290-12975.

Allen MJ, Tung VC, and Kaner RB (2010). Honeycomb Carbon: A Review of Graphene. Chem. Rev., 110: 132-145.

Al-MashatLaith, Shin K, Kalantar-zadeh K, Plessis JD, Han SH, Kojima RW, KanerRB, Li D, Gou X, Ippolito SJ, and Wlodarski W (2010). Graphene/Polyaniline Nanocomposite for Hydrogen Sensing. J. Phys. Chem. C, 114: 16168-16173.

Bano F, Fruk L, Sanavio B, Glettenberg M, Casalis L, Niemeyer CM, and Scoles G (2009). Toward Multiprotein Nanoarrays Using Nanografting and DNA Directed Immobilization of Proteins. Nano Letters, 9: 2614-2618.

Barone PW, Baik S, Heller DA and Strano MS (2005). Near-Infraed optical sensors based on single-walled carbon nanotubes. Nature Materials, 4: 86-92.

Becke AD (1993). Density functional thermochemistry. III. The role of exact exchange. J. Chem. Phys. 98: 5648-5652.

Chandra SS and Swathi RS (2014). Stability of Nucleobases and Base Pairs Adsorbed on Graphyne and Graphdiyne. J. Phys. Chem. C, 118: 4516-4528.

Chen L, Cooper AC, Pez GP, and Cheng H (2007). Mechanistic Study on Hydrogen Spillover onto Graphitic Carbon Materials. J. Phys. Chem. C, 111: 18995-19000.

Chen RJ, Bangsaruntlp S, Drouvalakls KA, Kam NWS, Shim M, Li Y, Kim W, Utz PJ, Dai H (2003). Noncovalent functionalization of carbon nanotubes for highly specific electronic biosensors. PNAS, 100: 4984-4989.

Chung C, Gautier C, Campidelli S, Filoramo A. (2010) Hierarchical Functionalization of Single-Wall Carbon Nanotubes with DNA through Positively Charged Pyrene. Chem. Commun, 46: 6539-6541.

Cornell WD, Cieplak P, Bayly CI, Gould IR, Merz KM, Ferguson DM, Spellmeyer DC, Fox T, Caldwell JW, and Kollman PA (1995). A Second Generation Force Field for the Simulation of Proteins, Nucleic Acids, and Organic Molecules. J. Am. Chem. Soc., 117: 5179-5197.

Cornell WD, Cieplak P, Bayly CI, Gould IR, Merz KM, Ferguson DM, Spellmeyer DC, Fox T, Caldwell JW, and Kollman PA (1995). A second generation force field for the simulation of proteins, nucleic acids, and organic molecules. Journal of the American Chemical Society, 117(19):5179-5197.

Denis PA (2011).Theoretical investigation of the stacking interactions between curved conjugated systems and their interaction with fullerenes. Chem. Phys. Lett., 516: 82-87.

Denis PA, Iribarne F (2009). On the hydrogen addition to graphene. Journal of Molecular Structure: Theochem, 907: 93-103.

Dewar MJS, Zoebisch EG, Healy EF, and Stewart JJP (1984). AM1: A New General Purpose Quantum Mechanical Molecular Model. J. Am. Chem. Soc., 107: 3902-3909.

Dion M, Rydberg H, Schrçder E, Langreth DC, and Lundqvist BI (2004a). Van derWaals Density Functional for General Geometries. Physical Review Letters, 92: 246401 (1-4).

Dion M, Rydberg H, Schrçder E, Langreth DC, and Lundqvist BI (2004b). Van derWaals Density Functional for General Geometries. Physical Review Letters, 92: 246401(1-4).

Ehrlich S, Moellmann J, and Grimme S (2013). Dispersion-Corrected Density Functional Theory for Aromatic Interactions in Complex Systems. Acc. Chem. Res., 46: 916-926.

Fredlake CP, Hert DG, Mardis ER, Barron AE (2006) What is the future of electrophoresis in large- scale genomic sequencing? Electrophoresis, 27: 3689-3702.

Ghaderi N and Peressi M (2010). First-Principle Study of Hydroxyl Functional Groups on Pristine, Defected Graphene, and Graphene Epoxide. J. Phys. Chem. C, 114: 21625-21630.

Gowtham S, Scheicher RH, Ahuja R, Pandey R and Karna SP (2007). Physisorption of nucleobases on graphene: Density-functional calculations. Physical Review B 76: 033401(1-4).

Gowtham S, Scheicher RH, Pandey R, Karna SP and Ahuja R (2008). First-principles study of physisorption of nucleic acid bases on small-diameter carbon nanotubes. Nanotechnology, 19: 125701 (1-6).

Grimme S (2004). Accurate Description of van der Waals Complexes by Density Functional Theory Including Empirical Corrections. Journal of Computational Chemistry, 25: 1463-1473.

Grimme S (2006). Semi empirical GGA-Type Density Functional Constructed with a Long-Range Dispersion Correction. Journal of Computational Chemistry, 27: 1787-1799.

Grimme S, Antony J, Ehrlich S, and Krieg H (2010). A consistent and accurate ab initio parametrization of density functional dispersion correction DFT-D for the 94 elements H-Pu. The J. Chem. Phys., 132: 154104(1-19).

Grimme S, Ehrlich S, Goerigk L (2010). Effect of the Damping Function in Dispersion Corrected Density Functional Theory. Journal of Computational Chemistry, 32: 1456-1465.

H-G Martin, Pople JA (1988). MP2 Energy Evaluation By Direct Methods. Chemical Physics Letters, 153: 503-506.

Hohenstein EG, Chill ST and Sherrill CD (2008). Assessment of the Performance of the M05-2X and M06-2X Exchange-Correlation Functionals for NoncovalentInteractions in Biomolecules. J. Chem. Theory Comput., 4: 1996-2000.

Hubert V, Gil A, and Frapper G (2010). Trends in the Adsorption of 3d Transition Metal Atoms onto Graphene and Nanotube Surfaces: A DFT Study and Molecular Orbital Analysis. J. Phys. Chem. C, 114: 14141-14153.

Johnson ER, Wolkow RA , DiLabio GA (2004). Application of 25 density functionals to dispersion-bound homomolecular dimmers. Chemical Physics Letters, 394: 334-338.

Johnsona ER, Mackieb ID and DiLabio GA (2009). Dispersion interactions in density-functional theory. J. Phys. Org. Chem., 22: 1127-1135.

Jonkheijm P, Weinrich D, Schrçder H, Niemeyer CM., and Waldmann H (2008). Chemical Strategies for Generating Protein Biochips. Angew. Chem. Int. Ed., 47: 9618-9647.

Kang N, Erbe A and Scheer E (2008). Electrical characterization of DNA in mechanically controlled break-junctions. New Journal of Physics, 10: 023030 (1-9).

Lee C, Yang W, and Parr RG (1988). Development of the Colic-Salvetti correlation-energy formula into a functional of the electron density. Physical Review B, 37: 785-789.

Lee G, Lee B, Kim J, and Cho K (2009). Ozone Adsorption on Graphene: Ab Initio Study and Experimental Validation. J. Phys. Chem. C, 113: 14225-14229.

Li J, Lu Y, Ye Q, Cinke M, Han J and Meyyappan M (2003). Carbon nanotube sensors for gas and organic vapor detection. Nano Lett., 3: 929-933.

Lim SH., Feng L, Kemling. JW, Musto. CJ, and Suslick KS. (2009). An optoelectronic nose for the detection of toxic gases. nature chemistry, 1: 562-567.

Liu Z, Yang K, and Lee ST (2011). Single-walled carbon nanotubes in biomedical imaging. J. Mater. Chem., 21: 586-598.

Lu G., Ocola, L. E. and Chen, J (2009). Gas detection using low-temperature reduced graphene oxide sheets. Appl. Phys. Lett., 94, 083111-083115.

Meijer EJ and Sprik M (1996). A density functional study of the intermolecular interactions of benzene. J. Chem. Phys. 105: 8684-8689.

Meng S, Maragakis P, Papaloukas C, and Kaxiras E (2007a). DNA Nucleoside Interaction and Identification with Carbon Nanotubes. Nano Lett., 7: 45-50.

Meng S, Wang WL, Maragakis P, and Kaxiras E (2007b). Determination of DNA-Base Orientation on Carbon Nanotubes through Directional Optical Absorbance. Nano Letters, 7: 2312-2316.

Meyer JC, Geim AK, Katsnelson MI, Novoselov KS, Booth TJ & Roth S (2007). The structure of suspended graphene sheets. Nature Letters, 446: 60-63.

Min SK, Kim WY, Cho Y and Kim KS. (2011). Fast DNA sequencing with a graphene-based nanochannel device. nature nanotechnology, 6: 162-165.

Moller C and Plesset MS (1934). Note on an Approximation Treatment for Many-Electron Systems. Physical Review, 46: 618-622.

Nelson T, Zhang B, Prezhdo OV (2010). Detection of Nucleic Acids with Graphene Nanopores: Ab Initio Characterization of a Novel Sequencing Device. Nano Letters, 10: 3237-3242.

Panigrahi S, Bhattacharya A, Banerjee S and Bhattacharyya D (2012). Interaction of Nucleobases with Wrinkled Graphene Surface: Dispersion Corrected DFT and AFM Studies. J. Phys. Chem. C, 116: 4374-4379.

Park S, Lee K-S, Bozoklu G, Cai W, Nguyen ST, and Ruoff RS (2008). Graphene Oxide Papers Modified by Divalent Ions-Enhancing Mechanical Properties via Chemical Cross-Linking. Acs Nano, 3: 572-578.

Patolsky F, Zheng G and Lieber CM (2006). Fabrication of silicon nanowire devices for ultrasensitive, label-free, real-time detection of biological and chemical species. Nature protocols, 1: 1711-1724.

Paul A and Bhattacharya B (2010). DNA Functionalized Carbon Nanotubes for Nonbiological Applications. Materials and Manufacturing Processess, 25: 891-908.

Prasongkit J, Grigoriev A, Pathak B, Ahuja R, Scheicher RH (2011). Transverse Conductance of DNA Nucleotides in a Graphene nano gap from first principles. Nano Letters, 11: 1941-1945.

Priyakumar UD and Sastry GN (2003). Cation-pi interactions of curved polycyclic systems: M+ (M = Li and Na) ion

complexation with buckybowls. Tetrahedron Lett. , 44: 6043-6046.

Pumera M, Ambrosi A, Bonanni A, Chng ELK, Poh HL (2010). Graphene for electrochemical sensing and biosensing. Trends in Analytical Chemistry, 29: 954-965.

Quintana Mildred, SpyrouKonstantinos, GrzelczakMarek, Browne Wesley R, Rudolf Petra, and Prato Maurizio (2010). Functionalization of Graphene via 1,3- Dipolar Cycloaddition. Acs Nano, 4: 3527-3533.

Rao CNR, Sood AK, Subrahmanyam KS, and Govindaraj A (2009). Graphene: The New Two-Dimensional Nanomaterial. Angewandte Chemie, 48: 7752-7777.

Ritter KA and Lyding JW (2009). The influence of edge structure on the electronic properties of graphene quantum dots and nanoribbons. Nature materials, 8: 235-242.

Rubes M and Bludsky O (2009). DFT/CCSD(T) Investigation of the Interaction of Molecular Hydrogen with Carbon Nanostructures. ChemPhysChem, 10: 1868-1873.

Rutledge LR and Wetmore SD (2010). The assessment of density functionals for DNA protein stacked and T-shaped complexes. Canadian Journal of Chemistry, 88: 815-830.

Rutledge LR, Durst HF, and Wetmore SD (2009). Evidence for Stabilization of DNA/RNA-Protein Complexes Arising from Nucleobase-Amino Acid Stacking and T-Shaped Interactions. J. Chem. Theory Comput., 5: 1400-1410.

Sanchez-Jimenez G, Childs B and Valle D (2001). Human disease genes. nature analysis, 409: 853-855.

Schedin F, Geim AK, Morozov SV, Hill EW, Blake P, Katsnelson MI and Novoselov KS (2007). Detection of individual gas molecules adsorbed on graphene. Nature Materials Lett., 6: 652-655.

Shapir E, Cohen H, Calzolari A, Cavazzoni C, Ryndyk DA., Cuniberti G, Kotlyar A, Felice RDF and Porath D (2008). Electronic structure of single DNA molecules resolved by transverse scanning tunnelling spectroscopy. Nature Materials, 7: 68-74.

Shtogun YV, Woods LM, Dovbeshko GI (2007). Adsorption of Adenine and Thymine and their Radicals on Single- Walled Carbon Nanotubes. J. Phys. Chem. C, 111:18174-18181.

Shukla MK, Dubey M, Zakar E, Namburu R, Czyznikowsk Z, Leszczynski J (2009). Interaction of nucleic acid bases with single-walled carbon nanotube. Chemical Physics Letters 480: 269-272.

Si Y and Samulski ET (2008). Exfoliated Graphene Separated by Platinum Nanoparticles. Chem. Mater., 20: 6792-6797.

Song B, Elstner M, and Cuniberti G (2008). Anomalous Conductance Response of DNA Wires under Stretching. Nano Letters, 8: 3217-3220.

Stepanian SG ,Karachevtsev MV, Glamazda AY , Karachevtsev VA, Adamowicz L (2008). Stacking interaction of cytosine with carbon nanotubes: MP2, DFT and Raman. Chemical Physics Letters, 459: 153-158.

Stewart JJP (1988). Optimization of Parameters for Semi empirical Methods II. Applications. Journal of Computational Chemistry, 10: 221-264.

Stewart JJP (1989). Optimization of Parameters for Semi empirical Methods I. Method. Journal of Computational Chemistry, 10: 209-220.

Stewart JJP (1990). Optimization of Parameters for Semi empirical Methods III. Extension of PM3 to Be, Mg, Zn, Ga, Ge, As, Se, Cd, In, Sn, Sb, Te, Hg, T1, Pb, and Bi. Journal of Computational Chemistry, 12: 320-341.

Stewart JJP (2007). Optimization of parameters for semi empirical methods V: Modification of NDDO approximations and application to 70 elements. J Mol Model, 13: 1173–1213.

Stoller MD, Park S, Zhu Y, An J, and Ruoff RS (2008). Graphene-Based Ultracapacitors. Nano letters, 8: 3498-3502.

Tachikawa H and Iyama T (2010). Density Functional Theory Method for Study of the Mechanism of C–H Bond Formation on Finite-Sized Graphene Surface. Japanese Journal of Applied Physics, 49: 06GJ12 (1-4).

Tang S and Cao Z (2011). Adsorption of nitrogen oxides on graphene and graphene oxides: Insights from density functional calculations. The journal of chemical physics, 134: 044710(1-4).

Tkatchenko A and Scheffler M (2009). Accurate Molecular Van Der Waals Interactions from Ground-State Electron Density and Free-Atom Reference Data. PRL, 102: 073005(1-4).

Tournus F and Charlier JC (2005). Ab initio study of benzene adsorption on carbon nanotubes. Physical Review B 71:165421 (1-8).

Umadevi D and Sastry GN (2011). Quantum Mechanical Study of Physisorption of Nucleobases on Carbon Materials: Graphene versus Carbon Nanotubes. J. Phys. Chem. Lett., 2:1572-1576.

Umadevi D, Sastry GN (2015). Graphane versus graphene: a computational investigation of the interaction of nucleobases, aminoacids, heterocycles, small molecules (CO2, H2O, NH3, CH4, H2), metal ions and onium ions. Phys. Chem. Chem. Phys., 17: 30260-30269.

Vidic JM, Grosclaude J, Persuy M-A, Aioun J, Salessea R and Pajot-Augy E (2006). Quantitative assessment of olfactory receptors activity in immobilized nanosomes: a novel concept for bioelectronic nose. Lab chip, 6: 1026-1032.

Vovusha H, Sanyal S and Sanyal B (2013). Interaction of Nucleobases and Aromatic Amino Acids with Graphene Oxide and Graphene Flakes. J. Phys. Chem. Lett., 4: 3710-3718.

Wang D, Kou R, Choi D, Yang Z, Nie Z, Li J, Saraf LV, Hu D, Zhang J, Graff GL, Liu J, Pope MA, and Aksay IA. (2010). Ternary Self-Assembly of Ordered Metal Oxide Graphene Nanocomposites for Electrochemical Energy Storage. Acs

Nano, 4: 1587-1595.

Wang H and Ceulemans A (2009). Physisorption of adenine DNA nucleosides on zigzag and armchair single-walled carbon nanotubes: A first-principles study. Physical Review B, 79:195419(1-6).

Wang P, Wu H, Dai Z, Zou X (2011). Simultaneous detection of guanine, adenine, thymine and cytosine at choline monolayer supported multiwalled carbon nanotubes film. Biosensors and Bioelectronics, 26: 3339-3345.

Wang X and Liew KM (2011). Silicon carbide nanotubes serving as a highly sensitive gas chemical sensor for formaldehyde. J. Phys. Chem. C, 115: 10388-10393.

Wang Y (2008). Theoretical Evidence for the Stronger Ability of Thymine to Disperse SWCNT than Cytosine and Adenine: self-stacking of DNA bases vs their cross-stacking with SWCNT. J Phys Chem C Nanomater Interfaces, 112: 14297-14305.

Wang Y, Shao Y, Matson DW, Li J, and Lin Y (2010). Nitrogen-Doped Graphene and Its Application in Electrochemical Biosensing. Acs Nano, 4: 1790-1798.

Wang Yi and Bu Y (2007). Noncovalent Interactions between Cytosine and SWCNT: Curvature Dependence of Complexes via π-π Stacking and Cooperative CH-pi/NH-pi. J. Phys. Chem. B, 111: 6520-6526.

Weizmann Y, Chenoweth DM, and Swager TM (2011). DNA-CNT Nanowire Networks for DNA Detection. J. Am. Chem. Soc., 133: 3238-3241.

Yan Z and Truhlar DG. (2005). Benchmark Databases for Nonbonded Interactions and their use to test Density Functional Theory. J. Chem. Theory Comput., 1: 415-432.

Yarotski DA, Kilina SV, Talin AA, Tretiak S, Prezhdo OV, Balatsky AV, and Taylor AJ (2009). Scanning Tunneling Microscopy of DNA-Wrapped Carbon Nanotubes. Nano Letters, 9: 12-17.

Zhang G, Qi P, Wang X, Lu Y, Li Xiaolin, Tu R, Bangsaruntip S, Mann D, Zhang L, Dai H (2006). Selective Etching of Metallic Carbon Nanotubes by Gas-Phase Reaction. Science, 314: 974-977.

Zhao X (2011). Self-Assembly of DNA Segments on Graphene and Carbon Nanotube Arrays in Aqueous Solution: A Molecular Simulation Study. J. Phys. Chem. C, 115: 6181-6189.

Zhao Y and Truhlar DG (2005). Benchmark Databases for Nonbonded interactions and their use to test Density Functional Theory. J. Chem. Theory Comput., 1: 415-432.

Zhao Y and Truhlar DG (2006a). A new local density functional for main-group thermochemistry, transition metal bonding, thermochemical kinetics, and noncovalent interactions. J. Chem. Phys., 125: 194101 (1-18).

Zhao Y and Truhlar DG (2006b). Density Functional for Spectroscopy: No Long-Range Self-Interaction Error, Good Performance for Rydberg and Charge-Transfer States, and Better Performance on Average than B3LYP for Ground States. J. Phys. Chem. A, 110: 13126-13129.

Zhao Y and Truhlar DG (2008). The M06 suite of density functionals for main group thermochemistry, thermochemical kinetics, noncovalent interactions, excited states, and transition elements: two new functionals and systematic testing of four M06-class functionals and 12 other functional. TheorChem Account, 120: 215-241.

Zhao Y and Truhlar DG. (2008). Density Functionals with Broad Applicability in Chemistry. Acc. Chem. Res, 41: 157-167.

Zhao Y and Truhlar DG. (2011). Applications and validations of the Minnesota density functional. Chemical Physics Letters, 502: 1-13.

Zheng M, Jagota A, Semke ED, Diner BA, Mclean Robert S, Lustig Steve R, Raymond Richardson E. And Tassi Nancy G. (2003). DNA-assisted dispersion and separation of carbon nanotubes. nature materials, 2: 238-242.

Zheng Y, Yang C, Pu W, Zhang J (2009). Carbon Nanotube-based DNA Biosensor for Monitoring Phenolic Pollutants. Microchim. Acta, 166: 21-36.

Zwolak Michael and Ventra M Di (2008). Colloquium: Physical approaches to DNA sequencing and detection. Rev. Mod. Phys., 80: 141-165.